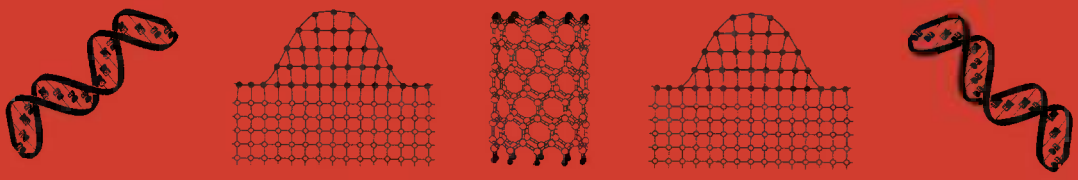

NANOSTRUCTURE SCIENCE AND TECHNOLOGY
Series Editor: David J. Lockwood

Controlled Synthesis of Nanoparticles in Microheterogeneous Systems

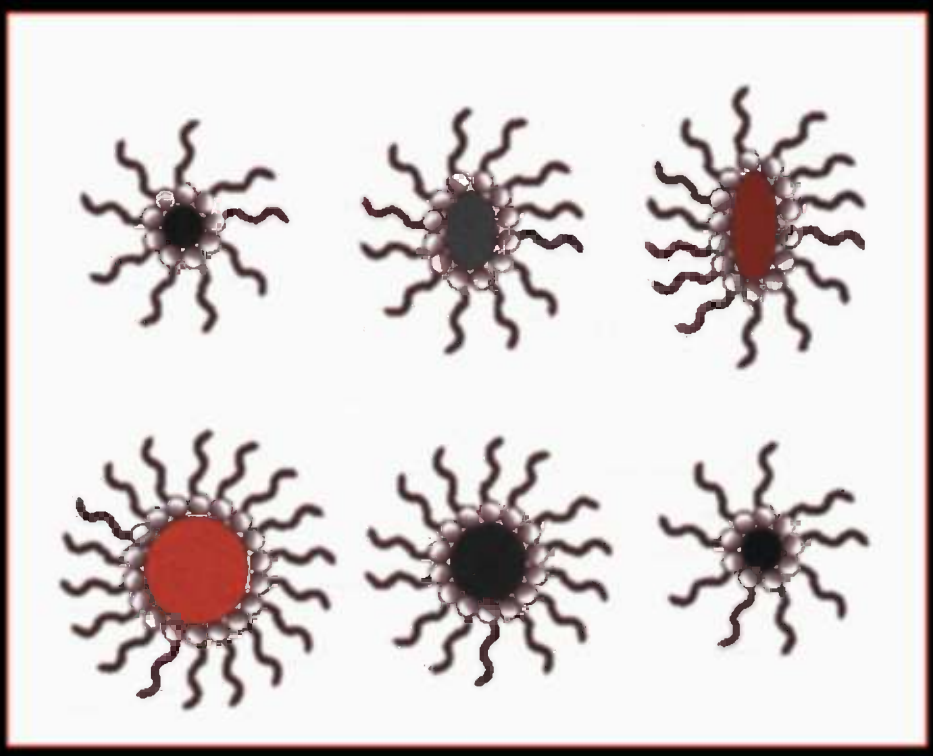

Vincenzo Turco Liveri

Controlled Synthesis of Nanoparticles in Microheterogeneous Systems

Nanostructure Science and Technology

Series Editor: David J. Lockwood, FRSC
National Research Council of Canada
Ottawa, Ontario, Canada

Current volumes in this series:

Controlled Synthesis of Nanoparticles in Microheterogeneous Systems
Vincenzo Turco Liveri

Ordered Porous Nanostructures and Applications
Edited by Ralf B. Wehrspohn

Nanoscale Assembly—Chemical Techniques
Edited by Wilhelm T.S. Huck

Surface Effects in Magnetic Nanoparticles
Dino Fiorani

Alternative Lithography: Unleashing the Potentials of Nanotechnology
Edited by Clivia M. Sotomayor Torres

Interfacial Nanochemistry: Molecular Science and Engineering at Liquid-Liquid Interfaces
Edited by Hitoshi Watarai

Introduction to Nanoscale Science and Technology, Vol. 6
Di Ventra, Massimiliano; Evoy Stephane; Helfin Jr., James R.

Nanoparticles: Building Blocks for Nanotechnology
Edited by Vincent Rotello

Nanostructured Catalysts
Edited by Susannah L. Scott, Cathleen M. Crudden, and Christopher W. Jones

Nanotechnology in Catalysis, Volume 1 and 2
Edited by Bing Zhou, Sophie Hermans, and Gabor A. Somorjai

Polyoxometalate Chemistry for Nano-Composite Design
Edited by Toshihiro Yamase and Michael T. Pope

Self-Assembled Nanostructures
Jin Z. Zhang, Zhong-lin Wang, Jun Liu, Shaowei Chen, and Gang-yu Liu

Semiconductor Nanocrystals: From Basic Principles to Applications
Edited by Alexander L. Efros, David J. Lockwood, and Leonid Tsybeskov

Controlled Synthesis of Nanoparticles in Microheterogeneous Systems

Vincenzo Turco Liveri
University of Palermo, Italy

Springer

Vincenzo Turco Liveri
Department of Physical Chemistry
University of Palermo
Viale delle Scienze
Parco d'Orleans II – Pad. 17
90128 Palermo
Italy
turco@unipa.it

Library of Congress Control Number: 2005928489

ISBN-10: 0-387-26427-2 e-ISBN 0-387-26429-9
ISBN-13: 978-0387-26427-1

Printed on acid-free paper.

Printed in the United States of America. (SPI/SBA)

9 8 7 6 5 4 3 2 1

springeronline.com

Foreword

Colloidal science is extremely diverse and is broadly defined as structural features in length scales ranging from nanometer to micron. These structures are either self-assembled or reduced in sizes and dispersed by applying energy. Some of the nanostructures will entrap gas while others will enclose liquids and/or active matter (micelles, microemulsions, vesicles, cubosomes, hesosomes, etc.) or will encapsulate active molecules in dispersed solid particles (capsules, spheres etc.). The micro- or nanoparticles can be of soft or hard matter.

There are almost endless variations to produce dispersed particles, droplets, and bubbles, and our imagination is short of visualizing the complexity and variability of nanostructures that can self-assemble.

Reducing the size of substances to the state of nanoparticles imparts properties and functionalities that are very different from molecules in a solution, bulk, or crystalline form and demonstrates properties of almost particular, isolated atoms and molecules. Nanotechnology opened the door to emerging new materials with very unique properties in areas of biology, pharmaceutics, cosmetics, and food and industrial products.

Professor Vincenzo Turco Liveri has written a very massive, monumental composition on the methods of producing nanoparticles with selected physico-chemical properties.

It is a difficult task to create some order in the jungle of information on particle size reduction or molecular (or atomic) aggregation, yet Professor Liveri has found the logic and the concept leading to such classification.

I am very impressed by Professor Liveri's intelligent work in categorizing the different techniques into classes and sub-classes, using growth and dimensional criteria as well as componential approach.

The progress that is made daily to better understand short- and long-range interactions, functionality of certain amphiphiles that self-assemble, and preferable organizations (micelles, microemulsions, lyotropic liquid crystals, aggregated biopolymers, membranes, etc.) provides new and fresh ideas to those of us who are engaged in the development of nano- and microdroplets, and particles. Professor Liveri, in his manuscript, did an excellent job in organizing this information.

The number of possible future applications seems to be promising, and Professor Liveri manages to clarify the scope and limitation of each technique while extending knowledge related to the science behind each and every technology. It is only a matter of time before the formation of colloidal particles becomes more of a science and less of "cook and look."

Of special importance is the contribution made by the science related to self-assemblies. It enables us to understand better the physical functionality of biological systems (membranes, cylomicrones, lipoproteins, cells, etc.) that can contribute greatly to the development of new biosensors, devices, methods, and carriers (vehicles) for the delivery of drugs, proteins, DNA, etc.

Professor Liveri's book stresses the fundamental subjects of thermodynamics and kinetics of nanoparticle formation and growing processes in homogeneous and heterogeneous systems, and his view on nucleation and growth is very refreshing.

The manuscript is logically and systematically divided into chapters that are easy to read and follow. Chapter 4 is devoted to a search for new methods with which to prepare nanoparticles and serves as a good starting point to those who are planning to be part of this exciting science.

Congratulations to Professor Liveri for his important contribution.

Jerusalem, Israel *Prof. Nissim Garti*

Preface

The production of materials with selected physico-chemical properties is pivotal for the development of new technologies. Apart from those directly taken from the environment and used after minor changes (stones, wood, minerals, etc.), this objective has been traditionally achieved by chemists and material engineers synthesizing new molecules or blending already known materials. Following these routes, many important classes of materials have been produced such as plastics, explosives, drugs, surfactants, metals, and metallic alloys. However, in the past decades, a novel strategy based on the reduction of well-known substances to the state of nanoparticles and the controlled manipulation of matter in space, time, and chemical composition at a very high degree of subdivision showed itself to be an alternative way to the two older and well-established techniques. Incidentally, it must be stressed that until now, no new material has been achieved by another very old route based on magic practices and esoteric rites finalised to obtain matter with miraculous properties such as the elixir of life and the philosopher's stone.

The reduction of well-known substances to the state of nanoparticles has captured the attention and the imagination of many researchers because, within a substance-specific size range, finely divided matter can exhibit properties and functionalities different from those of the same material in the bulk state as well as from those of isolated atoms and molecules. For many substances, this domain is very often located in the range of a few nanometers ($1\,\text{nm} = 10^{-9}\,\text{m} = 10\,\text{Å}$). Quantum size effects, confinement of charge carriers, size-dependence of nanoparticle electronic structure, effects due to the unique properties of surface atoms, and huge value of the surface-to-volume ratio are only some of the most frequently cited causes of the exotic behaviour of nanoparticles. As a consequence of their peculiar properties, the synthesis of nanoparticles has opened the door to the production of many technological and pharmacological products such as catalysts with high activity and specificity, materials for specialized optical applications, electrorheologic and electrochromic systems, superconductors, antiwear additives, enhanced adsorbents, drug-carriers, and specialized diagnostic tools.

From a different point of view, the control of matter at the nano-size level could permit the realization of miniaturized devices with specific functionalities like nano-carriers, sensors, nano-machines, and high density data storage cells. Moreover, given their intrinsic smallness, a huge number of nano-components could be rationally assembled to build very highly complex man-size machines.

Further, more sophisticated applications can be devised, looking at biological systems where out of equilibrium nanostructures direct the synthesis, blending, and assembling of a wide range of molecules, their auto-replication and inter-connection; affording in such way the existence and evolution of living beings and the expression of their astonishing capabilities. From this prospect, the production of "artificial" nanostructures far from chemical equilibrium and/or self-assembling and/or self-replicating could greatly amplify the actual potentialities of nanotechnologies allowing the realization of supra-nanodevices with high density of component elements and characterized by complex and interconnected functionalities.

It can be reasonably expected that the realization of nanotechnologic products and their introduction in the market will deeply affect the human quality of life, reducing drastically the waste of raw materials and energy and leading to a planetary revolution of social relations. Moreover, some of these products could enhance and amplify the actual capability of the scientific world to explore the universe and to investigate physico-chemical phenomena with fast computing machines and advanced research instruments.

Together with the benefits that can be expected by the development of nanotechnological products, it is helpful to consider also the potential risks for living beings, cultural heritages, and ecosystems arising from the introduction of nanotechnology in the environment. Being so small, nanoparticles can easily penetrate inside whatever system, while, being so reactive, they could trigger off very dangerous reactions. This implies that, together with the development of synthetic methods and applications of nanomaterials, investigations on their effects and the exploitation of suitable procedures for their safe manipulation must be carried out. From a more general point of view, it must be also stressed that nanotechnology has its inherent limits so that it will disappoint those who believe to have found the panacea to all the ills of our society.

Nanoscience is not a new discipline, but, rather, it can be viewed as a network of knowledge taken from some well-established sciences: physics, chemistry, biology, and engineering. Many of the theoretical foundations needed to build up nanoscience have been developed in the past so that most of the future work is the untrivial application of these principles aiming to the realization of a broad range of technological products.

Obviously, the first necessary step to develop novel nanotechnologies is the production of nanoparticles. A wide variety of physico-chemical phenomena have been used to set up an enormous number of efficient protocols to synthesize nanomaterials of technological and biotechnological interest.

These protocols can be distinguished according to the starting point of the synthetic route:

- From macroscopic bodies through their subsequent subdivision in ever smaller particles by the input of external energy (top-down methods). Typical top-down methods are the grinding of solids by ball milling or the high-temperature vaporization.
- From atomic and molecular precursors, through spontaneous chemical reaction and/or self-assembling processes (bottom-up methods). Examples are those based on the preparation of colloidal solutions and the use of mesoporous materials.

or to their capability to allow:

- the mere synthesis of nanoparticles
- the spatial control of nanoparticles to obtain a more or less ordered arrangement within a suitable matrix or upon a surface to obtain the so-called nanomaterials

or to the degree of matter dimensionality restriction reached:

- quasi-zero-dimensional particles (quantum dots)
- one-dimensional structures (quantum wires)
- two-dimensional structures (quantum wells)
- three-dimensional fractal-like structures

or to their ability to generate mixed nanoparticles formed by two or more components or nanoparticles with peculiar shape:

- core-shell nanoparticles
- doped nanoparticles
- sandwich nanoparticles
- hollow nanoparticles
- spherical, rod-like, and multifaceted nanoparticles

or to the physicochemical phenomenon employed to stabilize nanoparticles against their spontaneous unlimited growth:

- charging of nanoparticles
- coating of nanoparticles with anisotropic molecules
- spatial segregation of nanoparticles on solid surfaces or embedded into appropriate supporting matrixes

These distinctions also delineate the questions that should be posed in order to plan the better synthetic method suitable for a given nanomaterial and its specific applications.

Because below specific critical threshold values, nanoparticle properties are generally strongly size and shape dependent, the judgement of the merit of each preparation methodology is related to its ability to finely control these structural parameters and the corresponding polydispersity degree. Moreover, taking into account that bare nanoparticles are thermodynamically unstable against an unlimited growth and very often display an enhanced chemical reactivity, every good synthetic protocol should allow not only reproducible size and shape control but also appropriate structural and chemical stability.

As a consideration of general validity, it is important to point out that there is not any best synthetic method for all nanomaterials and their specific applications, but each one can be efficient for some substances and unsuitable for others. This implies that the choice of the most convenient route for the synthesis of a specific nanomaterial requires the knowledge of the advantages and disadvantages of each synthetic strategy including its cheapness.

Here will be described one of the most powerful synthetic bottom-up methods based on the use of some surfactant-containing microheterogeneous systems (liquid crystals, monolayers and multilayers, solutions of direct and reversed micelles, direct and reversed vesicles, water-in-oil and oil-in-water microemulsions) as peculiar solvent and reaction media. Thanks to the nano-sized microheterogeneities characterizing the microstructure of these systems, appropriate species can be hosted in spatially separated domains that, as a consequence of specific diffusion processes, can come in contact and react, forming the precursors of the nanoparticles. The accumulation of these precursors in confined space leads to the formation of nanoparticles shaped by their boundaries, whereas their dispersion in the medium and surfactant adsorption on the nanoparticle surface could prevent nuclei agglomeration and precipitation, providing size and shape control. The advantages of such strategy are

- Nanoparticles synthesis can be performed at mild conditions implying a low cost technology and unnecessary expensive apparatus.
- The synthetic method can be easily scaled up for high-volume production of nanomaterials.
- Nanoparticles of a wide class of substances (metals, semiconductors, superconductors, magnetic materials, biomaterials, polymers, water soluble inorganic and organic compounds, etc.) can be produced.
- The synthesis can be easily modulated to obtain coated, doped, mixed, onion or hollow nanoparticles. This capability is of particular industrial importance because the physico-chemical properties of these nanoparticles are frequently found to be very different from those of the single components, showing significant changes in the electronic structure and enhanced catalytic activity.

- Good control of nanoparticle composition, size, shape, polydispersity, and stability of these parameters with time is generally achieved by appropriate selection of the experimental conditions.
- Specific physico-chemical properties can be conferred to nanoparticles by confinement and surface effects, and enhanced potentialities can be given by their random or ordered dispersion in microheterogeneous systems.
- By changing the nature and/or the composition of the microheterogeneous system, different local structures and dynamics can be achieved leading to the production of a great variety of nanomaterials.
- Microheterogeneous systems represent not only the media where nanoparticles can be synthesized but also can be considered suitable for their transport, preservation, and application. They possess also potentials to realize specialized out-of-equilibrium nanoparticle containing systems to model or minic biological processes.
- By simple evaporation of the volatile components of nanoparticle-containing surfactant solutions, it is possible to prepare mono-, bi-, and three-dimensional spatial configurations of nanoparticles in surfactant matrixes, the so-called nanoparticle/surfactant composites, showing very interesting collective properties. By changing the experimental conditions, nanoparticle size and internanoparticle distance can be easily regulated. It is worth noting that at present, the major efforts are directed to establish suitable techniques to assemble nanoparticles in 1D, 2D, and 3D architectures that have important applications in photonics, biotechnology, and microelectronics.
- Nanoparticle/surfactant composites can be easily manipulated, layered on suitable supports, transferred, and resuspended.
- Being some microheterogeneous systems composed of biocompatible, biodegradable, and/or ecocompatible substances, the nanoparticle synthesis in such media is particularly adapted to pollution-free productions. Moreover, interesting nanomaterials for pharmacological and environmental applications can be exploited
- Since microheterogeneous systems share many of the fundamental properties of biomembranes, nanoparticle synthesis in these environments allows a realistic simulation of important biological functions such as the formation and reconstruction of solid constituents of the human body.
- Considering the huge value of the numerical density of nanosized domains contained in microheterogeneous systems, in principle, a relevant number of identical nanoparticles can be synthesized and hosted in such systems. As a quantitative estimate, it can be easily calculated that, in a litre of a 0.1 mol dm^{-3} micellar solution of a typical surfactant having a head group area of 50 $Å^2$, about 10^{20} nearly identical nanoparticles with a size of 50 Å can be synthesized and hosted.

- From a theoretical point of view, the encapsulation of nanoparticles within the peculiar microheterogeneities characterizing surfactant-based systems gives the opportunity to investigate a wide spectrum of quite intriguing and unexplored phenomena such as reaction and crystallization in confined space, preferential adsorption of surfactant molecules on certain nanoparticle crystallographic facets, growth inhibition, and structural organization within self-assembled structures

In the past few decades, many investigations have been carried out with the aim to synthesize nanoparticles in microheterogeneous systems and to control their physico-chemical properties. All these studies have confirmed the great potentials and versatility of the inherent synthetic methods. Besides, starting from an initial tendency to use microheterogeneous systems for the mere control of the nanoparticle size, now it is increasingly becoming the tendency to realize specialized nanoparticle containing microheterogeneous systems with specific structural and dynamical peculiarities for technological or biological applications. A lot of supra-nanoparticular assemblies with peculiar architectures have been prepared to date.

Even if these studies have not produced a general theory enabling the selection a priori of the optimal conditions for the synthesis of nanoparticles of a given material with the wanted properties, nevertheless, some general criteria and pivotal external parameters governing their synthesis have been underlined. Here, an attempt to collect together theoretical and experimental results and to furnish a unified approach is addressed. However, given the huge amount of knowledge accumulated in this field, the account of the contributions of all the researchers working in this area is practically impossible due to time and space constraints of both the writer and the readers. For this reason, this book has been written with the intention to be suggestive more than comprehensive. From a different prospect, the strict content of this book is not the most important thing but rather the interaction between the mind and imagination of the readers with its physical content. I think and hope that, from some of these interactions, new discoveries and interesting interconnections will be triggered.

This book was intended to furnish a systematic but introductory-level treatment of the basic topics necessary to the neophytes for the preparation of nanomaterials through surfactant-based media. It should help them avoid the need to go into the jungle of the bibliographic world to achieve a panoramic view of this specific research field.

Because the correct use of microheterogeneous systems aiming at nanoparticle synthesis requires the knowledge of their structural and dynamical properties, an overview of these aspects will first be presented. Besides, it must be emphasized that a preliminary and unavoidable step of nanoparticle syntheses in these systems is the solubilization of appropriate precursors and reactants. For this reason, general information on the microscopic processes

governing the solubilization phenomenon and some guidelines for solute entrapment in such systems will also be given. Taking into account that reaction rates and mechanisms show distinctive features due to the peculiar structure of microheterogeneous systems, some information concerning these aspects, focused on reactive processes leading to nanoparticle formation, will be furnished. All these arguments will be treated in Chapter 1.

Other fundamental subjects are the thermodynamics and kinetics of the nanoparticle formation and growing processes in homogeneous and microheterogeneous systems together with the molecular phenomena responsible for the possible growth inhibition and nanoparticle stabilization. These arguments are helpful to understand the differences and analogies among the various strategies employed to control the nanoparticle size and to obtain stable nanomaterials. They are useful guidelines for nanoparticle synthesis. This matter will be considered in Chapter 2.

An overview of the peculiar properties of nanoparticles and nanomaterials will be considered in Chapter 3 not only to appreciate the potentialities of these systems but also because the knowledge of their exotic properties is also necessary to delineate a successful synthesis. In particular, quantum size and surface effects will be considered.

Finally, some specific recipes for nanoparticle synthesis will be presented in Chapter 4. The intention is to underline the wide variety of the methodologies employed to prepare nanomaterials by microheterogeneous systems that can be easily transposed for the synthesis of other nanomaterials. In particular, the recipe ensemble can also be taken as a container of microheterogeneous systems with well-known structural and dynamical properties. However, to save space, these recipes are not sufficiently detailed, and for the interested reader the direct reference to the reported bibliography is strongly suggested.

Palermo, Italy *Vincenzo Turco Liveri*

Contents

1

Structural and Dynamical Properties of Microheterogeneous Systems

1.1 Introduction

Excluding phenomena in which very high energies are involved, ordinary matter can be treated as an ensemble of a limited number of some invariant constituents: nuclei and electrons. These quantistic particles self-assemble according to their mysterious capability to interact with each other, thus forming a potentially infinite number of systems ranging from nanometric to macroscopic where with some approximations, the more or less invariant dynamic aggregates of these particles can be identified: atoms, molecules, and ionic species.

For many purposes, however, matter can be more plainly described as a collection of these aggregates. Even if this picture is basically incorrect and a holistic approach should be used, it must be stressed that a lot of macroscopic physico-chemical properties and phenomena can be foreseen and rationalized using this simplified model of reality. There is in fact a close relation between the properties of these quasi-invariant constituents and the laws of physics and chemistry governing the behaviour of macroscopic bodies. Another advantage is the possibility to represent the state of matter at a very fine dimensional scale. But, the most important aspect is that the setting up and the control of complex systems can be achieved only by a detailed knowledge of their structures and dynamics at the molecular level. This can be achieved by careful experiments, theoretical models, simulations, and ab initio or semi-empirical calculations.

According to this model, molecules are treated as hard objects having, in some cases, a well-defined size and shape. However, as a consequence of conformational and vibrational dynamics and intermolecular interactions, more generally molecular size and shape can vary significantly with time, temperature, pressure, system composition, and nature of surrounding molecules. This variability of the steric properties of molecules introduces some restrictions to the possibility to predict their structural arrangements in condensed phases using fixed geometric parameters.

It is worth emphasizing that molecular size and shape are a simplified expression of the force field created around them by the self-assembled nuclei and electrons forming the molecule. Then, the molecular conformational and

vibrational dynamics is the appearance of the internal movements caused by these forces and their continuous time variation. Moreover, the reciprocal action of these force fields between neighbouring molecules determines intermolecular interactions and the mutual structural and dynamical perturbations of molecules. Thus, molecular force fields and intermolecular interactions are inextricably entangled.

In this respect, the behaviour of ions, small molecules, and parts of large molecules is generally described in simplified manner by three electric properties arising from the spatial distribution and dynamics of nuclei and electrons: electric charge, dipole moment, and polarisability. Electric charge is due to the presence of an unequal number of protons and electrons, the dipole moment to an unsymmetrical distribution of electron density around nuclei, and the polarisability to the strength by which nuclei and electrons are bonded to each other. All species are polarisable while ions possess also a net charge and dipolar molecules also a dipole moment. However, the above reported considerations suggest that these properties are not fixed molecular peculiarities, depending more or less strongly on the instantaneous molecular state, nature of neighbouring molecules, and their relative positions.

An important consequence of the existence of a limited number of distinct building blocks of matter, the so-called "elementary" particles, is that all physico-chemical phenomena (mixing or separation of substances, phase transitions, chemical reactions, nuclear and particle transmutations, etc.) can be explained as a change of the spatial arrangement of the same particles. In particular, chemical properties of matter are connected with the ability of molecules to break and/or combine, forming different nuclei-electrons ensembles, whereas collective physical properties are mainly described in terms of their actual steric hindrance, dynamics, and ability to interact. Intermolecular interactions, in fact, triggered by the molecular size and shape as well as diffusive and conformational motions determine in condensed phases the formation of a hierarchy of transient structures of increasing size and extending along one or more dimensions. The configurational multiplicity of these structures increases steeply with size while the accessibility to each configuration is regulated by the ratio between its potential energy and kT. Depending on the nature of the system and the strength of intermolecular interactions, some of these structures are separated from neighbouring states by small activation energies and characterized by short lifetimes; others by large activation energies and long lifetimes.

The continuous development, refinement, and application of the relationship between macroscopic physical and chemical properties and molecular picture of every system can be considered one of the principal aims of physical chemistry. Obviously, within the constraints imposed by the uncertainty principle, the realization of a microscopic technique allowing the "direct" and contemporaneous observation of structural and dynamical properties of single molecules represents the dream of many physical chemists.

1.2 Microscopic Picture of Molecular Ensembles

The use of the molecular model of matter is of particularly great help to describe and to rationalize the structural and dynamic aspects of the peculiar self-assembling patterns shown by some amphiphilic molecules called surfactants in various experimental conditions. Then, the subsequent step is to rely on the macroscopic physico-chemical properties to the structural and dynamic properties of the specific aggregation pattern of these molecules. This micro-macro correlation is the key to achieve the rationale control of many physico-chemical phenomena.

1.2.1. Intermolecular Interactions

To rationalize the self-assembling of surfactant molecules in condensed fluid phases, it must be taken into account that molecules are in contact because attractive intermolecular interactions dominate the tendency of thermal agitation to spread molecules in the space but not so much to freeze their dynamics and thus inhibit conformational motions and diffusion. It must be also considered that some of these interactions are always attractive independently of the molecular orientations such as ion-induced dipole, dipole-induced dipole interactions, and dispersion forces. Dispersion forces, also called induced dipole–induced dipole interactions, arise from the correlated fluctuations of the electron density of neighbouring molecules determining on average instantaneous dipoles favourably oriented. The transition from uncorrelated to correlated fluctuations, occurring when two apolar molecules approach, corresponds to the building up of the dispersion force and the bond energy release to thermal motions. It must be stressed that, in general, if there are not efficient channels by which the energy arising from the establishment of the interaction can be dissipated, the probability of the elastic collision increases and that of the interaction set up decreases.

On the contrary, other interactions are attractive only when the involved species are favourably oriented such as ion-dipole and dipole-dipole forces becoming repulsive in the opposite orientations. Since attractive orientations are energetically favoured, after the establishment of the interaction, they occur more frequently than those repulsive and the resulting average force is attractive. Concerning the electrostatic ion-ion forces, the repulsive or attractive nature of their interactions is simply dictated by the sign of their charges. All these kinds of physical interactions show a smooth dependence on the relative intermolecular orientation and their strength decreases more or less fast with distance.

At short intermolecular distances, very strong repulsive forces arising from the inherent attempt to overlap double occupied orbitals occur. This is stated by the Pauli exclusion principle, which excludes the coexistence in the same orbital of two electrons with the same spin. Just these mysterious

forces make condensed matter able to sustain very high pressure with little volume change, avoiding its collapse to very small and dense objects.

In many textbooks, some equations based on elementary electrostatic principles are given to describe all these interactions. However, it must be stressed that they are obtained introducing some severe restrictions to their validity such as punctiform particles or intermolecular distance much greater than molecular size, two-body interactions, time averaged forces, and intermolecular interactions averaged on all the possible mutual orientations. Moreover, these equations are particularly unsuitable to describe structural and dynamical properties of ensembles of large and/or anisotropic molecules forming condensed phases.

Less severe restrictions can be posed by calculating the forces acting on a given molecule as the resultants of the forces exerted on each atom of that molecule by all the other atoms of the same molecule and of the surrounding molecules. This is the way followed in the molecular dynamics method allowing to simulate the motions of all molecules of the system. Such approach generally requires a lot of computer power, and its accuracy is determined by that of the relationships used to describe the interatomic potential energy. Then, the force is calculated by the derivative of the potential energy along the three spatial coordinates. Some typical expressions of interatomic potential energy (ε_p) are:

$$\varepsilon_p = \frac{B_{ij}}{r_{ij}^{12}} \text{(for short range repulsion)} \tag{1.1}$$

$$\varepsilon_p = -\frac{A_{ij}}{r_{ij}^{6}} \text{(for London attraction)} \tag{1.2}$$

$$\varepsilon_p = \frac{Cq_iq_j}{r_{ij}} \text{(for Coulomb interaction)} \tag{1.3}$$

where r_{ij} is the interatomic distance and the constants A_{ij} and B_{ij} depend on both atoms i and j.

In order to grasp similarities and differences among various molecular systems, it is useful to show some examples of the distance (d) dependence of the total potential energy (E_p) of two molecular species arising from the overall intermolecular interactions (Fig. 1.1). According to the above reported considerations, these plots should be considered a qualitative description of the potential energy changes occurring when a molecule is approached by another, maintaining their reciprocal orientation constant and changing the position of the surrounding molecules opportunely.

It can be noted the total repulsive case (A), that involving long range attractive and short range repulsive interactions (B), and those involving the existence of some repulsive/attractive regimes (C, D).

The behaviour of the above-mentioned physical interactions is in contrast with that typical of intermolecular chemical bonds such as hydrogen bonding and donor-acceptor bonds, which are generally characterized by a

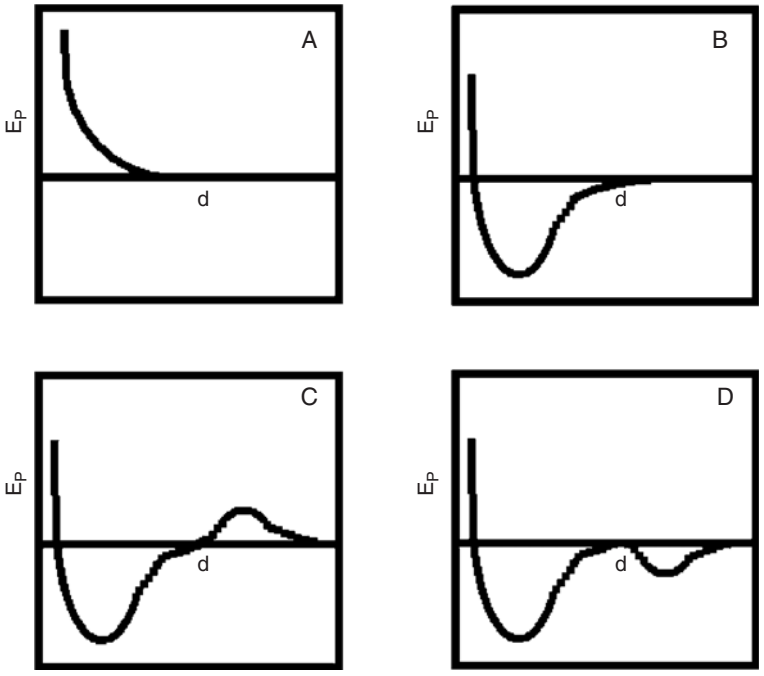

FIGURE 1.1. Various examples of the potential energy change occurring by approaching two molecules in condensed phase.

stronger strength and a marked dependence on the relative orientation and intermolecular distance. These interactions are exerted among contacting molecules, and the dependence of the potential energy from distance and relative orientation can be calculated by the molecular orbital method.

In conclusion, the complex and intricate action of all the interactions among molecules and their thermal agitation determine the structural and dynamic properties of the system as well as the molecular self-assembling. From all the above considerations, it can be easily inferred that it is a hard task to attempt to gain a quantitative prediction of the bulk properties of condensed matter.

1.2.2. Dynamical Picture of Molecular Ensembles

To predict the thermodynamic equilibrium condition of an ensemble of molecules at constant volume and temperature, two driving forces must be considered: energy and entropy. The first quantity tends to push the collection of molecules to the lowest energy configuration and the latter to the highest number of distinct microscopic states continuously explored by the system. At each macroscopic state corresponds, generally, an enormous number of microscopic ones consistent with the constraints operating on

the system and physical laws. Within the molecular model and the uncertainty principle, each microstate is characterized by the specific position and energy of every molecule of the system. In turn, the state of each molecule is defined by its librational, rotational (internal and as a whole), vibrational, and electronic states.

The mechanisms by which molecules change their energy are intermolecular collisions and the absorption and spontaneous or stimulated emission of photons. This involves that molecules coexist and are in dynamic equilibrium with a spectrum of photons continuously created and annihilated. Intermolecular collisions and absorption/emission of photons are also the mechanisms by which systems out of equilibrium reach the thermal, mechanical, composition, and chemical equilibrium through the superposition of several relaxation processes. However, it must be stressed that this is a simplified picture because it does not consider that the occurrence of intermolecular interactions prevents the assignment of well-defined energy packets to each molecule.

The ensemble of microscopic states can be represented in the configuration space by the potential energy of the N particles constituting the system as a function of their 3N spatial coordinates. The resulting hypersurface of each system is characterized by the density of minima and the depth of the potential energy barriers. Fragile systems display a density of minima larger than strong ones. It must be stressed that the specific topology of the hypersurface controls the system dynamics. The probability (p_i) and the time fraction (τ_i) that a system can be found in the generic microscopic state with total energy E_i is given by the equation

$$p_i = \tau_i = \frac{e^{-\frac{E_i}{kT}}}{\sum_i e^{-\frac{E_i}{kT}}} \qquad 1.4$$

where the summation is extended to all the distinct system microstates. This equation can be also applied to small pockets of molecules as well as to a single molecule or even to a specific freedom degree of the molecule. It says that p_i and τ_i decrease exponentially with the energy and that significant values of these quantities can be reached at E_i up to kT, i.e., at about $4\ 10^{-21}$ J at room temperature. On the other hand, the multiplicity or degeneracy of microscopic states generally increases steeply with E_i and the number of particles composing the system leading to a maximum of p_i and τ_i corresponding to the mean, i.e., thermodynamic, value of the system energy.

It is well-known that, at constant volume and temperature, the macroscopic state thermodynamically favoured is that characterized by the lowest Helmholtz free energy (A). This quantity is related to the possible E_i values of the system by the equation

$$A = -kT \ln \sum_i e^{-\frac{E_i}{kT}} \qquad 1.5$$

However, if the activation energy barrier associated with the transition to a specific microscopic state from neighbouring ones is greater than 5–10 kT, then that state is practically unreachable by spontaneous fluctuations.

The existence of large energetic barriers between microscopic states accounts for the formation of kinetically but not thermodynamically stable systems. This is a question frequently encountered in microheterogeneous systems making experimentally arduous the distinction between these two conditions. It occurs also frequently that, by the external input of energy (mechanical, electric, magnetic, etc.), some microheterogeneous systems can be trapped in a spectrum of microscopic states separated by large energetic barriers from those corresponding to the thermodynamic stable system. This leads to a quite surprising situation, i.e., the realization with the same substances in the identical experimental conditions (concentrations, temperature, etc.) of systems showing different macroscopic physico-chemical properties and different behavior. To describe this phenomenology, it is useful to build up ideally a multidimensional diagram where the free energy of each possible thermodynamic state of the system is reported as a function of the macroscopic variables characterizing the system. Looking to the topology of the resulting hypersurface, it can be observed the presence of hills, mountains, and valleys as well as local minima and only one absolute minimum. One of the points of the hypersurface represents the initial state of the system: the possibility to reach the thermodynamic stable state (the absolute minimum) depends on the existence of a path joining both states along which by spontaneous thermal fluctuations the system can walk.

At the molecular level, the interplay of energy and entropy leads to an endless dynamics among all the accessible microscopic states characterizing the life of macroscopic systems in thermodynamic equilibrium. Microscopic states can be ideally grouped according to their energy (degenerate or quasi-degenerate states) or their close similarity in the spatial arrangements of molecules (degenerate or quasi-degenerate snapshots). Within characteristic system-dependent timescales, the molecular dynamics determines the formation and the breakage of transient supramolecular structures that can be identified as short-living building blocks of the macroscopic system.

In the case of microheterogeneous systems, it will be found that the constant peculiarity of the supramolecular structures is the coexistence of two nanosize polar and apolar pseudophases separated by an huge interface and characterized by local orientational order at short times and fluidity at long times. It can be easily understood that these properties are essential for building up molecular machines with complex functionalities such as self-organization, self-replication and recognition. In fact, the same features can be observed in the most complex biological systems of which they are the "artificial" counterpart. It is quite astonishing to be aware that the wide variety of supramolecular structures observed in microheterogeneous systems is the expression of a simple structural property of the molecules invariably present within such systems, i.e., surfactant molecules.

1.3 Surfactants and Surfactant Molecule Self-Assembly

Some examples of typical surfactant molecules together with their structures are shown in Table 1.1. It can be noted that surfactant molecules are characterized by molecular anisometry, i.e. elongated shape, wide spectrum of molecular conformations, and the coexistence of spatially separated hydrophobic (only polarizable) and hydrophilic (both polar/ionic and polarizable) moieties. The hydrophobic part is constituted by one or more long

TABLE 1.1. Structure of some typical surfactant molecules

1. Cationic surfactants Hexadecyltrimethylammonium chloride, CTAC $CH_3(CH_2)_{15}N^+(CH_3)_3Cl^-$	
2. Anionic surfactants Sodium dodecyl sulfate, SDS $CH_3(CH_2)_{11}OSO_3^- Na^+$	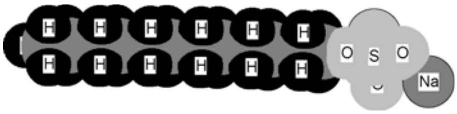
Sodium bis(2-ethylhexyl) solfosuccinate, AOT $CH_3(CH_2)_3CH(C_2H_5)CH_2COOCH_2CHSO_3Na$ | $CH_3(CH_2)_3CH(C_2H_5)CH_2OCO$	
3. Zwitterionic surfactants Lecithin $CH_3(CH_2)_{14}COOCH_2$ | $CH_3(CH_2)_7CH{=}CH(CH_2)_7COOCH{-}CH_2PO_4^-(CH_2)_2N^+(CH_3)_3$	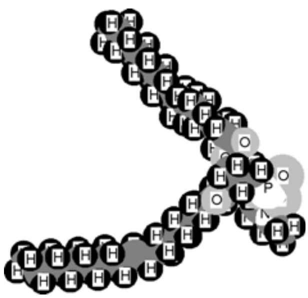
4. Nonionic surfactants Triton X-100 $(CH_3)_3C{-}CH_2{-}C(CH_3)_2{-}C_6H_4{-}(O{-}CH_2{-}CH_2)_{10}OH$	

and flexible hydrocarbon or fluorocarbon chains, whereas the hydrophilic one is generally concentrated in a smaller domain of the entire molecule and is formed by a polar or ionic head group. Depending on the nature of the head group attached to the alkyl chains, surfactants are distinguished as non-ionic (polar), ionic (cationic or anionic), and zwitterionic (carrying both positive and negative charged groups). In the case of anionic surfactants, the presence of some metal ions as counterions could provide additional features such as color, magnetism, and catalytic capability.

In order to confer specific properties and to extend their widespread applications, in the past few decades chemists have synthesized a lot of new surfactant molecules by inserting functionalised head groups or by changing intentionally the architecture of the apolar part. As examples of bio-functionalised surfactants, it can be mentioned the hexadecylphosphoryl adenosine and the hexadecylphosphoryl uridine[1].

Recent developments in the synthesis of surfactants have led to novel classes such as polymerizable, polymeric, gemini, glycolipidic, dendritic, bolaform, and multifunctional surfactants, or according to their potential applications as hydrophilic, lipophilic, photosensitive, degradable, biocompatible, and ecocompatible surfactants. The structural features of some of these surfactants are shown in Fig. 1.2.

Most probably, the oldest class of surfactants is constituted by the alkali salts of long-chain fatty acids. Other well-known surfactants are the alkylarylsulfonates, phosphoric acid esters, and polyoxyethylene alcohols.

Gemini surfactants are characterized by two amphiphilic moieties linked by a spacer. Many different compounds of this kind can be synthesized by changing

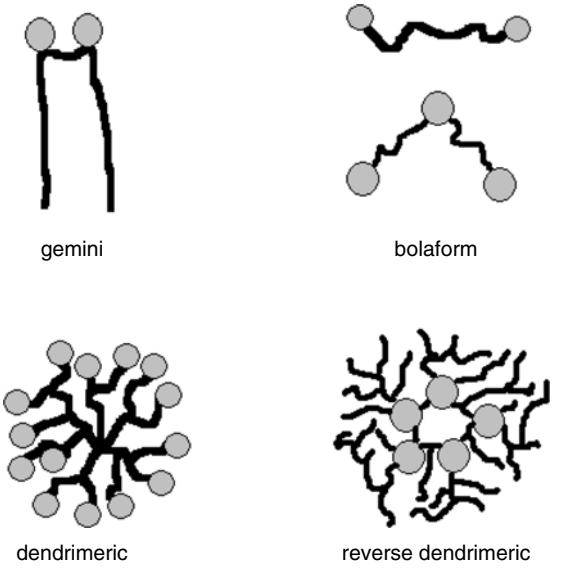

FIGURE 1.2. Structural features of some novel classes of surfactants.

the length of the alkyl chains and of the spacer as well as the nature of the two hydrophilic groups. Gemini surfactants show marked effect on the water surface tension, low cmc, and Krafft temperature. Moreover, their structure and high molecular weight confer to these substances low skin penetration.

Bolaform amphiphiles are characterized by the presence of two polar head groups at the ends of one or two hydrophobic chains. This peculiar molecular architecture confers to bolaform surfactants specific self-assembling properties[2].

A large variety of amphiphilic triblock copolymers, composed by a hydrophobic poly(oxypropylene) middle block and two hydrophilic poly(ethylene) end blocks, are commercially available. These surfactants, called polaxamers or pluronics, are characterized by their molecular weight and the ratio between the hydrophilic and hydrophobic parts.

1.3.1. Surfactant Packing Parameters

Several attempts to correlate the surfactant self-assembling properties with the structure of their molecules have been tried. In particular as a first order approximation, it has been emphasized the role played by the size and shape of the head group and hydrophobic chain[3,4]. It has been suggested that the quantity determining the preferred supramolecular structure is the critical packing parameter (CPP) defined as

$$\mathrm{CPP} = \frac{\mathrm{v}}{\mathrm{a_0 l_c}} \tag{1.6}$$

where v is the volume of the surfactant alkyl chain, a_0 is the head group area, and l_c the length of the fully extended chain. In the case of mixed surfactant aggregates formed by component 1 and 2, the working equation becomes

$$\mathrm{CPP} = \frac{\mathrm{v_1 X_1 + v_2 X_2}}{(\mathrm{a_1 X_1 + a_2 X_2})\mathrm{l_c}} \tag{1.7}$$

where X indicates the mole fraction of each surfactant in the mixed aggregate and l_c is the length of the longest chain.

Based on geometric considerations, it has been stated that, if CPP$<$1/3, the surfactant is well-suited to form structures where the hydrophobic chain point toward the interior and the hydrophilic head group protrudes toward the exterior, i.e., spherical direct micelles. If CPP occurs between 1/3 and 1/2, the preferred structures are the direct hexagonal phases and cylindrical direct micelles. If CPP occurs between 1/2 and 1, then the preferred structures are lamellar phases, bilayers, direct vesicles, and oil-in-water microemulsions. Finally if CPP is greater than 1, reversed hexagonal phases, reversed micelles, reversed vesicles, and water-in-oil microemulsions should result.

As an alternative analysis of the geometric surfactant properties, looking at the molecular structure of surfactants, it can be noted that they can be approximated as a frustum characterized by a set of four distinct param-

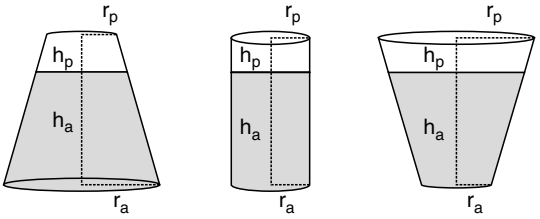

FIGURE 1.3. Schematic representation of surfactant molecules with various packing parameters (white, polar part; grey, apolar part).

eters: the radii r_p and r_a and the heights h_p and h_a, where p and a refer to the polar and apolar moiety (see Fig. 1.3).

It can be noted that as limiting cases, the frustum could become a cone (r_p or $r_a = 0$) or a cylinder ($r_p = r_a$). Remembering that in condensed phases molecules are in contact and, as a consequence of intermolecular interactions, surfactants self-assemble head-to-head and tail-to-tail giving compact supramolecular structures, it can be foreseen the effect of geometrical parameters on the natural radius of curvature of surfactant aggregates and consequently on their aggregational patterns[5].

In particular, considering the ratio r_p/r_a, the preferred structure can easily be predicted: if $r_p/r_a > 1$, direct hexagonal phases, spherical and cylindrical micelles and o/w microemulsions; if $r_p/r_a \approx 1$, lamellar phases, bilayers and vesicles; if $r_p/r_a < 1$, reversed hexagonal phases, reversed micelles and w/o microemulsions. It must be also noted that both $r_p/r_a < 1$ and $r_p/r_a > 1$ conditions emphasize a tendency to a spontaneous curvature of the interface formed by surfactant molecules.

On the other hand, the h_a value can be taken as a rough measure of the hydrophobicity/hydrophilicity of the surfactant: small h_a values indicate high solubility in water and poor solubility in apolar solvents, intermediate h_a values high solubility in apolar solvents and poor solubility in water, large h_a values scarce solubility both in hydrophilic and hydrophobic media. Moreover, $2(h_a + h_p)$ can be taken as a rough estimate of the cross-section diameter of direct and reversed micelles or the thickness of surfactant bilayers and vesicles. It is worth to note that, depending on the various r_p/r_a ratios, there is a general symmetry between the supramolecular aggregates characterizing microheterogeneous systems: direct and reversed hexagonal phases, direct micelles/reversed micelles, direct vesicles/reversed vesicles, water in oil and oil in water microemulsions.

Another frequently used parameter related to the surfactant self-assembling peculiarities and based on experimental measurements is the ability to interact with aqueous and apolar media. This property is described by the hydrophile-lipophile balance (HLB), and it is dependent on the strength of the surfactant/water and surfactant/apolar media interactions. The HLB property allows to distinguish surfactants as hydrophilic (high solubility in

water, strong tendency to form micelles), lipophilic (preferentially soluble in apolar solvents, strong tendency to form reversed micelles), amphiphilic (soluble both in water and apolar solvents), and amphiphobic (scarcely soluble in polar and apolar media, strong tendency to form direct and reversed vesicles). Further aspects arising from geometrical properties and intermolecular interactions will be described in more detail when each kind of surfactant self-assembling pattern is considered.

More generally, it can be said that critically depending on their molecular peculiarities (shape and size of apolar and polar parts, molecular flexibility, anisometry of structure, anisotropic interactions hydrogen bonding capability), and the experimental conditions, surfactants can realize spontaneously a wide variety of structurally different systems: liquid crystals, mono- and multilayers, solutions of direct and reversed micelles, water-in-oil and oil-in-water microemulsions, and direct and reversed vesicles. The interconversion of one of such structures into the others is also in principle possible by changing some external parameters, and this greatly amplifies the freedom degrees of their applications. This interconvertibility arises because very often the difference in energy among the various aggregation patterns are small so that thermal

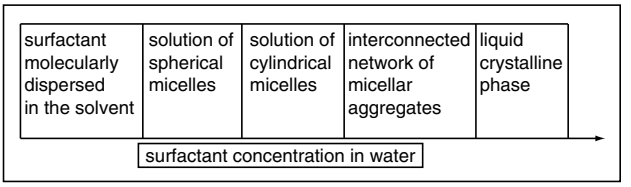

SCHEME 1.1. Typical qualitative composition dependence of the various structural patterns formed by hydrophilic surfactants in water.

fluctuations could induce marked local changes of the surfactant self-assembling while modest changes of temperature and/or composition could determine structural transitions. As an example, Scheme 1.1 shows qualitatively the various structures and transitions that occur by changing the composition of water/surfactant systems.

Structural changes are often revealed by sudden changes in some physical properties such as viscosity, conductivity, permittivity, solubilization capability, and scattering patterns.

1.3.2. Nonspontaneous Aggregation Patterns of Surfactant Containing Systems

In addition to the thermodynamically stable surfactant aggregates above cited that form spontaneously by mixing the system components, other nonspontaneous kinetically stable structures can be obtained by suitable techniques such as shear, ultrasonication, microwave irradiation, application of high electric fields, and mechanical manipulation of surfactant systems. An inter-

esting example of the last methodology is the micro-manipulation of surfactant aggregates to produce nanofluidic devices constituted by lipidic nanotubes (radius 50–150 nm) connected on both sides with unilamellar lipid vesicles (size 5–25 μm). These nanofluidic systems could allow controlled transport as well as detection of single nanoparticles[6,7].

It is also possible, starting from lamellar phases and by applying shear in controlled conditions, to obtain surfactant reorganization into a new phase constituted by multilamellar vesicles (200–1000 nm), called onions or spherulites[8].

Other thermodynamically unstable systems that could show long-term kinetic stability are emulsions and multiple emulsions. These systems can be prepared by many mechanical methods and show a wide variety of local transient structures. In particular, multiple emulsions are characterized by small droplets of phase A confined in larger droplets of phase B, which in turn are dispersed in a continuous phase A. Depending on the nature of phase A, they can be distinguished as water/oil/water or oil/water/oil emulsions[9].

Further nonspontaneous or kinetically too-slow-forming aggregates are obtained by ultrasound. Ultrasonic irradiation is widely employed because it allows, through the introduction of mechanical energy in the system, to significantly increase solubilization rates and to induce some physical and chemical effects due to acoustic cavitation. Ultrasound is also an effective tool to induce emulsification and vesicle formation.

A percolation transition accompanied by an increase of the viscosity can be induced in w/o microemulsions by applying high electrical fields[10,11]. The effects of an electric field on the structure of lecithin organogels composed by water, cyclohexane, and lecithin have been also investigated. It has been observed by oscillatory rheology that the electric field triggers off an extended fusion of rod-like lecithin reversed micelles[12].

1.3.3. General Correlation between Supramolecular Structure and Solubilization Properties of Microheterogeneous Systems

The most frequent use of microheterogeneous systems is as peculiar solvent and reaction media. Additional applications are as specialized carriers, stabilizers, and nanocontainers of solubilizates. Solubilization and enhancement of chemical reactions have been exploited in a wide range of applications (detergency, drug carrier, tertiary oil recovery, micellar catalysis, stereoselective synthesis, pseudo-homogeneous reactions, etc.) but, in the present context, both processes are of utmost importance because they are the fundamental steps by which the in situ nanoparticle synthesis is carried out. In particular, the knowledge of the location of appropriate species and of their diffusional dynamics and the rationalization of confinement, interfacial, catalytic, and template effects on their reactivity are pivotal to direct consciously the synthesis of nanoparticles. Fortunately, many of these features can be grasped, at least qualitatively, using some elementary principles.

As previously stated, all the more or less transient structures formed by surfactants are invariably characterized by the coexistence of nano-size hydrophilic and hydrophobic domains separated by a very large interface. These nanodomains are distinguished by different local physico-chemical properties (polarity, ionic strength, viscosity, orientational order, lifetime, etc.). In particular, the coexistence of polar and apolar regions confers to microheterogeneous systems the ability to solubilize even contemporaneously a wide class of ionic, polar, apolar, and amphiphilic substances, locating them in the various domains characterizing their microscopic structure and according to the solubilizate-domain affinity. In particular, ionic and polar substances are located in the hydrophilic regions, apolar compounds in the hydrophobic ones, while amphiphilic substances are partitioned between these regions and most often preferentially located at the interface between hydrophilic and hydrophobic domains. This selectivity on the location of solubilizate molecules entails:

- inhomogeneous distribution at small spatial scale and local solubilizate concentration different from the overall[13]
- confinement effects such as low translational diffusion coefficients and enhancement of correlation times of the solute molecules
- significant change of the intrinsic reactivity of the solubilized species[14]
- re-organization of finite amounts of solute in nanoscopic domains leading to the formation of ordered arrangements such as zero- or bi-dimensional molecular clusters[15]
- the coexistence of ionic, polar, apolar, and amphiphilic molecules located in different but close domains could allow frequent encounters and interesting chemical reactions
- structural and dynamical properties of the solubilizate as well as that of the hosting domain can be modified. The changes of the hosting medium depend on the nature of the system and are more marked at high solubilizate concentration and/or when its molecular size is large[16].
- the contemporaneous or sequential solubilization of finite amounts of appropriately chosen molecules in confined space could allow realization of highly complex and intriguing supramolecular structures

Because of these features, in complex fluids like microheterogeneous systems, all physico-chemical properties such as surface tension, vapour pressure, viscosity, activity, solubility, dissociation constants, reaction equilibria, oxydo-reduction potentials, reaction mechanisms and rates, nucleation and growing processes, stability of reactants, products, and intermediates can be significantly altered with respect to that found in homogeneous systems[17]. This means that the use of the physico-chemical properties determined in homogeneous systems could lead to large errors and wrong expectations. Generally, these changes can be invariably reconducted to intermolecular interaction, local composition, compartmentalization, and interfacial effects.

Experimental and theoretical investigations on reaction rates and mechanisms in restricted geometries have shown large deviations compared to

that in bulk systems. Some of these deviations can be attributed to the inherent large fluctuations in the number of reagent species when they are confined in nanoscopic space[18].

In the field of chemical kinetics, a well-known application of the peculiar properties of microheterogeneous systems is micellar catalysis[19]. It is also worth noting that many biological reactions occurring in nature are directed by organized media such as photosynthesis.

In microheterogeneous systems characterized by low viscosity, the solubilization process can be achieved by simply contacting the solubilizate with the micellar solution and improved by manual or mechanical stirring. However, for very viscous media, the complete solubilization could become a time consuming process. In this case, it could require recourse to some tricks such as increase of the temperature, ultrasonication, milling, or solubilization in the less viscous micellar solutions and then composition change by evaporation of the volatile components. On the other hand, reaction rates are generally performed by mixing two or more microheterogeneous systems, each containing one of the various reactants. In the case of microheterogeneous systems whose structure is sensitive to mechanical or electrical stresses or of reactions controlled by diffusion, significant effects on the reaction rates and mechanisms can be expected by applying stirring or electric fields.

Given the importance of the structure and dynamics of the various microheterogeneous systems to control nanoparticle size, shape, and stability through the peculiarity of the solubilization of appropriate species, of the reaction between these species to synthesize the nanoparticle precursors, and of the precursor aggregation to form the nanoparticles, in the following, these subjects will be treated considering separately each kind of system to take into account their specific behaviour.

1.4 Pure Surfactants and Liquid Crystals

From a molecular point of view, pure surfactants self-assemble forming a more or less ordered array of opportunely oriented molecules. In general, the peculiar aggregation state of surfactants as pure components is dictated by the two different parts that ideally constitute the surfactant molecule: the head and the tail. The number of possible conformations of surfactant head (H) and tail (T), their respective steric hindrances, and the nature and strength of their mutual attractive/repulsive interactions are the most important aspects that must be considered. Intra and intermolecular steric hindrances are an evidence of the short-range repulsive forces arising from the attempt to overlap double occupied orbitals increasing steeply with decreasing distance. On the other hand, intra and intermolecular attractive interactions arise invariably from all the electric forces among nuclei and electrons of atoms of the same molecule or of neighbouring molecules.

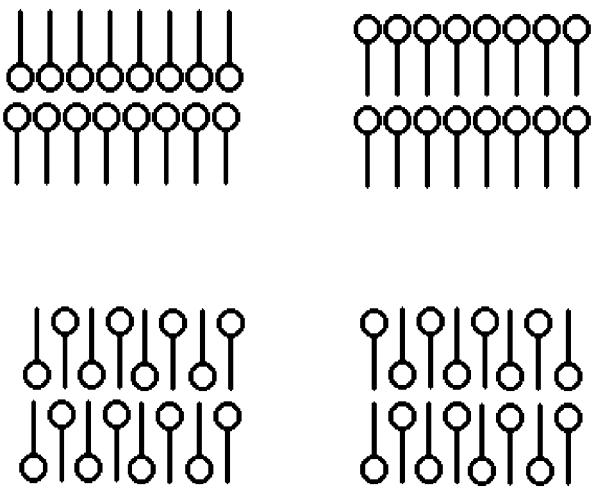

FIGURE 1.4. Some arrangements of surfactant molecules in the plane (O, head; ——, tail).

Taking into account the specific nature of surfactant heads and tails, the H-H interactions can be attributed to ion/ion, ion/(induced) dipole, (induced) dipole/(induced) dipole interactions, hydrogen bonding and other specific chemical bonds, the T-T interactions only to induced dipole/induced dipole forces and H-T interactions to ion/induced dipole and (induced) dipole/induced dipole forces. Summing up all these contributions, a pivotal role can be assigned to the value of the strength (S) of H-H, T-T, H-T interactions and on their dependence on distance and reciprocal orientation. Some possible bidimensional arrangements of surfactant molecules are shown in Fig. 1.4.

As the most frequent behaviour, it is found that, in the pure state, surfactant molecules display a marked tendency to self-assemble arranged so that one molecule is close to the other and placed head-to-head and tail-to-tail. The relation among S values leading to this typical surfactant self-assembling is $S_{H\text{-}H} \gg S_{H\text{-}T}$ and/or $S_{T\text{-}T} \gg S_{H\text{-}T}$. Alternatively, some surfactants show interdigitated and monolayer structural elements[20,21].

It is worth noting that the S values do not control only the surfactant aggregation state at room temperature (solid or liquid crystal) and its self-assembling but also determine the existence of energetic barriers that modulated the thermally activated diffusional, conformational, and flip-flop dynamics. These processes can be described in the liquid crystalline phases as concerted and collective jumps of surfactant molecules among favourable orientations and conformations. Given the long-range order along certain directions, the diffusional coefficient of surfactant molecules in liquid crystals is characterized by marked anisotropy. Moreover, the difference among S values causes different conformational mobility and disorder of tails and chains.

From a molecular point of view, surfactants in the solid or liquid crystalline state can be distinguished in terms of positional and orientational order. In the solid state, surfactant molecules possess positional and orientational order, whereas as liquid crystals the positional order is lost although a consistent part of the orientational order is maintained. Moreover, the ordering characterizing surfactant structures suggests that generally there is an unfavourable conformational contribution to the entropy of the system that can tend to shift the system toward less ordered arrangements. This tendency can be enhanced by increasing the temperature. As a consequence, it can be expected that the structural disorder of surfactants in equilibrium state increases with temperature. In addition, structural disorder can be introduced in the system through the input of mechanical energy (agitation) while the application of static and variable electric fields could influence not only structure but also the dynamics.

A schematic representation of some typical thermodynamically stable structures arising from self-assembled surfactant molecules in the pure state is shown in Fig. 1.5.

In the figure is emphasized the role played by size and shape of surfactant head group and hydrophobic moiety in determining the overall supramolecular structure. It is worth to say again, however, that size and shape of surfactant hydrophilic and hydrophobic parts are not fixed molecular properties because they can be critically influenced by some external parameters such as temperature, pressure, presence and concentration of other species.

Techniques well suited to investigate the structure of liquid crystals are the low-angle X-ray diffraction and polarizing microscopy[22,23]. In the lamellar

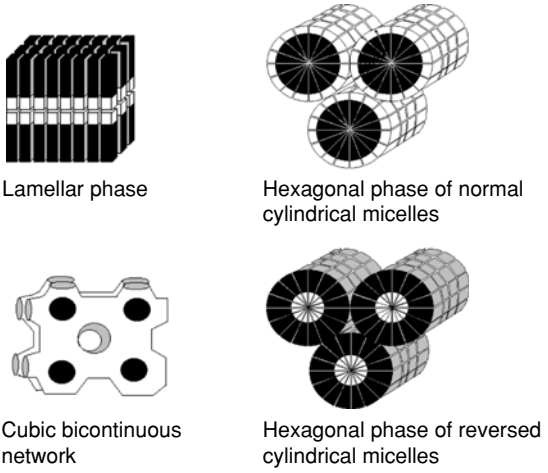

FIGURE 1.5. Some of the most frequent liquid crystalline structures shown by pure surfactants (in black the hydrohobic part, in white the hydrophilic moiety of the surfactant molecule).

phase, the bidimensional structural element composed by parallel oriented surfactant molecules virtually extends without limits along the plane, whereas it is limited with respect to the molecular dimension perpendicularly to the plane. The superposition of many of such structural elements leads to macroscopic lamellar phases. Inverting the spatial orientation of all the surfactant molecules along the principal axis the same structure is obtained: the lamellar phase is the symmetric counterpart of itself. A lamellar phase is expected when $r_p \approx r_a$ and it is generally shown by single-chain surfactants. It is characterized by X-ray diffraction peaks corresponding to interplanar distances in the ratio: 1:1/2:1/3:1/4. An example of a non-ionic surfactant forming at room temperature a lamellar phase is tetraethylene glycol monododecyl ether[24].

Direct and reversed hexagonal phases are characterized by close-packed supramolecular rods of infinite length. Such phases are expected for surfactants having $r_p > r_a$ and $r_p < r_a$, respectively. It can be noted the existence of "infinitely" extended uni-dimensional domains embedded in a three-dimensional one. Besides, by inverting the spatial orientation of all the surfactant molecules along their principal axis, the hexagonal phases transform from direct to reversed and vice versa. They are characterized by X-ray diffraction peaks corresponding to interplanar distances in the ratio: $1:1/\sqrt{3}:1/2$. For example, AOT in the pure state forms a reversed hexagonal phase[25].

From the broadening of the most intense peak observed in the diffractograms, information on the average domain size (d) of the liquid crystals can be achieved by the Debye-Scherrer equation

$$d = \frac{K\lambda}{B\cos\theta} \qquad 1.8$$

Where λ is the X-ray wavelength, B is the full width at half height of the peak (in radians) corrected for instrumental broadening, θ is the Bragg angle, and K is a factor, approximately equal to unity, related to the domain shape[26].

Finally, a cubic phase is composed of spherical aggregates formed by oriented surfactant molecules arranged in a cubic lattice. Depending on the surfactant orientation, such phases are expected for surfactants having $r_p > r_a$ or $r_p < r_a$. It can be noted the existence of zero-dimensional domains forming a quite ordered network embedded in a three-dimensional one. An interesting liquid crystal showing the bicontinuous cubic phase structure which, due to its biocompatibility, can be used as a vehicle for hydrophobic and/or hydrophilic drugs is glycerol monooleate.

It has been observed that the layers at the liquid crystal surface show smaller lattice constants, meaning higher packing density, as compared to those in the bulk liquid crystal. The thickness of this surfacial domain is quite extended (about 300 nm)[28].

In addition to single phase domains, many surfactants show polymorphism, i.e., the coexistence of different structural arrangements. This condition can be observed in both thermodynamically stable states (equilibrium polymorphs) and kinetically stable ones (metastable polymorphs)[29].

As previously stated, by increasing temperature, an increasing disorder and fluidity characterize these systems, and some structural transitions could take place before an isotropic phase is formed or the decomposition of surfactant molecule occurs. The temperature dependence of the phase behaviour is called thermotropism, whereas lyotropism is that determined by solvent addition.

By changing the pressure, phase changes can be also induced. Generally, the effects arising from a pressure increase are opposite to that due to an increase of the temperature; however these effects become significant when the pressure is increased considerably.

Phase transitions must be viewed not only as changes in the spatial arrangement of surfactant molecules but also as the result of the activation/deactivation of one or more molecular freedom degrees. For example, melting can be described as the significant activation of the hopping mechanism, allowing the surfactant molecule diffusion and the loss of the positional order.

1.4.1. Solubilization in Surfactant Liquid Crystals

Of utmost importance for our purpose is that the peculiar pure surfactant self-assembling ability leads to the formation of a spatially ordered arrangement of long living polar and apolar microdomains where solute molecules or small particles can be selectively hosted. The apolar region is generally characterized by relatively high alkyl chain mobility and consequently it can be considered a liquid-like domain disposed to accommodate hydrophobic species. This is experimentally put into evidence by the lack of the typical sharp peak at about $2\Theta = 19$ degrees in the X-ray diffractograms of surfactant liquid crystals, which is instead observed in the case of hydrocarbon chains in the crystalline state and, obviously, by the possibility to solubilize large amounts of many apolar species.

However, many experimental evidences suggest that the chain mobility in liquid crystalline phases is more restricted than that in micellar solutions. For this reason, in the pure state and at room temperature, surfactant liquid crystals appear as highly viscous liquids or waxy solids with anisotropic physico-chemical properties. This involves that the attainment of the thermodynamic equilibrium state as well as the solubilization of selected species and their diffusion in the surfactant structure are generally a slow and time-consuming process. In order to circumvent this drawback, solubilization of appropriate species can be performed in surfactant solutions with low viscosity and then the homogeneous solubilizate/surfactant composite could be obtained by solvent evaporation under vacuum[30].

This procedure cannot be applied always. In fact, it must be taken into account that the progressive evaporation of volatile components of the surfactant solutions involves a progressive increase of surfactant concentration and consequently the formation of viscous phases so that some intermediate structures could be frozen due to the reduced diffusion rate, which could inhibit the formation of the thermodynamically stable phase. Other procedures take advantage of the separation of a liquid crystalline phase

produced by an intentional composition or temperature change of low-viscous water/surfactant/additive systems[31].

Looking at Fig. 1.5 and considering the simple and very old rule "similis similia solvuntur" (like dissolves like), the preferential solubilization site of single quite small polar, apolar, and amphiphilic solubilizate molecules in the various liquid crystal structures can be easily predicted. As a specific example, Fig.1.6 shows their solubilization sites in the hexagonal phase of cylindrical reversed micelles.

It must be emphasized that confinement of finite amounts of selected small-size polar substances in reversed hexagonal phases could lead to the formation of zero- and unidimensional aggregates entrapped within the hydrophilic domain, whereas their solubilization in lamellar phases to zero-, uni-, and bidimensional aggregates. As an example, solubilization of urea in the typical two-dimensional reversed hexagonal structure of AOT liquid crystals leads to the formation of uni-dimensional urea nanoparticles trapped in the hydrophilic core of the AOT rods[15,32]. Such nanoparticles can be viewed as interesting confined reactants for specialized solid-solid chemical reactions involving locally a limited number of molecules.

Similar considerations can be made for hydrophobic substances solubilized in direct hexagonal or lamellar phases. Simple geometric considerations generally allow to evaluate the effects of solute entrapment on the size of the hosting domains[33].

On the other hand, solubilization of amphiphilic substances could lead to an ordered array of their molecules at the hydrophilic/hydrophobic interface. In the case of large molecules such as polymers, more complex situations

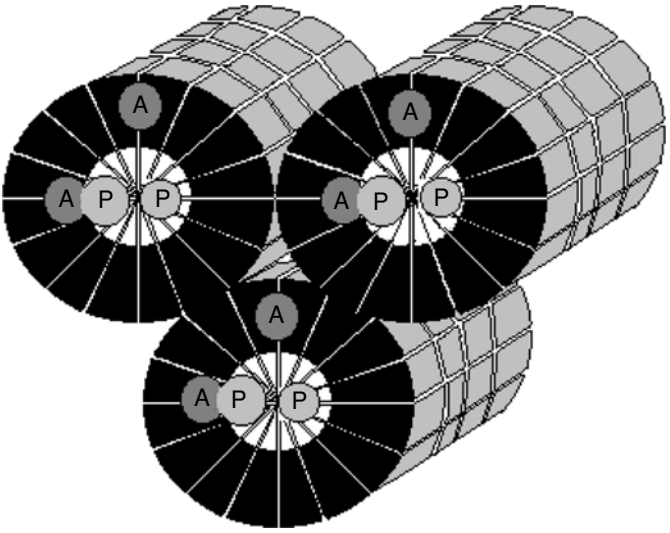

FIGURE 1.6. Solubilization sites of apolar (A), amphiphilic (AP), and polar (P) substances in the hexagonal phase of cylindrical reversed micelles.

can be determined depending on their structural properties. Accordingly, long chains can form random coils confined within a specific domain or random wires connecting and extending across many domains.

Moreover, the long-range order existing in surfactant liquid crystals makes these systems particularly interesting as nanoparticle hosts because they could allow a long-range spatially ordered distribution of nanoparticles embedded in the surfactant matrix. Taking into account that the typical length scale of hydrophobic and hydrophilic domains characterizing liquid crystals comprises in the range 1–50 nm, nucleation restricted by the boundaries of these domains is expected to lead to nanoparticles of comparable size.

Depending on the molecular volume and the amount of solubilizate confined in each domain, the surfactant structure and more generally its phase behavior can be more or less influenced. As an example, it has been reported that the addition of finite amount hexachloroplatinic acid to oligoethylene oxide/water systems strongly influences the temperature and composition ranges where the various liquid crystalline phases are stable[34]. Phase transitions have been also observed when a fluorocarbon oil (perfluorodecalin) is solubilized in a non-ionic fluorinated surfactant/water system[35].

Of particular importance are the effects arising when water is added to pure surfactants. Considering the addition of water to direct hexagonal phases, a localization of water molecules among the surfactant rods leading to a progressive increase of the distance among the rods and their breaking in shorter pieces can be expected. This ideal dilution process should allow to find a connection between hexagonal phases and rod-like micellar solutions, and, at greater dilution, to solutions of small spherical micelles. On the other hand, the progressive addition of an apolar solvent to a reversed hexagonal phase should produce an analogous phenomenon leading to solutions of rod-like reversed micelles and finally of spherical reversed micelles dispersed in an apolar medium.

It is also interesting to consider the evolution of the lamellar phase by adding water or an apolar solvent. The initial addition of water involves an increase of the interlamellar distance, being water localized in the hydrophilic domain. As the width of this domain increases, it becomes more and more easy to break the "infinite" layers in smaller ones as a consequence of the thermally activated undulation motions. But these smaller pieces are less energetically stable than closed layers, i.e., direct vesicles. Analogously, the addition of an apolar solvent should bring the system to the formation of dispersions of reversed vesicles. The phase behaviour of surfactants as a function of solvent addition is called lyotropism.

The addition of water could also affect the surfactant packing parameters leading to phase transition. As an example, by adding water to phytantriol, a surfactant frequently employed as a cosmetic additive, reversed micellar, lamellar and cubic phases were observed[36].

A more complex phase behavior can be observed in systems composed by three or more components. Depending on the composition range, the

ternary system formed by water, 1-decanol, and sodium octanoate shows hexagonal, lamellar, and reversed hexagonal phases as well as isotropic micellar solutions[37]. At high surfactant concentration, the system composed by a novel Gemini surfactant (disodium 2,3-didodecyl-1,2,3,4-butanetetracarboxylate), decane, and water forms hexagonal, cubic, and rectangular-ribbon phases[38].

Till now it has been delineated what happens when polar, apolar, and amphiphilic substances are added to a liquid crystalline phase forming monophasic systems. However, it must be stressed that the free energy minimum of a system could also correspond to two or more macroscopically separated or interpenetrated and coexisting phases. This means that at some composition thresholds, the system is saturated and further solubilizate addition leads to the appearance of a new phase. Both structural features and number of equilibrium phases are embodied in the system phase diagram. In the ambit of microheterogeneous systems, this field has been widely investigated for decades, and many phase diagrams are reported in the literature.

More generally, a flight inside the multidimensional phase diagram of a system where all the external parameters have been reported (pressure, temperature, composition) should allow to move through the various surfactant aggregation states. To evaluate the number of external parameters, it must be remembered that for a system in thermodynamic equilibrium constituted by C components and F phases, the total number of variables is $(C\text{-}1)F + 2$ and, considering that the maximum number of phases that can coexist in thermodynamic equilibrium is $F_{max} = C + 2$, the corresponding number of external parameters (NP) necessary to describe the system is $NP = C(C + 1)$.

1.5 Mono- and Multilayers

When very small amounts of surfactants are added to water, as a consequence of their amphiphilic nature, some molecules are located as monomers at the water/air interface with the hydrophilic group dipped in the aqueous phase and the coiled alkyl chain laying flat on the surface. These molecules are in dynamic equilibrium with those dissolved monomerically in the bulk medium. This equilibrium can be treated as a partitioning between surface and bulk domains according to the Nernst distribution law

$$K_N = \frac{a_S}{a_B} \qquad 1.9$$

where K_N is the thermodynamic distribution constant, a_S and a_B the surfactant activity in the surface and bulk domains, respectively.

The surfactant partitioning corresponds to a minimum of the free energy of the system and is dictated by a delicate equilibrium between water/surfactant head group and water/surfactant alkyl chain interactions as well

as by entropic contributions. It is of interest the preferential coiled conformation of the alkyl chains emphasizing the existence of attractive interactions (dipole-induced dipole and dispersion forces) both intramolecular and with water molecules. By progressively increasing the overall surfactant concentration, also the concentration at the surface increases and, as a consequence of its tendency to cooperatively self-assemble and above specific concentration threshold, surfactant molecules form at the surface small aggregates called hemimicelles or admicelles in dynamic equilibrium with surfacial monomers and bulk species. At sufficiently high surfactant concentration, the surface is saturated, and a monolayer (Langmuir monolayer) of oriented molecules covering completely all the water surface is formed (see Fig. 1.7).

At the surface, it can be noted the existence of two domains with different local properties; the quite anhydrous surfactant alkyl chain region and the hydrated surfactant hydrophilic head group one. The boundaries and thickness of both domains are not well-defined due to local thermal fluctuations arising from the frequent intermolecular collisions with species coming from the gas phase and the aqueous solution leading to fast molecular and collective dynamics. An additional contribution to the molecular disorder of the surfactant monolayer can be introduced externally by mechanical stirring and ultrasound irradiation. It follows that the order degree of the monolayer can be increased by decreasing the temperature and avoiding any form of disturbance of the system surface. Moreover, both domains are characterized by a composition different from that in the bulk, varying with the depth and

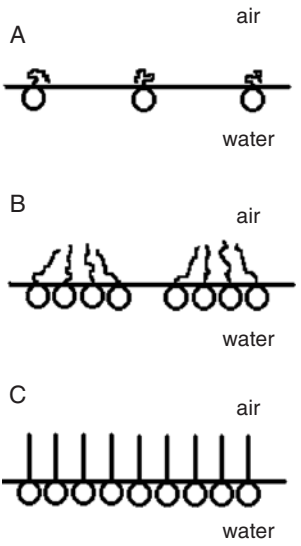

FIGURE 1.7. Surfactant monomers (A), hemimicelles (B), and oriented monolayer of surfactant molecules (C) at air/water interface.

showing ordering and marked directionality. It is of interest to consider the connection between these structural peculiarities and the specific behavior of surfactant monolayers as specialized solvent and reaction media.

In the case of ionic surfactants, dissociation leads to the partial release of counterions with the formation of a charged surface and an oppositely charged diffuse electric layer extending in the subphase (see Fig. 1.8).

As a first order approximation, the dependence of the electric potential (V) on the distance (x) from the surface can be described by

$$V = V_0 e^{-\frac{x-\delta}{x_0}} \tag{1.10}$$

where δ is roughly the distance of closest approach of the surfactant counterions to the surfactant head groups, V_0 the potential at $x = \delta$, and x_0 the Debye length corresponding approximately to the double layer thickness. This last term is correlated to the ionic strength (I, $I = \frac{1}{2}\sum c_i z_i^2$) and the dielectric constant (ε) of the medium by the equation

$$x_0 = \sqrt{\frac{\varepsilon kT}{8\pi e^2 I}} \tag{1.11}$$

where e is the electronic charge. It can be noted that the double layer thickness increases with the temperature and decreases with the ionic concentration. In water, typical x_0 values are in the 0.1–10 nm range. On the other hand, V_0 can be evaluated by

$$V_0 = \frac{\sigma x_0}{\varepsilon} \tag{1.12}$$

where σ is the surface charge density; which can be estimated by the surfactant dissociation degree and concentration at the surface. Then, the ionic concentrations (c_+ and c_-) at a point near the surface where the electric potential is V can be calculated by the equations

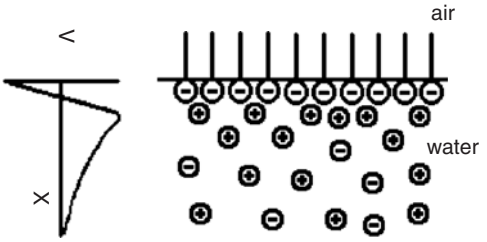

FIGURE 1.8. Stern model of the electric double layer originated by an oriented monolayer of anionic surfactant molecules at air/water interface.

$$c_+ = c_0 e^{-\frac{z_+ eV}{kT}} \quad c_- = c_0 e^{\frac{z_- eV}{kT}} \tag{1.13}$$

where z_+ and z_- are the the ionic valence and c_0 the bulk concentration.

It is worth noting that even in the case of non-ionic surfactant dissolved in solutions of electrolytes, a charged surface can be formed as a consequence of preferential ionic adsorption at the surfactant hydrophilic head group layer. Moreover, additional properties can be conferred to monolayers by the specific nature of the surfactant molecules like coordination and inclusion capability or hydrogen bonding. All the above underlined features of surfactant monolayers at water/air interface make them wzell-suited to drive many interesting phenomena such as nucleation and oriented crystallization[39].

Macroscopically, the progressive increase of the surfactant concentration at the water surface is accompanied by a parallel marked decrease of the surface tension of the system. This peculiarity is at the basis of the employment of surfactants as wetting and detergent agents. From the concentration dependence of the surface tension (γ), the surface excess concentration (Γ_2) of the surfactant in dilute solutions can be evaluated by the equation

$$\Gamma_2 = -\frac{1}{RT}\frac{d\gamma}{d\ln c} \tag{1.14}$$

Obviously, many other physico-chemical properties as well as phenomena dependent on the structural and dynamical properties of the surface are affected by surfactant addition to aqueous solutions.

In addition to the direct solubilization of surfactants in water, monolayers can be prepared by laying drops of an appropriate surfactant/apolar organic solvent system on the water surface and waiting for solvent evaporation. This procedure is suggested in the case of surfactants showing scarce solubility in water and/or low solubilization rate. In order to speed up the process, organic solvents with low boiling point are preferred. Moreover, complete spreading of the organic solution on water can be achieved only when the spreading coefficient $S_{o/w}$ is positive; otherwise, it will form a lens on water. It must be reminded that the spreading coefficient $S_{b/a}$ for liquid b on liquid a is defined as

$$S_{a/b} = \gamma_a - \gamma_b - \gamma_{ab} \tag{1.15}$$

where γ_a and γ_b are the surface tensions of liquid a and b, respectively; and γ_{ab} is the interfacial tension between the two liquids.

Another interesting experimental condition is represented by the surfactant arrangement at an oil-water interface. In this case, surfactant molecules are oriented perpendicularly to the interface with the hydrophilic head dipped in the water phase and the tail fully extended in the oil phase even at small interfacial surfactant concentration, i.e., as monomers. By increasing the surfactant concentration, the number of amphiphilic molecules

randomly located at the interface increases until a compact monolayer is formed. This because in addition to water/surfactant and surfactant/surfactant interactions, also oil/surfactant ones contribute to the interface structure (see Fig.1.9). Concerning the electric double layer, the interfacial tension and surfactant excess concentration at the interface, many of the above reported considerations on monolayers at air/water interface can be applied also to the oil/water one.

Obviously, the formation of an oriented monolayer occurs in many other conditions, i.e., whenever surfactant molecules find interfaces. An interface, in fact, implies the existence of two contacting media with different composition and properties and consequently different affinity for hydrophilic and hydrophobic groups. Investigations on the state of surfactant molecules adsorbed on interfaces have emphasized that their arrangement depends on the surfactant concentration and the nature of the interface (gas-liquid, gas-solid, liquid-liquid, liquid-solid, and solid-solid). When solid surfaces are involved, adsorption is also influenced by crystal planes, surface heterogeneities, and roughness.

The peculiar self-assembling of surfactants at interfaces can be directed to form a wide variety of two-dimensional organized bi- and multilayers called Langmuir-Blodgett (LB) layers. These films can be liquid-like or solid-like depending on the surfactant molecular properties as well as on substrate nature, temperature, and surface pressure, i.e., the difference between the surface tension of the pure liquid and that of the film-covered surface. Most frequently, the transfer of these monolayers from water to selected solid substrate is simply performed by dipping it in the aqueous solution (see Fig.1.10).

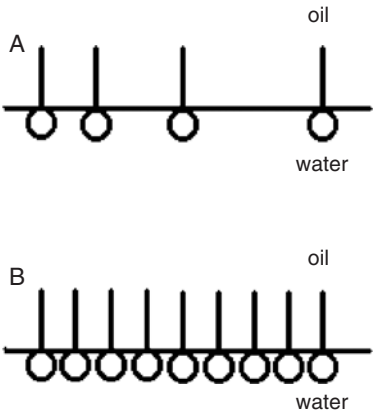

FIGURE 1.9. Random distribution of surfactant monomers (A) and oriented monolayer of surfactant molecules (B) at oil/water interface.

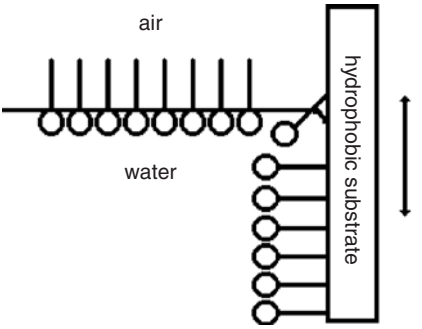

FIGURE 1.10. Transfer of an oriented monolayer of surfactant molecules on a hydrophobic surface.

During the transfer process, the surface pressure is maintained constant by reducing progressively the monolayer area to compensate for the surfactant molecules adsorbed to the substrate. LB films constituted by n layers are obtained by repeating this procedure n times. Depending on the specific interactions between substrate surface and surfactant molecules, different self-assembled multilayers can be obtained (see Fig. 1.11).

Other two-dimensional structures can be obtained by interposing surfactant layers between hydrophilic/hydrophilic, hydrophilic/hydrophobic, and hydrophobic/hydrophobic substrate walls (see Fig. 1.12).

Of particular importance is the arrangement of surfactant monolayers on metal surfaces. Investigations on this subject find interesting applications in several fields such as detergency, lubrication, corrosion inhibition, and nanoparticle synthesis. In general, the physical or chemical adsorption of surfactant molecules at the metal surface and the binding strength can be controlled by selecting the surfactant head group and the nature of the surrounding medium.

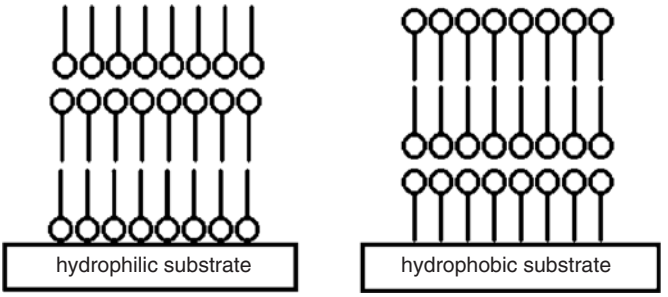

FIGURE 1.11. Self-assembled multilayers of surfactant molecules on hydrophilic or hydrophobic substrates.

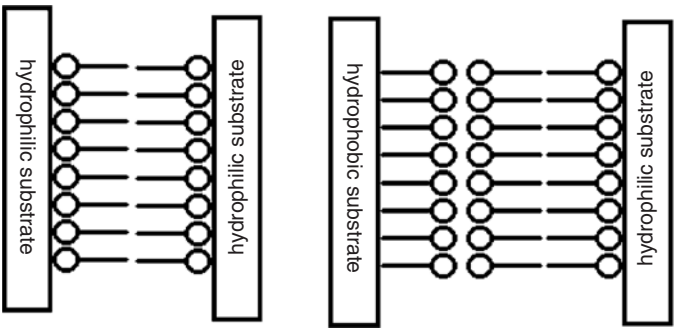

FIGURE 1.12. Self-assembled multilayers of surfactant molecules between two substrate walls.

Recent studies have shown that the surfactant self-assembling and orientation on metal surfaces can also be controlled by applying an electric potential. In particular, it has been observed by in situ scanning tunnelling microscopy that, at 0.5 V, a gold electrode immersed in an aqueous solution of sodium dodecylsulphate (SDS) is coated by hemimicelles and that the surfactant molecules are oriented so that their hydrophilic groups protrude toward the aqueous solution. However, by increasing the potential to 1V, the structure on the surface is significantly changed and the SDS molecules are arranged forming a compact and uniform bilayer. Finally, by restoring the initial potential, SDS molecules are pushed away from the surface. The absence of a reversible behaviour was attributed to an irreversible structural change of the Au surface[40].

Monolayers and multilayers can host solubilizate molecules according to their structural properties. In particular, the solubilization of finite amount of water (or oil) leads to the formation of an aqueous (or apolar) domain interposed between surfactant layers (see Fig. 1.13).

These domains in turn can host hydrophilic (or hydrophobic) species or can be the place where specialized chemical reactions could happen. In this contest, of particular interest are the reactions leading to the formation of nanoparticles or ultra-thin layers of specific materials interposed between surfactant sheets and deposited on suitable substrates. Generally, reactants in molecular form come from the two contacting phases and are directed towards the surfactant n-layers by spontaneous diffusion.

An alternative route consists in a preliminary nanoparticle synthesis in a suitable medium followed by their addressing to the surfactant n-layers. Also in this case the entrapment of nanoparticles is controlled by the general trend imposing the segregation in hydrophobic or hydrophilic domains according to their nature (see Fig. 1.14).

Surfactant-coated nanoparticles can be firmly adsorbed on solid supports by modifying opportunely the support surface (see Fig. 1.15).

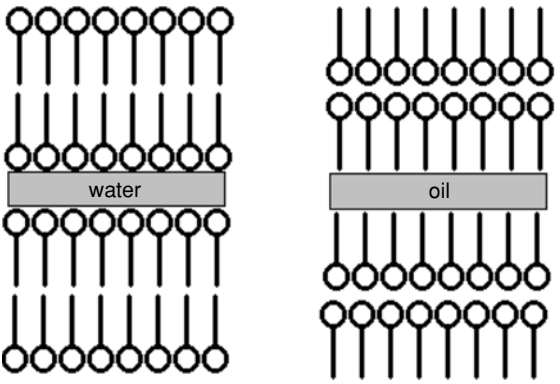

FIGURE 1.13. Water or oil containing multilayers of surfactant molecules.

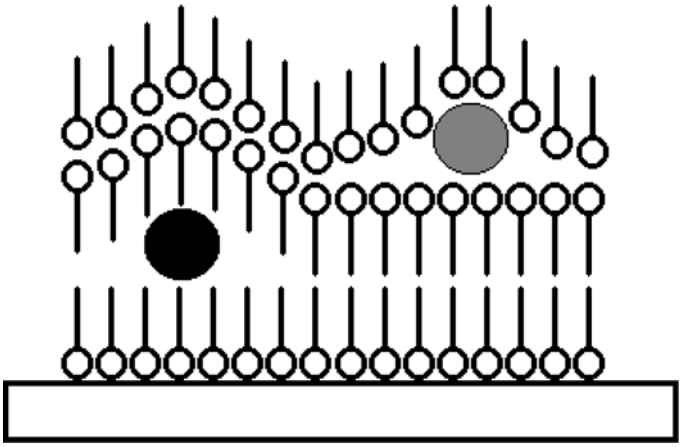

FIGURE 1.14. Entrapment of nanoparticles according to their hydrophilic or hydrophobic nature.

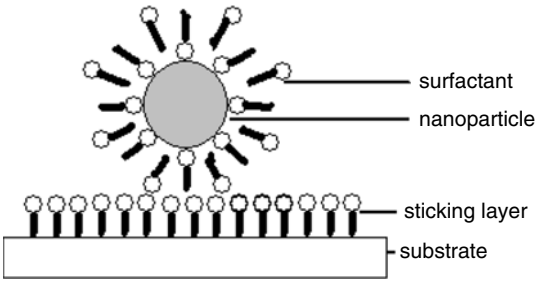

FIGURE 1.15. Binding of surfactant-coated nanoparticles to appropriately modified support.

1.6 Surfactant Aggregates in Liquid Media

A wide spectrum of very interesting supramolecular living aggregates can be formed by dissolving surfactants in strongly polar or totally apolar solvents in the dilute and semidilute regimes. These aggregates are generally distinguished as direct/normal micelles or, simply, micelles, mixed micelles (bicelles), reversed micelles, and vesicles both direct and reversed. Other interesting more complex supramolecular aggregates are obtained by adding appropriate additives to binary surfactant/solvent solutions leading to water in oil and oil in water microemulsions. All these systems are very often characterized by low viscosity, i.e., high molecular diffusion coefficients, allowing many useful technological applications as peculiar solvent or reaction media.

1.6.1. Surfactant/Surfactant Interactions in Liquid Media

When surfactant molecules are dissolved in liquid media in addition to the surfactant head-head (H-H), tail-tail (T-T), and head-tail (H-T) interactions, also the solvent/solvent (S-S), solvent/head group (S-H), and the solvent/tail (S-T) interactions must be considered to rationalize the surfactant state in solution and its self-assembling. The tangled interplay of these interactions could lead to a very small solubility of the surfactant in some solvent media due to H-H and/or T-T interactions overwhelming S-H and/or S-T interactions or to the formation of a rich variety of different supramolecular aggregates in dynamic equilibrium with monomers due to the predominance of S-S and S-H or H-H interactions. Moreover, in the frequent presence of additional components, the number of possible interactions increases steeply making even more complex the theoretical treatment of these systems but at the same time opening the door to a wider spectrum of accessible structures and dynamics. Generally, all these interactions are physical and not chemical, implying low energy barriers stabilizing the aggregates and consequently high fluidity and penetrability joined with short mean lifetimes of each surfactant molecule in the aggregates and of the entire aggregate. This also implies that polar and apolar regions in surfactant aggregates are not so strongly separated as is often shown in many schematic representations to stress their structural peculiarity.

The possible aggregates can be distinguished in terms of their size (in the range of about 2–100 nm), shape (spherical, ellipsoidal, cylindrical, disk-like, worm-like), aggregation number (in the range of about 20–10,000) as well as their dynamic properties. Making some rough approximations, in such class of surfactant aggregates are included direct micelles, reversed micelles, oil-in-water and water-in-oil microemulsions, direct vesicles, and reversed vesicles.

For a well-suited surfactant/solvent system, it generally occurs that, above a threshold concentration (the so-called critical micellar concentration, cmc),

i.e., when the concentration-dependent favourable entropic contribution arising from the surfactant dispersion as monomers in the solvent decreases so that further increase of their concentration is not possible, solubilization of additional amounts of surfactant is achieved by a system-specific self-assembling of surfactant molecules. Experimentally, the crossing over of the cmc is often emphasized by an abrupt change of the colligative properties, i.e., properties dependent upon the number density of particles in the solvent medium, with the surfactant concentration. This behavior can be explained, at least qualitatively, assuming that, below the cmc, the number density of particles (N_p) changes with the surfactant concentration (c) according to

$$N_p = N_{Av}c \tag{1.16}$$

whereas above the cmc as

$$N_p = N_{Av}cmc + \frac{N_{Av}(c - cmc)}{N_{agg}} \tag{1.17}$$

where N_{Av} is the Avogadro's number and N_{agg} is the mean number of surfactant molecules forming the aggregate (aggregation number). It can be noted that above the cmc, being N_{agg} of the order 20–10,000, the number of particles increases with surfactant concentration with a much lower rate.

The system-specific surfactant self-assembling in liquid media is controlled not only by the structural peculiarity of its molecules but also by many external parameters such as concentration, nature of the solvent, presence of additives, temperature, and pressure. This means that by changing these parameters, marked structural changes could be observed and that the molecular picture of the system can be stated only after the values of these parameters have been specified together with the kind of molecular species of which the system is composed.

From a thermodynamic point of view, it should be recognized that steric and entropic factors tend to auto-limit the aggregation process. In fact, surfactant self-assembling involves a decrease of the configurational contribution to the entropy due to the non-random spatial distribution of surfactant molecules. Other entropic contributions arise from the partial loss of molecular translational and rotational degree of freedom. These entropic terms could be counteracted by other entropic factors coming from hydrophobic interaction, hydrogen bonding, molecular dissociation, change of (internal) rotational and conformational degree of freedom, and of the associated enthalpic effects. Generally, from direct calorimetric measurements or temperature dependence of the cmc, it results that the aggregational process is accompanied by small values of enthalpy of formation of the aggregate lying in the range $-10/+10$ kJ/mol (of surfactant molecules)[41,42].

1.6.1.1. Surfactant Aggregation Models in Liquid Media

Among the models used to describe the surfactant aggregation process, i.e., the transition from the monomeric state to the monomers/aggregates equilibrium, the most simple is the pseudo-phase transition model, which describes the phenomenon as a solubility equilibrium. Below the solubility limit (the cmc), surfactant molecules are dispersed monomerically in the bulk medium. Above the solubility limit, the micellar pseudo-phase dispersed in the bulk medium is in equilibrium with surfactant monomers dissolved in the solvent at a concentration equal to the cmc. In such condition, the monomer concentration ([m]) in the bulk phase is related to the chemical potential of monomers in standard state, μ_m^*, and to the surfactant molecules in the micellar pseudo-phase, μ_M, by the equation

$$\ln [\mathrm{m}]\gamma_{\mathrm{m}} = -\frac{\mu_m^*}{RT} + \frac{\mu_M}{RT} \tag{1.18}$$

where γ_m is the activity coefficient of monomers. This equation shows the thermodynamic factors influencing the cmc and suggests why the addition of solutes could affect this value by changing γ_m and/or μ_M. On the other hand, the temperature dependence of the monomer concentration can be obtained by

$$\frac{\partial \ln [\mathrm{m}]\gamma_{\mathrm{m}}}{\partial T} = \frac{\Delta H_M}{RT^2} \tag{1.19}$$

where ΔH_M is the molar enthalpy of micellization.

The pseudo-phase model can be usefully applied for systems characterized by small cmc values and consequently by abrupt transition from surfactant molecules monomerically solubilized to the monomers/aggregates equilibrium. However, the pseudo-transition model does not allow to gain information on the surfactant mean aggregation number as well as on aggregate polydispersity and structural parameters.

More realistic and omni-comprehensive is the model based on the law of mass action. According to this model, association of surfactant S is described by multi-steps equilibria

$$\begin{aligned} \mathrm{S} + \mathrm{S} &\leftrightarrows \mathrm{S}_2 && \mathrm{K}_1 \\ \mathrm{S}_2 + \mathrm{S} &\leftrightarrows \mathrm{S}_3 && \mathrm{K}_2 \\ &\cdots\cdots\cdots\cdots \\ \mathrm{S}_{n-1} + \mathrm{S} &\leftrightarrows \mathrm{S}_n && \mathrm{K}_n \end{aligned}$$

where each equilibrium is characterized by a specific thermodynamic constant ($\mathrm{K_i}$) linked to the activity (a) of the involved species by

$$K_i = \frac{a_{S_i}}{a_{S_{i-1}} a_S} \tag{1.20}$$

In principle, this model allows to foresee the polydispersion phenomenon, the mean aggregation number, and the relationship between the concentration of the various aggregates including that of monomers with the overall surfactant concentration. Moreover, the effects of temperature and pressure changes can be predicted by standard thermodynamic equations. Also the influence of additive addition can be accounted by considering the involved changes of the activities of Eq. 1.20. However, its application to a specific system requires a preliminary knowledge of the thermodynamic equilibrium constants and activity coefficients of each species. These quantities can be achieved by making reasonable hypothesis on the aggregation process or by the analysis of suitable experimental data. On the other hand, this model cannot furnish direct indication on size and shape of the various populations of surfactant aggregates, which can be achieved by suitable theoretical models and experimentally by scattering measurements (light scattering, SAXS, SANS, etc.). Other basic information that cannot be obtained by the mass action model is the detailed description of aggregate dynamics.

Given their peculiar closed structure, aggregation of surfactants can be generally described by a cooperative association below a critical aggregation number and an anticooperative association above this value. However, depending on the cooperativity degree connected with surfactant association, surfactants can be classified into two main groups. The first, characterized by a low cooperativity of the intermolecular interactions, low mean aggregation number, and high polydispersity, is well described by many monomer/n-mer equilibria, whereas the second, characterized by high cooperativity, high aggregation number, and low polydispersity, is well described by a single or a limited number of monomer/n-mer equilibria. The aggregation number (N) dependence of the mole fraction $[X_N]$ of aggregates for a noncooperative system (A) and another one (B) characterized by strong cooperativity is shown in Fig. 1.16.

1.6.1.2. Clustering of Surfactant Aggregates and Interaggregate Interactions

In sufficiently dilute solutions, surfactant aggregates are generally nearly spherical and randomly dispersed in the bulk solvent medium. By increasing the surfactant concentration, two main effects can be predicted: i) an increase of the aggregate size and of the aggregation number and ii) the establishment of attractive or repulsive interactions among aggregates influencing their mean distance and spatial distribution. In the case of ionic surfactants, it has been suggested that a pivotal role in the establishment of interaggregate interactions is played by micellar charge and surfactant ion hopping among contacting aggregates[43]. For non-ionic or zwitterionic surfactants, important contributions to interaggregate attractions can be due to hydrogen bonding[44].

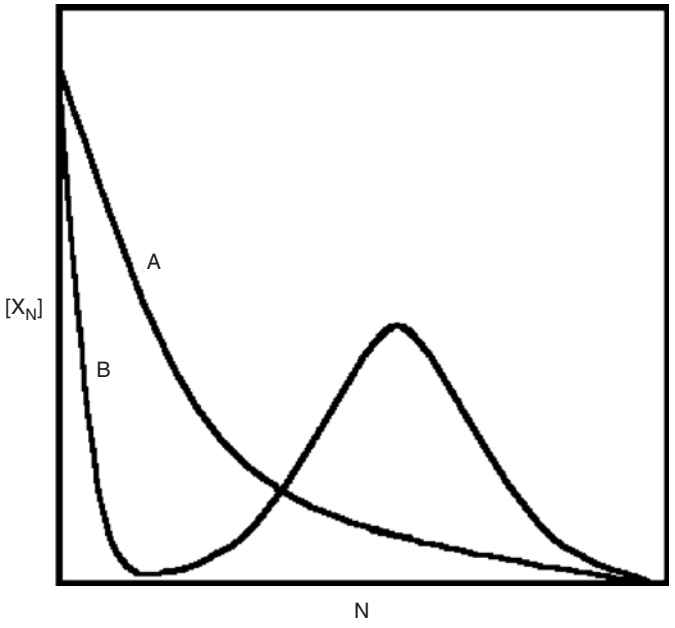

FIGURE 1.16. Aggregate concentration as a function of the aggregation number for noncooperative and cooperative systems.

The formation of interaggregate adhesion or the temporary fusion due to interaggregate attractions leads to more or less extended dynamic aggregate clusters and, above system-specific critical parameters (temperature, surfactant concentration), to an infinite aggregate cluster extending along all the system; this phenomenon is called percolation[45–47]. The extended interaggregate connectivity could also occur for simple topological reasons[16,48].

A schematic representation of different distribution of aggregates (random, attractive, and repulsive) is shown in Fig. 1.17, while percolated system for topological reasons (A) or as a consequence of attractive intermicellar interactions (B) is shown in Fig.1.18.

Depending on the nature of the system, the interconnection between surfactant aggregates can be better described as contacting aggregates or fused aggregates. Fusion leads to cylindrical aggregates with increased aggregation number. However, from a dynamic point of view, this difference cannot be clearly established because both contacting and fused aggregates coexist in the same system resulting from the continuous fusion/fission processes so that the most important point that needs to be established is the time fraction that an aggregate passes as isolated, contacting, and fused.

The formation of infinitely extended clusters has a marked effect on the system physico-chemical properties of the system. A dramatic increase of some properties such as viscosity, conductance, and permittivity are generally

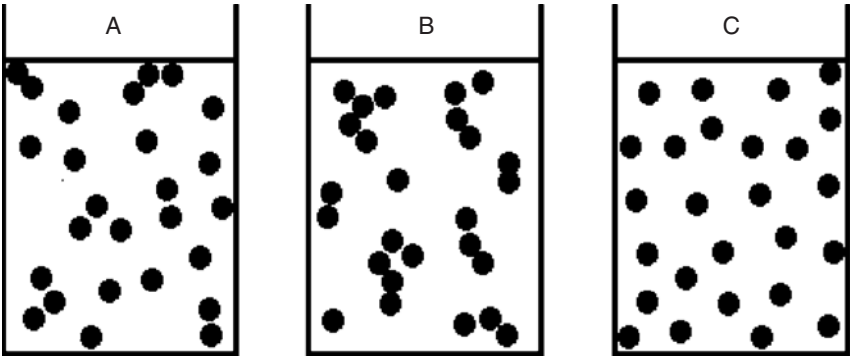

FIGURE 1.17. Random (A), attractive (B), and repulsive (C) distribution models of surfactant aggregates.

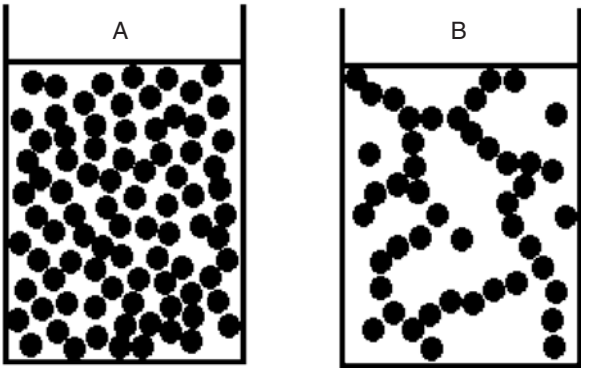

FIGURE 1.18. Microscopic structure of percolated systems due to topological (A) reasons or intermicellar attractive interactions (B).

a clue of the formation of extended clusters of aggregates. Percolation is also at the basis of the formation of gel-like systems[49,50].

1.6.1.3. Dynamical Properties of Surfactant Aggregates in Liquid Media

The frequent breaking and reforming of the labile intermolecular interactions stabilizing the surfactant aggregates, the diffusion of surfactant molecules in the bulk medium and within the aggregate, and the diffusion of the entire aggregates maintain in thermodynamic equilibrium a more or less wide spectrum of aggregate populations. Diffusion rates depend on the aggregate size and can be varied by changing the temperature or the nature of the solvent, i.e., the thermal agitation and the viscosity of the bulk medium. It can be hardly overemphasized the role of these processes because they are at the basis of the mechanism by which equilibrium concentrations of all the aggregate

populations are reached and maintained, solubilizate molecules are transported and can come in contact and react. In particular, the transport and interaggregate exchange of appropriate species is at the basis of nanoparticle formation in surfactant solutions. To emphasize the peculiarities of the diffusion mechanism in condensed phases, a schematic representation of the typical paths of molecules in gas, liquid, and solid is shown in Fig. 1.19.

Even if, at the same temperature, the speed of a molecule is quite independent on the aggregation state, the constraints due to collisions with neighbouring molecules drastically influence the diffusion rate.

The Brownian translation movement of surfactant aggregates of radius R can be depicted as thermally activated jumps of mean length λ among favourable positions with a characteristic time τ. These quantities are related to the diffusion coefficient (D) by the Einstein-Smoluchowski equation

$$D = \frac{\lambda^2}{2\tau} \tag{1.21}$$

It is generally assumed that λ is equal to aggregate diameter; then the mean translation velocity v of aggregates is $v \approx D/R$. Considering the relative velocity of aggregates and that the frequency of collisions (ν) experienced by an aggregate corresponds to the number of aggregates (N_m) in the volume visited in one second, then

$$\nu = 16\pi DRN_m \tag{1.22}$$

The diffusion coefficient of surfactant aggregates can be estimated by the Stokes-Einstein equation

$$D = \frac{kT}{6\pi\eta R} \tag{1.23}$$

where T is the temperature, η the viscosity of the medium, and R the hydrodynamic radius of particles. Then, the rate constant k_{diff} for the diffusional collision of aggregates can be calculated by the Smolochowski equation

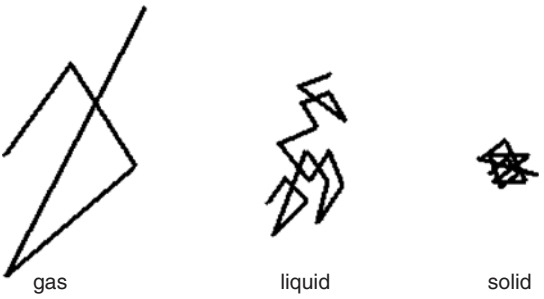

FIGURE 1.19. Schematic representation of the typical molecular paths in gas, liquid, and solid.

$$k_{diff} = 16\pi \, RDN_{Av} \tag{1.24}$$

where N_{Av} is Avogadro's number. Combining the above equations, the simple relationship can be obtained

$$k_{diff} = \frac{8kTN_{Av}}{3\eta} \tag{1.25}$$

allowing to calculate the interaggregate collision frequency (ν) by

$$\nu = k_{diff}\left(\frac{c - cmc}{N_{agg}}\right)^2 \tag{1.26}$$

Obviously, the actual value of D and k_{diff} can deviate from that predicted by the above equation in the presence of attractive or repulsive interaggregate interactions. Moreover, it must be taken into account that in absence of interaggregate interactions, the most probable spatial distribution of aggregates in the bulk medium is a random one, in the case of attractive interactions a more or less marked clustering of aggregates results, whereas a tendency to a spatially ordered distribution occurs if aggregates interact through long-range repulsive forces.

1.6.1.4. Solubilization in Surfactant Aggregate-Containing Liquid Media

A lot of question arises if a solute is added to a surfactant solution. How is it partitioned among the various nanodomains characterizing the structure of the system? What is its preferential location and orientation in each domain? Which are the interactions that drive their solubilization? What are its physico-chemical properties in each nanodomain? How are the structural and dynamical properties of surfactant aggregates modified by the solubilizate presence and its local concentration? How are all these phenomena affected by the nature of solvent and surfactant or affected by an increase of the temperature, pressure, and overall solubilizate concentration?

The most simple question regards the preferential solubilization site, which can be qualitatively answered taking into account the nature (hydrophilic, hydrophobic, amphiphilic) of the solubilizate. On the other hand, a quantitative description of the partitioning process requires the development of suitable models.

At low solubilizate concentration, the solubilizate binding to surfactant aggregate is described by a dynamic equilibrium that can be represented by the scheme

$$X + A \leftrightarrows XA$$

where X indicates the solubilizate species and A the "mean" surfactant aggregate. The magnitude of the binding can be measured by the corresponding equilibrium constant K_b

$$K_b = \frac{a_{XA}}{a_X a_A} \tag{1.27}$$

where a_{XS} is the activity of the solubilizate compartmentalized in the surfactant aggregates, while a_X and a_A are the activities of the free solubilizate and bare aggregates, respectively. It is worth noting that K_b values depend on the choice of the standard states. In molarity scale, the equation can be rewritten

$$K_{b,\,M} = \frac{\gamma_{XA,\,M}[XA]}{\gamma_{X,\,M}\gamma_{A,\,M}[X][A]} \tag{1.28}$$

where γ indicates the activity coefficients in molarity scale, and the terms in square brackets are the molar concentrations.

Alternatively, the solubilization equilibrium can be treated as a portioning of the solute between the micellar and the bulk solvent pseudo-phases, then the partition constant K_p is defined by the equation

$$K_p = \frac{a_b}{a_f} \tag{1.29}$$

where a_b and a_f are the activities of the solute species in the micellar and the bulk solvent pseudo-phases, respectively. Obviously, also in this case care must be taken with the choice of the standard states. Very often, activities are substituted by the corresponding concentrations, but marked nonideal behavior can be expected in surfactant aggregates especially at high solute/surfactant molar ratios.

At very low solubilizate/surfactant ratios, the system consists of bare aggregates and single occupied aggregates. However, by increasing this ratio, it becomes increasingly probable that an aggregate is occupied by more than one solubilizate molecules. In such condition, a distribution model is required.

Several distribution models of solubilizate molecules among surfactant aggregates can be hypothesized. At low solubilizate concentration, a random distribution is generally hypothesized. Assuming that the inclusion of the solubilizate molecule into the aggregate is independent of the presence of other molecules and that it does not cause a significant change in the micellar aggregation and structure, it can be shown that the distribution of the solubilizate among aggregates follows the Poisson distribution function

$$P(m) = \frac{x^m e^{-x}}{m!} \tag{1.30}$$

where P(m) is the probability of finding a surfactant aggregate containing m solubilizate molecules and x is the average number of solubilizate molecules per aggregate. Alternatively, x is the ratio between the concentration of solubilizate molecules entrapped in surfactant aggregates and the aggregate concentration. The same equation can be obtained by a kinetic treatment

based on the hypothesis that the kinetic constant of the solubilizate binding is independent of the number of solubilizate molecules in the surfactant aggregate while that of the unbinding process is proportional to m[51].

When there is a strong solubilizate/solubilizate attractive interaction or the solubilization of the first molecule makes the aggregate more apt to entrap other molecules, they tend to accumulate within some of them (attractive distribution). In contrast, solubilizate/solubilizate repulsions will lead to a dispersion among surfactant aggregates more ordered than that corresponding to a random distribution.

The solubilization mechanism of a solid or liquid solute could be mainly driven by the molecular solubilization in the bulk solvent and then the solute entrapment in the surfactant aggregates or by the adsorption of surfactant aggregates on the solute/surfactant solution interface followed by their desorption as aggregates containing some solute molecules (see Fig. 1.20).

The first mechanism is more plausible for solutes showing an appreciable solubility in the bulk solvent while the latter is more reasonable for substances scarcely soluble in the pure solvent. The second one could also be claimed to explain the dispersion and enhanced stabilization of small particles in surfactant solutions.

In order to estimate the interaggregate exchange rate of solubilized species, it must be taken into account their preferential location in the surfactant aggregate. For amphiphilic solubilizates, i.e., species located at the surfactant interface and in the bulk medium, in addition to the contribution arising from its self-diffusion, the exchange rate is practically controlled by the aggregate diffusion and collision rate because the transfer during collision requires only the facile jump and reorientation of solubilizate molecules.

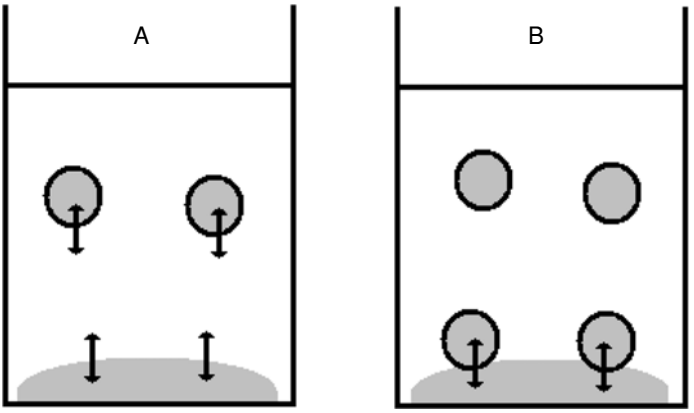

FIGURE 1.20. Solubilization mechanisms of solid or liquid substances in surfactant solutions by molecular diffusion and entrapment in micellar aggregates (A) or surfactant aggregate adsorption/desorption mechanism (B).

In the case of amphiphilic molecules preferentially located in the micellar palisade layer, the solubilizate exchange rate (v_{ex}) can be estimated by

$$v_{ex} = k_{diff} N_s \left(\frac{c - cmc}{N_{agg}} \right)^2 \qquad 1.31$$

where N_s is the mean number of solubilizate molecules per aggregate. The above equation considers that the exchange probability of each solubilizate molecule between aggregates is 1/2.

On the other hand, the exchange rate of species solubilized in the core of the surfactant aggregates is generally slower than is predicted by diffusion controlled processes. This is because solute transfer could happen only after the temporary interaggregate fusion followed by separation. The need to overcome the energy barrier due to the opening of the surfactant layer leads to exchange rates controlled by the slower interaggregate coalescence. In such condition, the solubilizate exchange rate can be estimated by the equation

$$v_{ex} = \beta k_{diff} N_s \left(\frac{c - cmc}{N_{agg}} \right)^2 \qquad 1.32$$

where β indicates the fraction of collisions leading to aggregate coalescence and consequently allowing a solubilizate transfer. The typical timescale for the material exchange between surfactant aggregates is of the order milliseconds, i.e., two or three orders lower than that associated with interaggregate collisions[52,53].

1.6.1.5. Surfactant Aggregates Containing Liquid Systems as Reaction Media

Reaction rates and mechanisms in solution can be strongly modified by the presence of surfactant aggregates due to changes of local concentrations and interfacial effects. These effects are obviously dependent on the specific location of each reactant. In the case of species solubilized in the aggregates or partitioned between aggregates and bulk medium, the treatment of reaction rates in liquid media containing surfactant aggregates requires the comparison of the reaction time constant with the residence time of the reactants in the aggregates and with the characteristic time of the aggregate breaking/reforming process. Then, reactions can be distinguished as activation energy or diffusion controlled processes.

Slow reactions occurring with characteristic time longer than lifetime of surfactant aggregates can be analysed in the same manner of those occurring in homogeneous systems, i.e., bulk concentrations must be considered and the observed rate must be attributed to an averaged medium effect. In the opposite case, the reaction rate must be considered as the sum of two contributions; one arising from the reactants in the bulk medium and the other from those confined in the aggregates[54]. To express both these contri-

butions, the partition constant of each reactant is needed in order to calculate their local concentrations.

1.6.2. Normal Micelles

All the physico-chemical properties of liquid water are mainly dominated by the ability of its molecules to form a maximum of four tetrahedrally oriented strong hydrogen bonds; two as proton donor and two as proton acceptor. Further contributions arise from effects due to water dipole moment and polarisability. The interlaced superposition of these forces and thermal agitation lead to the building up of local, dynamic, short-living, three-dimensional hydrogen-bonded networks characterized by collective breaking and reforming of these quite strong intermolecular interactions and large local energy fluctuations. The lifetime of these networks is of the same order of magnitude of the water single dielectric time relaxation (8 ps) while their size is strongly temperature dependent. On the other hand, the characteristic mean lifetime of each hydrogen bond is about 0.6 ps[55–57]. These features make liquid water the prototype of structured solvents.

Of particular interest in this contest is the rearrangement of the water structure in the presence of apolar species. It is generally believed that the interplay of water/water and water/apolar species attractive interactions leads to a slowing down of the hopping and reorientational movements of the water molecules surrounding the apolar species and of the solute molecule itself, a strengthening of water-water hydrogen bonding, and the formation of a more ordered local structure. This effect is called hydrophobic hydration and is emphasized by the large and negative entropy of transfer of a hydrocarbon molecule from an apolar liquid phase to water, small positive or negative enthalpy of transfer, large and positive standard free energy of transfer, and large partial molar heat capacity. Moreover, the anomalously small partial molar volumes of hydrocarbons in water suggest that apolar solutes tend to be constrained within the void spaces of the typical open structure of water. It has been found that all these quantities change linearly with the number of solute carbon atoms.

As a consequence of the hydrophobic hydration, apolar substances show very small solubility in water, and the molecules solubilized in water tend to minimize the area of the water/apolar species interface. One way to satisfy this tendency is reached by suitable conformational change of the apolar molecule (from elongated to coiled conformation), a second one is by the coming in contact of two or more apolar species (formation of associated entities), and a third one is phase separation and interface formation. The totality of all the peculiar interactions leading to conformational changes and aggregation of apolar species in water is called hydrophobic interaction.

On the other hand, the interaction of water molecules with hydrophilic (polar or ionic) species is enthalpically favoured due to the establishment of strong dipole-dipole, ion-dipole, and/or hydrogen bonds. This is emphasized

by large and negative hydration enthalpies and the formation of a first ordered solvation shell of oriented water molecules surrounding the polar or ionic species. In the case of ionic species, the binding and the mean residence time of water molecules is greater for smaller and higher charged ions. Further secondary enthalpic effects arise from short and long-range perturbation of the water structure. It is believed that the first solvation shell is surrounded by another one where water molecules are more disordered than in bulk water due to the competition of different orienting effects determined by water/water and ion/water interactions. For gas, liquid, and solid with not too high reticular energy, the favourable hydrophilic species/water interactions lead to high solubility.

Taking into account the amphiphilic nature of surfactants, in dilute or semi-dilute aqueous solutions, their aggregation is mainly driven by the scarce tendency of the water to host in its three-dimensional H-bonded network apolar species (unfavourable S-T interactions) joined to the strong affinity towards polar and ionic groups (favourable S-H interactions). In other words, a significant contribution to the driving force of surfactant association in water is the gain in entropy due to the elimination of the unfavourable chain-water contacts. From a dynamical point of view, this means that there is a strong tendency to reduce the time fraction during which apolar groups are in contact with water molecules. To fulfil these requirements, a suitable number of surfactant molecules must transiently self-assemble in order to avoid contacts between water and hydrophobic chains.

As a result, above the critical micellar concentration (cmc), surfactant monomers are in dynamical equilibrium with self-assembled globular aggregates characterized by a nano-size liquid-like hydrophobic core constituted by the surfactant tails and an external shell formed by the hydrated head groups that constitute the boundary between the micellar phase and bulk medium. This kind of aggregation leads to the formation of "supermolecules" that appear from the outside as hydrophilic objects dispersed in the aqueous medium.

In the case of ionic surfactant, the partial dissociation of the head groups leads to the formation of a charged micellar surface (Stern layer), the formation of an oppositely charged diffuse layer of counterions surrounding the micelle (Gouy-Chapman electrical double layer), and the development of an intermicellar electrostatic repulsion as well as an intramicellar electrostatic repulsion among the charged head groups. Both these effects stabilize micelles against coalescence and indefinite growth, i.e., against phase separation.

The spherical form of direct micelles occurs more frequently at low surfactant concentrations while an increase of the aggregation number accompanied by a one-dimensional growth as rod-like micelles of increasing length or as disk-like micelles can be observed at high concentration or in presence of appropriate additives. At the highest surfactant concentration, a new phase in equilibrium with the micellar one is formed, which is most often a hexagonal or a lamellar phase.

Given the smallness of the micelles, the micelle/water interface has a huge value. With a typical value of 50 $Å^2$ of the surfactant head group area and taking into account that virtually all surfactant molecules lie at the interface, an interfacial area of about 30,000 m^2 in a liter of a 0.1 molar surfactant solution can be calculated. For this reason, the physico-chemical properties of aqueous surfactant solutions are dominated by interfacial effects.

The aggregation number ranges from tens to thousands of monomers depending on the nature of the surfactant and on some external parameters such as temperature, concentration, and presence of additives. This means that about 10^{19} to 10^{21} nearly identical self-assembled aggregates, which can also be viewed as nanoreactors, nanocarriers, or nanocontainers, are dispersed in a liter of a 0.1 molar surfactant solution. A schematic representation of a direct micelle is shown in Fig. 1.21.

As it can be expected, micellization process, cmc, and micelle size and shape depend on the structure of surfactant molecules as well as on the presence of additives, counterion complexation, and temperature. However, the primary factor is the size of the surfactant hydrophobic part. For long chain surfactants, the micelle formation can be well described as a pseudo-phase separation process while for short chain surfactants, a multi-step equilibrium is preferable. In particular, by increasing the surfactant alkyl chain length, the micelle size increases and the cmc decreases. For a homologous series of surfactants, the relationship between the cmc and the number (n_C) of carbon atoms of the alkyl chain generally found is

$$\log \text{cmc} = a - bn_C \tag{1.33}$$

where a and b are constants. The a value is specific for each homologous series while b is in the range 0.3–0.5.

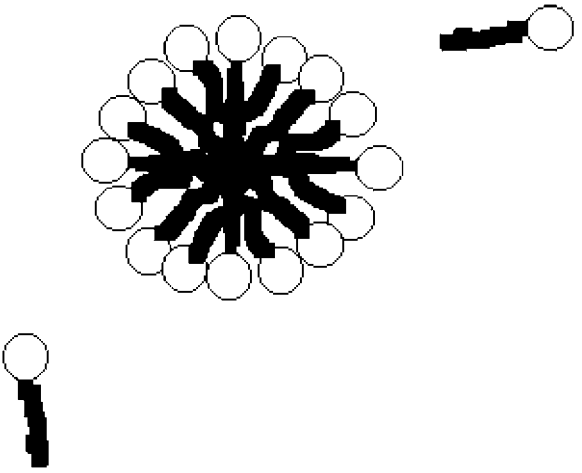

FIGURE 1.21. Schematic representation of a direct micelle.

Formation of micelles requires a minimum number of carbon atoms of the hydrophobic chain, which is 8–10. Chain branching or the presence of double bonds in the alkyl chain destabilizes the micelles and consequently increases the cmc. In the case of ionic surfactants, the micelle size increases and the cmc decreases with the concentration of added salt. Non-ionic surfactants are less sensible to the presence of electrolytes, and for a given alkyl chain length their cmc is lower than for ionic ones.

The shape of the smaller micelles is nearly spherical, whereas that of the larger ones can be rod-like, disk-like, or worm-like. Intermicellar interactions can drive their distribution in the system maximizing (repulsive interaction) or minimizing (attractive interactions) the mean distance with the next neighbouring micelles (see Fig. 1.17).

As a consequence of the existence of various channels by which amphiphilic molecules can fulfil the hydrophobic interaction, the solubility of surfactants in aqueous solutions shows a typical temperature dependence. In particular, below a certain temperature, the so-called Krafft point, the solubility is scarce and lower than the cmc. In such circumstances, the surfactant is dissolved monomerically in the aqueous medium, and its solubility is dictated by that of monomers. Above the Krafft point, the solubility is greater than the cmc, and it increases dramatically with temperature. Now, the surfactant solubility is dictated by that of micelles, which is much higher than that of monomers.

Increasing surfactant concentration or the addition of appropriate solubilizates can lead to the formation of rod-like micelles and for very concentrated systems to percolated systems and finally to liquid crystals. Percolation could arise for topological reasons or can be driven by strong intermicellar attractive interactions. A schematic representation of percolated system of interconnected micelles is shown in Fig. 1.18.

It is believed that the size of non-ionic surfactant micelles increases with temperature while for ionic surfactants it decreases. The radius of spherical micelles can be roughly identified with the length of the surfactant molecules and by considering that the average length of surfactant alkyl chain is of the order the full extended length.

Further interesting effects are originated by dynamical properties characterizing the life of surfactant aggregates. The dynamics of aqueous micelles is characterized by conformational movements of alkyl chains and surfactant head groups, lateral diffusion of surfactant molecules within the aggregate, diffusion and rotation of the entire aggregate, size and shape of micellar fluctuation, and exchanging of monomers with the surrounding medium or between contacting micelles. All these processes are directly or indirectly triggered by the surrounding water molecules. It has been observed that different parts of surfactant molecules embodied in a micelle show distinct conformational mobility; it decreases proceeding from the head group towards the most internal methyl groups[1].

The micelle/surrounding exchanging process of surfactant molecules (S), represented by the dynamic equilibrium

$$S_n \leftrightarrows S_{n-1} + S$$

occurs in the $10^{-3} - 10^{-8}$ second timescale.Micellization being a cooperative process, the transient elimination of surfactant molecules could lead to the complete dissolution of the micelle, and conversely monomers could associate in a micelle. This process, represented by the dynamic equilibrium

$$S_n \leftrightarrows nS$$

occurs on the 10^{-3} to 1 second timescale[58].

The most investigated surfactant able to form direct micelles in water is sodium dodecylsulfate (SDS). Dissolved in water, this surfactant forms quite monodisperse and spherical aggregates that are in equilibrium with monomers at a concentration (cmc) of 8.3×10^{-3} M. Its Krafft point is 20°C, the mean aggregation number is about 65 at 25°C, the degree of counterion binding is about 0.6, and the hydration number of the micellar head group region per amphiphile is about 8.

A particular kind of micelles can be formed by solubilizing in water a long-chain phospholipid and a hydrophilic surfactant. The resulting molecular aggregates are called bicelles and are characterized by a discoid shape with an inequal distribution of the two amphiphiles: a lipid-rich bilayer and surfactant-rich edges. The bicelle size can be modulated by changing the lipid/surfactant ratio. As an example, bicelles can be formed by solubilizing in water 1,2 dihexanoyl-3-sn-phosphatidylcholine and 1,2 dimiristoyl-3-sn-phosphatidylcholine[59].

1.6.2.1. Solubilization in Aqueous Micellar Systems

One of the most important properties of solutions of micelles both for practical applications and theoretical implications is their solubilizing power. This is because many substances otherwise insoluble in water show a marked increase of their solubility in the presence of surfactants. Generally, this behaviour is explained in terms of solubilizate entrapment in the micelles.

Taking into account the effects of hydrophobic interactions, the most easily addressed question is the preferential micellar solubilization site of apolar, amphiphilic, and polar solutes (see Fig. 1.22).

It can be noted that micellar solubilization involves the establishment of specific interactions and an oriented location.

However, to understand the solubilization process, all the possible interactions occurring in the system (solubilizate-solubilizate, solubilizate-micelle, solubilizate-bulk solvent) as well as all the possible resultant modifications in the structure and dynamics of solubilizate molecules, micelles, and surrounding medium should be considered.

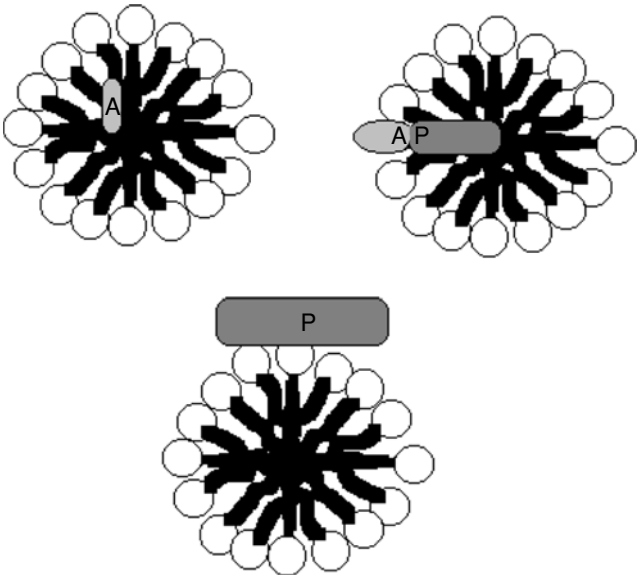

FIGURE 1.22. Solubilization sites in direct micelles of apolar (A), amphiphilic (AP), and polar (P) solutes.

Apolar substances that are slightly soluble in water can be readily solubilized in aqueous surfactant solutions as a consequence of their entrapment in the hydrophobic micellar core. This is macroscopically pointed out by the progressive increase of the solubility of many apolar substances with the surfactant concentration, i.e., the number density of micelles, occurring above the cmc. The possibility to incorporate apolar solubilizate in the micelle interior demonstrates that the micellar core can be considered liquid-like. Generally, an increase of the length of the surfactant alkyl chain determines an increase of the solubilization ability of micelles, whereas chain branching often results in its decrease. As a general rule, a change of external parameters such as temperature and pressure involving an increase of micellar stability leads to an increase of the maximum amount of apolar substances that can be solubilized. Because the solubilization capability of micelles is governed by geometric constraints, it can be easily predicted that increasing the size of the apolar solubilizate, its solubility decreases. Moreover, it can also be predicted that the solubilizate entrapment in the micellar core induces a micellar swelling and it modifies more or less the structural and dynamical properties of micelles. One of such effects is the decrease of the cmc induced by the presence of apolar substances.

Often the addition of appropriate substances generally called cosurfactants, such as medium-chain alcohols and amines, enhances the stability of micelles thus strongly increasing the solubilization power of apolar sub-

stances. When a finite amount of apolar substances is entrapped in the micellar core, the micellar size increases markedly and the system is generally indicated as an oil-in-water (o/w) microemulsion. A schematic representation of o/w microemulsions is shown in Fig. 1.23.

On the other hand, amphiphilic molecules are dynamically partitioned between the aqueous bulk medium and micellar phase[13,60]. Those solubilized in micelles are preferentially located, opportunely oriented, in the micellar palisade layer. The partition constant between aqueous and micellar pseudophases is correlated to the standard chemical potential difference of the solubilizate in both phases. This, in turn, depends on the change in the partial molar enthalpy and entropy of the solubilizate accompanying its transfer from the aqueous to the micellar phase. The solubilization of amphiphilic substances induces some changes such as a decrease of the cmc and, in the case of ionic surfactants, an increase of their ionization degree[61]. By increasing the solubilizate/surfactant molar ratio, increasing changes in the micellar structure and deviations from the ideal behaviour are observed.

Polar solutes are totally solubilized in the aqueous medium but solute/micellar surface interactions should occur. Examples are ion binding to micelles and the marked effect of electrolytes on the stability of ionic micelles through changes in the ionic strength of the medium. According to their specific properties, polar solubilizates are preferentially located within the electric double layer of ionic micelles or can be trapped between the hydrophilic groups of the surfactant molecules. Ion binding to micelles is a basic process in the enhancement or inhibition of reactions in micellar solutions.

Other effects could be devised by considering the possibility that micelles can bind to macromolecules, nanoparticles, and surfaces by favourable hydrophobic, hydrophilic, and/or electrostatic interactions. In particular, ionic surfactants form charged micelles that can bind to oppositely charged

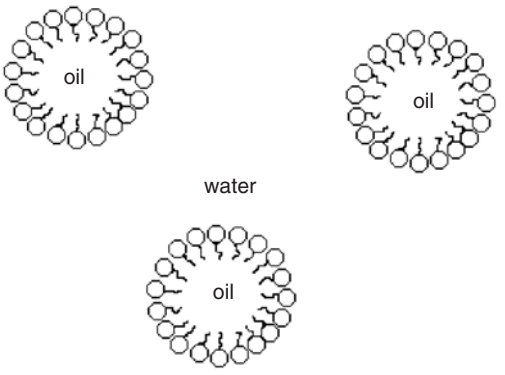

FIGURE 1.23. Schematic representation of an oil-in-water microemulsion.

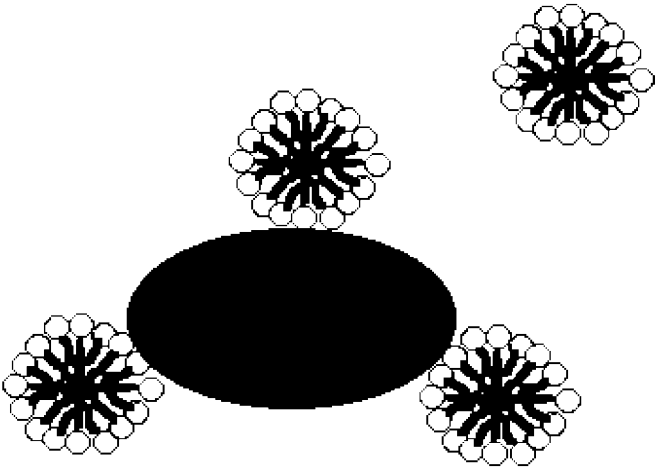

FIGURE 1.24. Binding of direct micelles to hydrophilic particles.

particles. Some of the possible arrangements of micelles or surfactant molecules on hydrophilic or hydrophobic nanoparticles leading to water-soluble aggregates are shown in Figs. 1.24, 1.25, 1.26, and 1.27.

It can be noted that the oriented adsorption of surfactant molecules on the surface of hydrophobic particles forming an electric double layer stabilizes the particle dispersion in water and inhibits particle aggregation. However, also the opposite effect could occur, i.e., the surfactant adsorption on the surface of

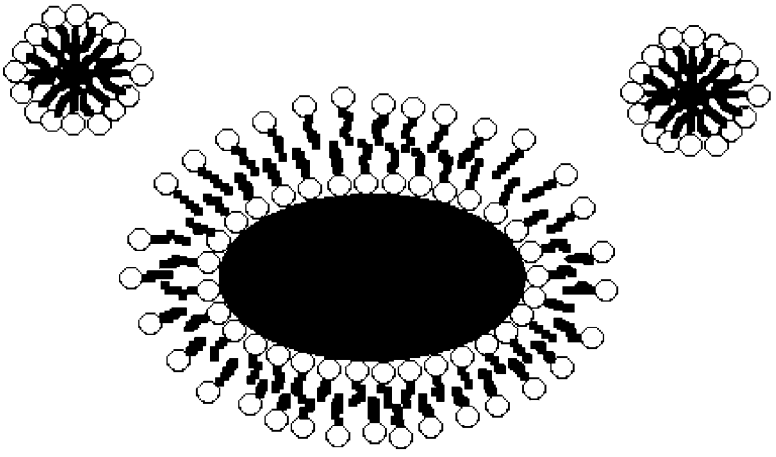

FIGURE 1.25. Binding of surfactant molecules to hydrophilic particles.

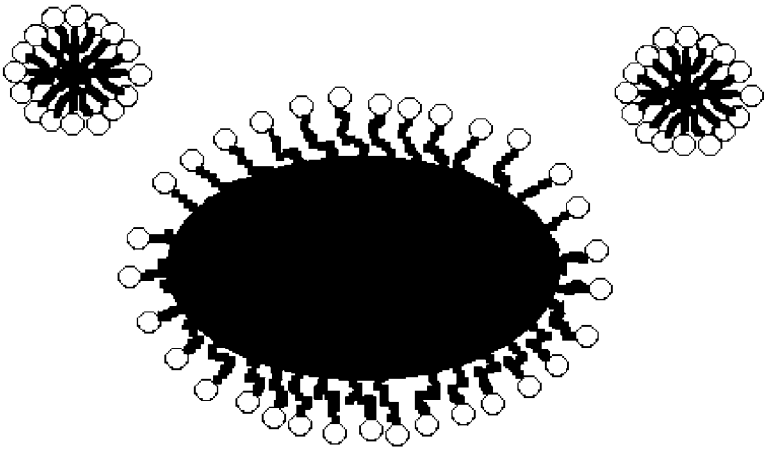

FIGURE 1.26. Binding of surfactant molecules to hydrophobic particles.

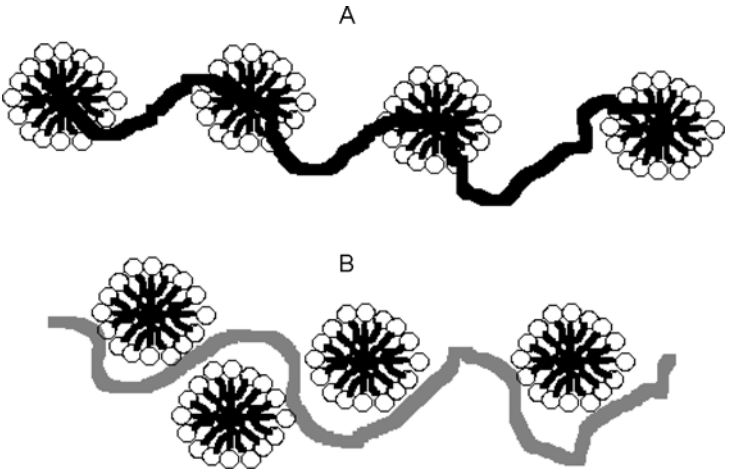

FIGURE 1.27. Binding of direct micelles to hydrophobic (A) and hydrophilic (B) macromolecules or uni-dimensional nanoparticles.

strongly hydrophilic particles could lead to the formation of a hydrophobic coat that makes the particle insoluble in the aqueous medium (Fig. 1.28).

It is worth noting that all these different situations depend on the nature of the involved species but in many cases can be driven by changing some external parameters such as concentration, temperature, and additive addition.

1.6.2.2. Aqueous Micellar Systems as Reaction Media

The main importance of surfactant aqueous solutions as specialized reaction media lies in the opportunity in monophasic liquid systems to perform

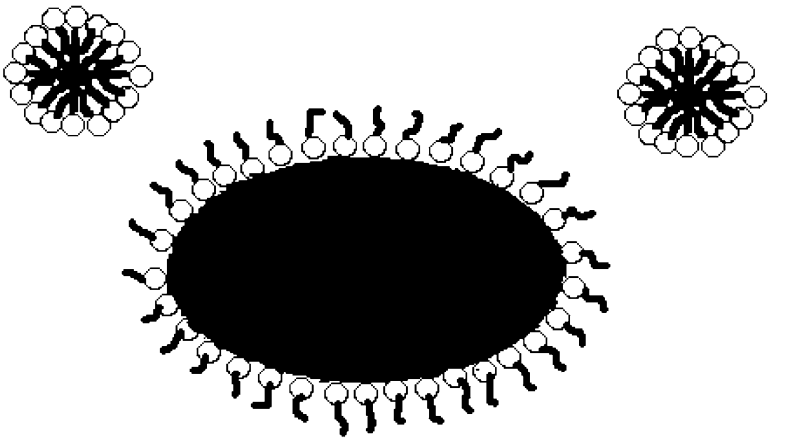

FIGURE 1.28. Binding of surfactant molecules to hydrophilic particles.

reactions among species with opposite hydrophilic/hydrophobic character. Because these reactions occur most frequently at the micellar interface, kinetic effects on reaction rate and products can be predicted.

The influence of micelles on reaction rates has been rationalized in terms of the pseudo-phase model and by hypothesizing that the overall reaction rate is the sum of two contributions due to reactive events occurring in the bulk medium and in the micellar phase. However, it is worth noting that this last hypothesis is valid only when the characteristic time of the reactive event is shorter than that associated with the formation/dissolution process of micelles. Moreover, according to the above hypothesis, the development of the kinetic model requires the knowledge of the concentration of the substrates in each possible solubilization site. Because in many cases the exchange of substrate molecules between micelles and surrounding medium is faster than the reactive process, it is generally assumed that reaction does not change significantly the local concentration at the equilibrium. For this reason, these quantities are generally calculated using the thermodynamic distribution constants.

Additional kinetic effects in aqueous surfactant solutions can arise also from specific surfactant/substrate interactions. For example, the rate of the disproportion reaction of copper sulfide nanoparticles from Cu_2S to $CuS{\cdot}S^{\circ}$ decreases significantly in the presence of surfactants due to their binding to surface catalytic sites of the nanoparticles[62].

1.6.3. Reversed Micelles

In apolar media, i.e., in solvent of low dielectric constant, surfactant molecules are quite un-ionized and so ion-ion interactions do not play a sign-

ificant role in surfactant self-assembling. For this reason, the formation of micellar aggregates is mainly driven by hydrogen bonding, dispersion forces, attractive dipole-dipole and/or ion pair interactions among the surfactant hydrophilic head groups while the solvent holds the secondary role of dispersing phase. It is worth noting the significant difference with respect to micellar aggregates formed in aqueous solutions where water structure plays a dominant role in the stabilization of micelles and interactions among solvated head groups destabilize micelles. Taking into account the molecular geometry and the solvent effect, it must be emphasized that the tendency of surfactants to form reversed micelles is more pronounced for surfactant molecules with $r_p/r_a < 1$ and when solubilized in less polar solvents. A consequence of these differences is that many common surfactants able to form micellar aggregates in water are scarcely soluble in apolar solvents and do not form reversed micellar aggregates. This critical dependence on the surfactant structure is emphasized by the observation that even small molecular variations have important impact on the physicochemical properties and aggregation behaviour of surfactants in apolar media[63].

Reversed micelle represents one of the most interesting aggregates formed by some surfactants when they are dissolved in apolar solvents above a concentration threshold value (cmc). They are globular aggregates with an interior constituted by the surfactant head groups while the alkyl chains protrude toward the external medium. The segments of chains near the head groups are less mobile than those in the periphery and surfactant molecules are disposed so that energetically unfavourable void spaces are avoided. A schematic representation of a reversed micelle is shown in Fig. 1.29.

Generally, reversed micelles are characterized by an aggregation number lower than that typical of direct micelles in aqueous solutions and by a

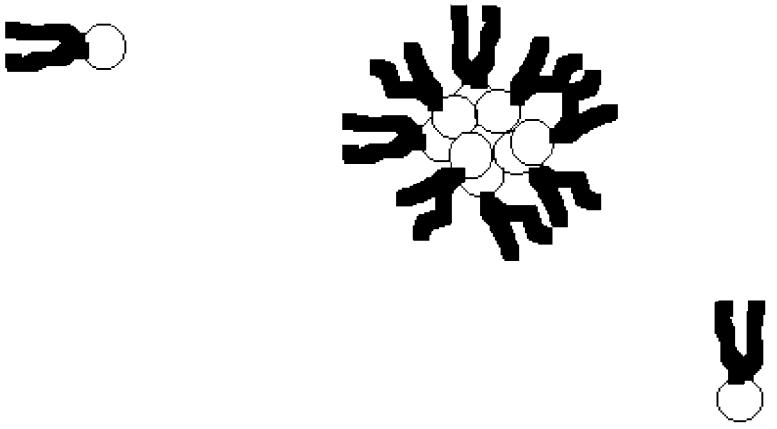

FIGURE 1.29. Schematic representation of a reversed micelle.

greater polydispersity. From a thermodynamic point of view, surfactant association in apolar solvents is driven by a favourable enthalpic effect whereas it is counteracted by an unfavourable entropic term. To the enthalpy of reversed micelle formation contribute attractive interactions (dipole-dipole, ion-dipole) and/or the formation of H-bonds. The negative entropic term arises from the non-random distribution of surfactant molecules in the dispersing medium and from the partial loss of translational and rotational degree of freedom accompanying the transition from monomeric to micellized surfactant molecules. While the interactions responsible for the formation and for the structure of micellar aggregates depend on the solvent nature (strongly polar or apolar), the thermodynamic approach for the association process is quite independent of these aspects so that the same models can be used for micellar aggregates in water and in apolar media. For both situations, this subject has been treated in section 1.6.1.1.

An interesting aspect of the life micellar aggregates is represented by their dynamic properties and those of surfactant monomers. Their dynamics is characterized by conformational and diffusive motions in the bulk medium and in the micellar aggregate, exchange of surfactant molecules between solvent and reversed micelles, structural collapse of the entire aggregate, and its re-formation. The aggregates undergo Brownian motions leading to diffusion, rotation of the entire aggregate, and micellar encounters. As a consequence of the collisions between micelles, the formation of short-lived dimers and their separation with material exchange occurs. Thanks to these dynamic properties, the relative populations of the various aggregates reach and maintain the equilibrium concentrations. It is worth noting that a dynamic picture of reversed micelles is important to understand why sometimes it is found that the nanoparticle size is not controlled by the micellar size.

The most investigated surfactant able to form reversed micelles in absence of cosurfactants is sodium bis(2-ethylhexyl) sulfosuccinate (AOT). Dissolved in hydrocarbons, this surfactant forms highly monodisperse quite spherical aggregates that are in equilibrium with monomers at a concentration (cmc) of 4×10^{-4} M. Moreover, the mean aggregation number is about 23, the micellar radius 15 Å, the timescale of the monomer exchange 10^{-6}s, and that of the micellar collapse/re-formation 10^{-3}s[64–66]. From this compound, by replacing the sodium counterion with other cations, many surfactants have been obtained. Interesting structural and dynamical changes of reversed micelles dependent on the nature and charge of the AOT counterion have been observed[67,68].

Given its biocompatibility, another very interesting reverse micelle forming compound is lecithin. It forms nearly spherical reversed micelles whose mean radius is strongly sensitive to temperature, surfactant concentration, and moisture[69]. Other frequently employed surfactants are didodecyldimethylammonium bromide[70], tetraethyleneglycol monododecylether ($C_{12}E_4$)[71], and sodium bis(2-ethylhexyl) phosphate[72].

As solvent media, quite all the low polar or apolar organic solvents have been employed; the most used being hydrocarbons. However, among the various apolar solvents employed as dispersing media of reversed micelles, much attention has been recently devoted to supercritical carbon dioxide as environmentally friendly and well-suited medium for green chemistry applications. The merits of this solvent are, in fact, non-toxicity, low-cost, non-flammability, tunable solvent strength, low viscosity, easy recycling, and rapid separation of dissolved species. Examples of surfactants able to form reversed micelles in supercritical CO_2 are fluorinated AOT and ammonium carboxylate perfluoropolyether.

1.6.3.1. Solubilization in Solutions of Reversed Micelles

The main peculiarity of reversed micelle solutions is their capability to increase noticeably the solubility of ionic, polar, and amphiphilic substances with respect to that in the same bulk solvent. This property has been exploited in numerous industrial and biotechnological applications[73,74].

Depending on the nature of the solubilizate, its preferential solubilization site in reversed micelles changes from the micellar core for hydrophilic substances, to the micellar palisade layer for the amphiphilic ones. While hydrophilic molecules practically spend all the time confined into the micellar core, amphiphilic solubilizates are virtually partitioned among the micellar core, the micellar palisade layer, and the surrounding medium. The fraction of these molecules residing opportunely oriented into the so-called micellar palisade layer or the mean time fraction that each solubilizates spends into it depend on the hydrophilic/lipophilic character of the amphiphile. Apolar substances are preferentially solubilized in the bulk apolar solvent (see Fig. 1.30).

At infinite dilution, the solubilization of small molecules does not involve significant change in the structural and dynamical properties of the reversed micelles hosting the solubilizate as well as of the entire micellar solution.

On the other hand, the solubilization of finite amount of substances or of macromolecules leads to more or less marked changes of the micellar properties. In particular, depending on solute/solute and solute/surfactant head group interactions, it can be found that polar species are dispersed among the surfactant head groups or form molecular clusters confined into the micellar core, while, in the case of amphiphilic molecules, it is possible to obtain a random or localized distribution of oriented molecules at the interface between the polar/apolar domains. These different solubilization models are schematically depicted in Fig. 1.31.

A simple geometrical model allows to predict the dependence of the micellar radius (r) upon the addition of polar and amphiphilic molecules to a solution of reversed micelles. This model is based on the reasonable hypothesis that polar substances are confined in the micellar core while amphiphilic ones are preferentially solubilized in the micellar palisade

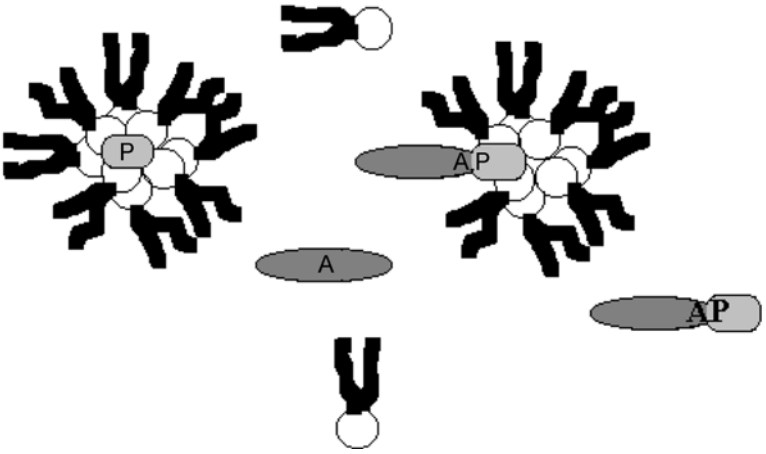

FIGURE 1.30. Solubilization sites of polar, amphiphilic, and apolar molecules in reversed micelles.

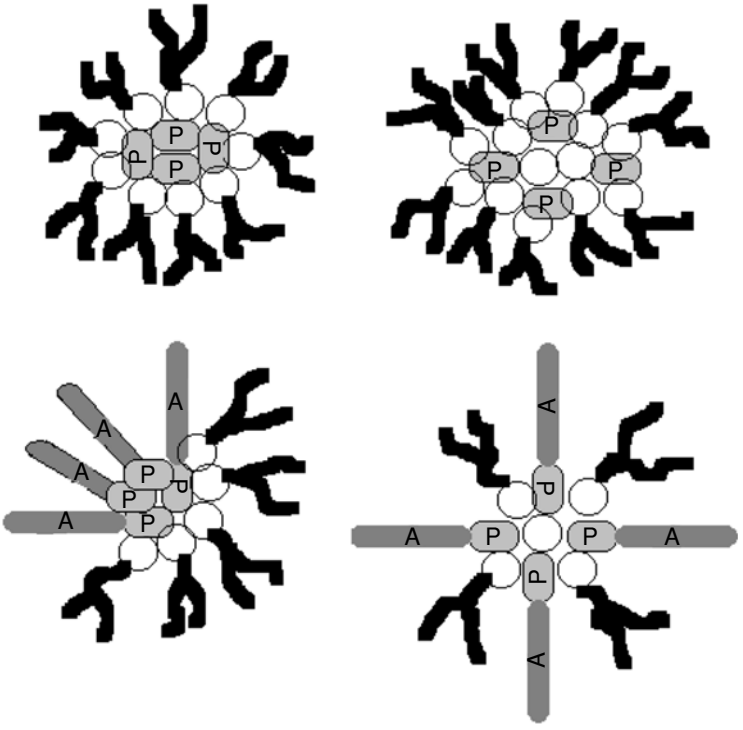

FIGURE 1.31. Schematic representation of solubilization models of a few polar and amphiphilic molecules in reversed micelles.

layer. Then, assuming spherical and monodisperse micelles, the volume V_m and the surface A_m of a reversed micelle are given by

$$V_m = \frac{4\pi r^3}{3} = n_s V_s + n_p V_p \tag{1.34}$$

$$A_m = 4\pi r^2 = n_s A_s + n_a S_a \tag{1.35}$$

where n_s, n_p, and n_a are, respectively, the number of moles of surfactant, polar, and amphiphilic solubilizates in one micelle, V_s and V_p the molar volumes of surfactant and polar compound, while A_s and A_a, the molar interfacial area of the surfactant and amphiphilic substance. Combining the above equation, it can be obtained

$$r = \frac{V_s + \frac{n_p V_p}{n_s}}{A_s + \frac{n_a S_a}{n_s}} \tag{1.36}$$

It can be noted that addition of polar substances induces an increase of the micellar radius while that of amphiphilic ones produces a decrease.

However, the addition of finite amounts of specific substances could involve structural changes more marked than that predicted by the geometric model arising from an enhancement of the intermicellar interactions and/or significant variations of the micellar size and shape. For example, the solubilization of finite amounts of some substances such as p-cresol, p-ethylphenol, benzenediols, and dihydroxynaphthalenes in solutions of AOT reversed micelles allows the formation of highly viscous and transparent gels. The high viscosity of these systems is attributed to the formation of an extended dynamic network of AOT reversed micelles linked to the solubilizate molecules through hydrogen bonds[75–77].

Being sustained by relatively weak interactions, these systems show a transition from a highly viscous organogel to fluid phase with low viscosity by increasing the temperature. Similar behaviour has been observed by adding water to reversed micellar solutions of lecithin in suitable solvents[49,78]. These systems are obviously very interesting candidates as nanoparticle entrapping substrates for technological applications.

The solubilization of finite amounts of hydrophilic liquids leads to the formation of discrete droplets of these substances stabilized by a surfactant monolayer[49,78]. A marked modification of the structural and dynamical properties of these substances due to confinement and interfacial effects has been observed.

It is also possible to solubilize finite amounts of hydrophilic organic or inorganic solid substances within reversed micelles[80,81]. This is performed by direct solubilization of the solute in the solution of reversed micelles or by solubilizing it in a solution of water containing reversed micelles and then, after complete evaporation of the volatile components (water and organic solvent), the solution is restored by adding the pure apolar medium. Physico-

chemical investigations on the state of these solubilizates entrapped in the micellar core have indicated that they are generally entrapped as small-size nanoparticles[32,82]. These systems appear to be well-suited for many specialized applications. For example, under dry organic solvent conditions, the photo-oxidation of organic substrates could be directed to the formation of chemical products of great practical importance[83].

Of particular interest is the solubilization of water in reversed micelles. This because in many reversed micellar systems, it is possible to dissolve a number of moles of water far exceeding that of the surfactant leading to the formation of discrete nano-size water droplets entrapped in the micellar core.

Water solubilization involves an increase of the micellar size transforming the reversed micelles from short-living aggregates to more stable ones with an enhanced persistence in size and shape of the entire aggregate but not in constituent molecules. When the amount of water solubilized is above the surfactant hydration limit, water containing reversed micelles is also called water-in-oil (w/o) microemulsion (see Fig. 1.32).

As a manifestation of confinement effect, the diffusion coefficient of water in solutions of reversed micelles is much lower than that in bulk[84].

Several investigations have shown that the physico-chemical properties of interfacial water are strongly different from those of bulk water[16,85,86]. At low water content, large deviations of the permittivity, viscosity, and structural order from bulk water have been observed.

The water solubility in reversed micelles can be significantly enhanced by adding appropriate cosurfactans such as medium-chain alcohols. The size and shape of water/surfactant aggregates are system specific. For example, AOT forms nearly spherical and monodisperse aggregates whose size can be regulated by changing the water to surfactant molar ratio. In particular, it has been found that the radius r of AOT reversed micelles quite

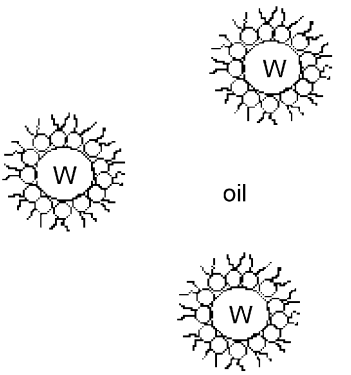

FIGURE 1.32. Schematic representation of water in oil (w/o) microemulsions.

independently of the surfactant concentration can be well described by the equation

$$r(\text{Å}) = 1.8R \qquad 1.37$$

where R represents the water-to-AOT molar ratio[87].

On the other hand, lecithin and copper bis(2-ethylhexyl) phosphate form elongated micelles that increase their size by increasing the water content.

Spherical water containing reversed micelles occur when water/surfactant interactions are less favourable than water/water and/or surfactant/surfactant interactions because in these conditions the interplay of all the interactions pushes the aggregates to have the smallest surface-to-volume ratio. On the other hand, rod-like water containing reversed micelles results when water/surfactant interactions are stronger than water/water and surfactant/surfactant interactions, because cylindrical aggregates maximize the water/surfactant polar head contacts.

The dynamics of water containing reversed micelles includes lateral diffusion of surfactant molecules at the water/surfactant interface, restricted motions of water within the micellar core, exchange of water and surfactant molecules with bulk solvent and neighbouring micelles, diffusion and rotation of the entire aggregate, intermicellar encounters, and possible micellar fusions. The lifetime of the fused dimers is of the order microseconds[88].

In spite of the apolar coat surrounding water containing reversed micelles and their dispersion in apolar solvents, reversed micelles of ionic surfactants are able to establish attractive interactions leading to more or less extended clusters. It has been suggested that the microscopic process responsible for these interactions is the intermicellar exchange of surfactant ions leading to the formation of oppositely charged reversed micelles[43]. Obviously, the formation of these clusters strongly influence the physico-chemical properties of the system: mass, moment, and charge transport within a cluster could be strongly enhanced as compared to a dispersion of randomly distributed micelles.

It is worth noting that, even if solvents hold the secondary role of dispersing media of the water containing reversed micelles, some specific effects are observed by changing it, the most marked being the maximum amount of water that can be dissolved in the micellar solution at a given temperature. This behaviour emphasizes the solvent triggering role of the intermicellar interactions.

1.6.3.2. Solubilization in Solutions of Water Containing Reversed Micelles

The water containing reversed micelles can be employed as suitable nanosize aggregates to host hydrophilic and amphiphilic substances[89–92]. The different location of solubilizates is depicted in Fig. 1.33. It is also emphasized the effect of finite amount of solubilizates on the micellar size.

It can be noted that polar substances are entrapped in the aqueous micellar core, whereas amphiphilic molecules are partitioned between the micellar

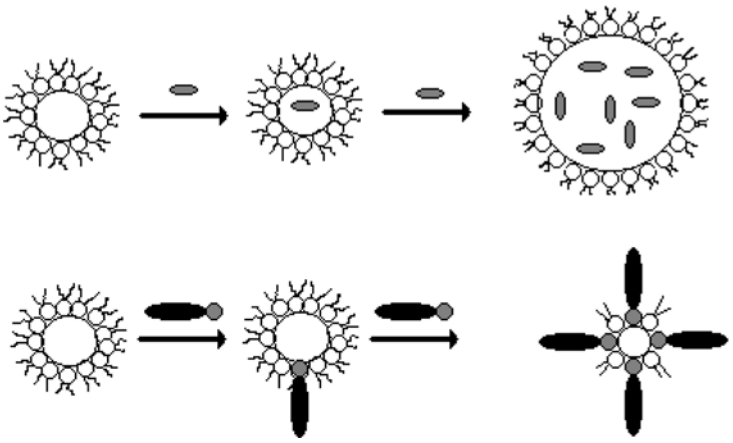

FIGURE 1.33. Solubilization sites in water containing reversed micelles.

palisade layer and the surrounding medium. Physical and chemical properties of solubilized species are modified by their confinement. For example, the enzymatic activity in reversed micelles is significantly enhanced[73,93,94].

Of utmost importance is the intermicellar material exchange process because it allows that hydrophilic reactants can be transported or can come in contact and react[95]. This process can be considered the result of some more elementary steps (see Fig. 1.34):

1. diffusion controlled motion of aggregates in the organic medium
2. intermicellar collisions and possible coalescence between micelles
3. diffusion of solubilizates molecules in the confined space of the transient micelle dimer
4. micelle separation

Obviously, the rate of the overall material exchange process is governed by the slowest of these consecutive steps and strongly depends on the preferred solubilization site of the exchanged species as well as of its size. Figure. 1.33 emphasizes also that the intermicellar exchange process of amphiphilic solubilizates occurs by intermicellar hopping or by diffusion through the solvent medium.

Factors involving a change of the material exchange rate such as temperature, nature of surfactant and apolar solvent, and composition can be altered to influence the intramicellar confinement effect.

From the knowledge of the micellar size, the average number of solubilizate molecules in each micelle can be calculated. However, the determination of their location and how they are distributed among micelles requires appropriate experimental measurements or a suitable model[96].

Several distribution models of solubilizate molecules among water containing reversed micelles can be hypothesized. At low solubilizate concentration, a

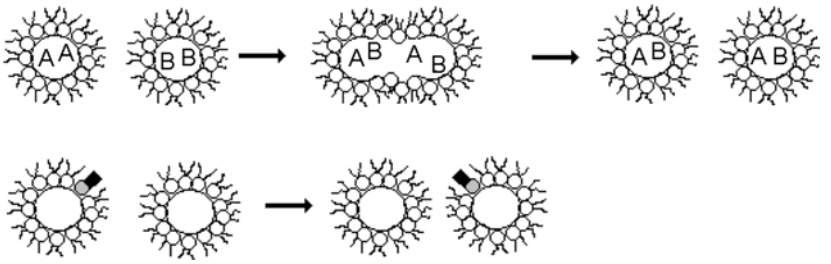

FIGURE 1.34. Intermicellar exchange processes.

random distribution is generally proposed. When there is a strong solubilizate/solubilizate attractive interaction or the solubilization of the first molecule makes the micelle more apt to entrap other molecules, they tend to accumulate within some micelles (attractive distribution). This situation dramatically occurs in the case of nanoparticle formation inside reversed micelles. On the contrary, if the swelling of the reversed micelle due to solute entrapment is against the solubilization of additional molecules, they tend preferentially to be solubilized in empty micelles (repulsive distribution).

1.6.3.3. Reaction Rates and Mechanisms in Solutions of Water Containing Reversed Micelles

Reaction rates and mechanisms in solutions of reversed micelles and water containing reversed micelles have been widely investigated. In addition to effects due to enhancement of local concentration, contributions arising from interfacial interactions, ordered molecular arrangement, and changes of water activity have been emphasized[97,98].

Specific investigations focused on the nanoparticle kinetic growth in reversed micellar solutions have been carried out. For example, the study of the growth rate of silica nanoparticles in tetraethoxysilane (TEOS)/ammonium hydroxide/polyoxyethylene nonylphenylether/cyclohexane system have emphasized that the process is controlled by the TEOS hydrolysis in the initial stages of the growth; whereas in the later stages the condensation rate becomes the rate determining step[99].

The influence of external parameters on the nanoparticle size has been carefully scrutinized. Studying the size of silver nanoparticles synthesized in water containing reversed micelles of an amphiphilic block copolymer dispersed in p-xylene, Zhang et al.[100] found that the diameter of nanoparticles increases with the size of the aqueous droplets; this because the average number of precursors in each micelle increases and the number of nuclei decreases with micellar size. Moreover, by increasing the reactant concentrations, the particle size decreases; this because the nucleation rate and the number of nuclei increase with the average number of precursors in each

micelle. In reversed micelles, simulation results lead to the conclusion that the particle size and their polydispersity increase with the aqueous core size[101].

Schematic representations of nanoparticles stabilized by reversed micelles and water containing reversed micelles are shown in Figs. 1.35 and 1.36.

1.6.4. Water-in-Oil and Oil-in-Water Microemulsions

In absence of surfactant, water and apolar solvents (generally indicated as oils) do not mix, forming two separate phases where only very small amounts of one component are dissolved in the other. As previously stated, the scarce solubility of oil in water can be rationalized in terms of the entropically directed hydrophobic hydration, while the scarce solubility of water in oil can be attributed to the fact that water/water interactions are much stronger than water/oil ones. This allows to predict, in accordance with the experiment, that solubilization of water in oil is an endothermic process[102].

Moreover, in addition to molecular solubilization, also the dispersion as small droplets of oil in water or water in oil is unfavoured as a consequence of the relatively high oil/water interfacial tension (about 52 mNm^{-1}) involving a work ($W = \gamma 4\pi r^2$) of 6.510^{-17} J to form a droplet of one phase in the other of 100 Å. This value is too large with respect to kT (4.110^{-21} J) at room temperature to allow the thermal driven spontaneous dispersion of oil in water or water in oil droplets.

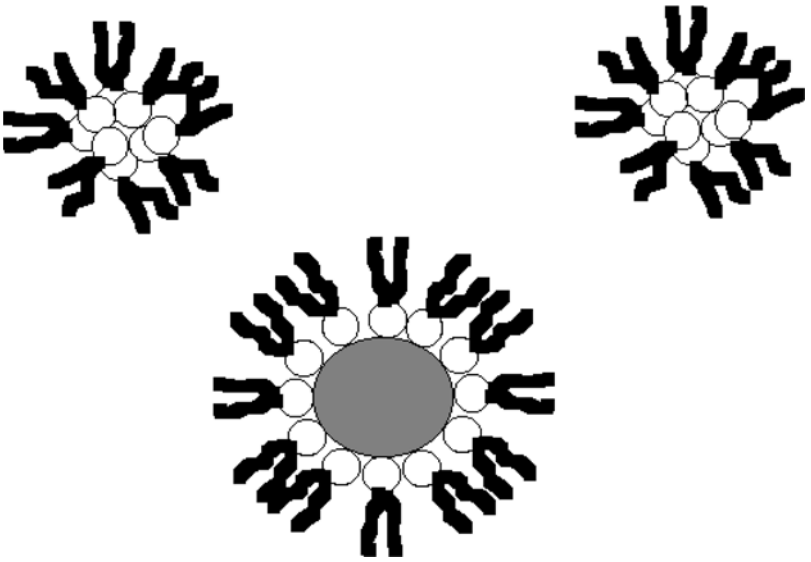

FIGURE 1.35. Nanoparticle stabilized by a reversed micelle.

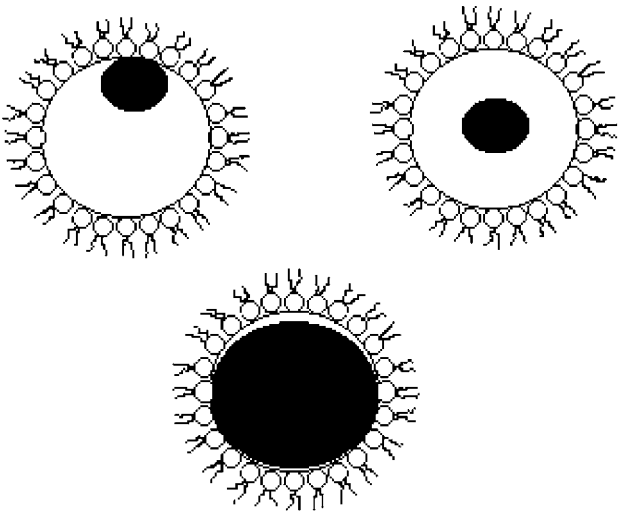

FIGURE 1.36. Possible locations of nanoparticles stabilized by water containing reversed micelles.

Adding a surfactant to the biphasic water/oil system, it can be easily recognized that it will be partitioned between the aqueous and the oil phases. Only a small amount will be located at the water/oil interface forming an oriented monolayer and determining a significant decrease of the interfacial tension[103].

In equilibrium condition and above the critical micellar concentration of the surfactant in both media, it can be predicted that potentially the surfactant forms direct micelles in water solubilizing in its interior the oil and reversed micelles in the oil phase entrapping water. However, according to the surfactant nature, one of the two structures (micelle or reversed micelle) is preferred so that macroscopically it is observed that the volume of one phase increases at the expense of the other. This unequal distribution of surfactant micelles has been widely employed in extraction chemistry. Moreover, these bi-phasic systems have found numerous applications as peculiar reaction media.

In appropriate conditions determined by the surfactant nature and concentration, relative amounts of oil and water, and the presence of suitable cosurfactants, one phase disappears leading to the formation of systems called oil-in-water (o/w) or water-in-oil (w/o) microemulsions. It can be noted that o/w and w/o microemulsions are related to and can be confused with solutions of normal micelles and reversed micelles solubilizing appropriate substances, respectively. However, conceptually the distinguishing element is that in micelles the emphasis is on the surfactant forming the aggregate, while in microemulsions the amount of solubilizates compart-

mentalized in the micellar core constitutes a relevant part of the entire aggregate. Generally, this involves some changes: a greater size, a lower diffusion coefficient, a variation of the interaggregate interactions, and a greater persistence in size and shape of the entire aggregate even if each surfactant molecule retains nearly the same dynamics.

To differentiate microemulsions from solutions of direct or reversed micelles, here is made the quite arbitrary convention that microemulsions are at least quaternary systems composed of significant amounts of water, oil, and more than one surfactant/cosurfactant. The reason of this choice is that, while many ternary mixtures composed of water, oil, and surfactant do not form a monophasic system, the further addition of appropriate amounts of another surfactant or cosurfactant leads to the formation of a thermodynamically stable monophasic one. This involves some subtle effects occurring in the presence of more than one amphiphilic molecules, which can be traced back to a wider spectrum of potential surfactant aggregates characterized by different structure and composition and by a specific contribution to the total free energy of the system.

Microemulsions are thus monophasic liquid systems that are isotropic and homogeneous on a macroscopic scale but heterogeneous on a molecular scale as they are divided into water and oil domains separated by a surfactant monolayer. The typical size of these domains is below the wavelength of visible light and hence these systems appear optically clear. From a molecular point of view, these systems are characterized by the coexistence of spatially separated polar and apolar microregions stabilized by a monolayer of amphiphilic molecules. In the case of water-in-oil (w/o) microemulsions, the water is dispersed in the oil as nanodroplets whereas in the case of oil-in water (o/w) microemulsions, the oil is dispersed as nanodroplets in water. In both cases, a monolayer of opportunely oriented surfactant molecules coating the droplet (diameter 10–100 Å) leads to an ensemble of thermodynamically stable aggregates dispersed in a bulk phase. These two structures are schematically represented in Figs. 1.23 and 1.31.

By assuming spherical aggregates and that all the surfactant molecules are located at the interface, the size (r) of the surfactant-coated water or oil droplets can be roughly estimated by the equation

$$r = \frac{3V_d R}{S_S} + h \tag{1.38}$$

where V_d is the water (oil) molecular volume, S_S the surfactant head group area, R the water (oil) to surfactant molar ratio, and h the surfactant molecule length. Then, the number of aggregates (N_{agg}) can be calculated by

$$N_{agg} = \frac{N_S S_S}{4\pi(r - h)^2} \tag{1.39}$$

where N_{agg} is the number density of surfactant molecules.

In the literature are also described microemulsions characterized by an interconnected network of canalicula of indefinite length, the so-called bicontinuous microemulsions. It is interesting to note, however, that as a consequence of the dynamic processes occurring at the molecular level, the the same system could show different structures when observed at different time or spatial scales. This is because more or less extended structures may be viewed as dynamical entities with a characteristic lifetime τ. On a timescale shorter than τ, the system appears as a collection of minimal entities undergoing independent diffusive motions and for times longer than τ behaves as an interconnected assemblies of minimal entities. This means that the same microemulsions can be seen as a bicontinuous structure or a collection of aggregates depending on the characteristic timescale of the physicochemical property used to study the system[104].

Generally, microemulsions exist as monophasic systems in a limited temperature range. Outside this range, microemulsions separate giving two or more phases whose compositions depend on the nature and relative amounts of the components.

Microemulsions as well as all the other microheterogeneous systems can be used as peculiar solvent and reaction media. A wide variety of apolar, polar, and amphiphilic substances can be solubilized separately or at the same time in these systems. Generally, microemulsions show a solubilizing capability greater than that of micellar solutions. This peculiarity makes microemulsions a sort of effective universal solvent media. According to the nature of the solubilizate, it will be preferentially solubilized in a specific domain of the microemulsions or partitioned among the various microenvironments. On the other hand, the dynamics of these domains and the huge value of the water/oil interface allow frequent encounters among the solubilizate molecules even if they are located in different nanodomains. The kinetics of solubilizate exchange among water droplets of water in oil microemulsions by micellar collision and transient fusion has been widely investigated[52,53,105].

It was observed that the rate constant of the intermicellar exchange of solubilizates entrapped in the inner part of microemulsion droplets is two to four orders of magnitude slower than that corresponding to droplet encounters. This emphasizes the existence of an energy barrier opposing the exchange process. Besides, it increases with temperature, the length of the solvent alkyl chain, the size and the number density of the aqueous droplets, while it decreases by solubilizing inorganic salts in the aqueous droplets.

The maximum amount of solubilizate that can be dissolved in microemulsions depends on its preferential location and specific interactions with surfactant interface[106]. Depending on the amount and/or size of the solubilizate molecules, more or less marked structural changes can be observed. Generally, the solubilization of hydrophilic macromolecules involves micellar swelling and, above specific threshold values (solubilizate concentration, temperature, etc.), structural transitions[107,108].

While small hydrophilic polymers are encapsulated inside the aqueous core of one water/surfactant aggregate, large ones require many aggregates to avoid polar/apolar contacts. This involves the formation of micellar clusters joined together by the polymeric chain[109].

The structural properties of microemulsions make these systems well suited for reactions between polar and non-polar reactants. For these species the reaction occurs at the water/oil interface[110]. For reactants partitioned between the aqueous, oil, and interfacial domains, the reaction rates can be quantitatively described in terms of the separate contributions of each domain[111].

Microemulsions are frequently employed as well-suited media for the synthesis of a wide variety of nanoparticles[112]. The kinetics and mechanism of formation of CdS nanoparticles in water/AOT/n-heptane w/o microemulsions has been investigated[113]. It has been found that the intermicellar exchange process of nanoparticle precursors is the rate determining step and that the total concentration of nanoparticles (c_t) can be modeled by the equation

$$c_t = \frac{c_0}{1 + k_{ex} c_0 t} \tag{1.40}$$

where c_0 is the initial concentration of nanoparticle precursor and k_{ex} the rate constant of the intermicellar precursor exchange. Moreover, the concentration of nanoparticles constituted by N precursor monomers is given by

$$c_N = \frac{c_0 (k_{ex} c_0 t)^{N-1}}{(1 + k_{ex} c_0 t)^{N+1}} \tag{1.41}$$

and the mean number ($\bar{N}$) of precursor monomers by

$$\bar{N} = \sum \frac{N c_N}{c_t} = 1 + k_{ex} c_0 t \tag{1.42}$$

1.6.5. Normal and Reversed Vesicles

Surfactant molecules showing a preponderance of the hydrophobic character with respect to the hydrophilic one, i.e., characterized by small head group and/or bulky hydrophobic part (two or more long hydrocarbon chains, branched chains), are sparingly soluble in aqueous solutions and, when dispersed in water, they tend to associate as multilamellar or unilamellar vesicles. Surfactants able to form vesicles show very small cmc (of the order 10^{-5} M or lower) in contrast with the cmc of many micelle forming surfactants (of the order 10^{-2} M). The low cmc reflects the poor water solubility of the vesicle-forming surfactant and it indicates very low exchange rate of the surfactant between the aggregate and the surrounding medium, long mean lifetime of the surfactant molecules in the bilayer, and

marked kinetic stability of vesicles. The stability and permeability of vesicles can also be improved using functionalised surfactants able to polymerise, forming intermolecular covalent bonds.

Multilammellar vesicles are constituted by closed surfactant bilayers spaced by aqueous layers, whereas unilamellar ones are constituted by only one aqueous domain entrapped inside a closed bilayer. In the case of some bipolar surfactants, vesicles constituted by a closed monolayer dispersed in water can also be obtained. Typical size and aggregation number of unilamellar vesicles are 50–200 nm and 10^4-10^5 monomers. A schematic representation of these structures is shown in Fig. 1.37.

Formation of vesicles is preferred with respect to micelles because the higher curvature radius allows a better accommodation of surfactant molecules while they are preferred with respect to extended bilayers because of the closed structure that avoids the existence of hydrophobic sides contacting water and of the greater mixing entropy associated with smaller structures. On the other hand, the formation of a closed structure involves the establishing of a mean curvature that can be more or less unfavourable from the energetic point of view.

According to the general structural symmetry existing among the surfactant aggregates, in addition to direct vesicles, it is also possible to realize dispersions of reversed vesicles in apolar solvents[114]. A schematic representation of a dispersion of reversed vesicles in oil is shown in Fig. 1.38.

In this case, the surfactant molecules are oriented so that the hydrophilic groups are in contact and the alkyl chains protrude in the oil phase.

Reversed vesicles are preferentially formed by hydrophilic surfactants with appropriate geometric packing parameters. They are consequently slightly soluble in apolar media and characterized by surfactant/surfactant interactions larger than surfactant/apolar solvent ones.

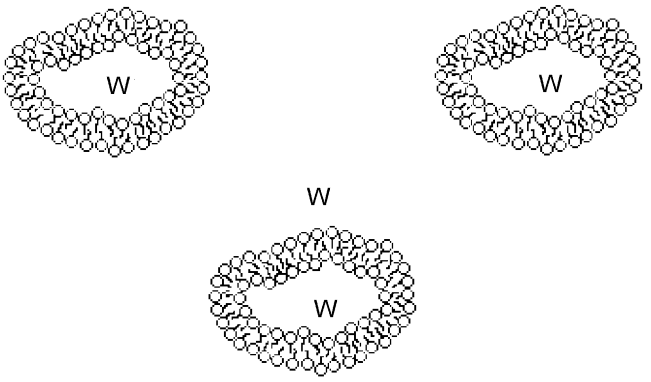

FIGURE 1.37. Schematic representation of unilamellar vesicles dispersed in water.

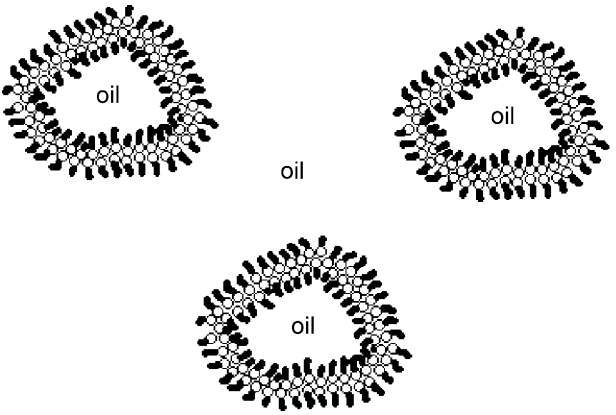

FIGURE 1.38. Schematic representation of a dispersion of reversed vesicles in oil.

Direct and reversed multilamellar vesicles can be prepared by mixing the components (surfactant, cosurfactant, and water or apolar solvent) in the appropriate composition or by the injection of an appropriate surfactant solution through a syringe equipped with a small hole needle. Heating of the mixture and the use of a low-power ultrasound bath generally allow the complete mixing of the components in a few minutes. Sonication is generally employed because it allows to overcome the activation energy barrier needed to transform extended bilayers in vesicles. The resulting dispersions appear quite cloudy as a consequence of the significant light scattering due to the vesicles with a mean size comparable with the visible light wavelength.

Dispersions of unilamellar vesicles are usually obtained using a high-power ultrasound bath and, being of smaller size, they appear clear with bluish reflections. Another method to prepare vesicle dispersion is based on the removal of the hydrophilic surfactant from an aqueous solution of mixed micelles constituted together with a lipophilic surfactant. The removal of the hydrophilic surfactant can be accomplished by dialysis.

By applying shear to lamellar structures in controlled conditions, surfactant reorganization into a new phase constituted by multilamellar vesicles (200–1000 nm), called onions or spherulites, is obtained[8]. Spherulites are dense multilamellar aggregates that can solubilize both hydrophilic and hydrophobic substances and for this reason have found many extended applications as drug-carriers and encapsulating systems.

Normal vesicles using dihexadecylphosphate or dioctadecyldimethyl ammonium chloride (DODAC) showing size in the range 150–300 nm can be formed in aqueous solutions. Particular mention must be devoted to phospholipid-based vesicles, also called liposomes, because they are of great interest being both biocompatible and stable in physiological environments. In living organisms, liposomes direct the synthesis (biomineralization) and

transport of inorganic crystals with controlled size, shape, and structure. Innovative uses of these aggregates as biomimetic systems, drug-carriers, and nanoparticle templates have been widely exploited.

Mixed unilamellar vesicles in water can be spontaneously formed by mixing two micellar solutions containing cetyltrimethylammonium bromide and dodecylbenzenesulfonic acid, respectively[115].

Distinctive properties of vesicles are their fluidity and selective permeability. These properties reflect the intermolecular interactions governing the aggregate stability and the thermally activated molecular dynamics. The vesicle dynamics is characterized by translational and rotational movements, thermally driven shape fluctuations, the lateral diffusion of surfactant molecules within the layer, and exchanges of surfactant molecules between the two leaflets of the bilayer (flip-flop). Other properties changing within specific timescales are bilayer local composition and density and membrane asymmetry. Exchanges of surfactant molecules with the surrounding medium are generally excluded as a consequence of its very low solubility in the bulk solvent, while flip-flops are rare due to the high energy barrier of the involved mechanism. Other important processes determined by vesicle dynamics are their breaking in smaller aggregates and their fusion in larger aggregates.

The thermodynamic stability of solutions of vesicles has been questioned. This because, in general, vesicles do not form spontaneously, requiring the input of energy, and that often solutions of vesicles show with time some changes[116]. It has been suggested that the existence of repulsive forces such as those arising from a net charge or a double layer could contribute to the stability of vesicle dispersions[117].

Depending on the specific permeability of the surfactant bilayer toward the species present in the system, concentration gradients between vesicle-entrapped and bulk water of the less diffusible species can be realized. The typical characteristic time for the transport of water molecules across the bilayer is of the order seconds while for large molecules it can be hours or more. This selective permeability, similar to that of semipermeable membranes, allows the achievement for several hours of an internal pH or ionic strength different from the exterior or the occurrence of a reaction only inside the aggregate. Also, vesicle strinkage or swelling can be determined in the case of an osmolarity gradient between the interior and the external parts.

1.6.5.1. Solubilization in Dispersions of Normal and Reversed Vesicles

Looking to the typical structure of vesicles, some different solubilization sites can be devised (see Fig. 1.39)

- the vesicle interior
- the hydrophilic domains constituted by the hydrated surfactant head groups on both sides of the bilayer
- the hydrophobic domain constituted by the surfactant tails

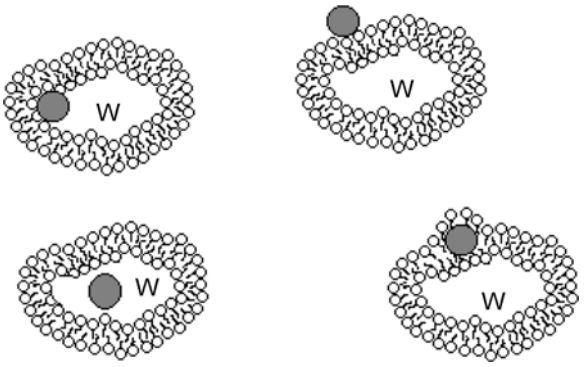

FIGURE 1.39. Solubilization sites of hydrophilic substances in aqueous vesicles.

- the so-called palisade layer, i.e., the domain between the surfactant head groups and the first carbon atoms of the alkyl chain
- the external medium

Hydrophilic substances are potentially solubilized in the i, ii, and v domains, hydrophobic molecules in the iii domain, and amphiphilic are preferentially located opportunely oriented in the iv domain[118].

While hydrophilic and hydrophobic molecules are almost entirely located in well-defined domains, the location of amphiphilic molecules is generally described as a partition equilibrium among all the possible sites. It is worth noting that, in the case of hydrophilic species showing large characteristic time of transport across the bilayer and depending on the preparation procedure of the system, it is possible to realize vesicle dispersions where the solubilizate is present both inside and ouside the vesicles, only outside or only inside. These conditions can be realized, i) by dissolving the solubilizate in the aqueous medium before the surfactant dispersion, ii) performing the solubilization of the hydrophilic molecules in the vesicle dispersion previously prepared, iii) starting from the solubilizate/vesicle/water system where the hydrophilic species is located both inside and outside the vesicles and removing the molecules located externally by dialysis.

Depending on the nature of the solubilizate and the solubilizate/surfactant molar ratio, more or less extended modification of the vesicle structure and dynamics can be expected. For example, the bilayer rigidity can be significantly increased by adding cholesterol. These changes could be more marked when nanoparticles are entrapped by vesicles.

1.6.5.2. Reaction Rates and Mechanisms in Dispersions of Normal and Reversed Vesicles

Reaction rates, mechanisms, and stereochemistry can be strongly influenced by the presence of vesicles[14]. In addition, these effects are critically depen-

dent on structure and dynamics. The main factor that must be taken into account is that a solution containing vesicles is characterized, potentially, by different reaction sites (the inner vesicular core, the internal water/surfactant head groups interface, the hydrophobic domain constituted by the quite ordered surfactant alkyl chains, the external water/surfactant head groups interface, and the external aqueous medium). The following step is the knowledge of the locations of substrates, their portioning among the various sites, and their diffusion rates among the various sites. This allows the determination of the local concentrations of all the substrates at the equilibrium and during the reaction. Because there is not a theory able to predict the reaction rate in each site, this information can be obtained by an analysis of experimental kinetic data through a suitable model that takes into account local substrate concentrations.

Following this strategy, many investigations have been carried out showing that rate changes can be mainly attributed to variations of local concentrations and of the substrate reactivity. As an example, measuring the rate of alkaline hydrolysis and thiolysis of p-nitrophenyl octanoate in aqueous dispersions of vesicles, a dependence on the vesicle size attributable to differences in ion dissociation, substrate binding constants, and intrinsic reactivities was observed[119].

Vesicles can play the role of nanoreactors where nanoparticles can be synthesized through appropriate reactions providing size and shape limits to their growth, of nanocontainers able to improve their time and chemical stability, and/or of nanocarriers to allow their transport. The closed structure of vesicles provides a means to control the precursor concentrations inside and outside the vesicles thus influencing the nucleation and growth of nanoparticles and representing an obstacle to particle agglomeration. In turn, this involves a control of the particle size and distribution. The internal vesicle wall could also influence the nucleation and growth rates.

REFERENCES

1. G. Zandomenighi, P. L. Luisi, L. Mannina, A. Segrè, *Helvetica Chimica Acta* **84**, 3710–3725 (2001)
2. N. Aydogan, N. L. Abbott, *J. Coll. Interf. Sci*., **242**, 411–418 (2001)
3. J. N. Israelachvili, D. J. Mitchell, BW Ninham, *J. Chem. Soc. Faraday Trans II*, **72**, 1525–1567 (1976)
4. D. J. Mitchell, B. W. Ninham, *J. Chem. Soc. Faraday Trans II* **77**, 601–629 (1981)
5. H. Hoffman, G. Ebert, *Angew. Chem. Int. Ed. Engl.* **27**, 902–912 (1988)
6. R. Karlsson, M. Karlsson, A. Karlsson, A. S. Cans, J. Bergenholtz, B. Akerman, A. G. Ewing, M. Voinova, O. Orwar, *Langmuir* **18**, 4186–4190 (2002)
7. A. Karlsson, M. Karlsson, R. Karlsson, K. Sott, A. Lundqvist, M. Tokacz, O. Orwar, *Anal. Chem*. **75**, 2529–2537 (2003)
8. F. Gauffre, D. Roux, *Langmuir* **15**, 3738–3747 (1999)
9. H. Liu, Y. Ni, F. Wang, G. Ying, J. Hong, Q. Ma, Z. Xu, *Colloids and Surfaces A* **235**, 79–82 (2004)

10. F. Runge, W. Rohl, J. H. Spilgies, G. Ilgenfritz, *Ber. Bunsenges. Phys. Chem*. **95**, 485–490 (1991)
11. F. Runge, L. Schlicht, J. H. Spilgies, G. Ilgenfritz, *Ber. Bunsenges. Phys. Chem*. **98**, 506–508 (1994)
12. Y. A. Shchipunov, T. Durrschmidt, H. Hoffmann, *Langmuir* **16**, 297–299 (2000)
13. R. De Lisi, C. Genova, V. Turco Liveri, *J. Coll. Int. Sci*. **95**, 428–434 (1983)
14. G. Savelli, R. Germani, L. Brinchi, *Reactions and Synthesis in Surfactant Systems*, (Ed J. Texter, Marcel Dekker Inc, NY, 2001) pp. 175–246
15. A Ruggirello, V Turco Liveri, *Chemical Physics* **288**, 187–195 (2003)
16. G. Giammona, F. Goffredi, V Turco Liveri, G. Vassallo, *J. Coll. Int. Sci*. **154**, 411–415 (1992)
17. A. T. Terpko, R. J. Serafin, M. L. Bucholtz, *J. Coll. Int. Sci*. **84**, 202–205 (1981)
18. R. F. Khairutdinov, N. Serpone, *Progr. Reaction Kinetics* **21**, 1–68 (1996)
19. F. P. Cavasino, C. Sbriziolo, M. L. Turco Liveri, V. Turco Liveri, *J. Chem. Soc. Faraday Trans* **90**, 311–314 (1994)
20. G. A. Jeffrey, H. Maluszynka, *Acta Cryst. B* **45**, 447–452 (1989)
21. A. Mueller-Fahrnow, V. Zabel, M. Steifa, R. Hilgenfeld, *J. Chem. Soc. Chem. Comm*. **198**, 1573–1574 (1986)
22. X. Auvray, T. Perche, R. Anthore, C. Petipas, I. Rico, A. Lattes, *Langmuir* **7**, 2385–2393 (1991)
23. D. J. Mitchell, G. J. T. Tiddy, L. Waring, T. Bostock, M. P. McDonald, *J. Chem. Soc. Faraday Trans. I* **79**, 975–1000 (1983)
24. E. Caponetti, P. D'Angelo, L. Pedone, V. Turco Liveri, *J. Chem. Phys*. **113**, 8783–8790 (2000)
25. P. Ekwall, l. Mandell, K. Fontell, *J. Coll. Int. Sci*. **33**, 215–235 (1970)
26. A. Kumar, H. Kuneida, C. Vazquez, M.A. Lopez-Quintela, *Langmuir* **17**, 7245–7250 (2001)
27. S. Puvvada, S. Baral, G. M. Chow, S. B. Qadri, B. R. Ratna, *J. Am. Chem. Soc*. **116**, 2135–2136 (1994)
28. P. Lang, *J. Phys. Chem. B* **103**, 5100–5105 (1999)
29. N. Filipovic-Vincekovic, V. Tomasic, *Thermal Behavior of Dispersed Systems*, (Ed N. Garti, Marcel Dekker Inc, NY, 2001) pp. 451–476
30. P. Calandra, A. Longo, V. Turco Liveri, *J Phys Chem B* **107**, 25–30 (2003)
31. P. T. Spicer, K. L. Hayden, M. L. Lynch, A. Afori-Boateng, J. L. Burns, *Langmuir* **17**, 5748–5756 (2001)
32. E. Caponetti, D. Chillura-Martino, F. Ferrante, L. Pedone, A. Ruggirello, V. Turco Liveri, *Langmuir* **19**, 4913–4922 (2003)
33. M. P. Pileni, *J. Phys. Chem*. **97**, 6961–6973 (1997)
34. G. S. Attard, P. N. Bartlett, N. R. B. Coleman, J. M. Elliot, J. R. Owen, *Langmuir* **14**, 7340–7242 (1998)
35. M. H. Ropers, M. J. Stebe, *Langmuir* **19**, 3137–3144 (2003)
36. J. Barauskas, T. Landh, *Langmuir* **19**, 9562–9565 (2003)
37. Y. Sasanuma, F. Nishimura, H. Wakabayashi, A. Suzuki, *Langmuir* **20**, 665–672 (2004)
38. D. P. Acharya, H. Kuneida, Y. Shiba, K. Aratani, *J. Phys. Chem. B* **108**, 1790–1797 (2004)
39. R. Tang, C. Jiang, Z. Tai, *J Chem Soc Faraday Trans* **93**, 3371–3375 (1997)
40. Z. Tang, E. Wang, *J. of Electroanalytical Chemistry* **496**, 82–87 (2001)

41. F. Y. Lo, B. M. Escott, E. J. Fendler, E. T. Adams, R. D. Larsen, P. W. Smith, *J. Phys. Chem.* **79**, 2609–2621 (1975)
42. D. Lichtenberg, E. Opatowski, M. M. Kozlov, in: *Thermal Behavior of Dispersed Systems*, edited by N. Garti, (Marcel Dekker, N.Y., 2001), vol. 93, pp. 295–334.
43. M. Goffredi, V. Turco Liveri, G. Vassallo, *J Solution Chemistry* **22**, 941–949 (1993)
44. V. Turco Liveri, In *Nanosurface Chemistry*, Ed M Rosoff, M Dekker, NY, pp. 473–504 (2002)
45. A. D'Aprano, G. D'Arrigo, A. Paparelli, M. Goffredi, V. Turco Liveri, *J. Phys. Chem.* **97**, 3614–3618 (1993)
46. M. Goffredi, V. Turco Liveri, *J. Solution Chem.* **22**, 941–949 (1993)
47. V. Arcoleo, M. Goffredi, V. Turco Liveri, *J. Solution Chem.* **24**, 1135–1142 (1995)
48. F. Goffredi, V. Turco Liveri, G. Vassallo, *J. Coll. Int. Sci.* **151**, 396–401 (1992)
49. F. Aliotta, M. E. Fontanella, G. Squadrito, P. Migliardo, G. La Manna, V. Turco Liveri, *J. Phys. Chem.* **97**, 6541–6545 (1993)
50. V. Arcoleo, F. Aliotta, M. Goffredi, G. La Manna, V. Turco Liveri, *Materials and Engineering C* **5**, 47–53 (1997)
51. R. De Lisi, V. Turco Liveri, *Gazzetta Chimica Italiana*, **113**, 371–379 (1983)
52. P. D. I. Fletcher, A. M. Howe, B. H. Robinson, *J. Chem. Soc. Faraday Trans. I* **83**, 985–1006 (1987)
53. J. Lang, A. Jada, A. Malliaris, *J. Phys. Chem.* **92**, 1946–1953 (1988)
54. P.D.I. Fletcher, B. H. Robinson, *Ber. Bunsenges. Phys. Chem.* **85**, 863–867 (1981)
55. H. Tanaka, I. Ohmine, *J. Chem. Phys.* **87**, 6128–6139 (1987)
56. I. Ohmine, H. Tanaka, P. G. Wolynes, *J. Chem. Phys.* **89**, 5852–5860 (1988)
57. C. J. Montrose, J. A. Bucaro, J. Marshall-Coakley, T. A. Litivitz *J. Chem. Phys.* **60**, 5025–5029 (1974)
58. H. Hoffmann, G. Platz, W. Ulbricht, *Ber. Bunsenges. Phys. Chem.* **90**, 877–887 (1986)
59. H. Sasaki, S. Fukuzawa, J. Kikuchi, S Yokoyama, H. Hirota, K. Tachibana, *Langmuir* **19**, 9841–9844 (2003)
60. R. De Lisi, A. Lizzio, S. Milioto, V. Turco Liveri, *J. Solution Chem.* **15**, 623–648 (1986)
61. M. Abu-Hamdiyyah, K. Kumari, *J. Phys. Chem.* **94**, 2518–2523 (1990)
62. R. H. Kore, J. S. Kulkarni, S. K. Haram, *Chem. Mater.* **13**, 1789–1793 (2001)
63. S. Nave, J. Eastoe, R. K. Heenan, D. Steytler, I. Grillo, *Langmuir* **18**, 1505–1510 (2002)
64. H. F. Eicke in F. L. Boschke, ed. *Topics in Current Chemistry*, vol 87. New York: Springer-Verlag, 1980, pp. 85–145
65. M. Wong, J. K. Thomas, T. Novak, *J. Am. Chem. Soc.* **99**, 4730–4736 (1977)
66. F. Heatley, *J. Chem. Soc. Faraday Trans. I* **83**, 517–526 (1987)
67. J. Eastoe, T. F. Towey, B. H. Robinson, J. Williams, R. H. Heenan, *J. Phys. Chem.* **97**, 1459–1463 (1993)
68. J. Eastoe, D. C. Steyler, B. H. Robinson, R. H. Heenan, A. N. North, J. C. Dore, *J. Chem. Soc. Faraday Trans. I* **90**, 2479–2505 (1994)
69. F. Aliotta, M. E. Fontanella, M. Sacchi, C. Vasi, G. La Manna, V. Turco Liveri, *J. of Molecular Structure* **383**, 99–106 (1996)
70. J. Eastoe, R. K. Heenan, *J. Chem. Soc. Faraday Trans. I* **90**, 487–492 (1994)
71. A. Merdas, M. Gindre, R. Ober, C. Nicot, W. Urbach, M. Waks, *J. Phys. Chem.* **100**, 15180–15186 (1996)

72. Q. Li, S. Weng, J. Wu, N. Zhou, *J. Phys. Chem.* **102**, 3168–3174 (1998)
73. P. L. Luisi, L. J. Magid, *CRC Critical Review in Biochemistry* **20**, 4091–4174, 1986
74. Y. X. Chen, X. Z. Zhang, S. M. Chen, D. L. You, X. X. Wu, X. C. Yang, W. Z. Guan, *Enzyme Microbial Techn.* **25**, 310–315 (1999)
75. X. Xu, M. Ayyagari, M. Tata, V. T. John, G. L. McPherson, *J. Phys. Chem.* **97**, 11350–11353 (1993)
76. M. Tata, V.T John, Y. Y. Waguespack, G. L. McPherson, *J. Mol. Liq.* **72**, 121–135 (1997)
77. Y. Y. Waguespack, S. Banerjee, P. Ramannair, G. C. Irvin, V. T. John, G. L. McPherson, *Langmuir* **16**, 3036–3041 (2000)
78. P. L. Luisi, R. Scartazzini, G. Hearing, P. Schurtenberger, *Coll. Polym. Sci.* **268**, 356–374 (1990)
79. P. D. I. Fletcher, M. F. Galal, B. H. Robinson, *J. Chem. Soc. Faraday Trans. I* **80**, 3307–3314 (1984)
80. G. Calvaruso, A. Minore, V. Turco Liveri, *J. Colloid Int. Sci.* **243**, 227–232 (2001)
81. V. Marcianò, A. Minore, V. Turco Liveri, *Colloid Polym. Sci.* **278**, 250–252 (2000)
82. P. Calandra, A. Longo, V. Turco Liveri, *Colloid Polymer Science* **279**, 1112–1117 (2001)
83. X. Li, X. Quan, C. Kutal, *Scripta Materalia* **50**, 499–505 (2004)
84. L. J. Schwartz, C. L. DeCiantis, S. Chapman, B. K. Kelley, J. P. Hornak, *Langmuir* **15**, 5461–5466 (1999)
85. A. D'Aprano, A. Lizzio, V. Turco Liveri, *J. Phys. Chem.* **92**, 1985–1987 (1988)
86. A. D'Aprano, G. D'Arrigo, M. Goffredi, A. Paparelli, V. Turco Liveri, *J. Chem. Phys.* **95**, 1304–1309 (1991)
87. B. H. Robinson, C. Toprakcioglu, J. C. Dore, *J. Chem. Soc. Faraday Trans. I* **80**, 13–27 (1984)
88. P. D. I. Fletcher, D.I. Horsup, *J. Chem. Soc. Faraday Trans.* **88**, 855–864 (1992)
89. L. J. Magid, K. Kon-no, C.A. Martin, *J. Phys. Chem.* **85**, 1434–1439 (1981)
90. A. D'Aprano, I. D. Donato, F. Pinio, V. Turco Liveri, *J. Solution Chem.* **18**, 949–955 (1989)
91. A. D'Aprano, I. D. Donato, F. Pinio, V. Turco Liveri, *J. Solution Chem.* **19**, 589–595 (1990)
92. J. J. Silber, A. Biasutti, E. Abuin, E. Lissi, *Advances in Colloid and Interface Science* **82**, 189–252 (1999)
93. S. Barbaric, P. L. Luisi, *J. Am. Chem. Soc.* **103**, 4239–4244 (1981)
94. E. Ruckenstein, P. Karpe, *J. Phys. Chem.* **95**, 4869–4882 (1991)
95. A. S. Bommarius, J. F. Holzwarth, D. I. C. Wang, T. A. Hatton, *J. Phys. Chem.* **94**, 7232–7239 (1990)
96. P. L. Luisi, M. Giomini, M. P. Pileni, B. H. Robinson, *Biochimica Biophysica Acta* **947**, 209–246 (1988)
97. C. Gomez-Herrera, M. Del Mar Graciani, E. Munoz, M. L. Moya, F. Sanchez, *J. Coll. Int. Sci.* **141**, 454–458 (1991)
98. R. Kubik, H. F. Eicke, *Helvetica Chimica Acta* **65**, 170–177 (1982)
99. K. Osseo-Asare, F. J. Arriagada, *J. Coll. Int. Sci.* **218**, 68–76 (1999)
100. R. Zhang, J. Liu, B. Han, Z. He, Z. Liu, J. Zhang, *Langmuir* **19**, 8611–8614 (2003)

101. U. Natarajan, K. Handique, A. Mehara, J. R. Bellare, K. C. Khilar, *Langmuir* **12**, 2670–2678 (1996)
102. R. De Lisi, M. Goffredi, V. Turco Liveri, *J. Chem. Soc. Faraday Trans. I* **76**, 1660–1662 (1980)
103. R. Aveyard, B.P. Binks, S. Clark, P. D. I. Fletcher, *J. Chem. Soc. Faraday Trans*. **86**, 3111–3115 (1990)
104. V. Turco Liveri, *Current Topics in Solution Chemistry* **2**, 143–156 (1997)
105. A. M. Howe, J. A. McDonald, B. H. Robinson, *J. Chem. Soc. Faraday Trans. I* **83**, 1007–1027 (1987)
106. J. Yano, H. Furedi-Milhofer, E. Wachtel, N. Garti, *Langmuir* **16**, 9996–10004 (2000)
107. M. J. Suarez, H. Levy, J. Lang, *J. Phys. Chem*. **97**, 9808–9816 (1993)
108. F. Aliotta, V. Arcoleo, G. La Manna, V. Turco Liveri, *Coll. Polym. Sci*. **274**, 989–994 (1996)
109. C. A. T. Laia, W. Brown, M. Almgren, S. M. Costa, *Langmuir* **16**, 465–470 (2000)
110. R. Schomaker, K. Stickdorn, W. Knoche, *J. Chem. Soc. Faraday Trans*. **87**, 847–851 (1991)
111. L. Garcia-Rio, J. R. Leis, J. C. Mejuto, *J. Phys. Chem*. **100**, 10981–10988 (1996)
112. S. Li, G. C. Irvin, B. Simmons, S. Rachakonda, P. Ramannair, S. Banerjee, V. T. John, C. L. McPherson, W. Zhou, A. Bose, *Colloid and Surfaces A* **174**, 275–281 (2000)
113. T. F. Towey, A. Khan-Lodhi, B. H. Robinson, *J. Chem. Soc. Faraday Trans*. **86**, 3757–3762 (1990)
114. H. Kuneida, V. Rajagopalan, In *Vesicles*, M Rosoff, ed.. New York: Marcel Dekker 1996, pp. 79–103
115. I. I. Yacobi, A. C. Nunes, A. Bose, *J. Coll. Inter. Sci*. **171**, 73–84 (1995)
116. D. D. Lasic, *J. Coll. Int. Sci*. **140**, 302–304 (1990)
117. H. Matsumura, T. Kuwamura, K. Furusawa, *J. Coll. Int. Sci*. **139**, 331–336 (1990)
118. E. Lasonder, W. D. Weriga, *J. Coll. Int. Sci*. **139**, 469–478 (1990)
119. M. K. Kuwamuro, H. Chaimovich, E. B. Abuin, E. A. Lissi, I. M. Cuccovia, *J. Phys. Chem*. **95**, 1458–1463 (1991)

2

Nucleation, Growth, and Arrested Growth in Confined Space

2.1 Introduction

The separation of solid phases from liquid ones is a very old practice and, at present, it represents a pivotal step involved in many industrial processes. The optimization of this step is of utmost importance both for the quality of the final product, environmental impact, and economic reasons. To achieve this goal, a wide range of experimental procedures and a framework of theoretical principles have been exploited. The notions of solubility, solubility product, the common ion effect, homogeneous and heterogeneous nucleation, crystal growth, precipitation and coprecipitation, crystallization, saturation, supersaturation, and filtration are normally learned in elementary courses of physical chemistry. The thermodynamic, kinetic, and statistical aspects of nucleation, crystallization (slow separation from a liquid phase of a solid compound characterized by relatively high solubility), and precipitation (fast separation of a solid with small solubility) have been well established as well as the effects of temperature, pressure, and additives.

For completeness, it is worth remembering that, in addition to those occurring in liquid systems, some important processes involving nucleation and crystal growth are performed in various other environments such as vapour phases, glass matrices, alloys, solid surfaces, and interfaces. In addition to the same general criteria, the development of specific treatments is required for the analysis of these phenomena.

Generally, the main requisites requested to a suitable precipitation protocol in liquid phase are the purity and the recovery of the highest fraction of the total amount of the product. Moreover, this process often occurs in homogeneous liquid media. Only seldom the crystallization or precipitation are performed in microheterogeneous fluid systems, and the control of the crystal geometrical parameters is needed. However, the recent interest to synthesize nanoparticles by bottom-up chemical methods in confined space has given rise to the exigency to develop appropriate theoretical principles and experimental methodologies allowing the rationale control of their mean size and shape, polydispersity,

and structure. Obviously, the knowledge of the mechanisms controlling the formation and stability of nanoparticles in surfactant-containing systems and of those opposing their unlimited growth is of utmost importance to plan a successful synthetic route. With this aim, here will be presented a thermodynamic and kinetic treatment allowing to put into evidence the phenomena involving significant deviations with respect to precipitation in homogeneous systems and the processes underlying the formation, growth, and arrested growth of nanoparticles.

2.1.1. Thermodynamic Considerations

The thermodynamic stability of a substance A in a solution with respect to the pure crystalline solid phase depends on the difference ($\Delta\mu$) between the chemical potential (μ_A) of A in both phases

$$\Delta\mu = \mu_{A,\ \text{solid}} - \mu_{A,\ \text{solution}} = RT \ln \frac{a_{A,\ \text{sat solution}}}{a_{A,\ \text{solution}}} \qquad 2.1$$

If $\Delta\mu > 0$, i.e., if the activity of species A in the saturated solution ($a_{A,\ \text{sat solution}}$) in equilibrium with A pure is greater than that in the actual solution ($a_{A,\ \text{solution}}$), the substance will stay entirely and molecularly dispersed in the liquid phase. Moreover, the system will be monophasic and thermodynamically stable. On the other hand, if $\Delta\mu < 0$, a part of A will form a solid phase moving from the solution to the solid phase until $\Delta\mu = 0$ and a condition of dynamic equilibrium between A in liquid and solid phases is realized. Given these properties, $\Delta\mu$ is also called the driving force for crystallization. Taking into account the relationship between activity, concentration (C), and activity coefficient (γ), the above equation can be rewritten as

$$\Delta\mu = RT \ln \frac{C_{A,\ \text{sat solution}}\gamma_{A,\ \text{sat solution}}}{C_{A,\ \text{solution}}\gamma_{A,\ \text{solution}}} = -RT \ln \frac{S\gamma_{A,\ \text{solution}}}{\gamma_{A,\ \text{sat solution}}} \qquad 2.2$$

where S ($S = \frac{C_{A,\ \text{solution}}}{C_{A,\ \text{sat solution}}}$) is the supersaturation ratio.

For sparingly soluble solutes, $\Delta\mu$ is related to the molar enthalpy (ΔH) and entropy (ΔS) of its transfer from the liquid to the solid phase by the equation

$$\Delta\mu = \Delta H - T\Delta S \qquad 2.3$$

This equation emphasizes the interplay of energetic and entropic terms as controlling factors of the crystallization process.

Other thermodynamic equations allow to predict the temperature and pressure dependence of $\Delta\mu$. Besides, thermodynamics furnishes the relationships between $\Delta\mu$ and the solubility of ionic and non-ionic solutes

through the knowledge of their activity coefficients in solid and liquid phases. The treatment of these aspects is quite cumbersome and out of the aims of the present book; for these reasons, the reference to standard physical chemistry textbooks is suggested.

These considerations can be formally extended to microheterogeneous systems taking into account that, at equilibrium, the chemical potential of species A in the various microenvironments marked by greek letters is equal ($\mu_{A,\alpha} = \mu_{A,\beta} =$ etc). Then, each microenvironment can be treated as a homogeneous system with the provision that the local concentration of the solute is generally different from the overall.

It is worth noting that, frequently, it occurs that the solute is practically solubilized only in a specific microdomain of the microheterogeneous system. In this case, the local concentration can be easily calculated from the overall without the need of the knowledge of distribution constants.

It must also be stressed that, due to specific and confinement effects, the solubility of species A in each domain of microheterogeneous systems can be found to be strongly different from that in bulk media, involving that the supersaturation value as well as all the thermodynamic parameters are different from those in homogeneous phase. Such consideration has important consequences on the thermodynamics and kinetics of nanoparticle formation in confined space. However, apart from direct experimental measurements, little help has been furnished by theory[1].

This is all that thermodynamics is capable to predict both for homogeneous and microheterogeneous systems. Further considerations require kinetic arguments.

2.1.2. Kinetic Considerations

Generally, above the solubility limit, precipitation/crystallization happens very quickly in the presence of a solid phase constituted by the same (secondary nucleation) or different substance (heterogeneous nucleation). The presence of a solid phase contacting the solution offers, in fact, sites and/or a surface on which A molecules could nucleate and grow. In this case, the factors controlling the rate of the process are i) the arrival of the species to the surface of the solid phase and vice versa by thermal diffusion, convection currents, or mechanical agitation, ii) the area and the nature of the solid phase exposed to the solution, and iii) the incorporation rate of the precursors to the crystal lattice. The incorporation step includes the adsorption of the precursors, the partial release of solvating species, and the effective entrapment into the lattice. Generally, a more or less marked preference to be entrapped into certain crystal faces leading to anisotropic morphologies is observed.

However, in the case of homogeneous nucleation, i.e., in absence of a preexisting solid phase, for statistical reasons the formation of that phase could not occur, and the liquid system will be described as kinetically stable. This because the formation of the crystalline phase is a multistep process requir-

ing the building up of molecular aggregates of increasing size according to the scheme:

$$A_{N-1} + A \leftrightarrows A_N$$

and/or through agglomeration processes:

$$A_i + A_j \leftrightarrows A_{i+j}$$

At the molecular level, the driving force of these processes is the Brownian diffusion of species allowing their haphazard encounters.

For this reason, the thermodynamic property that must be considered to know if the solid phase will be really formed or not from molecular or ionic precursors is the free energy of formation of a nucleus constituted by N molecules, ΔG_f, given by:

$$\Delta G_f = N\Delta\mu + \Delta G_S \qquad 2.4$$

This equation is constituted by the term $N\Delta\mu = NkT \ln \frac{a_{A,\text{ sat solution}}}{a_{A,\text{ solution}}}$, which takes into account the thermodynamic driving force for the aggregate formation, and another one, ΔG_S, due to the formation of an interface between the aggregate and the surroundings. This last term is given by

$$\Delta G_s = A_N \gamma_s \qquad 2.5$$

where A_N is the aggregate surface ($A_N = K_N N^{2/3}$) and γ_s is the interfacial energy per unit surface.

From a molecular point of view, the interfacial energy ΔG_s measures nothing more than the difference in the energetic state between species located in the surface and in the particle interior. This quantity must be necessarily positive, i.e., the energetic state of a species at the surface should be higher than that in the bulk, otherwise the interface would increase indefinitely leading to a molecular dispersion of the substance in the solution. In fact, while the time average of the resultant of all the forces acting on the molecules is zero independently if they are in the bulk or in the surface, the number and strength of chemical bonds formed by bulk species is larger than that of surface ones. This is the reason of the higher energy of surface species and that small-size crystallites (embryos) are thermodynamically unstable against an unlimited growth.

Here, for simplicity, only two states have been taken into account (surface and bulk species). However, it must be considered that, when two phases are in contact, an interfacial and not well-defined domain where the properties change proceeding from one region to the other is generated. This implies the existence of more than two states of species A in the particle.

For super-saturated solutions ($a_{A,\text{ solution}} > a_{A,\text{ sat solution}}$), the first term is negative while the second is always positive. In such circumstances, the typical dependence of these contributions and of ΔG_f upon the aggregation number N is shown in Fig. 2.1.

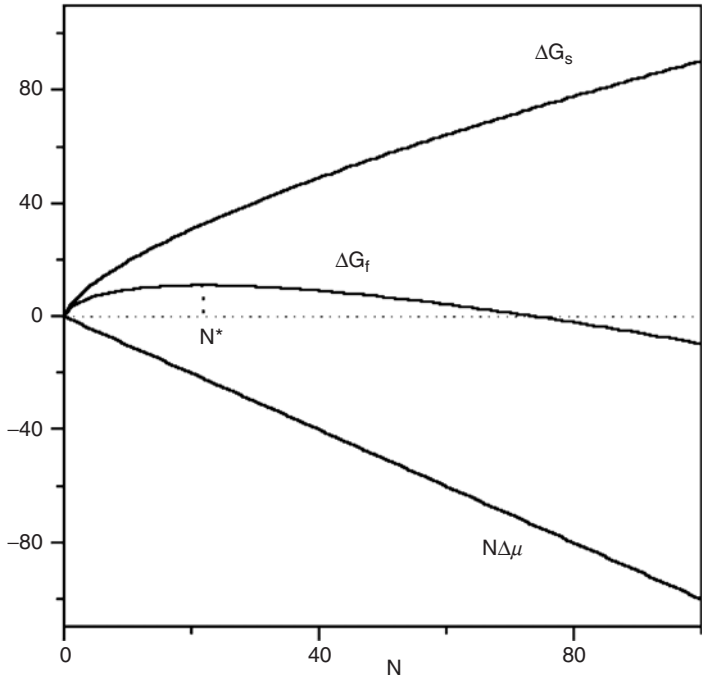

FIGURE 2.1. N dependence of the free energy of the formation of a nucleus (ΔG_f), the bulk crystal ($N\Delta\mu$), and the interface (ΔG_S).

The N* value corresponding to the maximum ΔG_f is the critical aggregation number; when an aggregate of N* molecules is formed, it is equally probable its growing as a bigger aggregate or decomposition in molecular precursors. The aggregates with N<N* are called embryos and tend to decompose because a decrease of N is accompanied by a reduction of the system free energy. Aggregates with N>N* are called nuclei and tend to grow spontaneously, because an increase of their size is accompanied by a decrease of the free energy. The N* value can be calculated by considering the maximum value of ΔG_f

$$\frac{d\Delta G_f}{dN} = \frac{d}{dN}(N\Delta\mu + K_N N^{2/3}\gamma_S) = 0 \qquad 2.6$$

i.e.,

$$N^* = -\frac{8K_N^3\gamma_S^3}{27\Delta\mu^3} \qquad 2.7$$

It can be noted that by increasing supersaturation, i.e., more negative $\Delta\mu$ value, the N* value decreases while higher interfacial energy per unit

surface shifts N* towards greater aggregates. Moreover, supersaturation being generally the result of a chemical reaction achieved by mixing two reactant-containing systems, it can be regulated not only by the initial reactant concentrations but also by addition and stirring rates of the two systems.

The corresponding free energy barrier ($\Delta G_f{}^*$) and the rate J of formation of aggregates of N* molecules are

$$\Delta G_f^* = \frac{4K_N^3 \gamma_S^3}{27\Delta\mu^2} \tag{2.8}$$

$$J = \Omega \exp\left(\frac{-\Delta G_f^*}{kT}\right) \tag{2.9}$$

where Ω is a factor correlated to the encounter frequency between the A molecules and consequently dependent on their diffusion coefficients[2].

In the case of microheterogeneous systems, as a consequence of confinement effects, it occurs frequently that the diffusion coefficients of solutes is smaller than that in homogeneous solutions (the diffusion coefficient of a solute is that of the supramolecular aggregate where it is entrapped) while the residence time in a certain nano-size domain (cage effect) is increased. This involves opposite contributions to the Ω value. On the other hand, J can be also influenced by specific surfactant/nanoparticle interactions involving changes of the ΔG_f^* value.

It is worth noting that if J is very small, i.e., if the probability of the formation of a critical aggregate is negligible, the embryos in the systems are stable in supersaturation conditions against an unlimited growth. This can be obtained at high ΔG_f^* and/or low Ω values. A high ΔG_f^* value is characteristic of particles with high interfacial energy and at low supersaturation levels, whereas small Ω values imply a low diffusion coefficient. According to Eq. 2.9, it is generally believed that a ΔG_f^* value of about 5–10kT represents a barrier adequate to avoid homogeneous nucleation only permitting the existence of short-living particles smaller than N*.

On the other hand, if the probability of the formation of critical aggregates is significant, the rate of nuclei formation increases with the precursor concentration and consequently also the number of crystallites. In contrast, the induction time (i.e., the time required for the formation of an experimentally detectable solid phase) and the particle size decrease with precursor concentration[3].

The various phases of the precipitation process are shown in Fig. 2.2. It must be stressed that these steps are not so well-disentangled as represented

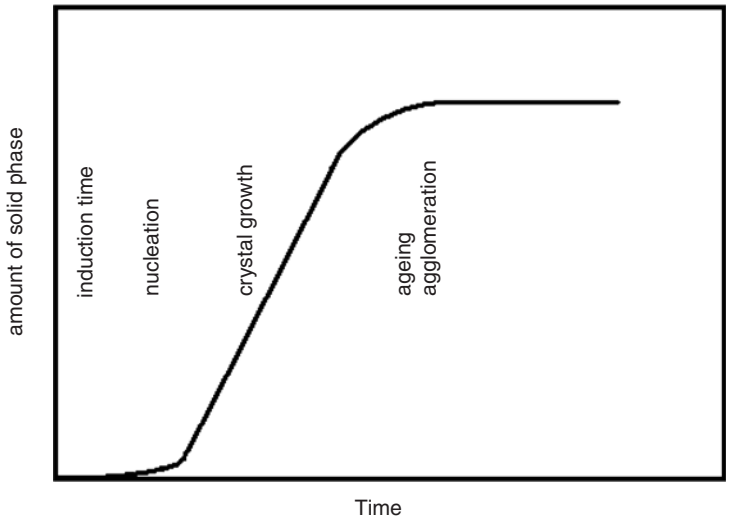

FIGURE 2.2. Processes involved during the precipitation process.

in the figure but, depending on the experimental conditions, more or less marked overlapping between the phases occurs.

2.2 Nanoparticle Growth, Growth Inhibition, and Size Control

According to the thermodynamic and kinetic premises, above the supersaturation threshold the unlimited nanoparticle growth is a spontaneous process whose rate can be controlled by altering some external parameters such as supersaturation degree, temperature, and additive presence. In order to inhibit this process, additional phenomena must come into play. Then, the appropriate use of the parameters regulating these phenomena could lead to the kinetic and/or thermodynamic fine nanoparticle size control. These features will be taken into account in the following subsections.

2.2.1. Time Dependence of Nanoparticle Size and Size Distribution

In supersaturated solutions where the probability of formation of critical aggregates is significant, the crystal growth in homogeneous conditions can be described in terms of three distinct processes, i.e., nucleation, normal growth, and competitive growth. In addition to these processes, sometimes, other phenomena could occur such as solid-phase transitions, aggregation,

and recrystallization. All these steps are not well separated in time so that overlapping zones occur.

The total number of crystals (N_c) formed by nucleation can be estimated by the equation

$$N_c = \frac{N_{Av} e^{\frac{-3\Delta G_f^*}{5kT}}}{3X_i^{0.2} V_m} \tag{2.10}$$

where X_i is the mole fraction of precursors and V_m their molar volume. By rearranging this equation, N_c can be directly related to the supersaturation ratio S by

$$\log N_c = A - \frac{B}{(\log S)^2} \tag{2.11}$$

where A and B are positive constants. It must be noted that, according to Eq. 2.11, an increase of the supersaturation value, i.e., higher precursor concentration, leads to a larger number of crystals meaning smaller nanoparticles.

The time dependence of the precursor concentration, C(t) can be evaluated by

$$C(t) = C_0 \left[1 - \left(\frac{t}{\tau}\right)^{\frac{5}{2}}\right] \tag{2.12}$$

where τ is the characteristic precipitation time, which can be calculated by the equation

$$\tau = \frac{V_m^{\frac{2}{3}} e^{\frac{2\Delta G_f^*}{5kT}}}{2DX_i^{0.2} N_{Av}^{\frac{2}{3}}} \tag{2.13}$$

After the appearance of the first nuclei through the random formation of embryos of increasing size, their normal growth occurs by means of the incorporation of molecular precursors reaching the nuclei by diffusion. In this phase, nuclei agglomeration is neglected because their low concentration and diffusion rate make the probability of their encounters practically zero. During normal growth, the time dependence of the mean cluster size ($\bar{r}$) is described by the equation

$$\bar{r} = (2DV_m C_0)^{0.5} t^{0.5} \tag{2.14}$$

where C_0 is the molar concentration of precursors, and the concentration of the precursors decreases with time. In stationary state condition, the radius distribution of nuclei is given by the Gaussian function

$$P(r) \propto e^{\frac{-K(r-r^*)^2}{kT}} \quad 2.15$$

where r* is the critical radius. Generally, a sharp size distribution results when experimental conditions are set so that agglomeration is prevented and nucleation and growth are temporally separated processes. This can be achieved by realizing an initial high supersaturation followed by an inhibition of subsequent nucleation obtained by a dilution at selected time or by a change of some external parameter (pH, temperature, etc.).

When the precursor concentration becomes negligible, the competitive growth dominates the entire process. During this stage, a mass transfer from smaller particles to larger ones occurs, and the time dependence of the cluster size is described by the equation

$$\bar{r} \propto t^{0.33} \quad 2.16$$

It must be noted that equation 2.16 emphasizes the spontaneous tendency to an unlimited increase of crystal size.

Generally, when the particle size reaches a system-dependent value as a consequence of a growing process and/or of association of smaller aggregates, they tend conspicuously to separate from the liquid phase as an effect of the gravitational force overwhelming that due to the Brownian movements. In such circumstances, an upper or lower solid phase depending on the densities of particles and bulk medium is formed. It is also worth noting that precipitation of scarcely soluble substances from homogeneous solutions generally leads to a broad size distribution due to random crystal growth. Moreover, after precipitation, secondary processes can occur (recrystallization, ageing, aggregation) involving further changes of size, shape, structure, and defectivity of crystals.

2.2.2. Nanoparticle Growth Inhibition and Size Control

In some cases, the particle growth is arrested as a consequence of the occurrence of some phenomena. The physico-chemical processes underlying these phenomena and allowing a size control are

- charging of the nanoparticles
- passivation of the nanoparticle surface by adsorption of suitable species
- compartmentalization of nanoparticles in spatially distinct regions

It must be pointed out that each of these mechanisms has its peculiarity and limitations that must be taken into account in the selection of the nanoparticle appropriate synthetic method.

A well-known contribution to the stability of particles is given by the presence of a net charge and/or the formation of an electric double layer surrounding the particle. This phenomenon is quite frequent in polar solvents because the particle could adsorb ionic species of the solution and/or species

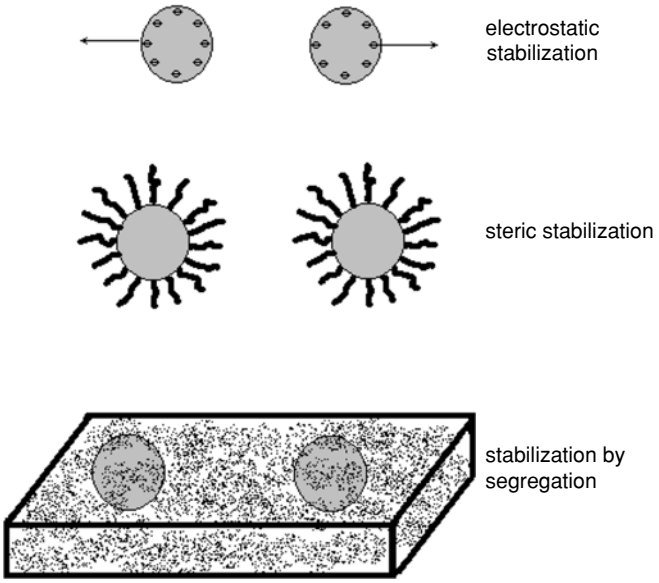

FIGURE 2.3. Mechanisms allowing nanoparticle size stabilization.

laying on the particle surface can dissociate, releasing ions on the surrounding medium. These processes together with the subsequent electrostatic effect on other nearby ionic species generate a double layer surrounding the particle.

Particles carrying the same charge and/or surrounded by an electric double layer repel due to electrostatic forces. In such conditions, a stable dispersion occurs when the particle-particle repulsive force arising by electric charges overcomes the attractive forces (van der Waals interactions, hydrogen bonding, etc.). Electrostatic stabilization is strongly sensitive to the presence of electrolytes, to their concentration and charge, and, generally, stable dispersions can be obtained at very low concentrations of nanoparticles. In particular, two opposite effects can be observed, i.e., ions coming from electrolyte dissociation can be selectively adsorbed, generating a charge on the nanoparticle surface or neutralizing pre-existent charges.

Moreover, it must be considered that when two particles approach each other, as a consequence of electrostatic forces and of the charge mobility on the particle surface and/or on the charged double layer coating the particles, the charge distribution around each particle is altered. The resulting charge distribution involves that the repulsive forces are decreased, the particles can move closer, and other distance-dependent interactions could come into play. Moreover, at sufficiently small distances, additional attractive forces such as the formation of chemical bonds and capillary forces can become operative[4]. For example, it has been observed that negatively charged silica particles readily deposit in presence of negatively charged polymer latexes[5].

It is worth noting that not only in aqueous media but also in apolar solvents the stability of particle dispersions can be governed by the presence of a net charge on the surface or by double-layer electrostatic repulsions[6,7]. It has been suggested that surface charging in solvents with low dielectric constant could be sustained by specific mechanisms such as exchange of protons between particle surface and surrounding medium[8].

Another phenomenon by which particles can be stabilized is the intentional use of appropriate capping agents. From a molecular point of view, the capping agents are molecules showing a physical or a chemical affinity for the species lying at the nanoparticle surface and forming a protective layer that makes the nanoparticle surface unreactive against agglomeration or precursor incorporation. Generally, the action of capping agents is based on their peculiar structure. In particular, they have a molecular moiety displaying an affinity to the nanoparticle surface and another unreactive moiety extending towards the environment that sterically prevents nanoparticle coalescence or precursor adsorption. As a consequence, the stabilization by surface capping is, generally, not sensitive to the presence of electrolytes and/or other unreactive additives. Capping with chemically bonded species is often contraindicated for nanoparticles to be used as catalysts.

Particles can also be stabilized against an unlimited growth by segregation or compartmentalization in spatially distinct domains. This strategy is based on the complete inhibition of nanoparticle encounters or material exchange process. This can be achieved by chemically anchoring particles on the surface of a suitable solid substrate or by dispersing them within a solid matrix. In such conditions, the freezing of the diffusive processes avoids the particle growth. This strategy is most frequently followed for the preparation of nanomaterials for optical applications or catalysis.

Stabilization of the nanoparticle size can also be achieved by performing their synthesis in microheterogeneous systems. This strategy has its distinct features even if it embodies all the above reported mechanisms. Thanks to the large difference of the diffusion coefficients of precursors and nuclei in microheterogeneous systems, in general the formation of nanoparticles occurs through two well-separated steps, i.e., the fast formation of nuclei and their slow growth. The separation is more evident at high reactant concentration[9,10].

Specific stabilization mechanisms are observed in microheterogeneous systems. Such systems, in fact, allow the stabilization of nanoparticles most often because their nanoscopic domains act as a physical boundary that inhibits precursor and nanoparticle diffusion, encounters, and agglomeration. As a consequence, the rate of formation of nanoparticles in microheterogeneous systems is generally slower than it is in homogeneous media. This strategy is similar to that followed by biological systems to accomplish the control of mineralization process within small spaces such as biological membranes or liposomes.

When the molecular aggregates are confined in nano-size domains, further contributions to the stability of the system could arise from:

1. A change of the particle/surrounding medium interfacial energy due to the adsorption on the aggregate surface of a monolayer of surfactant molecules. Concerning this point, it must be considered if the aggregate surface is hydrophilic or liphophilic, because this aspect determines the orientation of the surfactant or of the micellar aggregate on the particle surface. If the surface is hydrophilic and the nanoparticle is dispersed in water, a second layer of surfactant molecules is generally formed, coating the first layer and forming a bilayer surrounding the particle.
2. A significant reduction of the encounter frequency due to the screening effect of the surfactant layer on the internanoparticle attractive interactions and to the dispersion of micelles in the solvent medium.
3. A decrease of the particle growing process due to the drastic reduction of diffusion rates, which gives enough time to other processes such as particle coating with specific molecules allowing stabilization and control of small-size particles.
4. An inhibition of the heterogeneous nucleation due to the coating effect of a monolayer of surfactant molecules on the possible solid surfaces or particles in the system.
5. A change of the microscopic processes leading to the formation and growth of particles.
6. A change of kinetic and thermodynamic parameters in confined space.

Concerning point 5, investigations on the growing process of ZnS nanoparticles in AOT reversed micelles allowed to point out that the time dependence of the nanoparticle size can be expressed by a power law whose exponent (0.074) is much lower than that expected for the same process in an homogeneous system (0.33)[11]. This was taken as an indication that the ZnS nanoparticles in AOT reversed micelles grow following a different mechanism. In contrast with homogeneous media where the particle growth is regulated by the diffusion rate of precursors, it has been found that in reversed micellar systems, the process is controlled by the intermicellar exchange of material.

From the analysis of the enthalpies of precipitation of calcium carbonate and calcium fluoride nanoparticles in various w/o micromeulsions, it was suggested that their energetic state is strongly different from that in the bulk. The observed behavior was attributed to smallness of the nanocrystals, changes of the equilibrium constants, and nanoparticle/surfactant interactions[12].

A generally overlooked question of all nanoparticle chemical synthetic methods is the destiny of secondary products that quite often accompany

the formation of nanoparticle precursors. Depending on the specific synthetic protocol, these substances could poison or dope the nanoparticle. This question is more important when the synthesis is carried out in confined space.

2.3 Internal and External Parameters Controlling Nanoparticle Formation and Stability in Microheterogeneous Systems

2.3.1. General Considerations

Size, shape, and polydispersity of nanoparticles can be regulated by selecting the appropriate system and experimental conditions. In the best condition, i.e., when the nanoparticle size and shape is controlled by that characterizing the structure of the microheterogeneous system, care must be taken for the suitable composition of the medium allowing selection of the dimensional parameters of the hosting space. It must be stressed that, in this case, important contributions to the control of nanoparticle structural parameters could arise by surfactant adsorption on their surface and strong reduction of diffusive motions.

More frequently, the size and shape of nanoparticles synthesized in microheterogeneous systems result from a fine balance between the tendency of the microdomains to maintain their original structure and that of nanoparticles to grow indefinitely. In these cases, the selection of the appropriate precursor to surfactant molar ratio could play a decisive role for a successful synthetic route. Because the formation of a nanoparticle requires the accumulation of precursors in a single nanodomain, the deformability of the surfactant layer, which controls the material exchange process among nanodomains, plays a pivotal role in determining the nanoparticle growing rate and its final size and shape. A lower material exchange rate involves a reduction of the precursor encounter frequency and consequently the formation of a greater number of nuclei and smaller nanoparticles.

Generally, the hindering to the diffusion process increases with the particle size, so that, when the nanoparticle reaches a critical size, it is stably entrapped in a single domain, and it can grow only by the arrival of further precursors in the molecular state. When all the precursors have been depleted, the nanoparticle reaches its final size. The flexibility of the surfactant layer is also involved if the nanoparticle size becomes comparable with that of the surfactant nanodomain because further growth requires an unfavourable swelling of the nanodomain. The final size is also influenced by the number density of nanodomains because an increase of their concentration involves an increase of the number of nuclei and consequently a smaller nanoparticle size.

Specific effects could also arise from the selective adsorption of surfactant molecules on certain crystallographic facets of the nanoparticles during their growth. It has been suggested that this phenomenon could significantly influence the nanoparticle shape[13].

Sometimes, to enhance the microheterogeneous system capability to inhibit the nanoparticle growth and for a better control of their size and polydispersity, specific capping agents are added during the synthesis.

Summing up all the above considerations, the factors influencing nanoparticle size and shape are[14–16]

- structural and dynamical properties of the microheterogeneous system
- structure and composition of the water/oil interface
- surfactant layer flexibility
- surfactant nature
- size and shape of microdomains
- nature of the reagents and their localization
- distribution law of reactants among nano-size domains
- reagent local and overall concentrations
- diffusion and material exchange rates among microdomains
- reaction rate leading to the formation of nanoparticle precursors
- local solubility of the nanoparticle precursors
- presence of suitable additives such as capping agents or electrolytes
- nature of the solvent medium
- presence of specific capping agent

Taking into account the sensitivity of the structure and dynamics of microheterogeneous systems to the presence and concentration of additives, it is worth noting that both features must be considered in the presence of reactants.

According to the above-reported considerations, after choosing the appropriate microheterogeneous system, the most frequently employed external parameters to control nanoparticle synthesis are

- the precursor to surfactant molar ratio
- surfactant aggregate concentration
- the nature of the solvent medium
- the temperature
- the addition of specific capping agents

2.3.2. Some Specific Examples

Using w/o microemulsions as microheterogeneous medium, it has been found that, in some conditions, the nanoparticle size is controlled by the size of the water containing reversed micelle, whereas this does not occur if the synthesis is performed in different experimental conditions[9,17].

It was suggested that many other factors can influence the final nanoparticle size, shape, and their distribution such as the number of reagent molecules per reversed micelle, the reversed micelle concentration, and the nature of the solvent medium[18]. This is because a change of these factors more or less affects the intermicellar material exchange, nucleation, and growth rates. It has also been found that an increase in the reagent concentration leads to an increase of the nanoparticle size.

The effect of various parameters on the synthesis of silver chloride nanoparticles obtained by adding an aqueous solution of $AgNO_3$ to dioctyldimethylammonium chloride/n-decanol/isooctane microemulsions has been investigated. It was observed that i) an increase of the surfactant or water concentrations caused an increase of the particle size, ii) an increase of the silver nitrate concentration led to the formation of more nuclei and consequently smaller nanoparticles, iii) high n-decanol concentration or water to surfactant molar ratio induced destabilization of reversed micelles and consequently nanoparticle agglomeration and flocculation[19].

The reshaping effect of silica-core gold-shell nanoparticles dispersed in aqueous solutions of cetyltrimethylammonium bromide has been investigated. In particular, it has been observed that nearly spherical nanoparticles are slowly transformed into elongated hollow toroidal gold nanoparticles with significant etching of the silica core[20].

Microheterogeneous systems can also be employed to realize stable dispersions of particles. This is achieved by directly suspending finely divided materials. It has been found that the adsorption of the surfactant molecules at the particle surface plays a key role in the stabilization process. The dispersion process can be divided in the following steps: i) formation of sufficiently small particles, ii) formation of a compact surfactant layer on the particle surface, iii) dispersion in the medium[21,22].

REFERENCES

1. C. Giordano, A. Longo, V. Turco Liveri, A. M. Venezia, *Coll. Polym. Sci.* **281**, 229–238 (2003)
2. O. Sohnel, J. Garside, *Precipitation, basic principles and industrial applications*, Butterworth Heinemann Ltd, Oxford, 1992, Oxford
3. J. K. N. Dhort, C. Smits, H. N. W. Lekkerkerker, *J. Coll. Int. Sci.*, **152**, 386–401, 1992
4. H. Shinto, D. Iwahara, M. Miyahara, K. Higashitani, *Langmuir* **18**, 4171–4178 (2002)
5. E. Matijevic, *Langmuir* **2**, 12–20 (1986)
6. D. N. L. McGown, G. D. Parfitt, E. Willis, *J. Coll. Science* **20**, 650–664 (1965)
7. C. A. Malbrel, P. Somasundaran, *J. Coll. Interface Science* **133**, 404–408 (1989)
8. D. F. K. Hughes, I. D. Robb, P. J. Dowding, *Langmuir* **15**, 5227–5231 (1999)
9. C. Tojo, M. C. Blanco, M. A. Lopez-Quintela, *Langmuir* **13**, 4527–4534 (1997)
10. C. Tojo, M. C. Blanco, M. A. Lopez-Quintela, *Langmuir* **13**, 1970–1977 (1997)

11. V. Turco Liveri, M. Rossi, G. D'Arrigo, D. Manno, G. Micocci, *Appl Phys A* **69**, 369–373 (1999)
12. V. Arcoleo, M. Goffredi, V. Turco Liveri, *Thermochim. Acta* **233**, 187–197 (1994)
13. Y. Sun, B. Mayers, T. Herricks, Y. Xia, *Nanoletters* **3**, 955–960 (2003)
14. E. Boakye, L. R. Radovic, K. Osseo-Asare, *J. Coll. Int. Sci*. **163**, 120–129 (1994)
15. S. Modes, P. Lianos, *J. Phys. Chem*., **93**, 5854–5859 (1989)
16. J. Gao, C. M. Bender, C. J. Murphy, *Langmuir* **19**, 9065–9070 (2003)
17. C. L. Chang, H. S. Fogler, *Langmuir* **13**, 3295–3307 (1997)
18. C. L. Kitchens, M. C. McLeod, C. B. Roberts, *J. Phys. Chem. B* **107**, 11331–11338 (2003)
19. M. Husein, E. Rodil, J. Vera, *Langmuir* **19**, 8467–8474 (2003)
20. C. M. Aguirre, T. R. Kaspar, C. Radloff, N. J. Halas, *Nanoletters* **3**, 1707–1711 (2003)
21. S. Krishnakumar, P. Somasundaran, *Colloids and Surfaces A: Physicochemical and Engineering Aspects* **117**, 37–44 (1996)
22. M. Goino, K. Esumi, M. Tagawa, *Colloids and Surfaces A: Physicochemical and Engineering Aspects* **135**, 135–139 (1996)

3

Physico-chemical Properties of Nanoparticles Entrapped in Microheterogeneous Systems

3.1 Introduction

The strict correlation between the number of materials available to human societies during the various historical periods and their quality of life is well known. This because the production of materials with suitable properties is at the basis of the development of technologies leading to the realization of a wide range of consumer goods and social infrastructures. Nowadays, the need of novel materials is hugely increased by the widespread possibilities offered by scientific knowledge.

These considerations are at the basis of the strong technological interest towards nanoparticles. In fact, by finely dividing a solid and controlling its size, shape, and spatial distribution within a suitable matrix, it is possible to generate a continuous spectrum of new materials starting from the same substance. Taking into account that this potentially holds for each solid substance, the enormous potentials offered by nanomaterials can be easily understood. Moreover, nanoparticles are the inevitable answer to miniaturization, i.e., the building up of devices in the nano-scale regime or with the highest concentration of constituent nanocomponents.

In this context, however, the knowledge of the peculiar properties of nanoparticles and of the microscopic processes responsible for their behaviour must be considered of basic importance not only to exploit their potential applications but also to plan a suitable synthetic protocol. In fact, their reactivity poses some limits to the substances employed for the synthesis of stable nanoparticles, nature of the surrounding medium used to entrap them, and the energy source at which they can be exposed. Moreover, their specific reactivity must be considered in order to take the necessary cautions for their manipulation, storage, and transport both in laboratories and industrial plants. Their size demands some additional requirements for their employment as building blocks of more or less complex devices. On the other hand, the knowledge of some of their exotic properties could be useful because it can suggest appropriate methods that can be applied during the

various phases of the synthetic process such as nanoparticle stabilization, extraction, and transfer.

Finally, the exotic properties of nanoparticles are interesting from the theoretical point of view because the attempt to find explanations of their peculiar behaviour stimulates significantly the development of the present theories.

3.1.1. Physico-chemical Properties of Nanoparticles

The reduction of bulk materials to the state of nanoparticles induces size-dependent effects arising from

- a significant increase of the surface to volume ratio involving a huge increase of the interfacial area and of the fraction of species at the surface
- a change of the physico-chemical properties of the species at the surface and in the nanoparticle interior with respect to that in the bulk or as isolated molecules
- changes of the electronic structure of the species composing the nanoparticle and of the nanoparticle as a whole
- changes in the arrangement (lattice structure, interatomic distances) of the species in the nanoparticle and presence of defects
- confinement and quantum-size effects (due to the confinement of charge carriers into a particle having a size comparable with the electron or hole De Broglie length)

These variations do not occur monotonously with the particle size but become significant by decreasing the particle size below system-specific size thresholds. As a rough reference value, a typical size threshold of 10 nm can be taken. Moreover, it is worth noting that in practical applications, nanoparticles are always embedded in a surrounding medium and consequently additional features arise from the specificity of contacting and/or adsorbed species at the nanoparticle surface.

As a consequence of these effects and being able to control the nanoparticle size and shape, various exotic and sometimes unexpected properties can be conferred to well-known materials leading to the formation of a continuous spectrum of new materials starting from the same substance. For example, superparamagnetism, due to single domain particles, is an interesting phenomenon that can be observed only in nanoparticles of magnetic substances[1].

The behavior of superparamagnetic materials can be exploited for the development of many useful applications including ferrofluids, magnetocaloric refrigeration, and enhanced contrast in magnetic resonance imaging. Some additional interesting applications of magnetic nanoparticles in biomedicine have been recently reviewed[2,3]. They are based on the possibility to manipulate magnetic nanoparticles after their introduction in the human

body by an external magnetic field gradient allowing their transport in specific organs, immobilization, and heating. This gives the opportunity of novel anti-cancer therapy, drug carrying, and targeting.

Below a critical size, the ionization potential of metal clusters increases by decreasing the cluster size, involving changes of their chemical properties (reactivity, catalytic activity, stability). The application of Pd and Pt nanoparticles for the treatment of car exhaust gas in catalytic mufflers[4] is well-kown.

Other chemical applications of metal clusters can be devised by their photoactivation. For example, Ag nanoparticles under visible laser irradiation act as photoelectron emitters and effective reducing agents[5].

The band gap and the radiative rate of the optical excitations of semiconductors increase by decreasing the size[6]. For example, the band gap of CdS can be varied from about 2.5 to 4 eV and the radiative rate from nanoseconds to picoseconds. Semiconductor nanoparticles coated with a higher band gap material are characterized by an enhancement of their photoluminescence due to the inhibition of the nonradiative recombination of the hole/electron pair at the nanoparticle surface[7]. These variations are also accompanied by color changes.

Interesting application of semiconductor nanoparticles to the photocatalytic degradation of a wide variety of organic pollutants has been deeply investigated[8–14]. Of particular importance are also the potentialities of semiconductor nanoparticles, for solar energy conversion[15].

The lattice of small particles (diameter ≈ 10 or smaller) is generally distorted and the cohesive energy, i.e., the heat of sublimation of bare nanoparticles, increases with the particle size trending to the bulk value[16].

The melting temperature of nanomaterials is influenced by the cluster size. This effect reflects the modification of the electronic structure of the nanoparticle with respect to the bulk and the presence of a significant fraction of species at the surface. It has been suggested that the melting temperature $T_{m(d)}$ of nanoparticles with a diameter d is given by

$$T_{m(d)} = T_{m(\infty)} \exp\left(\frac{1-\alpha}{\frac{d}{d_0}-1}\right) \qquad 3.1$$

where d_0 is a critical diameter, $T_{m(\infty)}$ the melting temperature of the bulk material, and α a size-independent parameter that depends on the nature of the nanoparticle and surrounding medium[17]. It must be noted that, if $\alpha < 1$, $T_{m(d)}$ decreases with d while, if $\alpha > 1$, the opposite behaviour occurs.

Reducing the size of crystals in the nano-size regime leads to an alteration of the phonon density of states at low energy. In nanocrystals, phonon modes become discrete because of the reduced number of atoms constituting the particle. For a bare spherical nanoparticle, it is predicted that internal vibration modes at frequencies less the Lamb mode (ν_L) do not occur. ν_L can be estimated by the equation

$$\upsilon_L = \frac{2\pi v_T}{d} \qquad 3.2$$

where v_T is the transverse sound velocity and d the nanoparticle diameter. It follows that physico-chemical properties that depend on the vibrational spectrum at low energy are affected by size reduction[18].

The equilibrium solubility of nanoparticles changes with the crystal size. This behavior is well-described by the Gibbs-Thomson equation

$$a_r = a_\infty e^{\frac{2k_a f V_m}{3k_v \nu RTr}} \qquad 3.3$$

where a_r and a_∞ are the activity of the substance in solution in equilibrium with nanoparticles of size r and size "infinite", respectively; k_a and k_v are the shape factors of nanoparticle area and volume, f is the surface stress, V_m the molar volume, and ν the number of ions arising from the substance dissociation[19]. According to equation 3.3, the equilibrium solubility increases with the decrease of the particle size, and this effect becomes markedly significant in the nano-size regime. For very small particles, it has been found that also the surface energy increases with the size[19].

Also the chemical reactivity of bulk materials can be strongly enhanced by reducing them to the state of nanoparticles. This effect results from the mere increase of the fraction of species at the surface that are ready to react with incoming reactants as well as from changes of the nanoparticle electronic structure. An enhancement of their reactivity is of great interest in the fields of catalysis, sensors, material processing, and in novel solid-solid reactions[20–23].

The huge value of the surface to volume ratio of nanoparticles leads to the production of nanomaterial showing enhanced adsorption of specific substances. This behavior can be exploited for several technological applications such as hydrogen storage systems[24,25].

Nanoparticle coating could influence their physico-chemical properties. For example, it has been shown that the blocking temperature of surfactant coated superparamagnetic iron nanoparticles is strongly influenced by the nature of the surfactant functional group[26].

The dispersion of nanoparticles in a suitable substrate could generate other interesting physical phenomena such as dielectric confinement arising when the refractive index of nanoparticles is higher than that of the surrounding matrix. Under exposure of light, the local enhancement of the field intensity compared to that of the incident radiation leads to interesting photophysical properties of the composite.

Another well-known optical property is the absence of scattering of the light if the particle size is less than its wavelength, leading to transparent and optically homogeneous media.

In suitable conditions, polarisable nanoparticles suspended in apolar solvent media give the electrorheologic effect, i.e., a sudden and reversible

marked increase of the system viscosity due to the establishment of strong electric fields. This behavior can be exploited in the realization of interesting electromechanical devices[27].

It has been reported that the thermal conductivity of particle dispersion in liquid systems increases steeply with decreasing their size in the nano-regime. The peculiar mechanism of heat transport in nanoparticles and their clustering allowing the formation of local percolated paths with high thermal conductivity have been considered responsible for the observed enhanced thermal conductivity of these dispersions (nanofluids)[28].

Specific effects are observed by dispersing nanoparticles in the typical structure characterizing microheterogeneous systems[29].

Nanoparticle containing microheterogeneous systems can be used as specialized reaction media in which nanoparticles carry out the role of catalysts[30].

Nanoparticles are also interesting as building blocks of geometric arrangements on suitable matrices showing interesting collective properties or of ultra-miniaturized devices. A potential application of nanoparticles is the construction of biomachines or devices based on quantum effects. A thorough overview of the complex nanostructures that can be formed by nanoparticle assembling can be found in the book of J. Zhang et al.[31] In particular, the rich variety of self-assembled structures formed by nanospheres, nanorods, nanocubes, and nanoplates functionalized with oligomeric tethers attached to specific positions of the nanoparticle surface has been emphasized[32].

Dispersion of nanoparticles on a suitable matrix could lead to the realization of nanomaterials with enhanced mechanical properties with respect to that of the components[33]. An interesting example of this potential application is offered by natural biological composites such as sea shells, bones, and teeth. These nanomaterials are in fact characterized by a complex microstructure constituted by inorganic nanoparticles embedded in a protein matrix[34].

Biological applications of nanoparticles have also been devised based on their ability to inactivate bacteria and viruses, suggesting their use as antimicrobial agents[35,36]. For example, the antimicrobial activity of silver nanoparticles against *E. coli* was investigated. It was found that these nanoparticles are an effective bactericide[37].

The reduction of slightly water soluble drugs to the nanometer size could improve their bioavailability through the increase of the total surface area of the particles involving an increase of the dissolution rate. Lipid nanoparticles have been suggested as improved drug delivery systems for the administration of biologically active substances. Their employment could allow chemical protection, controlled release, and targeting of drugs[38,39]. The potential of nanoparticles in anti-cancer therapy and diagnosis has also been highlighted[40].

Interesting applications of biomaterials as bionanomotors, bionanochips, biological sensors, and drug delivery systems have been thoroughly treated by Cui et al.[41]

Together with the benefits that can be obtained by the exploitation of nanoparticle properties, it is helpful to mention also the potential risks for living beings arising from their introduction in the environment. Being so small, nanoparticles can easily penetrate through the skin and the lungs, reaching the internal organs of living beings where, being so reactive, they could trigger off very dangerous reactions. For example, it has been ascertained that liver and kidney granulomatosis can be caused by non-biodegradable nanoparticles of some inorganic materials, such as porcelains and alumina, generally considered inert, non-toxic, and biocompatible substances. This involves the necessity to revise the definition of biocompatible materials to take into account not only their chemical composition but also the particle size[42].

Other potential health risks, including asthma, chronic bronchitis, and ischemic heart diseases, can be originated by atmospheric nanoparticles. Moreover, these nanoparticles could act as photocatalysts enhancing the ozone production in the atmosphere or acting as carriers of toxic substances[43].

Cultural heritages and ecosystems could also be severely damaged by uncontrolled nanoparticle dispersion in the environment.

Many human activities are responsible for nanoparticle introduction in the environment. For example, nanoparticle emissions determined by vehicular traffic and their impact on air quality have been thoroughly investigated[44].

The particular physico-chemical properties conferred to nanomaterials are also dependent on the kind of dimensional restriction. The size of a bulk material can be restricted along one dimension giving a bi-dimensional structure (quantum well), along two dimensions leading to a mono-dimensional structure (quantum wire), and finally along three dimensions forming the so-called quantum dot. According to their three-dimensional arrangement, quantum wells and quantum wires extending along the three dimensions can give a wide variety of interesting three-dimensional nanostructures (see Fig. 3.1).

The restriction of the nanoparticle dimensionalities involves some changes in the energy (E) and density ($\rho(E)$) of electronic and phononic states and of the mechanism and rate of the electron-hole recombination. By the simple particle in a box model, the E dependence of $\rho(E)$ for each electronic band can be predicted (see Fig. 3.2).

It can be expressed in the form $\rho(E) \propto E^{\frac{\delta}{2}-1}$, where $\delta(\delta = 1, 2, 3)$ is the dimensionality of the nanomaterial and E is relative to the bottom of the electronic band. In the three-dimensional case, $\rho(E)$ changes with $E^{1/2}$ whereas for $\delta = 2$ and 1 the band can be considered composed by some subbands and the previous equation describes the density of states within each subband. For $\delta = 0$, a number of discrete states is obtained.

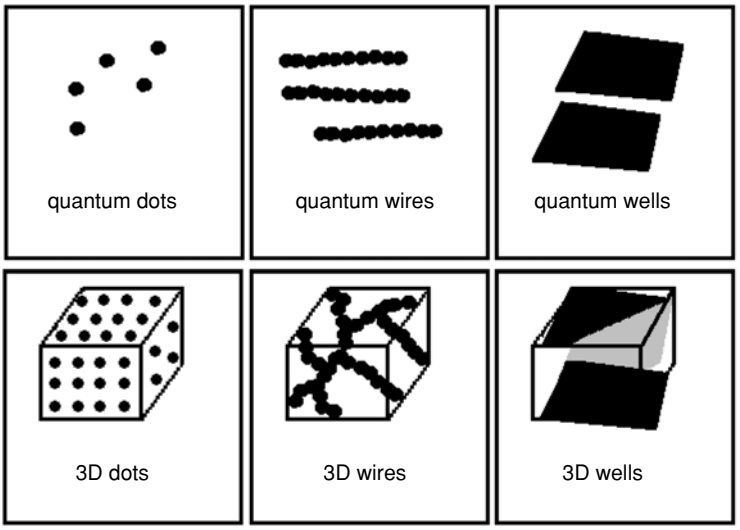

FIGURE 3.1. 0D, 1D, 2D, and 3D nanostructures.

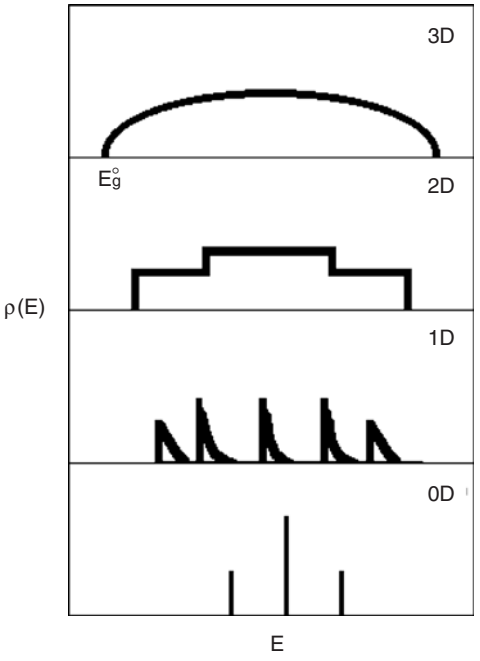

FIGURE 3.2. Density of electronic states from 00 to 30 nanostructures.

3.2 Quantum Size Effects

Quantum size effects originate from the progressive variation of the energy and density of the electronic levels with reducing the system size. Taking into account that quite all physico-chemical properties are strongly impacted by the electronic state, this involves the capability to tune the behaviour of a material by simply changing its degree of subdivision.

These effects are more often observed in solids characterized by strong interatomic interactions such as metals and semiconductors where the overlap of atomic orbitals is more efficient, while they are usually considered negligible in molecular solids where the properties are mainly those of the single molecules more or less perturbed by relatively weak intermolecular forces. However, it must be stressed that also nanoparticles of molecular solids could display exotic properties as a consequence of confinement, structural and interfacial effects[45].

As a general trend, below a substance-specific threshold, a decrease of the number of atoms composing the nanoparticle involves a lower density of electronic energy levels, narrower band widths, and larger interband energy gaps. These changes in turn influence the electronic distribution among the energy levels of the nanoparticle in the fundamental state as well as the energies required for their excitations. These effects become significant when the nanoparticle size is smaller than the Bohr exciton radius (R_B) given by

$$R_B = \frac{\varepsilon_0 \varepsilon h^2}{\pi \mu e^2} \qquad 3.4$$

where ε_0 and ε are the permittivities of vacuum and nanomaterial, μ is the reduced mass of the electron/hole couple ($\mu = m_e m_h/(m_e + m_h)$), and e is the electronic charge. For many substances, the Bohr radius is of the order a few nanometers.

Using the Schrödinger equation, the electronic structure of a solid system could be calculated exactly including the terms due to the kinetic energy of every electron and nucleus and the potential energy arising from the electron-electron, electron-nucleus, and nucleus-nucleus interactions. However, being impossible to solve this equation even for the simplest case, approximate methods have been developed to find reasonable wavefunctions and energy values.

Considering that nuclei are heavier than electrons, the Schrödinger equation can be split in two equations: one for a system of motionless nuclei and moving electrons and another for a system of moving nuclei and smeared electrons (Born-Hoppenheimer approximation). Because the electronic properties of solids are mainly determined by the valence electrons, a second approximation allows to rewrite the electronic part of the Schrödinger equation for a system of external electrons and motionless

nuclei+internal smeared electrons. Within the Hartree-Fock MO-LCAO treatment, these approximations lead to the secular determinant

$$|\langle\phi_i|H|\phi_j\rangle - E\langle\phi_i|\phi_j\rangle| = 0 \tag{3.5}$$

where E is the electronic energy, ϕ is the shared atomic orbital, and the indexes i and j run over these atomic orbitals. Finally, considering a unidimensional solid formed by atoms sharing only one atomic orbital and that only interactions among first neighbour atoms are significant (Hückel approximation), the following eigenvalues are obtained by solving Eq. 3.5:

$$E_k = \alpha + 2\beta\cos\left(\frac{k\pi}{N+1}\right) \tag{3.6}$$

where $1 \leq k \leq N$ and N is at the same time the number of atoms, atomic orbitals, and eigenvalues. E takes the maximum value (E_{max}) when k = 1 and the minimum one (E_{min}) when k = N; so that the quantity $\Delta E = E_{max} - E_{min}$ is the band width. Looking to Eq. 3.6, it can be noted that the band width is α independent and, as shown in Fig. 3.3a, it increases with N, tending to 4β for $N \to \infty$. Besides, the mean density of electronic level ($N/\Delta E$) and their mean separation are N, i.e., size dependent (see Fig. 3.3b).

It must be noted that higher β values involve wider band width and more marked N dependence of the band width, electronic level density, and mean separation. β being a measure of the strength of interaction among first neighbour atoms, it can be argued that more marked quantum size effects are observed for systems composed by strongly interacting species.

More generally, it must also be considered that each atom has more than one atomic orbital that can be combined with other atomic ones. There are thus various basis sets $\{\phi\}_i$ leading to various energy bands, as many as the number of $\{\phi\}_i$. The N evolution of the electronic structure of two bands of a "unidimensional" solid formed by a single atomic species arising from the overlap between orbitals with energies E_1 and E_2 is shown in Fig. 3.4.

For a three-dimensional solid system, the number of first neighbours of each atom is regulated by the crystal lattice. The treatment becomes formally more complex than that above reported, but qualitatively the same conclusions still hold.

Of utmost importance is the fact that the physico-chemical properties of the material are strictly correlated to the electronic level energies of each band, the energy gaps between neighbouring bands, and the degree of band electronic occupancy. The relationship between the occupancy of electronic states and some well-known properties describing the electronic behaviour of metals, semiconductors, and insulators is shown in Fig. 3.5 and Fig. 3.6.

It can be noted that metals are characterized by a partially filled highest energy band (conduction band) leading to easily accessible electronic states, i.e., easily excitable conduction electrons. In such conditions, some electrons

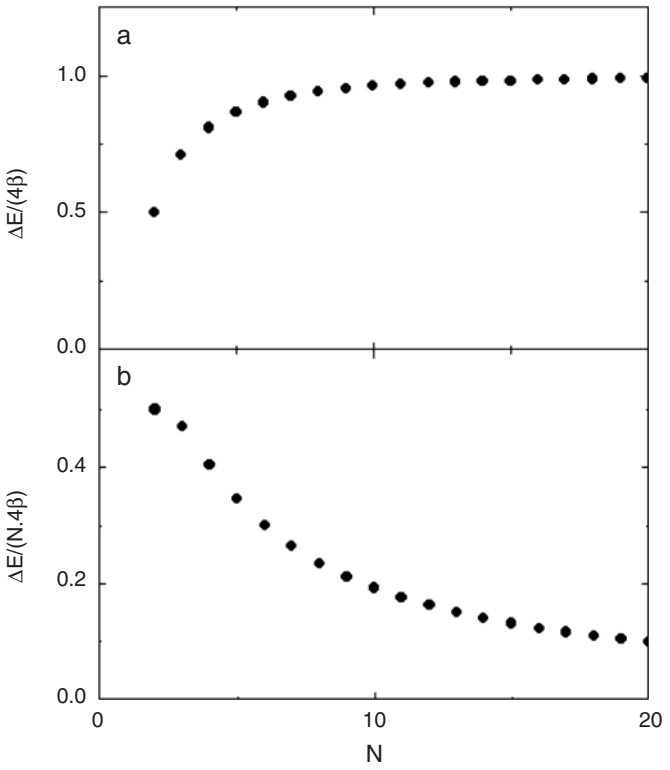

FIGURE 3.3. Size dependence of the band width (a) and mean density of electronic states (b).

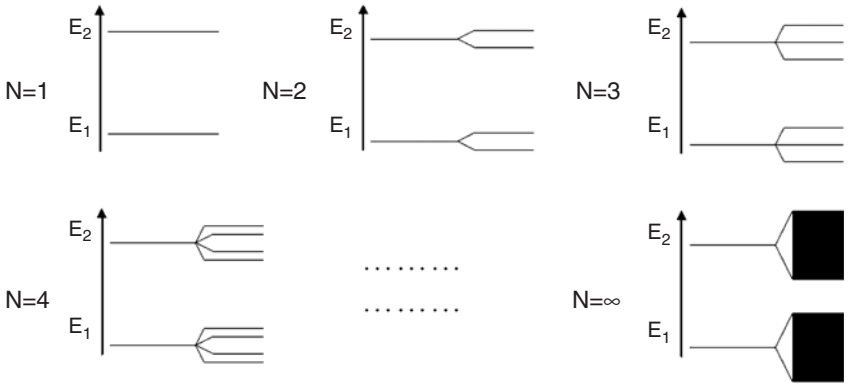

FIGURE 3.4. N evolution of the electronic structure of two bands of a unidimensional solid.

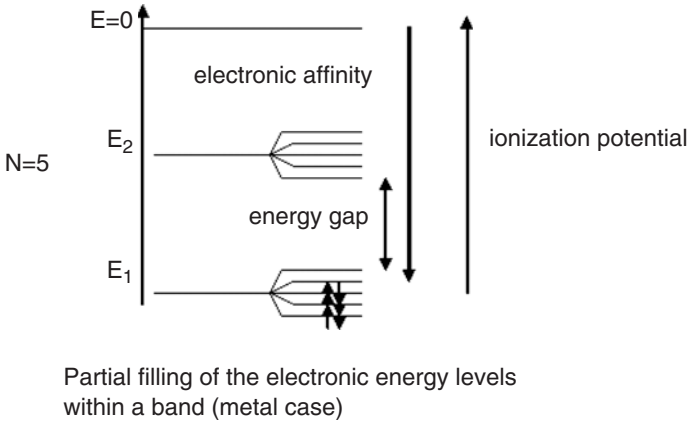

FIGURE 3.5. Electronic structure of two bands of a unidimensional solid (metal case).

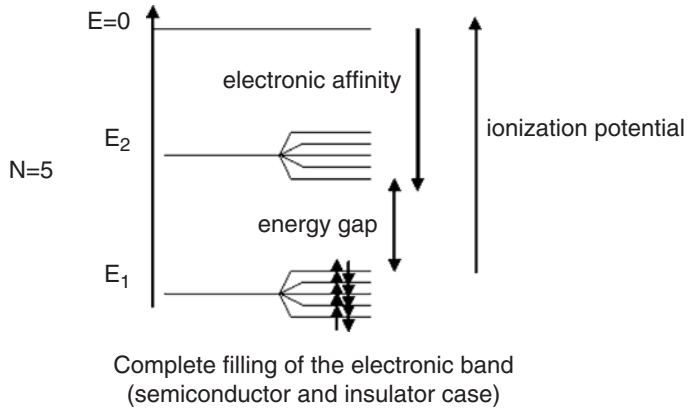

FIGURE 3.6. Electronic structure of two bands for a unidimensional solid (semiconductor and insulator case).

are delocalized and behave like molecules in the liquid state. On the other hand, at 0 K, semiconductors and insulating substances are characterized by the energy gap value between the totally unoccupied lowest energy conduction band and the underlying totally filled (valence) band. Now, all electrons are localized like molecules in the solid state. In contrast with insulating materials, semiconductors are characterized by relatively small energy gaps. This involves that, by increasing the temperature of semiconductors, an increasing number of electrons are promoted to the conduction band, leaving positive holes in the valence band. The mobility of these charge carriers is

substantially larger than that of many conductors. As a consequence of both effects, the semiconductor conductivity shows a peculiar increase with temperature. The changes of the electronic structure of a 3D solid due to size restriction are shown in Fig. 3.7.

The most evident effects of the changes in the structure of the electronic bands determined by a decrease of the nanoparticle size can be observed in the optical absorption or emission spectra. In the case of colloidal metals, absorption bands arise from the excitation of collective oscillations of conduction electrons (plasmons) or interband electronic transitions driven by the external electromagnetic field. The absorbance (A) is related to the number (N) of the nanoparticles by the equation

$$A = \frac{CNl}{2.303} \tag{3.7}$$

where C is their absorption cross-section and l the optical pathlength. According to the Mie theory with a good approximation, the absorption cross-section of spherical nanoparticles is given by

$$C = \frac{18\pi\varepsilon_2 V}{\lambda[(\varepsilon_1 + 2)^2 + \varepsilon_2^2]} \tag{3.8}$$

where λ is the radiation wavelength, V the nanoparticle volume, and ε_1 and ε_2 are the real and imaginary parts of the metal permittivity relative to that of the surroundings[46].

The above equation is applicable when the interparticle distance is larger than λ and the nanoparticle size is smaller than $\lambda/2\pi$. According to Eq. (3.8), the absorption coefficient shows a maximum whose position and width are determined by the frequency dependence of ε_1 and ε_2. Below a nanoparticle size threshold, a broadening and blue shift of the absorption band is observed. These deviations from the Mie theory predictions have been

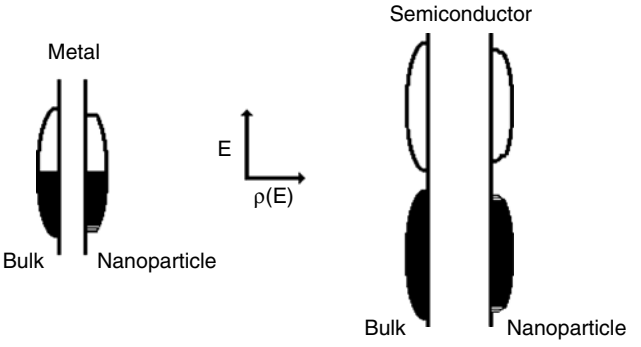

FIGURE 3.7. Changes in the electronic band structure of 3D metals and semiconductors due to size restriction.

accounted in terms of size dependence of metal nanoparticle permittivity. Further deviations arise from specific physical and chemical interactions between nanoparticles and surrounding medium, determining effects often larger than that due to nanoparticle size[47].

In the case of semiconductor nanoparticles, absorption of a photon with energy equal to or higher than its band gap promotes an electron from the valence to the conduction band, leaving a positive hole. Because the photon wave vector is small, the momentum conservation law leads to the selection rule of these electronic transitions, i.e., the electron wave vector k ($k = 2\pi/\lambda$) should be conserved. Direct band gap semiconductors are characterized by transitions with conservation of k and large absorption coefficients, whereas indirect band gap ones are characterized by transitions with large change of the electron wave vector and low absorption coefficients.

The absorption of a photon of suitable energy can lead to the generation of a bound electron-hole pair (Wannier exciton). When these species are confined within a nanoparticle, their interaction is strongly nanoparticle size dependent and so is also the energy needed for the excitation (excitonic energy, E_g). A simple model leads to the equation

$$E_g = E_{g(bulk)} + \frac{\hbar^2\pi^2}{2R^2}\left(\frac{1}{m_e^*} + \frac{1}{m_h^*}\right) - \frac{1.8e^2}{\varepsilon R} + E_{Rydberg} \qquad 3.9$$

where R is the nanoparticle radius, and m_e^* and m_h^* are the effective masses of the electron and hole, respectively, ε is the nanoparticle dielectric constant, and $E_{Rydberg}$ is a substance-specific constant[48].

However, recent experimental observations have put into evidence i) the validity of a more simple relationship between the energy gap and nanoparticle size ($E_g = AR^B$) and ii) that the energy gap does not uniquely depend on the nanoparticle size[20,49,50].

Due to increasing overlapping of the wave functions of electron and hole, the absorption coefficient increases by decreasing the nanoparticle size[51]. Moreover, using a tight-binding model, it has been predicted that shape changes of semiconductor nanoparticles have modest effects on energy gap. On the other hand, the oscillator strengths and consequently the intensity of optical spectra are strongly influenced by changes in nanoparticle morphology[52].

Experimentally the excitonic energy, i.e., the energy gap of the nanoparticle, can be found by an analysis of the absorption band through the equation

$$\sigma h\nu = A(h\nu - E_g)^{1/2} \qquad 3.10$$

where σ is the molar absorption coefficient and $h\nu$ the photon energy.

After photoexcitation, the annihilation of the electron/hole couple can occur by radiative or nonradiative processes. The lifetime of the couple, its redox potential, and the fraction of nonradiative recombinations are mainly triggered by the nanoparticle size and the existence of surface or internal

defects acting as charge carrier traps[53,54]. In particular, the increase of the band gap energy by decreasing the nanoparticle size involves more negative redox potential (E_e) for the electrons and a more positive one (E_h) for holes. These changes can be assessed by[31]

$$\Delta E_e = \frac{E_g - E_{g(\infty)}}{1 + \frac{m_e^*}{m_h^*}} \tag{3.11}$$

and

$$\Delta E_h = E_g - E_{g(\infty)} - \Delta E_e \tag{3.12}$$

The number of trap states for each nanoparticle is strongly sensitive to experimental conditions of the synthetic procedure[55].

The radiative electron/hole couple recombination leads to photon emission whereas nonradiative processes lead to the energy transfer to lattice vibrational motions and to redox reactions with electron donor or acceptor species adsorbed at the nanoparticle surface. As a consequence of the higher lifetime of trapped electrons and holes, reactions are due to these species rather than free charge carriers[56]. The various processes following the photon capture from a nanoparticle are shown in Fig. 3.8.

The change of the band gap energy of semiconductors with size involves also a change of their electron/hole conductivity (σ) according to the equation

$$\sigma = \sigma_0 e^{-\frac{E_g}{kT}} \tag{3.13}$$

It can be noted that an increase of the band energy gap determines a decrease of the conductivity.

3.3 Surface Effects

In addition to specific effect on the electronic structure arising from the nanoparticle small size, further effects could derive from the huge surface to volume ratio, shape, and surface topology such as corners, edges, and surface defects. Taking into account that surface atoms as well as those contained in an underlying thin layer are embedded in a force field different from that sensed by bulk ones, they are in a different energetic state and so they contribute differently to the total energy and free energy of the particle. Moreover, the position of surface atoms and their dangling bonds allow them to interact with the surrounding species, establishing specific physical or chemical interactions. Bare nanoparticles, in fact, can be obtained as dilute dispersion in high vacuum and after elimination of surface adsorbed species, i.e., in a very physically unusual condition. It follows that normally, nanoparticle size and shape as well as the surfacial shell composition are not well-

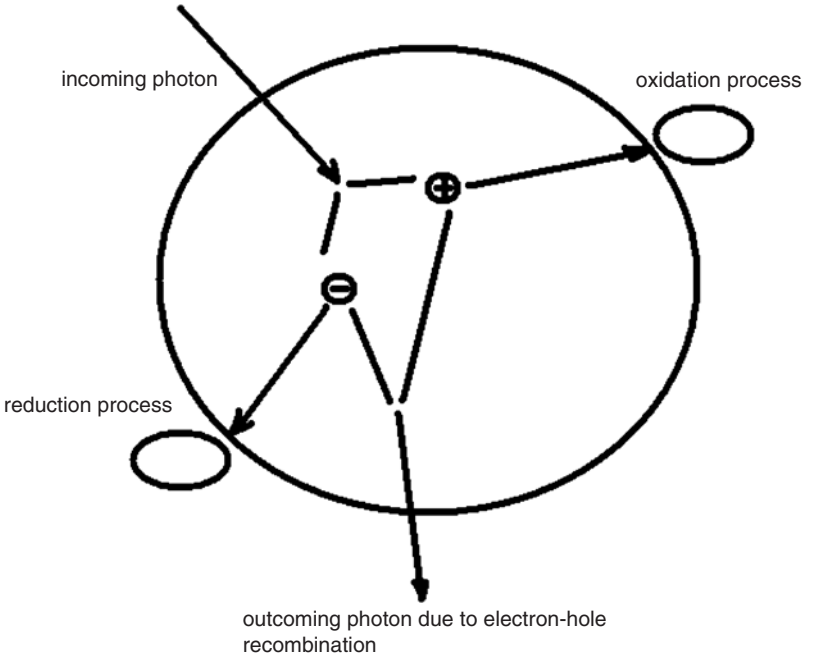

FIGURE 3.8. Radiative excitation and radiative or nonradiative processes of nanoparticles.

defined quantities. In addition to the well-known correlation between surface nature and catalytic efficiency, all these features cause changes in the thermodynamic properties of the material such as surface tension, melting temperature[57], solid-solid phase transition pressure[58], and magnetic properties[59]. Another property particularly sensitive to surface modifications is the fluorescence yield[60].

Obviously, the atom fraction at the surface of bulk materials is negligible so that all the properties resulting from the mean behaviour of all the species composing the sample are determined by those lying in the inside. This situation, however, changes in a typical way by decreasing the particle size, and the observed trend can be semiquantitatively described by making some very simple geometrical considerations.

Let us consider the partitioning of a cube having a volume of $1\,cm^3$ and a surface area of $6\,cm^2$ in N smaller cubes of identical size L, volume L^3, and surface area $6\,L^2$. Taking into account that subdivision does not involve a change of the overall volume, it follows that the total surface and the surface to volume ratio (S/V) of the smaller cube ensemble are given by $6L^{-1}$. Thus for example, if $L = 100$ Å, the total surface area increases by 10^6 times, becoming $6^*10^6\,cm$. Similar results are obtained by considering particle shapes different from the cubic one.

The L dependence of S/V in the range 0–100 Å is shown in Fig. 3.9. It can be noted that S/V changes little in a wide L region while, below a threshold L value, S/V rapidly increases with increasing the degree of subdivision. This feature is at the basis of the employment of small particles in the field of catalysis or enhanced adsorption because the number of active sites increases as S/V.

Another interesting aspect connected with the subdivision of matter as small particles can be perceived by considering that each cube could constitute a bit of information in a data storage system. For bidimensional devices of area $1\,cm^2$ storing information on a surface subdivided in N square elements of area L^2, the number of information elements is L^{-2}. So, the most recent information density of about 10 Gbit cm^{-2}, implying a bit size of approximately 100 nm, can be enhanced to 1 Tbit cm^{-2} for a bit size of 10 nm and even to 100 Tbit cm^{-2} if a bit size of 1 nm could be exploited. Furthermore, realizing three-dimensional devices as data-storage systems, the data density is even more strongly dependent upon the bit size, being equal to L^{-3} and reaching 10^9 Tbit cm^{-3} for a bit size of 1 nm. This emphasizes the importance of miniaturisation to increase the information density and the potentials of nanoparticles as building blocks of data storage systems. In recent years, bits of information formed by less than 100 atoms have been deposited on appropriate matrices by an atomic force microscope.

On the other hand, if nanoparticles are considered as building blocks of complex devices and machines, the possibility to concentrate so big an amount of constitutive elements in a reasonable volume suggests that a lot of astonishing applications can be addressed in the future.

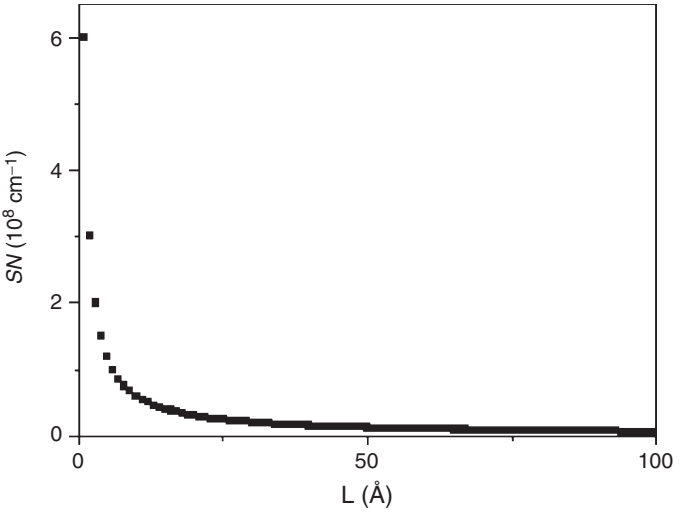

FIGURE 3.9. Size dependence of the surface to volume ratio (S/V).

Additional features are related to the nanoparticle shape. In fact, for a hypothetical spherical particle, all the atoms at the surface are in an identical topological and energetic state. On the other hand, this does not occur for particles having a different shape such as parallelepipeds, pyramids, or cubes. In order to put into evidence these features, here we consider the simplest case, i.e, cubic particles.

Considering a cubic lattice composed of atoms of size L_0 forming a cubic nanoparticle of size L in the vacuum, it can be observed that internal and surface atoms are surrounded by a different number of next neighbours. In particular, atoms can be divided into four classes according to their specific location: atoms at corners, edges, flat surfaces, and internal. It can be noted that these classes are characterized by a different number of next neighbours or coordination number (c.n.). In particular,

1. Atoms at corners with c.n.=3 and 3 dangling bonds
2. Atoms at edges with c.n.=4 and 2 dangling bonds
3. Atoms at flat surfaces with c.n.=5 and one dangling bond
4. Internal atoms with c.n.=6 and 0 dangling bonds

with f_3, f_4, f_5 and f_6 being the fractions of atoms with c.n. of 3, 4, 5, and 6, respectively, and from simple geometrical considerations it follows:

$$f_3 = \frac{8}{\left(\frac{L}{L_0}\right)^3} \tag{3.14}$$

$$f_4 = 12\frac{\frac{L-2L_0}{L_0}}{\left(\frac{L}{L_0}\right)^3} \tag{3.15}$$

$$f_5 = \frac{6\left(\frac{L-2L_0}{L_0}\right)^2}{\left(\frac{L}{L_0}\right)^3} \tag{3.16}$$

It is worth noting that as a consequence of the different topological and energetic states of these surface species, they give a distinct contribution to the surfacial and overall nanoparticle properties. The size dependence of the total fraction of surface atoms f_{sur}

$$f_{sur} = f_3 + f_4 + f_5 = 6(L_0/L) - 12(L_0/L)^2 + 8(L_0/L)^3 \tag{3.17}$$

together with the single contributions f_3, f_4, f_5 is shown in Fig. 3.10.

Looking at Fig. 3.10, it can be observed that the fraction of surface atoms is negligible for particles larger than 100 nm, while below this threshold value, by decreasing the nanoparticle size, it increases steeply with an increasing

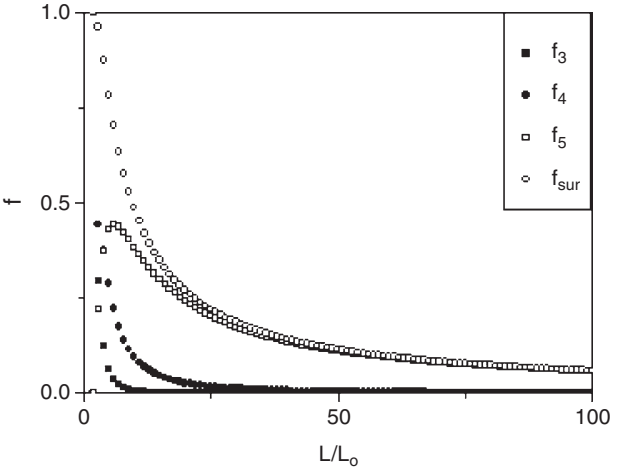

FIGURE 3.10. Size dependence of f_3, f_4, f_5, and f_{sur}.

preference for the species with lower coordination number. This means that the decrease of the nanoparticle size leads also a change of the relative proportions of the various surface atoms involving additional effects. This is summarized in Fig. 3.11, where the mean coordination number c.n. calculated by

$$c.n. = 3f_3 + 4f_4 + 5f_5 + 6f_6 \qquad 3.18$$

is shown as a function of size.

All these argumentations are based on the simplifying assumption that the nanoparticle can be considered composed of only two species: internal and surfacial ones. However, it must be stressed that this clear-cut view is not real and the local properties change smoothly proceeding from the external to the internal. Moreover, the assumption of perfectly cubic or spherical nanoparticles is not generally true: it has been argued that nanoparticle surface is not quite smooth, possessing a fractal-like structure[49].

The presence of irregularities increases the surface-to-volume ratio and the fraction of atom at the surface, enhancing the nanoparticle exotic character. Moreover, surface species, and in particular surface defects, as well as internal vacancies could add additional features by modifying the nanoparticle electronic structure thus altering their overall properties. On the other hand, driven by the reduction of the nanoparticle free energy, surfacial and internal atoms can rearrange or migrate leading to a decrease of the surface-to-volume ratio, number of defects, and/or to a structural change. The energy barriers to these processes are smaller than in the bulk[61].

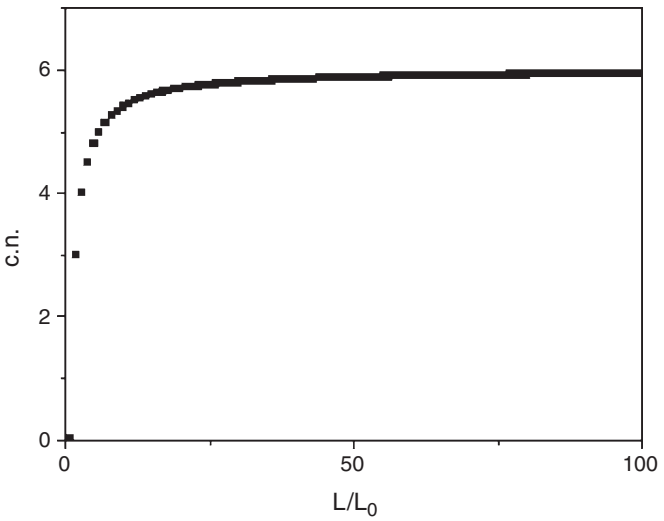

FIGURE 3.11. Size dependence of the mean coordination number c.n.

Surface plays an important role both for the optical and chemical properties of nanoparticles. First of all, surface species and defects can act as stabilizing traps for the photogenerated electron-hole pair so increasing their lifetime and lowering the molar extinction coefficient. In particular, Wang and Herron showed that nanoparticles cannot absorb additional photons until the electron-hole pair annihilates[48].

Moreover, because the energetic state of surface atoms is consistently different from bulk ones, their orbitals can less efficiently mix with those of the internal atoms. As a consequence, electronic states with energy composed between the conduction and the valence bands known as surface levels occur. The existence of these intermediate energetic levels involves some changes on the nanoparticle physical and chemical properties. In particular, the optical absorption and emission properties are influenced as a consequence of the increased number of possible electronic transitions[62–64].

It must be pointed out that surface is also the place on which eventual excess charges are accumulated and reactive processes could happen. The charging of nanoparticles can be due to several phenomena such as non-stoichiometric composition, release of charged species to the surrounding medium, or adsorption of ions coming from the surrounding medium. Charge accumulation involves nanoparticle-nanoparticle repulsion and electrostatic stabilization of nanoparticle against agglomeration. On the other hand, the enhancement of reactive processes at the nanoparticle surface is at the basis of their employment as catalysts or as reactants for fast solid-solid reactions[21].

The thermodynamic instability of nanoparticles toward an unlimited growth is determined by the tendency of surface atoms to saturate their dangling bonds. This phenomenon can take place through several different mechanisms[19,65] but it can be expected that the more efficient is the saturation of surface dangling bonds by growing, the more powerful is the driving force of the nanoparticle growth process. The variation of the number of surface atoms with increasing the particles size is given by the derivative of Eq. (3.17):

$$\frac{df_{sur}}{d(L/L_0)} = -6(L/L_0)^{-2} + 24(L/L_0)^{-3} - 24(L/L_0)^{-4} \qquad 3.19$$

This curve is shown in Fig. 3.12, and it clearly shows that the driving force diminishes very rapidly with size.

It follows that nanoparticles are thermodynamically unstable against an unlimited growth and that a synthetic protocol to be efficient in the nano-size regime should inhibit effectively the nanoparticle growth to allow the size control. As previously stated, this can be achieved by:

- compartmentalization in distinct domains, so nanoparticles cannot come into contact to aggregate
- charging of nanoparticles, so that they cannot aggregate owing to the repulsive inter-particle forces
- adsorption of suitable molecules at the nanoparticle surface.

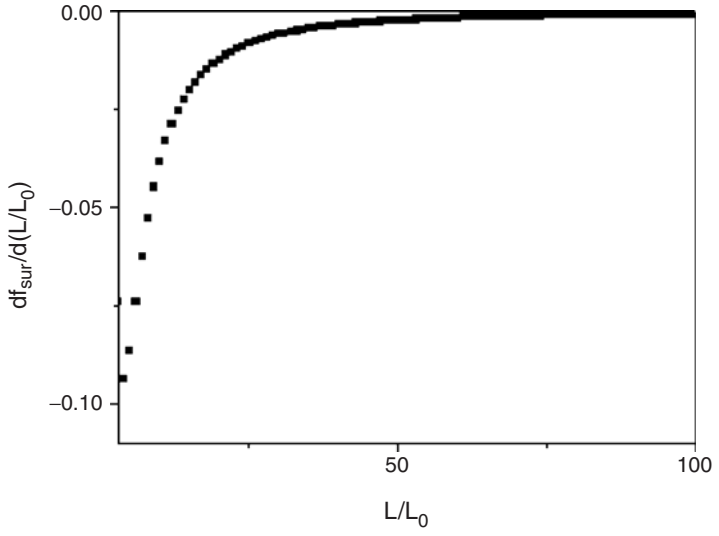

FIGURE 3.12. Size dependence of $df_{sur}/d(L/L_0)$.

It is worth noting that all these processes are mainly controlled by molecular events occurring at the nanoparticle surface. Of course, the control of the microscopic processes enabling growth inhibition are of utmost importance in determining the microscopic structure of the nanoparticles and, consequently, their properties. The choice of the synthetic method must therefore take it into account and be finalised to the subsequent use of the nanoparticles. In fact, the manipulation of nanoparticles without changing their properties after preparation remains a challenging question.

In conclusion, the reduced size of semiconductors and metals leads directly to changes of the physico-chemical properties with respect to the bulk solid while, for molecular solids or liquids, it is mainly the interaction with surrounding molecules inducing changes in the physico-chemical properties. Moreover, the entrapment within microheterogeneous systems can influence the physico-chemical properties of nanoparticles as a consequence of specific surfactant/nanoparticle interactions. The specific synthetic method leads to dangling bonds, adsorbed species, and surface roughness, which could produce electron and hole traps significantly influencing their lifetimes and radiative/nonradiative recombinations.

REFERENCES

1. C. R. Vesta,. Z. J. Zhang, *Chem. Mater*. **14**, 3817–3822 (2002)
2. Q. A. Pankhurst, J. Connelly, S. K. Jones, J. Dobson, *J. Phys. D. Appl. Phys*. **36**, R167–R181 (2003)
3. P. Tartaj, M Del Puerto-Morales, S. Veintemillas-Verdaguer, T. Gonzales-Carreno, C. J. Serna, *J. Phys. D. Appl. Phys*. **36**, R182–R197 (2003)
4. M. Shelef, G. W. Graham, *Catal. Rev. Sci. Eng*. **36**, 433–457 (1994)
5. K. Kim, J. Lee, S. J. Lee, *Chemical Physics Letters* **377**, 201–204 (2003)
6. K. P. Johansson, A. P. Marchetti, G. L. McLendon, *J. Phys. Chem*. **96**, 2873–2879 (1992)
7. B. O. Dabbousi, J. Rodriguez-Viejo, F. V. Mikulec, J. R. Heine, H. Mattoussi, R. Ober, K. F. Jensen, M. G. Bawendi, *J. Phys. Chem. B*. **101**, 9463–9475 (1997)
8. N. Serpone, R. F. Khairutdinov, *Semiconductor nanoclusters. Studies in Surface Science and Catalysis* vol. 103, pp. 417–444 (P.V. Kamat, D. Meisel Eds, Elsevier Science B.V. 1996)
9. N. Serpone, D. Lawless, R. F. Khairutdinov, *J Phys Chem*. 99, 16646–16654 (1995)
10. A. Di Paola, L. Palmisano, M. Derrigo, V. Agugliaro, *J. Phys. Chem. B* **101**, 876–883 (1997)
11. B. H. Korgel, H. G. Monbouquette, *J. Phys. Chem. B* **101**, 5010–5017 (1997)
12. N. Serpone, R. F. Khairutdinov, *Studies in Surface Science and Catalysis* **103**, 417–444 (1996)
13. B. M. Wckhuysen, G. Mestl, M. P. Rosynek, T. R. Krawietz, J. F. Haw, J. H. Lunsford, *J. Phys. Chem. B* **102**, 3773–3778 (1998)
14. V. Stengl, S. Bakardjeva, M. Marikova, P. Bezdicka, J. Subrt, *Materials Letters* **57**, 3998–4003 (2003)
15. A. Chang, J. H. Fendler, *J. Phys. Chem*. **93**, 2538–2542 (1989)

16. W. H. Qi, M. P. Wang, *J. Materials Science Letters* **21**, 1743–1745 (2002)
17. Q. Jang, L. H. Liang, J. C. Li, *Vacuum* **72**, 249–255 (2004)
18. M. R. Geller, W. M. Dennis, V. A Markel, K. R. Patton, D. T. Simon, H. Yang, *Physica B* **316**, 430–433 (2002)
19. O. Söhnel and J. Garside, *Precipitation*, Butterworth-Heinemann Ltd 1992, Oxford
20. P. Calandra, A. Longo, V. Turco Liveri, *J. Phys. Chem. B* **107**, 25–30 (2003)
21. P. Calandra, A. Longo, V. Marcianò, V. Turco Liveri, *J. Phys. Chem. B* **107**, 6724–6729 (2003)
22. H. Fissan, M. K. Kennedy, T. J. Krinke, F. E. Kruis, *J. Nanoparticle Research* **5**, 299–310 (2003)
23. O. P. Yadav, A. Palmqvist, N. Cruise, K. Holmberg, *Colloid Surfaces A* **221**, 131–134 (2003)
24. R. Janot, A. Rougier, L. Aymard, C. Lenain, R. Herrera-Urbina, G. A. Nazri, J. M. Tarascon, *J. Alloys and Compounds* **356**, 438–441 (2003)
25. Y. Isobe, M. Yamauchi, R. Ikeda, H. Kitagawa, *Synthetic Metals* **135**, 757–758 (2003)
26. G. Katabe, Y. Koltypin, A. Ulman, I. Felner, A. Gedanken, *Applied Surface Science* **201**, 191–195 (2002)
27. T.C. Halsey, *Nature* **258**, 761–766 (1992)
28. P. Keblinski, S. R. Phillpot, S. U. S. Choi, J. A. Eastman, *Int. J. of Heat and Mass Transfer* **45**, 855–863 (2002)
29. T. Liu, L. Guo, Y. Tao, T. D. Hu, Y. N. Xie, J. Zhang, *Nanostructured Materials* **11**, 1329–1334 (1999)
30. D. M. De Jesus, M. Spiro, *Langmuir* **16**, 4896–4900 (2000)
31. J. Zhang, Z. Wang, J. Liu, S. Chen, G. Liu, in *Self-assembled Nanostructures*, Ed D. J. Lockwood, Kluver Academic/Plenum Publishers, N.Y., 2003
32. Z. Zhang, M. A. Horsch, M. H. Lamn, S. C. Glotzer, *Nanoletters* **3**, 1341–1346 (2003)
33. M. Zhang, R. P. Singh, *Materials Letters* **58**, 408–412 (2004)
34. B. Ji, H. Gao, *Materials Science and Eng. A* **366**, 96–103 (2004)
35. C. Faure, A. Darrè, W. Neri, *J. Phys. Chem. B* **107**, 4738–4746 (2003)
36. P.K. Stoimenov, R. L. Klinger, G. L. Marchin, K. J. Klabunde, *Langmuir* **18**, 6679–6686 (2002)
37. I. Sondi, B. Salopek-Sondi; J. Colloid Interface Science 275, 177–182 (2004)
38. B. Heurtault, P. Saulnier, B. Pech, J. E. Proust, J. P. Benoit, *Biomaterials* **24**, 4283–4300 (2003)
39. J. Williams, R. Lansdown, R. Sweitzer, M. Romanowski, R. Labell, R. Ramaswami, E. Unger, *J. Controlled Release* **91**, 167–172 (2003)
40. I. Brigger, C. Dubernet, P. Couvreur, *Advanced Drug Delivery Reviews* **54**, 631–651 (2002)
41. D. Cui, H. Gao, *Biotechnol. Progr*. **19**, 683–692 (2003)
42. A. M. Gatti, F Rivasi, *Biomaterials* **23**, 2381–2387 (2002)
43. J. J. Bang, L. E. Murr, *J. of Materials Science Letters* **21**, 361–366 (2002)
44. D. B. Kittelson, W. F. Watts, J. P. Johnson, *Atmospheric Environment* **38**, 9–19 (2004)
45. A. Ruggirello, V. Turco Liveri, *J. Colloid Int. Sci*., **258**, 123–129 (2003)
46. J. A. Creighton, D. G. Eadon, *J. Chem. Soc. Faraday Trans*. **87**, 3881–3891 (1991)

47. U. Kreibig, M. Gartz, A. Hilger, *Ber. Bunsenges. Phys. Chem*. **101**, 1593–1604 (1997)
48. Y. Wang, N. Herron, *J. Chem. Phys*. **95**, 525–532 (1991)
49. P. Calandra, M. Goffredi, V. Turco Liveri, *Coll. Surf. A* **160**, 9–13, (1999)
50. E. Caponetti, L. Pedone, D. Chillura-Martino, V. Pantò, V. Turco Liveri, *Materials Science and Engineering C* **23**, 531–539 (2003)
51. T. Trindade, P. O'Brien, N. L. Pickett, *Chem. Mater*. **13**, 3843–3858 (2001)
52. V. Albe, C. Jouanin, D. Bertho, *J Crystal Growth* **184**, 388–392 (1998)
53. D. Y. Godovski, *Advances in Polymer Science* **119**, 79–122 (1995)
54. J. Z. Zhang, *J. Phys. Chem. B* **104**, 7239–7235 (2000)
55. R. Doolen, R. Laitinen, F. Parsapour, D.. Kelley, *J. Phys. Chem. B* **102**, 3906–3911 (1998)
56. D. Beydoun, R. Amal, G. Low, S. McEvoy, *J. of Nanoparticle Research* **1**, 439–458 (1999)
57. A.N. Goldstain, C.M. Echer, A.P. Alivisatos, *Science* **256,** 1425–1427 (1992)
58. L. E. Brus, J. A. W. Harkless, F. H. Stillinger, *J. Am. Chem. Soc*. **118**, 4834–4840, (1996) and references therein.
59. C. R. Vestal, Z. J. Zhang, *J. Am. Chem. Soc*. **125**, 9828–9833 (2003)
60. A Henglein, *Chem. Rev*. **89**, 1861–1873 (1989)
61. P. Morierty, *Reports on Progress in Physics* **64**, 297–381 (2001)
62. Z. Du, W. Zhang, Y. Huang, G. Ma, W. Zhao, Z. Zhu, *Supramolecular Science* **5**, 453–455 (1998)
63. L. Brus, *J. Phys. Chem*. **90** (12), 2555–2560 (1986)
64. Y. Li, Y. Ding, Y. Zhang, Y. Quian, *Journal of Physics and Chemistry of Solids* **60**, 13–15 (1999)
65. Frank-Peter Ludwig and Jürn Schmelzer, *Zeitschrift für Physikalische Chemie* **192**, 155–167 (1995)

4

Methods of Nanoparticle Synthesis in Microheterogeneous Systems

4.1 Introduction

The production of systems consisting of nanoparticles entrapped in microheterogeneous systems is of great interest because of their potential technological and biotechnological applications. This is because in addition to the quantum size effects and the huge surface to volume ratio characterizing the nanoparticle properties, new distinct features and functionalities can be conferred by their confinement, adsorption of surfactant molecules at the nanoparticle surface, and more or less ordered dispersion in the typical structure of microheterogeneous systems. As examples, the coating of the nanoparticle surface with a specific surfactant could inhibit the recombination of photogenerated electron/hole couples of semiconductor nanoparticles, increasing their mean life time and consequently the charge transfer at the nanoparticle/surrounding interface, and solid lipid nanoparticles have been suggested as suitable drug carrier systems affording a controlled and localized release of active drugs[1].

Often, the entire nanoparticle containing microheterogeneous system constitutes the final product of the preparation. For example, some nanoparticle containing microheterogeneous systems have been suggested as interesting nanofluids having peculiar magnetic, electric, wetting, and lubricating behavior that can be exploited for practical applications. Nanoparticle/surfactant composites are of special interest thanks to the long-time stability of their physical and chemical properties, the surfactant matrix being potentially able to prevent nanoparticle oxidation and coalescence. By varying the nanoparticle volume fraction, systems ranging from noninteracting to interacting nanoparticles can be realized, i.e., from a dilute dispersion of nanoparticles to an infinite extended network of interconnected particles and/or to a nanoparticle ordered array. Interesting physical phenomena such as insulator to metal transition can be observed especially in the threshold zone where percolation generally occurs.

The synthetic methods based on the use of microheterogeneous systems (liquid crystals, gels, solutions of micelles and vesicles, microemulsions, mono- and multi-layers) to manipulate matter at the molecular level are typical bottom-up techniques. They all are generally rapid and low-cost

methods and potentially allow the synthesis of a wide range of nanosized inorganic materials such as metals, oxides, sulphides, water-insoluble substances, and, quite recently, also water-soluble inorganic and organic substances[2,3].

The synthesis can be easily directed to form mixed nanoparticles (core-shell, doped, sandwich, hollow)[4]. Confinement of small organic molecules as well as polymers has been also achieved.

Generally, the synthesis can be carried out at room temperature and by performing very simple laboratory procedures, allowing a fine size and polydispersity control and the preparation of 1D, 2D, and 3D nanoparticle arrays. The nanoparticle size usually being less than 100 nm, these systems are optically clear and suitable for UV-vis and IR absorption investigations. Moreover, because this approach works at the atomic/molecular level, it is possible to coat or dope nanoparticles with other materials or, by a suitable selection of the microheterogeneous system, a control of the nanoparticle shape can be achieved.

The templating effect of microheterogeneous systems is based on the existence of a peculiar fragile structure, which can be easily permeated by appropriate species leading to their solubilization and, on the other hand, allowing their local non-homogeneous distribution in the dynamic nanoscopic domains. It is worth noting that, as a consequence of its fragility, the structure of some microheterogeneous systems can be drastically modified by applying constant or variable external forces such as electric and magnetic fields and shear giving the opportunity to have with the same system different synthetic routes. According to the nature of the system and the specific synthetic procedure, the resulting nanomaterial can retain the same order pre-existing before synthesis or be a cast of it or could show a new order.

An inspection of the literature in this specific research field puts into evidence a huge number of contributions and a wide variety of synthetic protocols used to produce nanoparticles and nanomaterials. This makes impracticable the attempt to give an account of all the innovative methods and to classify them in a reasonable and clear-cut number of different synthetic strategies. The way out is the presentation of a panoramic view of the field and the introduction of some arbitrary generalizations and rough approximations. Besides, I have chosen to report on the most recent literature aiming to show the actual state of the art and the tendency to prepare more and more complex nanoparticle containing microheterogeneous systems.

It is worth noting that the best conditions to obtain the desired nanomaterial can be generally found performing direct experiments by changing some external parameters or adjusting the procedure coupled with the check of the physico-chemical properties of the final product. This because a general theory allowing to select a priori the optimal conditions for the synthesis of a given nanomaterial by microheterogeneous systems with the

wanted properties has not yet been produced and there are reasonable argumentations suggesting that this will never be obtained. Long life to the experimentalists!

A block diagram showing the steps of the most frequent synthetic procedures of nanoparticles in microheterogeneous systems is shown in Fig. 4.1. In this scheme, it is emphasized the need to i) select the microheterogeneous system appropriate for the wanted nanomaterial, ii) inspect its structure after the solubilization of reactants, and iii) characterize the physico-chemical properties of the system resulting from the mixing process and their time dependence.

All the information collected during steps ii) and iii) and their analysis are pivotal to minimize the number of experiments necessary to find the optimal synthetic protocol. In particular, even if frequently neglected, the study of the time dependence of the nanomaterial physico-chemical properties is of utmost importance to establish its chemical and temporal stability.

Obviously, each physico-chemical property furnishes a window to get information on the molecular picture of the system. However, the most frequently employed techniques to characterize the nanomaterials are the microscopic (TEM, SEM, AFM) and scattering (SAXS, SANS, light scattering) ones allowing to state the structural properties of the nanocomposites. Further characterization of the nanoparticle properties is achieved by the use of quite all the physico-chemical techniques. Among these, a relevant

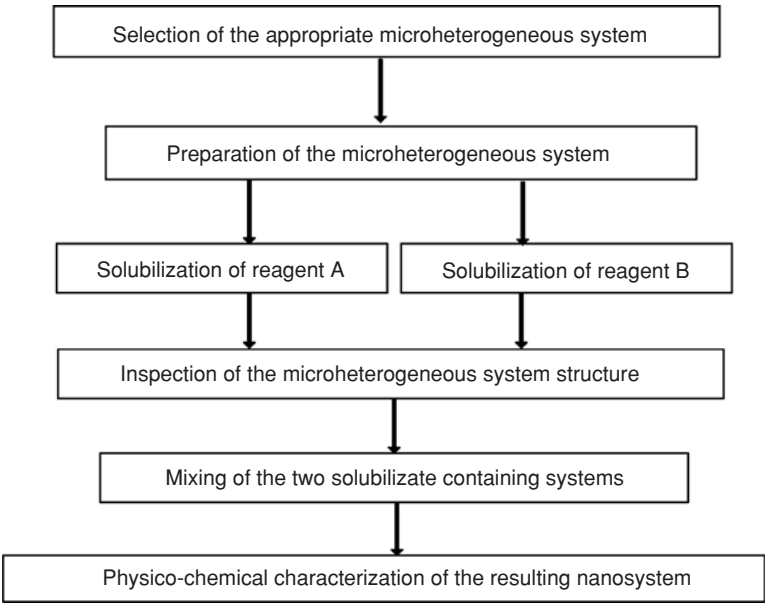

FIGURE 4.1. Block diagram of nanoparticle synthetic procedures.

place is occupied by spectroscopic methods and investigations on the chemical reactivity.

In the following parts, the various recipes taken from the literature have been distinguished according to the kind of microheterogeneous system employed to emphasize the structural peculiarities conferred to nanoparticles by a specific surfactant self-assembling. Within such partition, they have been in turn subdivided according to the kind of substance composing the nanoparticles, as metals, semiconductors, magnetic materials, and miscellaneous nanoparticles. This partitioning is dictated by the fact that each class of substance includes nanoparticles with common potential applications. Metal and semiconductor nanoparticles, in fact, are widely investigated because of their potentials in catalysis, photoreactions, sensors, and as components of optical and electronic devices. Magnetic nanoparticles, on the other hand, find interesting applications just for their sensitivity to magnetic fields as ferrofluids and building blocks of magnetic devices. Finally, miscellaneous nanoparticles include many different classes of substances such as polymers and biomaterials.

All the below reported recipes can be simply used in a pure imitative way allowing the synthesis of the same or similar nanomaterial. However, the hope is that their critical reading together with the considerations reported in the other parts of this book could stimulate the conception of novel synthetic procedures. In particular, quite unexplored routes are those directed to the self-assembling of multicomponent nanoarchitectures.

4.2 Nanoparticle Synthesis in Liquid Crystals

The geometric arrangement of nanoparticles on suitable matrices determines interesting collective properties. Thus, it is of utmost importance not only the control of the nanoparticle size and shape but also that of their spatial distribution. Liquid crystals possess the suitable structural and dynamical properties for this purpose. Looking to the typical structures of liquid crystals and taking into account that nanoparticles are selectively confined into the hydrophilic or hydrophobic domains, it can be argued that the potential nanomaterials that can be obtained are a random or ordered three-dimensional distribution of nanoparticles confined in the polar or apolar domains, bidimensional wells in the case of lamellar structures, and unidimensional wires for liquid crystals characterized by an hexagonal structure. A schematic representation of the nanoparticle synthesis in liquid crystals and one of the possible final structures is shown in Fig. 4.2.

Moreover, organic and inorganic mesoporous materials characterized by canalicula with nano-size cross section can be, in principle, prepared using liquid crystals as templates. This can be achieved by selecting precursors preferentially solubilized in the apolar or polar domain. After the synthesis of the mesoporous solid material, the surfactant can be easily removed by

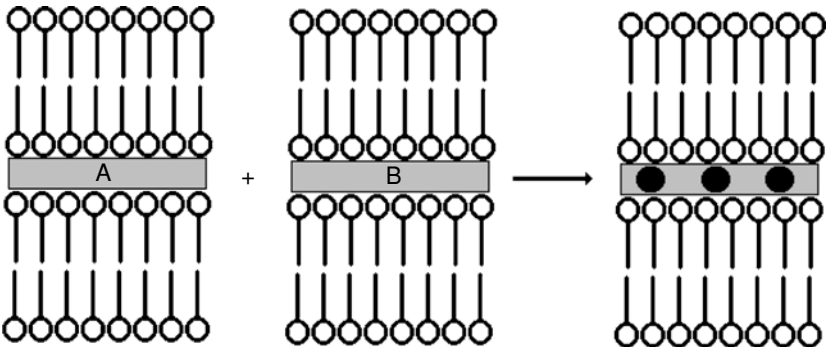

FIGURE 4.2. Schematic representation of nanoparticles synthesis in liquid crystals.

washing with the appropriate solvent. The most frequent problem arises from the mechanical constraints introduced by the progressive aggregation of precursors leading to the destruction of the local structure and the vanishing of the template effect. As a general rule, the successful synthesis can be achieved by the patient research of the appropriate experimental conditions.

4.2.1. Synthesis of Metallic Nanoparticles in Liquid Crystals

Silver nanoparticles were introduced in the lamellar phase formed by water/sodium dodecylsulfate/hexanol/dodecane liquid crystals using the following procedure. Negatively charged surfactant coated hydrophilic silver nanoparticles were synthesized by mixing aqueous silver nitrate with aqueous sodium borohydride and sodium oleate. On the other hand, by adding aqueous H_3PO_4 and dodecane or cyclohexane, hydrophobic silver nanoparticles were obtained in the organic phase. Coated nanoparticles were subsequently introduced in liquid crystals by adding the silver hydrosol or the silver organosol to the water/sodium dodecylsulfate/hexanol/dodecane system. As expected, it was found that the silver hydrosol is mainly solubilized in the aqueous layers whereas the silver organosol in the organic layers. In both cases, only an increase of the interlamellar distance was observed without variation of the basic structure of the liquid crystals[5].

Silver nanostructures were synthesized in the lamellar phase formed by tetraethylene glycol monododecylether $C_{12}E_4$ (Brij 30) by adding an 0.02 M aqueous solution of $AgNO_3$ to the pure surfactant. The solubilization of water among the surfactant layers allowed the contemporaneous entrapment of Ag^+ and NO_3^- ions. On the other hand, the formation of silver nanoparticles resulted from the reducing action of the oxyethylene groups of $C_{12}E_4$. TEM investigation indicated a bimodal particle size distribution constituted

by a larger proportion of smaller nanoparticles with a size in the range 2–3 nm and a smaller proportion of larger particles. The smaller nanoparticles were found to be arranged roughly close packed, forming very wide and long ribbons. The observed clustering of these particles revealed long-range nanoparticle/nanoparticle attractive interactions, whereas the partial inhibition of nanoparticle coalescence indicated a surface poisoning of the nanoparticle due to the surfactant hydroxyl groups. On the other hand, ribbons formation was dictated by the bidimensional domain characterizing the surfactant lamellar structure. By increasing the thickness of the hydrophilic domain of the lamellar structure, the size of the smaller nanoparticles was found unchanged whereas that of the larger particles and/or their amount was increased. Ageing of silver/$C_{12}E_4$ nanocomposites involved an increase of the larger particle proportion[6].

Macroscopically aligned silver nanoparticles have been obtained using as template the reverse hexagonal liquid crystal phase formed by poly(ethyleneoxide)-*block*-poly(propyleneoxide)-*block*-poly(ethyleneoxide) with the composition $EO_{20}PO_{70}EO_{20}$ (Pluronic P123). The synthesis strategy is based in the insertion of a silver nitrate solution in the hydrophilic core of the surfactant hexagonal structure and the slow reduction of the silver ions by means of the reducing ethyleneoxide groups. In particular, the procedure consisted in the mixing of Pluronic 123 with butyl acetate and a 1% aqueous solution of silver nitrate in the weight ratio 10:7:3. The resulting mixture was a clear and highly viscous gel. To allow the complete reduction of silver ions, the gel was maintained for six months in a covered glass beaker at room temperature. In such conditions, the formation of silver/liquid crystal composite fibers of several millimeters constituted by 3 nm silver nanoparticles in length was achieved. The authors reported that the formation of silver nanoparticles is accompanied by the partial destruction of the reverse hexagonal structure resulting from the contemporaneous oxidation of the EO groups. This effect most probably could be minimized by reducing the silver-to-surfactant molar ratio leading to a less marked composition and structural change of the template[7].

By reduction of hexachloroplatinic acid dissolved in the aqueous domain of the hexagonal phase formed by some oligoethylene oxide nonionic surfactants, mesoporous metallic platinum with pores disposed on a hexagonal lattice has been obtained. It can be argued that the application of this method to appropriate substances should allow the realization of mechanically robust mesoporous metals with interesting applications as catalysts, specialized electrodes, and semipermeable and robust filters with enhanced selectivity[8].

High concentrations of pure metallic copper nanoparticles with fcc structure have been synthesized in aqueous solutions of cetyltrimethylammonium bromide and ammonia by reduction of cupric chloride with hydrazine. The synthesis of metallic Cu nanoparticles was performed in a capped bottle by mixing two aqueous solutions of CTAB, one containing cupric chloride plus

ammonia and the other hydrazine. From the analysis of TEM data, it was ascertained that, after an initial decrease, the mean diameter of Cu nanoparticles approaches a constant value with the increase of hydrazine concentration. It was suggested that the formation of a bilayer structure of CTAB molecules prevents the particle agglomeration and precipitation[9].

4.2.2. *Synthesis of Semiconductor Nanoparticles in Liquid Crystals*

Cadmium sulfide nanoparticles were synthesized using as templating medium the lyotropic liquid crystals formed by cholesteryl oligo(ethylene oxide). The synthesis was carried out by adding an aqueous solution of cadmium nitrate to the pure surfactant. Then, the mixture was homogenized by shaking and heating and successively placed in contact with gaseous H_2S. After reaction, the samples were washed and centrifuged. Lamellar or hexagonal CdS nanoparticles embedded in the organic matrix were obtained by changing the structure of the surfactant mesophase. This was accomplished by varying the number of methylene oxide units of the amphiphile[10].

Zinc sulfide nanoparticles were synthesized by mixing two water/Triton X-100/n-decanol lamellar liquid crystals containing $Zn(CH_3COO)_2$ and Na_2S, respectively. The size of nearly spherical ZnS nanoparticles was about 10 nm and mainly controlled by the thickness of the hydrophilic layer. It was observed that the presence of ZnS nanoparticles influences the anti-wear properties of the bare liquid crystal[11].

Stable lead sulphide nanoparticles were synthesized in the bicontinuous cubic phase formed by sodium bis(2-ethylhexyl)sulfosuccinate (AOT)/water/Na_2S liquid crystals by contacting with an aqueous solution of $Pb(NO_3)_2$. The nanoparticles were subsequently stabilized by n-dodecanethiol as capping agent. The size of nanoparticle (4–14 nm) was controlled by changing the initial Na_2S concentration in the liquid crystals[12].

PbS nanoparticles with size in the range 10–15 nm were synthesized by directly mixing solid $Pb(CH_3COO)_2 \cdot 3H_2O$ with a mixture of $Na_2S \cdot 9H_2O$ and polyoxyethylene 10 stearyl ether. The resulting product was isolated by washing with water and ethanol and finally dried[13].

Hexagonal mesoporous silica layers were synthesized by hydrolysis of tetraethoxysilane (TEOS) in alkyltrimethylammonium bromides liquid crystals as templating phases. Initially a mixture of TEOS, ethanol, and water was aged and then water and surfactant were added. In some samples, silica nanoparticles were introduced as seeds. Subsequently, the samples were deposited on glass or silicon slides and thermally treated. The resulting surfactant-free silica layers showed a well-ordered structure with a preferential orientation induced by the air/solution and solution/slide interfaces. This preferential orientation was absent in the samples obtained by adding silica nanoparticle seeds. The effect of the structural order on the layer permeability was investigated[14].

It has been reported that transition metal aquo-complexes of nitrates and perchlorates form 2D and 3D hexagonal and cubic liquid crystals when solubilized in some alkyl oligo(ethylene oxide) non-ionic surfactants. By reaction with H_2S gas, the $[Cd(H_2O)_4(NO_3)_2]$/surfactant liquid crystals produce CdS spherical nanoparticles. For the synthesis, thin films of the liquid crystalline phase were deposited on quartz windows and then exposed to H_2S gas leading to a fast nanoparticle formation[15].

Cu_2O nanowires were obtained by electrodeposition through two narrowly spaced electrodes from reversed hexagonal liquid crystalline phases composed of sodium bis(2-ethylhexyl)sulfosuccinate (AOT), *p*-xylene, $CuCl_2$, and water. It was observed that the alignment of the liquid crystalline phase could be enhanced by controlling the electrode distance. It was emphasized that this method can be easily exploited for the synthesis of many metal, semoconductor, and polymer nanowires[16].

4.2.3. *Synthesis of Magnetic Nanoparticles in Liquid Crystals*

γ-Fe_2O_3 nanoparticles were obtained by addition of alkali to an aqueous solution of Fe(III) and Fe(II) salts followed by acidification and oxidation with ferric nitrate. After dialysis, the resulting magnetic fluid was mixed with solid dodecyldimethylammonium bromide (DDAB) and the mixture was homogenized by centrifugation. This procedure allowed to obtain a dispersion of γ-Fe_2O_3 nanoparticles in the lyotropic lamellar phase formed by DDAB[17].

Positively charged ferrite nanoparticles were introduced in potassium laurate/1-decanol/water liquid crystals leading to the formation of stable ionic ferrofluids. Magnetic nanoparticles (γ-Fe_2O_3) were synthesized by adding alkali to an aqueous solution containing a mixture of ferric and ferrous salts. The resulting colloidal dispersion was subsequently added to potassium laurate/1-decanol/water liquid crystals previously prepared. These ferromagnetic systems appear to be viscous and birefringent fluids, which under the application of a low magnetic field display a reversible orientational transition. Modifications of the phase diagram of the liquid crystalline system due to the nanoparticle presence were observed[18,19].

4.2.4. *Synthesis of Miscellaneous Nanoparticles in Liquid Crystals*

Calcium carbonate was synthesized in hexagonal and reversed hexagonal liquid crystals formed by triblock copolymers (Pluronics). The liquid crystalline phases obtained by mixing an aqueous solution of $CaCl_2$ with the copolymer were exposed to carbon dioxide. It was observed that the resulting $CaCO_3$ crystals were located in the aqueous nanoregions. $CaCO_3$ with

vaterite structure was obtained at low $CaCl_2$ concentrations while calcite resulted at high salt concentrations[20].

By photopolymerization of metal *p*-styryloctadecanoate inverted hexagonal liquid crystals, polymeric networks with the same structural features were obtained. The feasibility of the templated synthesis of CdS nanoparticles within the hydrophilic nanochannels of these polymerized phases was also ascertained[21].

Polymeric nanoparticles were synthesized by free radical polymerization of divinylbenzene and styrene in the reversed hexagonal liquid crystals formed by sodium bis(2-ethylhexyl)sulfosuccinate. After mechanical stirring and centrifugation of surfactant and water, the divinylbenzene or styrene monomers were added together with the initiator, potassium peroxodisulfate and 2,2′ azobis(2-methylproprionitrile). Polymerization was carried out at 60°C for 24 h. The formation of extended layers arising from the alignment of polymeric nanospheres into parallel linear chains was observed[22].

By ultrasound, an orientationally ordered dispersion of carbon nanotubes in a liquid crystal formed 4′-pentyl-4-cyanobiphenyl has been obtained. Moreover, it has been observed that their preferential orientation can be driven by applying external forces such as magnetic and electric fields[23].

Nanostructured polyacrylamide was synthesized in lyotropic liquid crystals formed by Brij-58 and Brij-56 by photopolymerization of monomeric acrylamide. As photoinitiator, Irgacure-2959 was used in the presence of bisacrylamide. The polymerization rate resulted to be significantly increased in such microheterogeneous systems. Structural effects on polyacrylamide nanoparticles due to diffusional constraints, segregation, and ordering phenomena was observed[24].

4.3 Nanoparticle Synthesis in Mono- and Multilayers

The growth of crystallites governed by mono- and multilayers allows the formation of random or ordered dispersion of 0D and 1D nanoparticles in thin layers and bidimensional inorganic or organic 2D nanoparticles placed on suitable supports[25,26].

The possibility to control finely the thickness of the surfactant layer and the low cost of the methodology make it a very interesting method for many technological applications. Moreover, this synthetic strategy can be considered an ideal method to mime the biomineralization processes occurrring at the surface of cell membranes. Various methods can be used to prepare nanoparticle containing films:

- binding of nanoparticles to layers
- synthesis in situ of nanoparticles
- growth in situ of nanoparticles

- by deposition of nanoparticle containing microheterogeneous system on appropriate surfaces

A panoramic view of various nanomaterials that can be obtained using surfactant mono- and multilayers has been reported by Stine et al. and Tieke et al.[27,28]

4.3.1. *Synthesis of Metallic Nanoparticles in Mono- and Multilayers*

Gold nanoparticles stabilized by sodium 3-mercaptopropionate (NaMP) were produced by the simultaneous addition of NaMP and sodium citrate to an aqueous solution of $HAuCl_4$. The particle size was easily controlled by changing the NaMP/$HAuCl_4$ ratio. Nanoparticle electrostatic stabilization is provided by the formation of a chemically bonded coat of oriented negatively charged MP^- ions. Then, these gold nanoparticles were introduced in the interlayer of *N*-[*p*-trimethylammonium hexyloxybenzoyl-*O*-*O'* -ditetradecyl-(L)-glutamate] bromide anchored on poly(tetrafluoroethylene) films by immersing the film into the aqueous dispersion of gold nanoparticles[29].

A stable suspension of gold nanoparticles was prepared by chemical reduction of aqueous $HAuCl_4$ with sodium borohydride. Subsequently, a solution of laurylamine in chloroform was added, and the two-phase mixture was vigorously shaken, leading to the complete transfer of laurylamine-capped gold nanoparticles in the organic medium. Then, the hydrophobized nanoparticles were extracted, washed, and dried. Finally, stable Langmuir-Blodgett films were obtained by spreading a mixture of coated gold nanoparticles and octadecanol in chloroform on water[30].

Gold nanoparticles synthesized in water were transferred into octadecylamine (ODA) monolayers lying at the air-water interface. The driving force of the transfer process was the chemical binding of ODA to the particles. Gold nanoparticles were obtained by chemical reduction of chloroaurate ions with glucose, and the octadecylamine monolayers were formed by spreading a ODA/chloroform solution on the surface of the aqueous dispersion of colloidal gold[31].

Pd and Au nanoparticles entrapped in a two-dimensional Langmuir monolayer were synthesized by in situ chemical reduction. In particular, solutions of the water-insoluble $Pd_3(CH_3COO)_6$ or $Au(P(C_6H_5)_3)Cl$ and arachid acid or octadecylamine in chloroform were spreaded on the surface of an aqueous solution of sodium borohydride. After evaporation of the organic solvent, nanoparticle containing monolayers were transferred onto solid substrates by the conventional dipping method. Size and shape of the nanoparticles were found to be dependent on the monolayer composition[32].

Silver nanoparticles coated by a monolayer of tri-*n*-octylphosphine oxide (TOPO) and self-assembled into multilayer films have been prepared. The synthesis of silver nanoparticles was carried out by chemical reduction of

aqueous $AgNO_3$ with sodium borohydride. Then, the colloidal suspension was mixed with a TOPO solution in toluene under vigorous stirring; this allowed nanoparticle coating and transfer into the organic phase. The resulting suspension of coated nanoparticles showed long-term stability of its optical properties. By immersing glass-slides in this suspension, a mirrorlike film of self-assembled silver nanoparticles is spontaneously formed. The nanoparticle binding was improved by thorough cleaning of the glass-slide surface. The film thickness was about 10 nm, and the absorption peak due to strong surface plasmon resonance was significantly red-shifted with respect to that of isolated nanoparticles in toluene. This finding was attributed to the close packing of silver nanoparticles resulting in an increase of the permittivity of the surrounding medium[33].

Capped platinum nanoparticles have been synthesized by chemical reduction of chloroplatinate ions in 4-hexadecylaniline Langmuir monolayers. Initially a solution of 4-hexadecylaniline in chloroform was spread on the surface of an aqueous solution of H_2PtCl_6. In such conditions, a monolayer of oriented surfactant molecules is formed at the air-water interface and at the same time the reduction of $[PtCl_6]^{2-}$ ions and the capping of resulting Pt nanoparticles is achieved. Nanoparticle containing monolayers were subsequently transferred onto various substrates (gold-coated quartz crystals, carbon-coated copper grids, and silicon). The aggregation of 4-hexadecylaniline-capped Pt nanoparticles and the formation of nearly linear superstructures was observed[34].

4.3.2. *Synthesis of Semiconductor Nanoparticles in Mono- and Multilayers*

The epitaxial growth of PbS nanoparticles was carried out in mixed monolayers of arachidic acid and octadecylamine as a function of the monolayer composition. The synthesis was performed by sending gaseous H_2S over an aqueous $Pb(NO_3)_2$ solution whose surface was antecedently coated by the surfactant mixture monolayer[35].

Thin layers of CuS were formed by exposing monolayers of copper stearate to an atmosphere of H_2S. These monolayers were obtained by dipping glass plates in a solution of $CuSO_4$ in water where a layer of stearic acid was previously deposited[36].

Cadmium sulfide nanoparticles were synthesized under monolayers of arachidic acid deposited on an aqueous $CdCl_2$ solution ($[CdCl_2] = 10^{-3}$M) by addition of gaseous H_2S. The monolayer was realized by dispersing an appropriate amount of a 10^{-3} M solution of arachidic acid in chloroform and allowing the complete evaporation of chloroform. The resulting nanoparticles were rod-like with widths of 5–15 nm and lengths of 50–300 nm[37].

By the hydrolysis of titanium tetraisopropoxide in a chloroform/1-propanol mixture containing hexadecyltrimethylammonium bromide (CTAB) and

tetramethylammonium hydroxide (TMAH), stable dispersions of TiO_2 nanoparticles (18–22 Å) were obtained. In such conditions, TMAH acts as catalyst and CTAB as coating agent. The formation of a stable coat was attributed to the binding of the cationic CTAB surfactant at the negatively charged TiO_2 particle surface. By spreading these dispersions on water surface, films of coated nanoparticles were obtained. It was found that the interparticle distance can be controlled by a heating treatment of the dispersion. This finding was attributed to some changes of the TiO_2 nanoparticle surface leading to a variation of the surfactant coat thickness[38].

Small-size CdS nanoparticles were synthesized in Langmuir-Blodgett films of stearic acid and tetra-tertoctyl-calix[4]arene-carboxyl acid. After solubilization of a cadmium salt, CdS nanoparticles were formed by exposing the LB films to H_2S gas. The time dependence of the nanoparticle size was explained in terms of a two-dimensional diffusion model[39].

Surfactant-coated CdS nanoparticles were spread on water surface to form Langmuir-Blodgett films. After preparation of CdS sols in aqueous solutions of sodium hexametaphosphate, the semiconductor nanoparticles were coated with dioctadecyldimethylammonium bromide and cetyltrimethylammonium chloride and extracted in chloroform and hexane. The role of sodium hexametaphosphate is to electrically passivate the nanoparticle surface. Subsequently, size-selective separation of surfactant-capped CdS nanoparticles was performed by adding increasing amounts of methanol or pyridine to the dispersions and centrifugation. By spreading the chloroform dispersions on water surface, Langmuir-Blodgett films were obtained. The fluorescence spectrum of these films showed sharp excitonic emission bands[40].

CdS nanoparticles were synthesized at the toluene/water interface containing an increasing amount of oriented cetyltrimethylammonium bromide molecules. The aqueous sub-phase contained $[CdEDTA]^{2-}$ while gaseous H_2S was produced by an aqueous Na_2S solution and directed toward the oil/water interface. After the reaction, toluene was evaporated and the films were transferred onto amorphous carbon. It was observed that, at low surfacial concentration of the surfactant, only single CdS nanoparticles are formed. However, as a result of the templating effect of the dish-like hemimicelles formed at higher surfactant concentration, disk-like aggregates of CdS nanoparticles were obtained by increasing the surfacial concentration of CTAB[41].

CdS and HgS nanoparticles have been synthesized in Langmuir-Blodgett films formed by behenic acid and deposited in quartz substrates. Initially, a solution of behenic acid in chloroform was spread on an aqueous subphase containing Cd^{2+} or Hg^{2+} or $Cd^{2+} + Hg^{2+}$ ions. Then, the monolayer was transferred on quartz plate hydrophobed with dodecanol and exposed to gaseous H_2S[42].

4.3.3. *Synthesis of Magnetic Nanoparticles in Mono- and Multilayers*

The synthesis of amorphous iron-containing magnetic nanoparticles controlled by applying electric and magnetic fields was carried out in a Langmuir monolayer by photocatalytical decomposition of iron pentacarbonyl. The Langmuir monolayer was prepared by spreading a chloroform solution of the iron compound and stearic acid on the water surface while the decomposition reaction was achieved by UV irradiation. By imposing magnetic and electric fields, marked increase of the size and shape anisotropy of nanoparticles was observed[43].

Magnetite nanoparticles coated by surfactant monolayer have been prepared by chemical co-precipitation method[44].

By chemical decomposition of $Co_2(CO)_8$ in toluene, cobalt oxide nanoparticles were prepared. AOT was used as stabilizing agent, and fine size control was achieved by varying the $Co_2(CO)_8$ to AOT molar ratio. Then, monolayer and multilayers of self-assembled nanoparticles coated by surfactant molecules were simply obtained by deposition of a drop of the nanoparticle containing solution on an amorphous carbon film controlling the solvent evaporation rate[45].

γ-Fe_2O_3 nanoparticles of about 8.3 nm were synthesized in aqueous solutions of $FeCl_3$ and NaOH. Nanoparticles were precipitated by a magnetic field and separated by decantation. After repeated washing steps, nanoparticles were treated with an aqueous solution of HCl leading to a clear hydrosol of γ-Fe_2O_3 that was used as subphase of Langmuir monolayers of arachidic acid. It was observed the formation of L-B films exhibiting superparamagnetic properties composed by a stable complex between arachidic acid and γ-Fe_2O_3 nanoparticles[46].

4.3.4. *Synthesis of Miscellaneous Nanoparticles in Mono- and Multilayers*

A nanocomposite constituted by 2D layers of decatungstate ions entrapped in dioctadecyldimethylammonium bromide (DODMA) bilayers has been synthesized. The experimental procedure consists in the mixing of two aqueous solutions containing Na_2WO_4 and DODMA, respectively. The precipitate was filtered, washed, and dried under vacuum. An analogous nanocomposite was prepared by substituting Na_2WO_4 with potassium hexachloroplatinate. From this composite, by reduction of Pt(IV), a system constituted by Pt nanoparticles dispersed in DODMA bilayers was prepared. Finally, nanocomposites formed by DODMA, $W_{10}O_{34}^{4-}$, and Pt nanoparticles were prepared by simply mixing two dispersions of $W_{10}O_{34}^{4-}$/DODMA and Pt/DODMA in

chloroform followed by the evaporation of the solvent under vacuum. It was observed that the $W_{10}O_{34}^{4-}$/DODMA composite dispersed in 2-propanol photocatalyzes the dehydrogenation of 2-propanol in acetone in presence of oxygen without hydrogen evolution. When the Pt/$W_{10}O_{34}^{4-}$/DODMA composite was utilized, the same reaction occurred in absence of oxygen with hydrogen evolution. It is suggested that Pt allows the reoxidation of the protonated $H_2W_{10}O_{34}^{4-}$ to $W_{10}O_{34}^{4-}$ with H_2 evolution[47].

Stable Langmuir films were formed by spreading a perylene-3,4,9,10-tetracarboxylic acid solution in dimethylsulfoxide/toluene onto the surface of an aqueous subphase containing copper (II) acetate. The films were transferred on solid substrates (quartz, CaF_2, mica) and investigated. It was found that they are formed by small nanoparticles arising from the aggregation of Cu(II)/perylene-3,4,9,10-tetracarboxylic acid complex molecules[48].

Thin films of mesostructured silica on silicon wafers were prepared by infiltration of vapour of tetraethoxysilane (TEOS) into a surfactant layer constituted by poly(ethylene oxide)-poly(propylene oxide)-poly(ethylene oxide) triblock copolymer acting as a templating agent. The silicon wafers were covered with a surfactant film by spin-coating with a solution of Pluronic F127 in water/ethanol while the TEOS vapour infiltration was achieved by placing the wafers in a closed vessel saturated with TEOS vapour. Finally, total removal of surfactant molecules was obtained by calcinations at 400 °C leading to the formation of stable mesostructured silica films[49].

4.4 Nanoparticle Synthesis in Direct Micelles

Historically, the formation of colloidal aqueous solutions is probably the oldest method to prepare stable nanoparticle dispersions. However, the occurrence of this phenomenon was most often considered an unwanted nuisance, and some procedures were exploited in the past to force the colloid separation from the liquid phase (heating, addition of electrolytes, etc.). The investigations directed to understand the microscopic processes responsible for the colloid formation have emphasized the role of the absorption of some species at the surface of the colloidal particles leading to their charging and/or to the saturation of their surface dangling bonds. Nowadays, the point of view being changed, these species are intentionally added to stabilize aqueous nanoparticle dispersions leading to the establishment of a lot of synthetic protocols in aqueous media[50]. Besides, the recognition that surfactant molecules are ideal stabilizing agents of small particles has suggested their employment for the same purpose. This idea has been confirmed by experimental observation so allowing to greatly increase the number of stable nanomaterials obtainable in aqueous solutions.

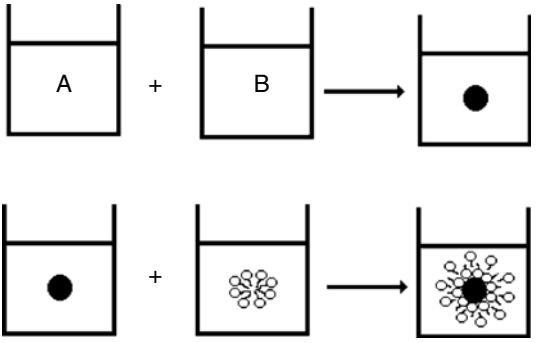

FIGURE 4.3. Microscopic processes involved in the nanoparticle synthesis in micellar solutions.

Micellar aqueous solutions are generally characterized by a low viscosity, which allows an easy homogenisation of the system and relatively more quick diffusion controlled reactions. After nanoparticle synthesis, the resulting solutions can be used for many interesting applications such as antiwear agents, photochemical systems, or specialized pseudohomogeneous catalytic or reaction media.

The microscopic processes involved in the synthesis of nanoparticles in micellar solutions are shown in Fig. 4.3.

It is worth noting that the stabilization effect resides in the oriented surfactant adsorption on the nanoparticle surface and in the hydrophilization of the entire aggregate. In some cases, the coating of the nanoparticles is intentionally directed to their separation from the aqueous medium through the formation of a hydrophobic shell covering the nanoparticle.

4.4.1. Synthesis of Metal Nanoparticles in Aqueous Micellar Solutions

Stable gold nanoparticles of various sizes and shapes have been synthesized in aqueous micellar solutions of Triton X-100 by UV photoactivation of $HAuCl_4$. Triton X-100 was chosen because it executes the dual role of reductant and stabilizer. By increasing the Triton X-100 concentration at fixed $HAuCl_4$ concentration, the Au nanoparticle mean size decreases significantly revealing the surfactant stabilizing effect. More recently, gold nanoparticles were obtained by UV irradiation of an aqueous micellar solution containing $HAuCl_4$, cetyltrimethylammonium chloride, sodium citrate, and NaOH. In such method, the citrate ions act as reducing agent at room temperature[51,52].

Pd and Au nanoparticles have been synthesized in aqueous micellar solutions of poly(2-vinylpyridine)-poly(ethylene oxide) (P2VP-b-PEO) diblock copolymers. Solid salts were firstly solubilized in the micellar

solutions by vigorous stirring. It was noted that the presence of the salt ions induces some changes in the structure of the micelles. Then, metal ions were reduced by adding an excess of a freshly prepared aqueous solution of sodium borohydride. The size and stability of nanoparticles was found to be influenced by the metal concentration and micellar structure. For both metals, it was observed the formation of two distinct populations that were attributed to different nucleation sites, i.e., the micellar core and the micellar periphery. It was hypothesized that the larger nanoparticles nucleate on the micellar periphery and their growth is sustained by metal ions exchange between neighbouring micelles[53].

Colloidal solutions of nanoparticles can be used as suitable media to build up organized assemblies of nanosized particle materials. CTAB-stabilized silver nanoparticles were synthesized in aqueous solution by $NaBH_4$ reduction. A monolayer of these nanoparticles was self-assembled on 3-mercaptopropionic acid (MPA) modified gold electrode by contacting the modified gold electrode with the silver colloidal aqueous solution for 24 h[54].

Au nanoparticles coated by an interdigitated bilayer constituted by a dodecylamine monolayer chemisorbed on the nanoparticle surface and a secondary layer of cetyltrimethylammonium bromide have been synthesized. Such particles can be easily dispersed in water, forming stable systems even at high particle concentration or in presence of electrolytes. Dodecylamine-capped Au nanoparticles were prepared by contacting a solution of dodecylamine in chloroform with a suspension of Au nanoparticles, obtained by reduction of chloroauric acid with $NaBH_4$. Vigorous shaking of this two biphasic system allowed the rapid transfer of Au nanoparticles to the organic phase. By solvent evaporation, the dodecylamine-capped gold nanoparticles were isolated and then washed with ethanol and redispersed in chloroform. Finally, the nanoparticles dispersed in the apolar solvent were transferred to an aqueous solution of cetyltrimethylammonium bromide by contacting and shaking the two immiscible phases[55].

Another synthetic strategy is based on the use of surfactants as surface stabilizers and controllers of the growth and shape of the particles. Gold nanorods capped with cationic bilayers and dispersed in water have been synthesized by an electrochemical method using as electrolyte a surfactant mixture constituted by cetyltrimethylammonium bromide and tetraoctylammonium bromide[56].

Elongated copper nanoparticles (about 50 nm in width and 500 nm in length) stabilized by an oriented monolayer of the zwitterionic surfactant, cetyltrimethylammonium *p*-toluene sulfonate, have been prepared by sonochemical decomposition of copper hydrazine carboxylate in surfactant/water solutions. The copper nanoparticle shape and morphology is attributed to the templating effect of the interconnected network of rod-like micelles formed by the surfactant[57].

High concentrations of pure metallic Cu nanoparticles with fcc structure have been synthesized in aqueous solutions of cetyltrimethylammonium

bromide and ammonia by reduction of cupric chloride with hydrazine. The synthesis of metallic Cu nanoparticles was performed in a capped bottle by mixing two aqueous solutions of CTAB, one containing cupric chloride plus ammonia and the other hydrazine. From the analysis of TEM data, it was ascertained that, after an initial decrease, the mean diameter of Cu nanoparticles approaches a constant value with the increase of hydrazine concentration. It was suggested that the formation of a bilayer structure of CTAB molecules prevents the particle agglomeration and precipitation[58].

Silver and gold nanoparticles stabilized by a double layer of sodium dodecylsulfate have been produced by laser ablation of a metal foil dipped in a SDS micellar solution. It was observed that nanoparticle size decreases with the surfactant concentration and by decreasing the laser power. The experimental findings were rationalized in terms of the rapid formation of nuclei from the dense cloud of atoms in proximity of the metal foil generated by the laser light followed by their growing process due to the residual metal atoms and/or by their coating with SDS molecules. Then, the final nanoparticle size resulted from the competition between these two last processes both sustained by the slow diffusion within the liquid medium. Advantages of this method are the easy size control by laser power and/or surfactant concentration and the absence in the final system of side products such as these occurring in chemical reduction of metal ions[59,60].

Gold nanoparticles were obtained by laser ablation of a gold metal plate immersed in an aqueous solution of sodium dodecylsulfate. The subsequent irradiation of the suspension with a laser at 532 nm allowed the controlled size-reduction of gold nanoparticles. This is because, when the laser wavelength coincides with that of a strong absorption band of the nanoparticles, the photon energy absorbed is significantly converted as thermal motion of the nanoparticle lattice leading to its fragmentation[61].

Bimetallic gold/palladium nanoparticles were prepared by ultrasound irradiation of an aqueous solution of sodium tetrachloroaurate (III) and sodium tetrachloropalladate (II) in the presence of sodium dodecylsulfate. It was suggested that the surfactant holds the double role of enhancher of the reduction rate of metallic ions and stabilizer of the bimetallic nanoparticles[62].

A stable aqueous dispersion of Ag nanoparticles coated by sodium oleate was prepared by chemical reduction of $AgNO_3$ with $NaBH_4$. After contacting the aqueous dispersion with toluene and by adding NaH_2PO_4, these nanoparticles were transferred at the water/toluene interface. At higher sodium oleate concentration, the surfactant coat makes Ag nanoparticles hydrophobic so that they are totally transferred in the organic phase. By immersing a hydrophilic slide in the two-phase system, it was observed that Ag nanoparticles spontaneously climb up the surface, forming a thin layer[63].

Silver, gold, and silver-coated gold nanoparticles have been synthesized by an electrochemical method in aqueous micellar solutions. The electrolytic cell was constituted by a gold electrode working as anode and a platinum plate as cathode. The solutions employed were obtained by dissolving

$AgNO_3$, CH_3 $COCH_3$, $C_{32}H_{68}BrN$, and $[CH_3(CH_2)_{15}]N(CH_3]_3Br$ in water. The electrolysis was carried out under ultrasound irradiation and at constant temperature[64].

4.4.2. *Synthesis of Semiconductor Nanoparticles in Aqueous Micellar Solutions*

A wide range of stabilizers is intentionally introduced in some reacting systems to improve nanoparticle stability in aqueous media or to confer specific properties, and their choice is based on their binding efficiency toward the surface atoms. For example, undoped ZnS nanoparticles have been synthesized by dropwise addition of an aqueous solution of Na_2S to aqueous solutions of zinc chloride and mercaptoethanol. The precipitate constituted by mercaptoethanol-capped Zn nanoparticles was washed and dried. It was found that the nanoparticle size can be regulated by varying the initial concentrations of $ZnCl_2$, Na_2S, and mercaptoethanol. Doped ZnS nanoparticles were simply obtained by adding $NiCl_2$ or $FeCl_3$ to the $ZnCl_2$+ mercaptoethanol solution. It was observed that the intense blue emission of undoped ZnS nanoparticles can be progressively quenched by increasing the amount of iron and nickel doping[65].

ZnS nanotubes (diameter 37–52 nm, length up to 3 μm) were synthesized by mixing an aqueous solution of zinc acetate with an aqueous solution containing Triton-X100, NH_4OH, and CS_2. After reaction, the precipitate was filtered and washed with water and ethanol. It was observed that the ZnS nanotube formation is affected by the surfactant concentration and aging time[66].

Tin oxide nanoparticles in the size range of 2–3 nm were prepared by pulsed laser ablation of tin metal plate in aqueous solutions of sodium dodecylsulfate leading to stable nanoparticle dispersions. It was suggested that tin oxide would be formed by the reaction between ablated tin species and water molecules while aggregation and growth of nanoparticles is assisted by surfactant molecules[67].

SnO_2 nanoparticles were prepared by mixing an aqueous solution of cetyltrimethylammonium bromide and NH_3 with an aqueous solution of $SnCl_4$. The resulting precipitate was separated, washed, and dried. By calcination, the amorphous SnO_2 was transformed into highly crystalline tin dioxide nanoparticles[68].

Size-controlled trigonal tellurium nanorods were synthesized in aqueous micellar systems containing $(NH_4)_2TeS_4$ by adding dropwise a sodium sulfite solution in water. As surfactants, sodium benzenesulfonate, sodium dodecylsulfate, sodium stearate, and sodium laurate were employed. It was suggested that the formation of nanorods is a consequence of the preferential adsorption of the surfactant for some crystal planes of the nanoparticles. Diameter and length of the nanorods was controlled by changing the nature of the surfac-

tant. It was observed, in fact, that an increase of the surfactant alkyl chain and head group polarity leads to a decrease of the diameter and length of the nanorods. It was also observed that tellurium nanorods of uniform size are able to self-assemble forming extended smectic-like arrays[69].

4.4.3. *Synthesis of Magnetic Nanoparticles in Aqueous Micellar Solutions*

Stable $Co_xFe_{3-x}O_4$ nanoparticles ($0.4 \leq X \leq 1$) having size varying from 6.3 to 10.5 nm have been synthesized by adding $Fe(NO_3)_3$ and $Co(NO_3)_2$ to an aqueous solution of sodium dodecylsulfate followed by NaOH addition[70].

$CoCrFeO_4$ nanoparticles have been synthesized by first mixing aqueous solutions containing $CoCl_2$, $CrCl_3$, and $Fe(NO_3)_3$, respectively. Then, an aqueous solution of sodium dodecylsulfate was added and the mixture was stirred continuously. Finally, as capping agent, methylamine was added. The size (8–16 nm) of $CoCrFeO_4$ nanoparticles was controlled by changing the temperature[71].

Nearly spherical Fe_3O_4 nanoparticles (mean size 9.3 nm) entrapped in bilayers of n-alkanoic acids dispersed in water have been synthesized. After coprecipitation of Fe(II) and Fe(III) ions by NH_4OH within an aqueous solution and addition of a fatty acid, the suspension was precipitated with acetone and methanol. This procedure allowed the preparation of Fe_3O_4 nanoparticles coated by a monolayer of surfactant molecules oriented so that the acidic group is chemisorbed to the nanoparticle surface and the alkyl chain protrudes toward the surroundings. In such condition, the nanoparticles become hydrophobic and are prevented against agglomeration. After careful washing, the precipitate was suspended in an aqueous solution of the ammonium salt of a fatty acid and vigorously stirred until a stable suspension was obtained. This step allowed to build up a second layer of surfactant molecules oriented so that the particle becomes hydrophilic leading to stable dispersions. It is worth noting that the two-step synthetic strategy permits to select separately the surfactant pair forming the primary and the secondary layers so that the control of the nanoparticle surface properties and of the stability of the aqueous suspensions can be achieved[72].

Superparamagnetic iron oxide nanoparticles with a size of few nanometers were synthesized by adding an aqueous mixture of ferric and ferrous salts to an aqueous NaOH solution. The product was separated from the solvent medium by a magnetic field and decantation. Subsequently, the nanomaterial was treated with an aqueous solution of sodium oleate to form stable surfactant-coated iron oxide nanoparticles[73].

Magnetite nanoparticles were synthesized by alkalinization of an aqueous mixture of ferrous sulphate and ferric chloride. By adding the surfactant *N*-oleylsarcosine, it was observed that at a surfactant to Fe_3O_4 molar ratio lower than 0.22 and pH in the range 5–9.5, only a monolayer of oriented surfactant molecules is adsorbed at the nanoparticle surface.

In such conditions, nanoparticles are hydrophobized and flocculate. On the other hand, at a molar ratio greater than 0.37 and pH in the range 6–8.5, a bilayer of surfactant molecules is formed. This involves that the nanoparticles are hydrophilic and the nanoparticle suspensions are stable[74].

Iron oxide and silver nanoparticles coated by oleic acid were synthesized by thermal treatment of iron pentacarbonyl and silver trifluoroacetate in the presence of oleic acid. Subsequently, the stable suspensions of these nanoparticles in *n*-hexane were mixed under stirring with an equal volume of an aqueous solution of α-cyclodextrin. In such circumstances, the complete transfer of capped nanoparticles in the aqueous phase was achieved. This phenomenon was attributed to the formation of an inclusion complex between surfactant molecules linked to the nanoparticle surface and α-cyclodextrin. It was also observed that the nanoparticles can be precipitated from the aqueous suspensions by salt addition[75].

A stable suspension of Fe_3O_4 nanoparticles coated by an inner hydrophobic layer of poly(propylene oxide) and an outer hydrophilic layer of poly(ethylene oxide) have been synthesized in aqueous solutions containing iron (III) and iron (II) chlorides, ammonium hydroxide, and a graft copolymer. The graft copolymer was prepared through the reaction between poly(acrylic acid) and amine-terminated poly(propylene oxide) and poly(ethylene oxide). The binding of the copolymer and magnetite growth inhibition was attributed to the formation of chemical bonds between carboxylic acid groups of the copolymer and the nanoparticle surfacial species[76].

Phosphorylcholine-coated iron oxide nanoparticles were synthesized by injecting aqueous solutions of $FeCl_2$ and $FeCl_3$ in tetramethylammonium hydroxide micellar solutions. Coating was achieved by mixing the nanoparticle suspension with PEG400 and phosphorylcholine. Phosphorylcholine was previously treated with a mixture of acidic and basic exchange resins to obtain a stable nanoparticle dispersion[77].

4.4.4. *Synthesis of Miscellaneous Nanoparticles in Aqueous Micellar Solutions*

Highly stable mesoporous metal oxides (zirconia, vanadia, and titania) were synthesized in aqueous solutions of hybrid Gemini surfactants. The synthesis was carried out by mixing under vigorous stirring an aqueous solution of the metal salt (zirconium sulphate, vanadyl sulphate, titanium sulphate) with an aqueous solution of Gemini surfactant characterized by the presence in its molecule of a siloxane moiety. Reactions led to the formation of precipitates that were filtered, washed, and calcinated. It was suggested that the siloxane moiety plays a pivotal role in determining the final structure of the mesoporous metal oxides[78].

Nanoparticles of vanadium (IV) oxo(phthalocyaninato) were obtained by laser irradiation of an aqueous solution of this substance. In the presence of some surfactants, an increase of the number and stability of

nanoparticlesand a decrease of their mean size was observed. It was also noted that the intensity of the irradiation needed to obtain nanoparticles is lowered. All these effects were attributed to an inhibition of the association tendency of the organic nanoparticles[79].

Functionalized silica-shell Fe_2O_3 + dye core nanoparticles have been synthesized in aqueous micellar solution. Initially, iron dodecylsulfate and methylamine were dissolved in water followed by the addition of the ASPI-SH fluorophore to the ferrofluid. To coat the Fe_2O_3 + dye nanoparticles with a silica layer, the suspension was treated with sodium silicate and, after purification, with tetraethylorthosilicate and NH_4OH. Finally, nanoparticles were functionalised by reaction with triethoxysilylpropyl-carbamoyl butyric acid. The selective uptake of these nanoparticles by specific cancer cells was ascertained[80].

Mesoporous silica particles were synthesized by spray drying aqueous solutions containing HCl, cetyltrimethylammonium chloride, and tetraethoxysilane. During solvent drying, silica and surfactant self-assemble forming well-ordered mesoporous materials. By changing composition and outlet temperature of the employed spray dryer, hollow spherical particles or spheres with the walls collapsed were obtained[81].

Boehmite (AlOOH) nanofibers were prepared by adding freshly prepared aluminium hydrate solution to the nonionic surfactant poly(ethylene oxide) ($C_{12-14}H_{25-29}O(CH_2CH_2O)_7H$). The aluminium hydrate was prepared by dropwise addition of an aqueous solution of $NaAlO_2$ to an acetic acid solution under vigorous stirring; then it was separated and washed. Subsequently, the freshly prepared aluminium hydrate was mixed with poly(ethylene oxide) and then maintained at 373 K. It was found that the surfactant plays a pivotal role in the nanofiber growth: the surfactant micelles interact with the hydroxyl groups on the surface of the bohemite nanoparticles through the formation of hydrogen bonds; so directing the uniaxial nanofiber growth[82].

Anthracene nanoparticles dispersed in water have been prepared by a novel sonication method. In a typical procedure, a solution of anthracene in acetone was injected in water or aqueous surfactant solutions during sonication. It was observed that in the presence of cetyltrimethylammonium bromide, sodium bis(2-ethylhexyl)sulfosuccinate, sodium dodecylsulfonate, and polyvinylpyrrolidone, a better control of nanoparticle size, morphology, and stability is reached. In particular, nanoparticles become smaller and more uniform in the presence of surfactants due to adsorption of micelles on the nanoparticle surface leading to inhibition of the nanoparticle-nanoparticle aggregation process. It was also found that as a consequence of surface effects, anthracene nanoparticles exhibit enhanced optical properties[83].

Electroconductive polyaniline nanoparticles were synthesized in aqueous micellar solutions of dodecylbenzene sulfonic acid (DBSA) by chemical oxidative polymerization of aniline. In particular, after solubilization of monomeric aniline in DBSA aqueous solution,

ammonium peroxydisulfate was added as initiator. The polymerization was stopped by adding methanol, leading to precipitation of polyaniline nanoparticles. It was observed that the electrical conductivity of the resulting nanomaterial varied with the initial DBSA to aniline molar ratio. A similar procedure was followed to synthesize poly(3,4-ethylene dioxythiofene) nanoparticles showing enhanced processability[84,85].

Hollow spherical polystyrene nanoparticles with a diameter of 15–30 nm and thickness of about 2–5 nm in poly(oxyethylene)-poly(oxypropylene)-poly(oxyethylene) triblock copolymer/water micellar solutions have been synthesized. The strategy of the synthesis consists in the formation, by in situ two-step polymerization, of polymethylmethacrylate/polystyrene core/shell nanoparticles confined in the micellar cores. Then, the polymethylmethacrylate cores were removed by using as etching solvent methylene chloride. Hollow nanospheres were separated from the reaction mixture by ethanol addition[86].

Nanoparticles of some electroconductive polymers (polyaniline, poly(3,4-ethylenedioxythiophene), showing enhanced conductivity, were prepared successfully in sodium dodecylsulfate and dodecylbenzene sulfonic acid micellar solutions[87].

4.5 Nanoparticle Synthesis in Reversed Micelles

Reversed micelles represent one of the most interesting structures able to synthesize and host nanoparticles, and for this reason a lot of different protocols based on these systems are reported in the literature. Solutions of reversed micelles have also been frequently employed as templates for nanoparticle and mesoporous materials[88].

The mechanism of formation of nanoparticles occurs by diffusion of the reversed micelles containing the reactants, collisions, and intermicellar fusions. This last step allows mass transfer, contact between reactants, and the formation of products (nanoparticle precursors). Only a fraction of all the intermicellar collisions leads to micellar fusion and material exchange process. This involves that the rate of precursor formation is controlled by the reversed micelle diffusion triggered by the fraction of the intermicellar collisions followed by an exchange event.

With the same mechanism, precursors are continuosly exchanged among micelles, but showing a strong tendency to aggregate, they progressively accumulate in some ''lucky'' micelles. This is because, as precursors accumulate within a micelle, the size of the precursor aggregate increases, making increasingly difficult their exchange with neighboring micelles. Above a threshold size, the precursor aggregates cannot be transferred among micelles. Obviously the growth of these aggregates stops when all the precursors have been incorporated in all the nanoparticles.

Some additional phenomena can change this mechanism. Adsorption of surfactant molecules on the nanoparticle surface and nanoparticle surface poisoning could inihibit the nanoparticle growth and lead to smaller nanoparticles. A schematic representation of the formation of nanoparticles in solutions of reversed micelles is shown in Fig. 4.4.

Many factors contribute to the control of the particle size, polydispersity, and dispersion stability in reversed micellar systems. Some leading factors are the size of reversed micelles and their concentration, the mean number of reactant molecules for each micelle, and the rate of the intermicellar material exchange process. As external parameters, the water to surfactant molar ratio, the nature and concentration of the surfactant, and temperature can be identified.

4.5.1. Synthesis of Metal Nanoparticles in Reversed Micelles

Copper nanoparticles with size in the range 10-120 Å were obtained by mixing solutions of AOT reversed micelles containing copper bis(2-ethylhexyl)sulfosuccinate with an aqueous solution of hydrazine. An increase of the size and polydispersity was observed by increasing the water content. Besides, the size increased by increasing the copper concentration or by decreasing the surfactant concentration. It was also observed that at a water to AOT molar ratio greater than 3, the formation of copper oxide occurs[89].

Silver nanoparticles were synthesized by mixing two solutions of AOT reversed micelles containing $AgNO_3$ and $NaBH_4$, respectively. In order to investigate the effect of the intermicellar exchange rate on the nanoparticle size, the organic solvent (cyclohexane, heptane, and decane) was changed or various additives (benzyl alcohol and toluene) and surfactants (SDS,

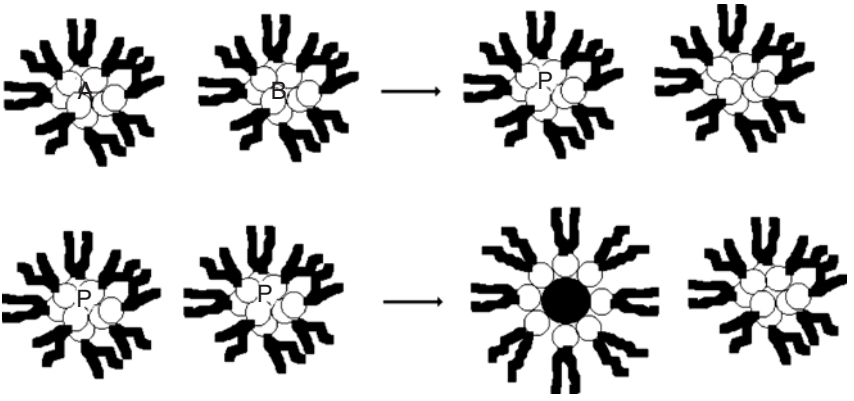

FIGURE 4.4. Nanoparticle formation mechanism in reversed micelles.

DTAB, NP-5) were added. It was observed that an increase of the intermicellar exchange rate promotes the formation of a greater number of nuclei giving smaller nanoparticles[90].

Silver nanoparticles were produced in silver nitrate containing water-AOT reversed micelles dispersed in compressed propane by reduction with $NaBH_4$. To recover nanoparticles from the high-pressure vessel, the content was directly transferred to a normal liquid micellar solution or after removal of the supercritical fluid depressurizing the reaction chamber and then collecting the resulting nanoparticle/surfactant composite[91].

Gold nanoparticles stabilized by a monolayer of cetyltrimethylammonium bromide were prepared by mixing under stirring a solution of CTAB in toluene with an aqueous solution of hydrogen tetrachloroaurate. The complexation of tetrachloroaurate anions with CTAB cations allowed the transfer of the metal from the aqueous solution to toluene where the surfactant forms reversed micelles. Then, an aqueous solution of sodium borohydride was added to the toluene solution leading to the formation of surfactant coated gold nanoparticles. By toluene evaporation, 2D and 3D networks of gold nanoparticles were obtained[92].

Silver nanoparticles were synthesized in solutions of reversed micelles formed by an amphiphilic block copolymer (L92, $(EO)_8(PO)_{50}(EO)_8$) in *p*-xylene. The size of nanoparticles was varied in the range 3–14 nm by changing the experimental conditions. The synthesis was carried out by mixing two reversed micelle solutions containing an aqueous solution of $AgNO_3$ and an aqueous solution of KBH_4, respectively. After the synthesis, Ag nanoparticles were recovered by increasing the system temperature. The separation is due to the sharp increase of the surfactant critical micellar concentration with temperature leading to reversed micelle breakage and nanoparticle precipitation while the surfactant remains in the organic phase[93].

Ag nanoparticles have been synthesized in solutions of AOT reversed micelles in isooctane by mixing two micellar solutions containing $AgNO_3$ and KBH_4, respectively. The application of ultrasound immediately after the mixing process led to the formation of needle-like and wire-like Ag nanoparticles while in absence of ultrasound nearly spherical ones were obtained[94].

Pd nanoparticles were synthesized in solutions of reversed micelles by reduction of hexachloroplatinic acid with hydrazine monohydrate. Then, Al_2O_3 powder was added to the nanoparticle dispersion under vigorous stirring. The complete transfer of the Pd nanoparticles on Al_2O_3 surface was achieved by the addition of tetrahydrofurane[95].

Cobalt nanoparticles, synthesized by the thermolysis of $Co_2(CO)_8$ in C-undecylcalix[4]resorcinarene tetraphosphate/toluene solutions, self-assemble forming chains and rings when re-dispersed in the presence of undecylcalix[4]resorcinarene. Chain and ring formation is due to magnetic interactions among Co nanoparticles[96].

Fe/Pt nanoparticles coated by a chemically bonded surfactant layer were synthesized by reaction between iron pentacarbonyl and platinum (II) acetylacetonate using as solvent medium a solution of oleic acid and oleylamine in dioctylether. After reaction, nanoparticles were separated from the solution by adding ethanol and centrifugation. It was found that the surfactant coated Fe/Pt nanoparticles can be dispersed in pure hexane[97].

Pt-core Co-shell nanoparticles were prepared by chemical reduction of cobalt acetate tetrahydrate and platinum (II) acetylacetonate with 1, 2 hexadecandiol dissolved in dioctylether. As nanoparticle stabilizers, oleic acid and lauric acid were added. The chemical reaction was carried out at about 300°C under stirring and in a nitrogen atmosphere. The resulting powder was washed and dried. It was observed that such nanoparticles form self-assembled spherical superaggregates and that the oxidation of the external cobalt layer is limited by the surfactant coating[98].

4.5.2. *Synthesis of Semiconductor Nanoparticles in Reversed Micelles*

CdS nanoparticles have been synthesized by adding tetrabutylammonium hydrogen sulphite to water/AOT/*n*-heptane solutions containing $CdSO_4$. Analysis of UV-vis absorption spectra recorded as a function of time indicated that an initial rapid formation of CdS nanoparticles is followed by a very slow growth process. This growth process was totally inhibited by the addition of bis(2-ethylhexyl)amine (BEA) leading to the formation of stable nanosized CdS nanoparticles coated by an oriented monolayer of chemically bonded BEA molecules. Depending on the BEA addition time, the growth inhibition can be achieved at any moment of the process leading to an easy and fine size control. Another advantage of this method is that BEA-coated CdS nanoparticles can be easily separated from the reaction medium and dispersed in a nonpolar media such as heptane and in polar media such as an aqueous surfactant solution[99].

Metal sulfide nanoparticles (CdS, ZnS, mixed CdS-ZnS, ZnS-coated CdS) have been synthesized in AOT reversed micelles. Then by in situ polymerization of diisocyanates, these nanoparticles were immobilized in polyurea particles. The resulting nanoparticle/polyurea composites were collected by centrifugation and tested as photocatalysts for the generation of H_2 from 2-propanol aqueous solutions or to produce nanoparticle containing transparent films[100].

CdS nanoparticles were prepared in self-reproducing reversed micelles dispersed in isooctane-octanol mixtures. The self-replication process is based on the hydrolysis of octyloctanoate catalyzed by lithium hydroxide confined in the aqueous core of sodium octanoate reversed micelles while that leading to CdS nanoparticles is the reaction of Cd^{2+} ions with H_2S occurring in the micellar confined space. The CdS were subsequently capped

with mercaptopropionic acid and separated by filtration. These coated nanoparticles resulted to be fully dispersible in water[101].

$Cd_yZn_{1-y}S$ mixed nanoparticles have been prepared by mixing three solutions of reversed micelles with the same water content and sodium (2-ethylhexyl)sulfosuccinate concentration (0.1 M) but containing Na_2S , $Zn(AOT)_2$, and $Cd(AOT)_2$, respectively. The formation of nanoparticles, ascertained by UV-vis spectroscopy, was emphasized by an absorption band occurring in the 250-450 nm range. The presence of a well-developed excitonic peak suggested that nanoparticle with a low size distribution are synthesized. Due to the rapid intermicellar material exchange process, the formation of nanoparticles occurs in a few seconds. It was also observed a progressive red shift with time suggesting a slow growing process of nanoparticles. However, by adding benzene thiol or dodecane thiol, this growing process was completely inhibited. This was attributed to the chemical reaction between thio-compounds and nanoparticle cations. It was also ascertained that, independently on the y value, the $Cd_yZn_{1-y}S$ nanoparticles size (15–30 Å) is controlled by the size of the aqueous micellar core[102].

Solutions of reversed micelles can be used as useful media to insert nanoparticles in mesoporous materials giving quite ordered nanostructures. Nanosize CdS particles synthesized in AOT reversed micelles dispersed in *n*-octane were confined in siliceous MCM-41 nanochannels by simply contacting the nanoparticle containing micellar system with the mesoporous material[103].

Depending on the nature of surfactant and experimental conditions, different nanosystems are obtained. ZnS nanowires with diameters of 40–80 nm and lengths up to tens of microns were prepared by mixing at room temperature equal volumes of two solutions of polyoxyethylene (9) dodecylether ($C_{12}E_9$) reversed micelles in cyclohexane containing zinc and sulfide ions, respectively[104].

It has been found that mixing two liquid solutions containing nanoparticles of opportunely chosen water-soluble materials allows the formation of the insoluble salt via a solid-solid reaction between nanoparticles. For instance, the blending of two AOT/*n*-heptane solutions containing Na_2S and $ZnSO_4$ nanoparticles, respectively, leads to the formation of ultrasmall (diameter $\leq$1 nm) ZnS surfactant-coated nanoparticles at relatively high concentration[105].

Even if tests on the extensibility of this synthetic route to other substances are currently being carried out, this method seems to be quite general and has specific advantages:

- nanoparticle size is generally very small
- nanoparticle concentration is very high
- because nanoparticles are formed by a fast solid-state reaction, they can have a structure very different from that of the nanoparticles synthesised so far, thus exhibiting exotic behaviour and enhanced photophysical properties.

For instance, AgCl and AgBr nanoparticles synthesised by this method showed marked quantum size effects and an unexpected lightfastness[106].

Superparamagnetic ferrite nanoparticles and semiconductor CdS nanoparticles have been trapped in the gel strands of the *p*-chlorophenol/AOT/CCl_4 organogel system. Because a trace of water inhibits the organogel formation, after the classic nanoparticle synthesis in the water/AOT/CCl_4 systems, the system was dried by evaporation of the volatile components and then the original concentration of the organic solvent was restored. Finally, by adding *p*-chlorophenol, the anhydrous micellar systems were transformed in a nanoparticle containing highly viscous organogels[107].

Silica nanoparticles have been synthesized by the hydrolysis of tetraethoxysilane (TEOS) in presence ammonium hydroxide occurring in the confined space of water containing AOT reversed micelles dispersed in *n*-decane. The surfactant concentration was in the range 0.1–0.24 M, the water to TEOS ratio 18.5, and the water to surfactant ratio R in the range 2–9.5. It was observed that below $R = 4$ no particles are formed. This indicated that the water present in the system is totally engaged in the solvation of sodium counterions and surfactant head groups and it is not available for TEOS hydrolysis. In the range $5 < R < 9.5$, spherical nanoparticles of mean size (100–350 Å) increasing with R and showing a broad size distribution were obtained. It must be noted that nanoparticle size exceeds significantly that of reversed micelles, emphasizing the dynamic nature of these aggregates. Finally, it was observed that the nanoparticle size increases with time and consequently the dispersions are not stable with time, leading eventually to the formation of gel-like precipitates. This is a drawback arising from the contemporaneous hydrolysis of AOT in presence of hydroxyl ions resulting in the formation of sodium carboxylate and 2-ethylhexanol[108].

Silica-network structure was formed by hydrolysis of tetraethoxysilane (TEOS) in solutions of reversed micelles composed by didodecyldimethylammonium bromide (DDAB), cyclohexane, and aqueous solution of HCl. Initially, an aqueous solution of HCl was dissolved in DDAB/cyclohexane solution followed by TEOS addition to the micellar system. Then, appropriate amounts of aqueous NaOH were added to neutralize HCl. The formation of spherical silica particles was observed, which, through a clustering process, were converted into an interconnected silica rod network upon HCl neutralization. Macroscopically, the network formation is accompanied by the system transition from a fluid sol to a highly viscous transparent gel[109].

By solubilizing titanium isopropoxide in solutions of water containing Triton X-100 or AOT reversed micelles, the formation of gels was observed. Gelling was attributed to the hydrolysis of titanium isopropoxide leading to an extended -O-Ti-O-Ti-network. These gels can be easily deposited on glass slides as thin and transparent TiO_2/surfactant films. It was suggested that TiO_2/Triton-X 100 composites are constituted by spherical TiO_2 nanoparticles coated by a surfactant layer while TiO_2/AOT ones are

characterized by an ordered array of surfactant capped cylindrical TiO_2 nanoparticles. Finally by heating at sufficiently high temperature these films, the surfactant was removed, obtaining interesting mesoporous films[110].

Nanoparticles of AgCl, AgI, Ag_2S, and silver tetraphenylborate have been synthesized in water containing AOT reversed micelles by mixing two micellar solutions at the same AOT concentration, one containing silver nitrate and the other NaCl, KI, $(NH_4)_2S$, or $Na(C_6H_5)_4B$. By calorimetric measurements, it was shown that the molar enthalpies of nanoparticle formation are independent of the surfactant concentration but are dependent on the reagent salt concentrations and the R value. Moreover, the molar enthalpies for the same processes in bulk water are not approached even at the highest R value. This behavior was attributed to the smalleness of the nanoparticles and to interactions between ions and the micellar interface[111].

4.5.3. *Synthesis of Magnetic Nanoparticles in Reversed Micelles*

Fe_3O_4 nanoparticles were prepared by mixing two water/AOT/isooctane micellar solutions containing $FeSO_4$ and NH_4OH, respectively. The size of nanoparticles was modulated by changing the solution composition. To prepare mixed ferrites, the metal containing micellar system is obtained by adding to the AOT/isooctane solution an aqueous solution containing $FeSO_4$ and $MnSO_4$ or $CoSO_4$. The use of a third micellar solution containing hydrogen peroxide allowing the total oxidation of Fe^{2+} to Fe^{3+} led to the synthesis of γ-Fe_2O_3[112].

Stable superparamagnetic surfactant-coated Fe_2O_3 nanoparticles of 5–16 nm in diameter have been synthesized in surfactant/decane solutions by sonochemical decomposition of $Fe(CO)_5$. Size control and nanoparticle stabilization was attributed to the formation of strong ionic bonds between the surfactants (11-undecenoic acid, dodecylsulfonic acid, and octyl phosphonic acid) and the Fe^{3+} ions at the nanoparticle surface[113].

Fe_2O_3 nanoparticles coated by sodium dodecylbenzene sulphonate were prepared by adding the surfactant to a two-phase system constituted by an aqueous $FeCl_3$ solution and toluene. Then, an aqueous solution of NaOH was added under stirring to the system. Fe_2O_3 nanoparticles of about 5 nm stabilized by a surfactant monolayer were found in the upper organic layer[114].

Pt/Fe_2O_3 core-shell nanoparticles have been synthesized in a mixture composed by 1,2 hexadecanediol, oleic acid, oleylamine, and octylether. Initially, a solution of platinum acetylacetonate in octyl ether was added to the mixture at 290°C. In such conditions, the formation of Pd nanoparticles was observed. Then, iron pentacarbonyl was added, and the mixture was refluxed for a certain period of time. Pt/Fe_2O_3 core-shell nanoparticles were washed with hexane and ethanol and separated by centrifugation. It was observed that nanoparticles can be dispersed in dilute solution of oleic acid

in hexane. By changing the experimental conditions, a control of the thickness of the Fe_2O_3 shell was achieved[115].

Superparamagnetic $MnFe_2O_4$ nanoparticles in the size range 4–14 nm were prepared in water containing dodecylbenzene sulfonate reversed micelles dispersed in toluene. The synthesis was carried out by mixing aqueous solutions of $Mn(NO_3)_2$ and dodecylbenzene sulfonate followed by the toluene addition. Then, to the clear reversed micelle solution, an aqueous solution of NaOH was added under vigorous stirring. The size of $MnFe_2O_4$ nanoparticles was controlled by changing the water to toluene ratio[116,117].

Nanosized Fe_3O_4 nanoparticles were synthesized in petroleum ether Isopar M solution of the surfactant TEGO EBE45 consisting of a polystyrene block and a poly(ethylene oxide) block. The synthesis was carried out by dispersing under ultrasound irradiation a concentrated solution of $FeSO_4 + HCl$ in TEGO EBE45/Isopar M solution. During this step, N_2 was bubbled to avoid total oxidation of Fe(II). The, methoxyethylamine was added to allow the formation of Fe_3O_4 nanoparticles[118].

Magnetic $MnFe_2O_4$ and $ZnFe_2O_4$ nanoparticles were prepared in water and then capped and transferred in toluene by the coupled action of two surfactants. In particular, MFe_2O_4(M = Mn or Zn) nanoparticles were synthesized by dissolving in water $MCl_2 \cdot 4H_2O$ and $FeCl_3 \cdot 6H_2O$. Then, a micellar solution of cetyltrimethylammonium bromide was added, maintaining the system temperature at 70°C. This treatment was followed by the addition of an aqueous solution of NaOH to reach a pH value of 12. The precipitate was washed with water and dried. Finally, a stable dispersion of capped MFe_2O_4 nanoparticles was obtained by dissolving the precipitate in a *n*-octylamine/toluene solution. It was observed that the nanoparticles can be precipitated by adding 2-propanol[119].

Cobalt nanoparticles coated by a chemically bonded oleic acid monolayer were synthesized in apolar media leading to magnetic particles with enhanced stability. $Co(CH_3COO)_2$ $4H_2O$, oleic acid, 1,2 dodecanediol, and trioctylphosphine were dissolved in diphenyl ether and heated at 250 °C. After reaction, cobalt nanoparticles were precipitated and washed several times with ethanol[120].

4.5.4. Synthesis of Miscellaneous Nanoparticles in Reversed Micelles

MgO nanoparticles were prepared by hydrolysis of magnesium methylate in water/methanol/toluene mixtures and thermally treated under pressure. After solvent evaporation, MgO nanoparticles were suspended in AOT/pentane or dodecyltrimethylammonium bromide/toluene solutions for 20 h. In such conditions, surfactant molecules are firmly adsorbed on the nanoparticle surface. It was found that, after nanoparticle surface modification, the dispersion capability of nanosized MgO is improved while its

reactivity is reduced due to steric hindrance and/or inhibition of Lewis acid sites[121,122].

Linear chains, rectangular superlattices, and long filaments constituted by barium chromate nanoparticles have been synthesized by mixing a solution of barium bis(2-ethylhexyl)sulfosuccinate with a solution of Na_2CrO_4 containing AOT reversed micelles. These different aggregation patterns have been obtained by changing the reactant molar ratio and has been attributed to the interdigitation of the surfactant monolayers coating adjacent nanoparticles[123].

Micrometer-long $BaSO_4$ nanowire has been synthesized by mixing a solution of $Ba(AOT)_2$ with a solution of AOT reversed micelles containing sodium sulfate. The proposed mechanism for the nanowire synthesis is based on the formation of nanoparticles inside reversed micelles followed by their fusion as surfactant-coated nanowires[124].

ZrO_2 nanoparticles have been synthesized in solutions of carbon nanotubes containing AOT reversed micelles. After dispersion of carbon nanotubes in AOT/cyclohexane solution, it was dropwise added under stirring a $ZrOCl_2$ aqueous solution and then an ammonium hydroxide one. Left to stand, the mixture formed two phases: an upper apolar phase containing ZrO_2 nanoparticles coated by AOT and carbon nanotubes and a lower aqueous phase. ZrO_2 nanoparticles were collected from the organic layer and thermally treated. It was ascertained that carbon nanotubes effectively inhibited nanoparticle coalescence and stabilized cubic ZrO_2[125].

Polyacrylamide nanoparticles confined in water containing reversed micelles dispersed in toluene have been prepared by in situ polymerization. Starting from a water/acrylamide/AOT/toluene system, after addition of azobisisobutyronitrile (AIBN), the reaction was initiated by the thermal or UV activation of AIBN. At the end of the process, a bimodal particle size distribution was found consisting of stable polymer+water and water containing AOT reversed micelles. It was proposed that the growth of polyacrylamide particles occurs by the monomer diffusion through the bulk apolar medium and by intermicellar exchanges[126].

Practically, nanoparticles of quite all water-soluble inorganic salts can be obtained using water containing reversed micelles by the following simple route. Starting from salt containing water/surfactant/organic medium reversed micellar systems, after evaporation of the volatile components (water and apolar solvent), the resulting salt/surfactant composite is resuspended in a dry organic solvent. Both in composites and resuspended composites, the presence of nanoparticles of the salt was observed. Following this route, nanoparticles of $CaCl_2$, Na_2HPO_4, $Cu(NO_3)_2$, $ZnSO_4$, Na_2S, $Co(NO_3)_2$, $AgNO_3$, KCl, and KBr have been synthesized[2,105,106,127,128].

By changing the experimental conditions (system composition, temperature, etc.), a fine size control can be reached.

Small size nanoparticles of strongly hydrophilic substances can be prepared by their direct solubilization in dry reversed micelle solutions.

Following this route, nanoparticles of urea, acetamide, and *n*-methylurea have been synthesized[3,129–134].

Reversed micelles encapsulated in a polymer matrix were obtained by radical polymerizations of styrene and divinylbenzene containing AOT reversed micelles entrapping in their interior water or formamide. The study of the lifetime of fluorescence emission of tris(22′-bipyridyl)dichlororuthenium (II) confined in the reversed micelles showed that in the polymerized samples, AOT aggregates retain a liquid-like core[135].

Trypsin nanoparticles with size in the range 3–15 nm were obtained by precipitation from a water/AOT/decane system applying compressed CO_2 at appropriate pressure. It was observed that the amount of precipitated protein increases with the CO_2 pressure and decreases by decreasing the water-to-AOT molar ratio. Moreover, larger nanoparticles are obtained by increasing the initial trypsin concentration[136].

4.6 Nanoparticle Synthesis in Microemulsions

Microemulsions have been widely employed for the synthesis of nanoparticles[137,138]. Their advantage is the possibility to solubilize a relevant amount of nanoparticle precursors within the typical nanoscopic domains characterizing these systems. This is because the size of the aggregates dispersed in the bulk medium is generally higher than that realized in direct and reversed micellar systems.

The nanoparticle synthesis is generally performed by mixing two water in oil (or oil in water) microemulsions containing the reactants confined in the aqueous (or apolar) cores of the aggregates. The interaggregate exchange of materials, occurring on a timescale of milliseconds, allows the reactants to come in contact and react, thus forming nuclei within the aqueous (or apolar) cores of the aggregates. The continuous interaggregate exchange of material fulfils the spontaneous nanocrystal tendency to unlimitedly grow, but their entrapment in the confined space and the surfactant adsorption at the nanoparticle surface could hinder the growth process. These processes as well as the conditions in which nucleation and growth take place are all factors governing final nanoparticle size and structure so that they allow to prepare nanoparticles with desired structural characteristics. The interaggregate exchange rate is found to be an important factor affecting size and growing rate of nanoparticles. A fast exchange rate leads to smaller nanoparticles and higher growing rates[139–141].

Nanoparticles of a wide range of materials with a fine size and polydispersity control have been synthesized using this technique[142].

A thorough review of the preparation of nano-size catalysts from microemulsions and their applications in heterogeneous catalysis has been reported[143].

Moreover, the high monodispersity that can be obtained through this route allowed study of the correlation between size/structure and physical properties, thus permitting to achieve further insights in quantum confinement effects[144]. Another advantage is the possibility of preparing doped, solid solution nanoparticles and nanocomposites with desired composition and structure[102]. For example, onion-like nanoparticles constituted by layers of different materials can be easily prepared by successive mixing of different microemulsions[145].

4.6.1. Synthesis of Metal Nanoparticles in Microemulsions

In order to protect nanoparticles of metallic Fe, Co, and their alloys from oxidation, the possibility to coat them with a layer of a noble metal has been explored. Fe/Au core-shell nanoparticles have been successfully synthesized using cetyltrimethylammonium bromide/butanol/water/octane w/o microemulsions as solvent media both for the metal salts and the reducing agent ($NaBH_4$). The gold shell was obtained by the successive addition of the appropriate amount of the aqueous gold salt[146].

Silver nanoparticles were synthesized by mixing two w/o water/Pluronic L92/p-xylene microemulsions containing $AgNO_3$ and KBH_4, respectively. This method possesses the peculiarity to allow the recovery of the silver nanoparticles by simply increasing the temperature. This is because the cmc of Pluronic L92 in *p*-xylene increases dramatically with the temperature, leading to destabilization of the surfactant aggregates and consequently to nanoparticle precipitation[93].

Silver and copper nanoparticles were synthesized in w/o microemulsions composed by water, sodium bis(2-ethylhexyl) sulfosuccinate, perfluoropolyether phosphate, and supercritical carbon dioxide. As reducing agents of silver or copper nitrate dissolved in the aqueous core of the microemulsions, sodium cyanoborohydride ($NaBH_3CN$) and *N,N,N′,N′*-tetramethyl-*p*-phenylenediamine (TMPD) were used. Metal reduction was accomplished by adding an ethanolic solution of $NaBH_3CN$ or pure TMPD[147].

Gold nanoparticles in the size range 10–100 nm were synthesized by mixing two w/o microemulsions composed of water, tetraethyleneglycoldodecyl ether (Brij30) or ammonium laurate and hexane, one containing tetrachloroauric acid and the other containing hydrazine. After reaction, the colloidal dispersions were sprayed into an air/acetylene flame allowing for complete combustion of the organic components and low-cost production of considerable amounts of gold-based nanomaterials[148].

Platinum nanoparticles have been synthesized by chemical reduction of $PtCl_4$ confined in water/AOT/cyclohexane microemulsions by dropwise addition of an excess of hydrazine. After addition of alumina and tetrahydrofuran, it was observed that platinum nanoparticles are quickly adsorbed at the alumina surface. The catalytic efficiency of the resulting nanocomposites was found to reach a maximum at a specific nanoparticle size[149].

Nearly monodisperse mixed platinum-ruthenium nanoparticles with a mean size in the range 2.5–4.6 nm and enhanced catalytic activity were synthesized by mixing two water/TRITON-X100/2-propanol/cyclohexane microemulsions, one containing dihydrogen hexachloroplatinate (IV) and ruthenium (III) chloride and the other containing hydrazine. The composition of the bimetallic Pt/Ru nanoparticles was regulated by changing the relative amounts of the two metal salts dissolved in the microemulsions, while their size can be reduced by decreasing salt concentration. It was observed that, at low precursor concentration, the nanoparticle size is controlled by nucleation, whereas at higher precursor concentration by inter-aggregate collisions[150].

Au-core Pt-shell nanoparticles with the diameter in the range 3–4.5 nm were synthesized by chemical reduction of chloroauric and chloroplatinic acid in water/AOT/isooctane microemulsions. The reduction reaction was performed by mixing two w/o microemulsions containing the metallic species and hydrazine, respectively. The structure of nanoparticles was determined by the fact that the nucleation rate of Au is faster than that of Pt. It was found that the size of nanoparticles is regulated by the number of nuclei initially formed, and it increases with the water-to-surfactant molar ratio[151,152].

Silica-coated rhodium nanoparticles have been synthesized using w/o microemulsions composed of water, polyoxyethylene (15) cetyl ether, and cyclohexane as reaction media. After solubilization of rhodium trichloride into the microemulsion, it was added in successive steps: i) hydrazine hydrate, ii) tetraethylorthosilicate and NaOH solutions. Nanoparticles were separated from bulk medium by adding propanol and by centrifugation. After washing and drying, coated nanoparticles were calcined and reduced with H_2[153].

Metal (Pt, Pd, Pt/Ag)-core inorganic aerogel (silica, ceria)-shell nanoparticles were synthesized in w/o microemulsions composed of water, cetyltrimethylammonium bromide, and toluene. After addition of the aqueous metal salt and NaOH solution to CTAB/toluene systems, chemical reduction of the metal was accomplished by dropwise addition of an excess of hydrazine hydrate. Subsequently, tetraethylorthosilicate was added to the colloidal solution and, after ageing, it was centrifuged and filtered. Surfactant was removed by washing the precipitate, and nanocomposites were chemically anchored to alumina, silica, or carbon by thermal treatment. The formation of a thin and porous layer of silica coating the nanoparticles allowing facile access to the internal metal core was ascertained[154].

Bismuth nanoparticles (about 20 nm) were prepared by mixing two microemulsions composed of poly(oxyethylene)$_9$ nonyl phenol ether, and poly(oxyethylene)$_5$ nonyl phenol ether in petroleum ether, one containing an aqueous solution of sodium borohydride and ammonia and the other an aqueous solution of bismuth citrate. The bismuth nanoparticles were separated by centrifugation and washed with ethanol[155].

4.6.2. Synthesis of Semiconductor Nanoparticles in Microemulsions

Star-shaped CdS nanoparticles in the size range 150–200 nm were prepared by mixing an aqueous solution of $CdCl_2$ and ethylendiamine with a solution of CS_2 and arachidic acid in benzene. The product was washed with ethanol and water and then dried under vacuum[156].

Monodisperse silica-cadmium sulfide nanoparticles were synthesized in w/o microemulsions by the controlled hydrolysis of tetraethylene ortosilicate (TEOS) in the aqueous micellar core and the addition of cadmium nitrate and ammonium sulfide. Initially, liquid TEOS is added to a stirred w/o microemulsion composed of IgepalCO-520 or Triton N-101 as nonionic surfactants, water, hexanol (in the case of Triton N-101), and NH_4OH. The TEOS hydrolysis is a slow process requiring a period of 24 h for the complete formation of SiO_2 nanoparticles, while the addition of w/o microemulsions containing cadmium nitrate and ammonium sulfide leads to the fast production of CdS. In such conditions, by changing the order and the timing of injection of reactants, nanoparticles with different spatial composition can be obtained[157].

CdS and ZnS nanoparticles were synthesized by mixing two water/fluorinated AOT/supercritical CO_2 microemulsions at the same water content, one containing Na_2S and the other $CdNO_3$ or $ZnNO_3$. The size of nanoparticles is controlled by the water-to-surfactant molar ratio[158].

TiO_2 nanoparticles were synthesized by the hydrolysis of titanium tetraisopropoxide in w/o microemulsions formed by water, toluene, and a mixture of dodecylbenzenesulfonate and sodium dodecylsulfate. After the synthesis, TiO_2 was separated from the reaction medium by centrifugation, washed to remove traces of surfactants and toluene from the nanoparticle surface, and dried. These nanoparticles showed a good photocatalytic activity, allowing the decomposition of dodecylbenzene sulfonate and sodium dodecylsulfate[159].

Nearly monodisperse and spherical NiS nanoparticles in the range 3–12 nm were synthesized by mixing two w/o microemulsions composed of water, 1-butanol, the nonionic, biodegradable and nontoxic sucrose fatty acid monoester (S-1170), tetradecane and $Ni(NO_3)_2$ or Na_2S, respectively. By centrifugation, a fine powder was obtained that was washed and dried before nanoparticle characterization. The size of NiS nanocrystals and the width of their size distribution was found to increase with the initial concentration of the reactants[160].

4.6.3. Synthesis of Magnetic Nanoparticles in Microemulsions

Iron oxide-doped alumina nanoparticles were synthesized in water-in-oil microemulsions formed by Igepal Co520 in cyclohexane. Microemulsions were prepared by adding to the micellar system an aqueous solution of

aluminium and iron nitrates. The hydrolysis of the metal salts was achieved by addition of an aqueous solution of ammonium hydroxide. The extraction of nanoparticles from the microemulsion was carried out by further addition of ethanol and centrifugation[161].

$CoFe_2O_4$- and $MnFe_2O_4$-core silica-shell nanoparticles have been synthesized in w/o microemulsions. After the preparation of the bare $CoFe_2O_4$ and $MnFe_2O_4$ nanoparticles, the respective powders were mixed with appropriate amounts of aqueous NH_4OH and polyoxyethylene(5)nonylphenyl ether (Igepal CO-520)/cyclohexane solution. To the resulting system, tetraethylene orthosilicate (TEOS) was added under stirring, and the core-shell nanoparticles were collected by a magnet[162].

Size-controlled polymer-coated iron oxide nanoparticles were synthesized by w/o microemulsions composed of water, AOT, and toluene. Firstly, aqueous dispersions of iron oxide were obtained by adding a concentrated solution of NaOH to a mixture of $FeCl_2$ and $FeCl_3$. After the addition of trisodium citrate solution, the magnetic particles were precipitated with acetone, and the precipitate was re-dispersed in water and dialyzed. Then, monomeric acrylamide and *N,N′*-methylene bis(acrylamide) were dissolved in the iron oxide aqueous suspension, and the total mixture was solubilized in AOT/toluene solution. The acrylamide polymerization was performed at 60 °C using 2,2′-azobis(isobutyronitrile) or 2,2′-azobis(2-amidopropane) dihydrochloride as initiators. After polymerization, aqueous dispersions of the magnetic polymeric nanoparticles were obtained by precipitation-redispersion or phase inversion. It was found that the particle size is controlled by the cross-linker concentration and surfactant to water ratio[163].

Silica-coated iron oxide nanoparticles have been synthesized by mixing under ultrasound irradiation two microemulsions, one containing $FeSO_4$ and $FeCl_3$ and the other tetraethylorthosilicate and NaOH or NH_3. Iron oxide is formed by the coprecipitation reaction of Fe(II) and Fe(III) ions with inorganic bases whereas the silica coating by the slow base-catalyzed hydrolysis of the tetraethylorthosilicate, leading to the formation of silicic acid polymer. After reaction, the resulting mixture was centrifuged and the precipitate washed several times with ethanol. To test the effect of surfactant nature on particle size, crystallinity, and magnetic properties, three different non-ionic surfactants were employed (Triton X-100, Igepal CO-520, Brij-97). It was suggested that, by adsorption of biomolecules (enzymes, antibodies, DNA, dextrans, starch, albumin) on the silica surface of these nanoparticles, some specialized biomedical application can be exploited[164].

Superparamagnetic nickel nanoparticles were synthesized by chemical reduction of nickel chloride with hydrazine in water/cetyltrimethylammonium bromide (CTAB)/*n*-hexanol microemulsions. Reaction was carried out at about 73°C by mixing two w/o microemulsions solubilizing $NiCl_2$ and $N_2H_4 + NH_3$, respectively. It was found that smaller nanoparticles can be obtained at high CTAB to hexanol ratio, as this involves a more rigid

interface. Moreover, it was observed that, at fixed concentration of the metal ions, the nanoparticle size decreases with the hydrazine concentration trending to a plateau value at high hydrazine to $NiCl_2$ ratio[165].

Nearly monodisperse magnetic MnZn-ferrite nanoparticles were synthesized in water-cetyltrimethylammonium bromide-hexanol microemulsions by in situ coprecipitation of the hydroxides of Mn^{2+}, Zn^{2+}, and Fe^{2+} followed by the oxidation of Fe(II) hydroxide. Initially, two water-CTAB-hexanol microemulsions, one containing tetramethylammonium hydroxide and the other $FeSO_4$, $MnSO_4$, and $ZnSO_4$, were mixed. Then, a third microemulsion containing H_2O_2 was added. It was found that the nanoparticle size can be controlled by selecting the appropriate microemulsion composition and reactant concentrations[166].

4.6.4. *Synthesis of Miscellaneous Nanoparticles in Microemulsions*

Nanosized cerium-terbium mixed oxides were prepared by mixing under stirring two w/o microemulsions formed by water, Triton X-100, *n*-hexanol, and *n*-heptane containing Ce(III) and Tb(III) nitrates and an alkali solution, respectively. After reaction, the resulting mixture was centrifuged, and the solid phase was separated by decantation, washed with methanol, dried, and calcinated. In such conditions, the formation of high-surface-area nanomaterials with average size in the 5–7 nm range and interesting catatlytic properties was ascertained[167].

Metal oxide nanoparticles were synthesized in w/o microemulsions composed by water, Triton X-100, *n*-hexanol, and *n*-hexane by adding under stirring functionalyzed metal alkoxides. The metal alkoxides were modified to obtain nanoparticles showing on their surface polymerizable groups. Subsequently, these nanoparticles were employed as initiators for radical polymerization using methyl methacrylate and styrene as monomers. This procedure allowed the preparation of amorphous metal-oxide-core polymer-shell nanoparticles of titanium, zirconium, tantalium, yttrium, and vanadium, showing good control of composition and morphology of the resulting nanomaterials[168].

Barium hexaaluminate nanoparticles were synthesized by mixing a solution of barium and aluminium alkoxides ($Ba(OC_3H_7)_2$;$Al(OC_3H_7)_3$) in iso-octane with a w/o microemulsion composed of water, polyethylene adducts, linear alcohols, and iso-octane. The microemulsion allowed the hydrolysis of the alkoxides and condensation in confined space so providing nanoparticle size control. In order to coat barium hexaaluminate nanoparticles with rare-earth and transition-metal oxides, nitrate or acetate salts of the desired metal were added to the reacting mixture 12–24 h after the mixing process. Nanoparticles were recovered by freeze drying and calcinated. It was found that nanoparticle morphology reflects that of the hydrophilic nanodomains characterizing the structure of microemulsion[169].

Cu_2O hollow nanoparticles of about 22 nm were synthesized using an o/w/o emulsion as a template. Initially, aqueous solutions of potassium sodium tartrate ($C_4H_4O_6KNa$), $CuSO_4$, NaOH, and dextrose were mixed and added to a solution of polyvinylpyrolidone in heptane. This led to the formation of a microemulsion. Then, the microemulsion was added to a solution of lauryl-polyoxyethylene (7) ether ($C_{12}H_{25}O(CH_2CH_2O)_7$) in order to obtain o/w/o multiple emulsion and was heated in a microwave oven. The precipitated nanomaterial was separated by centrifugation, washed, and dried[170].

Polyaniline nanoparticles were synthesized in w/o microemulsions through confined polymerization of aniline induced by ultrasound irradiation. The microemulsions were prepared by mixing cetyltrimethylammonium bromide, *n*-hexanol, and a concentrated aqueous solution of HCl. Then, an aniline/*n*-hexanol solution was added under ultrasound irradiation and polyaniline was precipitated by induced separation using ethanol. The resulting polyaniline nanoparticles are quite monodisperse, spherical, and their size was controlled by that of the microemulsion droplets[171].

Poly(methylmetacrylate) (PMMA) nanoparticles were synthesized in o/w microemulsions composed of methylmetacrylate, sodium bis(2-ethylhexyl)-sulfosuccinate and water. The polymerization was carried out at 60°C using potassium persulfate as initiator. The resulting latex was added to an acrylamide and *N, N′*-methylenebisacrylamide aqueous solution and polymerized to obtain microstructured hydrogels. In such conditions, the polymerization of acrylamide leads to the formation of a dendritic network that incorporates the PMMA nanoparticles. These structures showed enhanced water uptake and mechanical properties[172].

Stable nanoparticles of the organic compounds cholesterol, Rhovanil, and Rhodiarome with a size of about 5–7 nm have been produced using water/AOT/*n*-heptane, water/Triton/decanol, and water/CTAB/hexanol w/o microemulsions. The method consisted in the dropwise addition of a solution of the organic compound in an organic solvent (acetone, ether, ethanol, chloroform) to the microemulsion, and then the resulting mixture was homogenized by ultrasound or by a magnetic stirrer. The formation of nanoparticles was assured by TEM. The mechanism hypothesized to explain nanoparticle formation is constituted by the following steps: i) the solution of the organic compound penetrates in the micellar core. In this step, the nature of the solvent influences the transport of the coumpound across the surfactant monolayer surrounding the water droplet. ii) The accumulation of the solute in the micellar core, the equilibration of the solvent concentration in the system and the intermicellar material exchange process determine the nanoparticle formation. Different hypotheses have been advanced to explain nanoparticle stability: a) the nanoparticles are stabilized by a monolayer of surfactant molecules oriented so that the alkyl chains point toward the bulk medium; b) the nanoparticles are surrounded by water and then by opportunely oriented surfactant molecules; c) nanoparticles are surrounded by a surfactant bilayer[173].

$Cu_2[Fe(CN)_6]$ nanoparticles have been synthesized by dropwise addition of a water/AOT/*n*-heptane microemulsion containing $CuSO_4$ to another one containing $K_4[Fe(CN)_6]$. It was observed that, following the inverse procedure, i.e., the addition of the $K_4[Fe(CN)_6]$ containing microemulsion to that containing $CuSO_4$, resulted in bulk precipitation[174].

4.7 Nanoparticle Synthesis in Vesicles

The resemblance of vesicles and liposomes to cell membranes has driven many researchers to use them as systems to model and/or to mimic the mineralization processes occurring in the more complex biomembranes. Moreover, many novel nanomaterials have been synthesized by vesicular dispersions. On the other hand, investigations on the molecular mechanisms underlying nuclei formation and growth in the vescicular space are of theoretical interest. A schematic representation of nanoparticle formation inside vesicles is shown in Fig. 4.5.

Two reaction domains can be recognized in the vesicles. The first is the vesicle inside where the growing nanoparticle will be confined, the second is the outer leaflet of the vesicle bilayer where the precursors can accumulate, forming quite spherical nanoparticles or as hollow particles. Many nanoparticles have been synthesized in direct vesicles. In the case of ionic surfactants, the dissociation leads to the formation of an electric double layer and ion accumulation, which could stabilize nuclei. Moreover, specific effect and molecular recognition between embryos and vesicle surface could favour nanoparticle formation.

4.7.1. Synthesis of Metal Nanoparticles in Vesicle Dispersions

2D and 3D platinum nanostructures have been obtained by chemical reduction of platinum salt with ascorbic acid in aqueous surfactant solutions. The control of the resulting nanostructures was achieved using Sn(IV) octaethyl porphyrin dichloride (SnOEP), allowing the initial formation of a large number of Pt nuclei. In particular, after solubilization of SnOEP in aqueous dispersions of 1,2 dioctadecanoyl-*sn*-glycero-3-phosphocholine and choles-

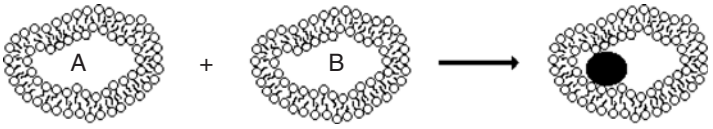

FIGURE 4.5. Nanoparticle synthesis in dispersions of vesicles.

terol liposomes and dropwise addition of aqueous solutions of Pt salt and ascorbic acid, the resulting mixture was irradiated with incandescent light. Similar protocols were followed but using sodium dodecylsulfate or polyoxyethylene (23) lauryl ether (Brij-35) as surfactant solutions[175].

Nano-size gold nanocrystallites were entrapped within multilamellar phosphatidylcholine vesicles by in situ reduction of $HAuCl_4$ due to the lipid itself[176].

Silver nanoparticles have been synthesized within the multilamellar vesicles formed by Genamin T020. Multilamellar vesicles were obtained by manual shearing of the surfactant with water followed by their dispersion in water by mechanical stirring. The subsequent addition of an aqueous solution of $AgNO_3$ led to the formation of Ag nanoparticles due to silver ions diffusion through the lamellae and their reduction assisted by Genamin T020. As an alternative procedure, the surfactant was directly sheared with the aqueous solution of $AgNO_3$, and the resulting multilamellar vesicles were dispersed in water. The two procedures determined significant differences in the nanoparticle growth rate and structural properties[177].

Stable polymerized diacetylene-coated silver nanoparticles have been synthesized by simultaneous silver photoreduction and diacetylene monomer photopolymerization under UV irradiation. Initially, an ethanolic solution of 10,12-pentacosadiynoic acid was mixed with aqueous silver nitrate and treated with ultrasound to allow the formation of diacetylene vesicles coated by silver ions on both internal and external bilayer surfaces. The binding of silver ions was attributed to chemical bonding with the carboxylic groups of diacetylene. Subsequently, the mixture was exposed to UV radiation to allow diacetylene photopolymerization and silver reduction[178].

4.7.2. Synthesis of Semiconductor Nanoparticles in Vesicle Dispersions

Nearly spherical CdS nanoparticles have been synthesized in aqueous suspensions of monolamellar lecithin vesicles. The size of CdS nanoparticles and their initial growing rate are regulated by the pH of the vesicle suspensions, presence of membrane modifiers, and Cd^{2+} ligands. By changing the preparation procedure, nanoparticles were located to the inner and/or outer surface of the lecithin vesicles[179].

Crystalline silicon nanoparticles coated by a chemically bonded monolayer of octanol molecules were successfully incorporated into phospholipid unilamellar vesicles dispersed in water. The capped nanoparticles were synthesized by decomposition of phenylsilane in supercritical octanol/hexane mixtures, allowing to obtain lipophilic particles stabilized against coalscence and oxidation of the nanoparticle surface[180].

Hollow nanoparticles of CdSe with size 100–200 nm in an aqueous dispersion of sodium dodecylsulfate (SDS) vesicles have been synthesized. An aqueous solution of $CdCl_2$ and SDS was exposed to low-intensity ultra-

sound. In this step, SDS micelles are transformed in vesicles and Cd^{2+} ions are absorbed on their surface. Then, a Na_2SeSO_3 aqueous solution was gradually added. During the reaction, the resulting mixture was irradiated with ultrasound probably to maintain SDS in the vesicular state. The resulting yellow precipitate was collected, washed, and dried under vacuum. To search for the best experimental conditions, the effect of surfactant concentration and temperature changes has been investigated[181].

Size-quantized CdS nanoparticles showing a very low polydispersity were synthesized in phosphatidylcholine vesicles dispersed in water. Higly monodisperse $CdCl_2$ containing vesicles were prepared by dialysis of an aqueous solution of phosphatidylcholine/*n*-hexyl-β-D-glucopyranoside mixed micelles and cadmium chloride. Residual cadmium ions external to the vesicles were eliminated effectively by a cation exchange column. Then, stable and monodisperse CdS nanoparticles entrapped in the vesicles were obtained by adding ammonium sulfite to the vesicle dispersion under vigorous stirring. It was found that CdS nanoparticle size is determined by the amount of cadmium ions initially entrapped in the vesicles[182].

Indium-tin hydroxide nanoparticles were formed by mixing two water/AOT lamellar liquid crystals, one containing indium nitrate and tin chloride and the other ammonium hydroxide. The application of shear force to the mixture caused the formation of spherical multilamellar vesicles (spherulites, diameter 300–10,000 nm) where the reaction took place, leading to small-size indium-tin hydroxide particles[183].

Multilamellar silica vesicles have been synthesized by hydrolysis of tetraethoxysilane in water/cetyltrimethylammonium bromide/diethylether systems. After solubilization of CTAB in aqueous ammonia solution, diethylether and TEOS was added under stirring. The precipitated matter was filtered, washed, and dried. By changing the diethylether concentration, as a consequence of the templating effect of the surfactant aggregates, star-like or bowl-like silica vesicles were obtained[184].

4.7.3. *Synthesis of Magnetic Nanoparticles in Vesicle Dispersions*

Iron oxide nanoparticles entrapped in aqueous vesicles formed by the photochromic amphiphilic spiropyran were obtained by mixing the vesicular dispersion with commercially available magnetic fluid. Such fluid was composed by surfactant-coated, nearly monodisperse iron oxide nanoparticles with a size of 10 nm. The resulting magnetic vesicles showed superparamagnetic properties at room temperature[185].

Monodisperse γ-Fe_2O_3 nanoparticles were entrapped in egg phosphatidylcholine liposomes by mixing the surfactant with a maghemite nanocrystal aqueous suspension followed by repeated extrusion through polycarbonate filters. Then, by gel exclusion chromatography, Fe_2O_3 nanoparticles lying in

the bulk aqueous medium were removed. It was observed that the permeability of liposomes can be altered by addition of the non-ionic surfactant octyl-β-D-glucopyranoside, leading to significant leakage of the magnetic nanoparticles[186].

Superparamagnetic monocrystalline magnetite nanoparticles have been synthesized in aqueous solution of unilamellar vesicles formed by cetyltrimethylammonium bromide (CTAB) and dodecylbenzenesulfonic acid. Initially, to an aqueous micellar solution of CTAB containing ferrous chloride, an aqueous solution of dodecylbenzenesulfonic acid was added dropwise leading to the formation of unilamellar vesicles entrapping ferrous ions. External metal ions replaced with sodium ions by gel permeation and subsequently sodium hydroxide was added to the vesicular solution. The permeation of OH^- ions across the bilayer allowed the formation of magnetite nanoparticles inside the vesicles. The existence of disordered surface layer involving interplanar spacings larger than those in the interior was observed[187].

Aqueous dispersions of superparamagnetic Fe_3O_4 nanoparticles encapsulated in phospholipid vesicles have been synthesized. Firstly, aqueous magnetite nanoparticle suspensions were prepared by dropwise addition of NH_3 solution to $FeCl_3$ and $FeCl_2$ solution in water. After addition of lauric acid, the resulting suspension was dialyzed with phospholipidic vesicular solution composed of dimyristoyl-phosphatidyl-choline and dimyristoyl-phosphatidyl-glycerol, leading to the formation of Fe_3O_4 nanoparticles stabilized by a phospholipid bilayer. Subsequently, poly(ethyleneglycol) derivatized dipalmitoyl-phosphatidyl-ethanolamine was introduced in the magneto-liposome bilayer by incubation with the corresponding vesicles[188].

4.7.4. *Synthesis of Miscellaneous Nanoparticles in Vesicle Dispersions*

Reduction of copper (II) ions encapsulated into spherulites of Genamin TO20 (R-N[$(C_2O_4O)_x$-X)][$(C_2O_4O)_y$-X)], where $x + y = 2$) by hydrazine led to the formation of Cu_2O nanoparticles (10–30 nm). The suspension of nanoparticles entrapped in spherulites was found to be stable. Lamellar phases composed of water/$CuSO_4$/Genamin TO20 were prepared by adding pure surfactant to copper sulfate aqueous solutions. To allow spherulites formation, the samples were placed in a plate-plate cell made of two parallel glass plates separated by a distance of 0.5 mm, and the shear was applied by rotating the lower plate at a controlled constant angular rate[189].

AgBr nanoparticles have been synthesized in unilamellar vesicles of dioleoylphosphatidylcholine by the reaction of Ag^+ ions confined inside the vesicles and Br^- ions placed in the bulk medium. Contacts between these reactants was provided by the application of a high-voltage electric field pulse to the aqueous suspension, which are able to produce the reversible and transient opening of pores in the vesicle bilayer[190].

Mixed electrolytes (aluminium/magnesium, aluminium/calcium, aluminium/barium chloride) dissolved in the aqueous core of unilamellar vesicles of phosphatidylcholine were made to react with hydroxyl ions coming from the extravescicular space and diffusing into the interior through the vesicle walls. It was suggested that nucleation occurs preferentially at the internal wall of vesicles, leading to the formation of nearly spherical and stable oxide nanoparticles[191].

4.8 Biological Microheterogeneous Systems

Cells and bacteria can be considered as natural occurring highly complex microheterogeneous systems. Their structural features can be exploited to set up additional innovative methods to synthesize nanoparticles. An advantage of this strategy is the production of nanoparticles by an eco-compatible process that does not require the use of toxic chemicals[192].

The idea to employ biological systems to synthesize nanoparticles must not be surprising, because it is routinely done by human cells, e.g., in the biosynthesis of bones and teeth.

The processes at the basis of nanoparticle synthesis by many bacteria and microorganisms are often functional to their defence mechanisms against the toxicity of many metal ions, consisting in changing its redox state and/or precipitating it intracellularly. This behaviour can be exploited by using microorganisms in processes as bioleaching, microbial corrosion, and nanoparticle synthesis. Actually, both prokaryotic and eukaryotic cells have proved to be able to synthesize nanosized particles of semiconductors (CdS and ZnS)[193–195] and metals (Au, Ag).[196,197]

Although biological systems are not widely exploited for nanoparticle synthesis, it looks a very simple and promising approach that deserves to be further investigated.

4.9 Final Remarks

In the past decades, many attempts to synthesize nanoparticles by microheterogeneous systems have been carried out, showing the relevant potentials of this methodology. The examples reported in this book should be convincing. From these examples in a pure imitative way, a lot of successful synthetic protocols can be derived. These protocols can be performed without expensive apparatus, and the control of the final structure of the nanomaterials can be achieved by the knowledge of some easy to understand theoretical principles and using a molecular picture of the employed systems.

The characterization of the resulting nanomaterials has shown that the confinement of nanoparticles in microheterogeneous systems confers to them peculiar physico-chemical properties. Synthesis in

microheterogeneous systems is not only an alternative route to other methods, but also it shows specific advantages, and sometimes it represents the unique way for nanoparticle preparation. Moreover, the investigations performed so far confirm that microheterogeneous systems are the right answer to the building of ordered 1D, 2D, and 3D architectures of nanoparticles embedded in a surfactant matrix with important chemical, optical, biotechnological, and microelectronic applications.

Being a typical bottom-up method, the synthesis by microheterogeneous systems can be directed to prepare nanoparticles of quite all the substances by simply changing the nature of the reacting species, i.e., it is potentially of general applicability. It can be expected that the extension to novel compounds could lead to the preparation of new and interesting nanomaterials. Future research should be focused on the selection of new microheterogeneous systems with improved or specific potentials for nanoparticle synthesis and the establishment of new synthetic routes.

Obviously, further efforts directed to a better understanding of the microscopic processes underlying the synthesis of nanoparticles in microheterogeneous systems and controlling their final structure and spatial distribution should lead to widely increase the number of nanomaterials of industrial interest that can be realized by microheterogeneous systems. Many novel nanoparticle containing microheterogeneous systems wait to be prepared and characterized in order to find nanomaterials for relevant applications in many fields.

The attempt to mimie biological systems by nanoparticle containing microheterogeneous systems should lead to the realization of "artificial" counterparts with increasing complexity, tending to reproduce many of their functionalities including evolution.

REFERENCES

1. W. Mehnert, K. Mader, *Advanced Drug Delivery Reviews* **47**, 165–196 (2001)
2. Marcianò, A. Minore, V. Turco Liveri, *Coll. Polym. Sci.* **278**, 250–252 (2000)
3. G: Calvaruso, A. Minore, V. Turco Liveri, *J. Coll. Int. Sci.* **243**, 227–232 (2001)
4. L. Levy, J. F. Hochepied, M. P. Pileni, *J. Phys. Chem.* **!00**, 18322–18326 (1996)
5. W. Wang, S. Efrima, O. Regev, *J. Phys. Chem. B* **103**, 5613–5621 (1999)
6. L. Qi, Y. Gao, J. Ma, *Colloids and Surfaces A* **157**, 285–294 (1999)
7. M. Andersson, V. Alfredsson, P. Kjellin, A. E. C. Palmqvist, *Nanoletters* **2**, 1403–1407 (2002)
8. G. S. Attard, P. N. Bartlett, N. R. B. Coleman, J. M. Elliot, J. R. Owen, *Langmuir* **14**, 7340–7242 (1998)
9. S. H. Wu, D. H. Chen, *J. Colloid Interface Science* **273**, 165–169 (2004)
10. B. M. Rabatic, M. U. Pralle, G. N. Tew, S. I. Stupp, *Chem. Mater.* **15**, 1249–1255 (2003)
11. H. Yang, R. Guo, H. Wang, *Colloids and Surfaces A* **180**, 243–251 (2001)
12. J. P. Yang, S. B. Quadri, B. R. Ratna, *J Phys. Chem.* **100**, 17255–17259 (1996)
13. W. Wang, Y. Liu, Y. Zhan, C. Zheng, G. Wang, *Materials Research Bulletin* **36**, 1977–1984 (2001)

14. M. Klotz, A. Ayral, C. Guizard, L. Cot, *Separation and Purification Technology* **25**, 71–78 (2001)
15. O. Dag, S. Aloyoglu, C. Tura, O. Celik, *Chem. Mater*. **15**, 2711–2717 (2003)
16. L. Huang, H. Wang, Z. Wang, A. Mitra, D. Zhao, Y. Yan, *Chem. Mater*. **14**, 876–880 (2002)
17. C. Menager, L. Belloni, V. Cabuil, M. Dubois, T. Gulik-Krywicki, T. Zemb, *Langmuir* **12**, 3516–3522 (1996)
18. V. Berejnov, Y. Raikher, V. Cabnil, J. C. Bacri, R. Perzynski, *J. Coll. Inter. Sci.* **199**, 215–217 (1998)
19. V. Berejnov, V. Cabmil, R. Perzynski, Y. Raikher, *J. Phys. Chem. B* **102**, 7132–7138 (1998)
20. P. Kjellin, M. Anderson, A.E.C. Palmqvist, *Langmuir* **19**, 9196–9200 (2003)
21. D. H. Gray, D. L. Giu, *Chem. Mater*. **10**, 1827–1832 (1998)
22. H. P. Hentze, E. W. Kaler, *Chem. Mater*. **15**, 708–713 (2003)
23. M. D. Lynch, D. L. Patrick, *Nanoletters* **2**, 1197–1201 (2002)
24. C. L. Lester, S. M. Smith, W. L. Jarrett, C. A. Guymon, *Langmuir* **19**, 9466–9472 (2003)
25. J. H. Fendler, *Reactions and Synthesis in Surfactant Systems*, (Ed J. Texter, Marcel Dekker Inc, NY, 2001) pp. 633–638
26. K. Grieve, F. Grieser, D. N. Furlong, *Reactions and Synthesis in Surfactant Systems*, (Ed J. Texter, Marcel Dekker Inc, NY, 2001) pp. 639–665
27. K. J. Stine, BG Moore, in *Nanosurface Chemistry*, Ed M Rosoff, M Dekker, NY, pp. 59–140 (2002)
28. B. Tieke, K.U. Falda, A. Kampes, in *Nanosurface Chemistry*, Ed M Rosoff, M Dekker, NY, pp. 213–242 (2002)
29. T. Yonezawa, T. Kunitake, *Coll Surfaces A* **149**, 193–199 (1999)
30. A. Swami, A. Kumar, P. R. Selvakannan, S. Mandal, M. Sastry, *J. Colloid Interface Science* **260**, 367–373 (2003)
31. K. M. Mayya, N. Jain, A. Gole, D. Langevin, M. Sastry, *J. Coll. Int. Sci*. **270**, 133–139 (2004)
32. G. B. Khomutov, S. P. Gubin, *Materials Science and Engineering C* **22**, 141–146 (2002)
33. Z. V. Saponjic, R. Csencsits, T. Rajh, N. M. Dimitrijevic, *Chem. Mater*. **15**, 4521–4526 (2003)
34. A. Swami, A. Kumar, R. Pasricha, A.B. Mandale, M. Sastry, *J. Coll. Inter.Sci*. **271**, 381–387 (2004)
35. J. Yang, J.H. Fendler, *J. Phys. Chem*. **99**, 5505–5511 (1995)
36. S. Erokhina, V. Erockhina, C. Nicolini, *Colloids and Surfaces A* **198**, 645–650 (2002)
37. J. Yang, F.C. Meldrum, J. H. Fendler, *J. Phys. Chem*. **99**, 5500–5504 (1995)
38. N. A. Kotov, F. C. Meldrum, J. H. Fendler, *J. Phys. Chem*. **98**, 8827–8830 (1994)
39. A. Nabok, I. Iwantono, A. Ray, I. Larkin, T. Richardson, *J. Phys. D Appl. Phys*. **35**, 1512–1515 (2002)
40. Y. Tian, J. H. Fendler, *Chem. Mater*. **8**, 969–974 (1996)
41. P. W. Wu, L. Gao, J. K. Guo, *Thin Solid Films* **408**, 132–135 (2002)
42. D. J. Elliot, D. N. Furlong, F. Grieser, *Colloids and Surfaces A* **155**, 101–190 (1999)

43. G. B. Khomutov, S. P. Gubin, V. V. Khanin, A. Y. Koksharov, A. Y. Obydenov, V. V. Shorokhov, E. S. Soldatov, A. S. Trifonov, *Colloids and Surfaces A* **198**, 593–604 (2002)
44. L. Fu, V.P. Dravid, D.L. Johnson, *Appl. Surface Science* **181**, 173–178 (2001)
45. J. S. Yin, Z.L. Wang, *J. Phys. Chem. B* **101**, 8979–8983 (1997)
46. Y. S. Kang, D. K. Lee, C. S. Lee, P. Stroeve, *J. Phys. Chem. B* **106**, 9341–9346 (2002)
47. I. Moriguchi, K. Orishikida, Y. Tokiyama, H. Watabe, S. Kagawa, Y. Tereoka, *Chem. Mater*. **13**, 2430–2435 (2001)
48. Y. Wu, B. Li, W. Wang, F. Bai, M. Liu, *Materials Science and Engineering C* **23**, 605–609 (2003)
49. S. Tanaka, N. Nishiyama, Y. Oku, Y. Egashira, K. Ueyama, *J. Am. Chem. Soc*. **126**, 4854–4858 (2004)
50. J. J. Ramsden, M. Grätzel, *J. Chem. Soc. Faraday Trans. 1*, **80**, 919–933 (1984)
51. M. Mandal, S.H. Gosh, S. Kundu, K. Esumi, T. Pal, *Langmuir* **18**, 7792–7797 (2002)
52. A. Pal, K. Ghosh, K. Esumi, T. Pal, *Langmuir* **20**, 575–578 (2004)
53. L. M. Bronstein, S. N. Siderov, P. M. Valetsky, J. Hartmann, H. Colfen, M. Antonietti, *Langmuir* **15**, 6256–6262 (1999)
54. W. Cheng, S. Dong, E. Wang, *Electrochemistry Communications* **4**, 412–416 (2002)
55. A. Swami, A. Kumar, M. Sastri, *Langmuir* **19**, 1168–1172 (2003)
56. B. Nikoobakht, M.A. El-Sayed, *Langmuir* **17**, 6368–6374 (2001)
57. R.A. Salkar, P. Jeevanandam, G. Kataby, S.T. Aruna, Y. Kolpin, O. Palchik, A. Gedanken, *J. Phys. Chem. B* **104**, 893–897 (2000)
58. S. H. Wu, D. H. Chen, *J. Colloid Interface Science* **273**, 165–169 (2004)
59. F. Mafunè, J. Kohno, T. Kondow, H. Sawabe, *J. Phys. Chem. B* **104**, 8333–8337 (2000)
60. F. Mafunè, J. Kohno, T. Kondow, H. Sawabe, *J. Phys. Chem. B* **105**, 5114–5120 (2001)
61. F. Mafunè, J. Kohno, Y. Takeda, T. Kondow, *J. Phys. Chem. B* **105**, 9050–9056 (2001)
62. Y. Mizukoski, K. Okitsu, Y. Maeda, T. A. Yamamoto, R. Oshima, Y. Nagata, *J. Phys. Chem. B* **101**, 7033–7037 (1997)
63. D. Li, S. Chen, S. Zhao, X. Hou, H. Ma, X. Yang, *Applied Surface Science* **200**, 62–67 (2002)
64. Z. Yian, W. Yongchang, L. Yimin, *Colloids and Surfaces A* **232**, 155–161 (2004)
65. P. H. Borse, N. Deshmukh, R. F. Scinde, S. K. Date, S. K. Kulkarni, *J. of Material Science* **34**, 6087–6093 (1999)
66. R. Lv, C. Cao, Y. Guo, H. Zhu, *Journal of Materials Science* **39**, 1575–1578 (2004)
67. C. Liang, Y. Shimizu, T. Sasaki, N. Koshizaki, *J. Phys. Chem. B* **107**, 9220–9225 (2003)
68. Y. Wang, C. Ma, X. Sun, H. Li, *Nanotechnology* **13**, 565–569 (2002)
69. Z. Liu, Z. Hu, J. Liang, S. Li, Y. Yang, S. Peng, Y. Qian, *Langmuir* **20**, 214–218 (2004)
70. X. Li, C. Kutal, *J. of Alloys and Compounds* **349**, 264–268 (2003)
71. C. R. Vestal, Z. J. Zhang, *Chem. Mater*. **14**, 3817–3822 (2002)
72. L. Shen, P.E. Laibinis, T.A. Hatton, *Langmuir* **15**, 447–453 (1999)

73. D. K. Kim, Y. Zhang, W. Voit, K. V. Rao, M. Muhammed, *J. of Magnetism and Magnetic Materials* **225**, 30–36 (2001)
74. X. Q. Xu, H. Shen, J. R. Xu, X. J. Li, *Applied Surface Science* **221**, 430–436 (2004)
75. Y. Wang, Y. F. Wong, X. Teng, X. Z. Liu, H. Yang, *Nanoletters* **3**, 1555–1559 (2003)
76. G. D. Moeser, K. A. Roach, W. H. Green, P. E. Laibinis, T. A. Hatton, *Ind. Eng. Chem. Res*. **41**, 4739–4749 (2002)
77. B. Denizot, G. Tanguy, F. Hindre, E. Rump, J. J. LeJeune, P. Jallet, *J. Coll. Int. Sci*. **209**, 66–71 (1999)
78. Y. Y. Lyu, S. H. Yi, J. K. Shon, S. Chang, L. S. Pu, S. Y. Lee, J. E. Yie, K. Char, G. D. Stucky, J. M. Kim, *J. Am. Chem. Soc*. **126**, 2310–2311 (2004)
79. B. Li, T. Kawakami, M. Hiramatsu, *Applied Surface Science* **210**, 171–176 (2003)
80. L. Levy, Y. Sahoo, K. S. Kim, E. J. Bergey, P. N. Prasad, *Chem. Mater*. **14**, 3715–3721 (2002)
81. P. J. Bruinsma, A. Y. Kim, S. Baskaran, *Chem. Mater*. **9**, 2507–2515 (1997)
82. H. Y. Zhu, X. P. Gao, D. Y. Song, Y. Q. Bai, S. P. Ringer, Z. Gao, Y. X. Xi, W. Martens, J. D. Riches, R. L. Frost, *J. Phys. Chem. B* **108**, 4245–4247 (2004)
83. P. Kang, C. Chen, L. Hao, C. Zhu, Y. Hu, Z. Chen, *Materials Research Bulletin* **39**, 545–551 (2004)
84. M. G. Han, S. K. Cho, S. G. Oh, S. S. Im, *Synthetic Metals* **126**, 53–60 (2002)
85. J. W. Choi, M. G. Han, S. Y. Kim, S. G. Oh, S. S. Im, *Synthetic Metals* **141**, 293–299 (2004)
86. J. Jang, H. Ha, *Langmuir* **18**, 5613–5618 (2002)
87. S. G. Oh, S.S. Im, *Current Applied Physics* **2**, 273–277 (2002)
88. R. Singh, M. Castagnola, P. K. Dutta, *Reactions and synthesis in surfactant systems*, (Ed J. Texter, Marcel Dekker Inc, NY, 2001) pp. 737–759
89. L. Lisiecki, M. P. Pileni, *J. Phys. Chem*. **99**, 5077–5082 (1995)
90. R. P. Bagwe, K. C. Khilar, *Langmuir* **16**, 905–910 (2000)
91. J. P. Cason, K. Khambaswadkar, C. B. Roberts, *Ind. Eng. Chem. Res*. **39**, 4749–4755 (2000)
92. W. Cheng, S. Dong, E. Wang, *Langmuir* **19**, 9434–9439 (2003)
93. R. Zhang, J. Liu, B. Han, A. He, Z. Liu, J. Zhang, *Langmuir* **19**, 8611–8614 (2003)
94. J. Zhang, B. Han, Z. Dong, J. Liu, D. Li, J. Wang, B. Dong, H. Zhao, L. Rong, *J. Phys. Chem. B* **107**, 3679–3683 (2003)
95. H. H. Ingelsten, J. C. Beziat, K. Bergkvist, A. Palmqvist, M. Skoglundh, H. Quinhong, L. K. L. Falk, K. Holmberg, *Langmuir* **18**, 1811–1818 (2002)
96. S.L. Tripp, S.V. Pusztay, A.E. Ribbe, A. Wei, *J. Am. Chem. Soc*. **124**, 7914–7919 (2002)
97. N. Shulka, C. Liu, P. M. Jones, D. Weller, *J. of Magnetism and Magnetic Materials* **266**, 178–184 (2003)
98. C. Luna, M. P. Morales, C. J. Serna, M. Vazquez, *Materials Science Engineering C* **23**, 1129–1132 (2003)
99. E. Caponetti, L. Pedone, D. Chillura Martino, V. Pantò, V. Turco Liveri, *Materials Science and Engineering C* **23**, 531–539 (2003)
100. T. Hirai, T. Watanabe, I. Kourosawa, *J. Phys. Chem*. B **103**, 10120–10126 (1999)

101. P. Dutta, J. H. Fendler, *J. Coll. Int. Sci.* **247**, 47–53 (2002)
102. J. Cizeron, M. P. Pileni, *J. Phys. Chem.* **99**, 17410–17416 (1995)
103. W.S. Chae, J. H. Ko, I. W. Hwang, Y.R. Kim, *Chem. Phys. Lett.* **365**, 49–56 (2002)
104. Q. Wu, N. Zheng, Y. Ding, Y. Li, *Inorganic Chemistry Comm.* **5**, 671–673 (2002)
105. P. Calandra, A. Longo, V. Turco Liveri, V. *J. Phys. Chem.* **107**, 25–30 (2003)
106. P. Calandra, A. Longo, V. Marcianò, V. Turco Liveri, V. *J. Phys. Chem.*, **107**, 6724–6729 (2003)
107. B. Simmons, S. Li, V. T. John, G. L. M. C. Pherson, C. Taylor, D. K. Schwartz, K. Maskos, *Nanoletters* **2**, 1037–1042 (2002)
108. F. J. Arriagada, K. Osseo-Asare, *J. Coll. Int. Sci.* **170**, 8–17 (1995)
109. M. Harada, S. Itakura, A. Shioi, M. Adachi, *Langmuir* **17**, 4189–4195 (2001)
110. E. Stathatos, P. Lianos, F. Del Monte, D. Levy, D. Tsiourvas, *Langmuir* **13**, 4295–4300, 1997
111. A. D'Aprano, F. Pinio, V. Turco Liveri, *J. Solution Chemistry* **20**, 301–306 (1991)
112. C. J. O'Connor, C.T. Seip, E. E. Carpenter, S. Li, V.T. John, *Nanostructured Materials* **12**, 65–70 (1999)
113. K. Shafi, A. Ulman, X. Yan, N. Yang, C. Estournes, H. White, M. Rafailovich, *Langmuir* **17**, 5093–5097 (2001)
114. W. Zhonghua, G. Lin, L. Qianshu, Z. Hesun, *J. Phys. Condensed Matter* **11**, 4961–4970 (1999)
115. X. Teng, D. Black, N. J. Watkins, Y. Gao, H. Yang, *Nanoletters* **3**, 261–264 (2003)
116. C. Liu, B. Zou, A. J. Rondinone, Z. J. Zhang, *J. Phys. Chem. B* **104**, 1141–1145 (2000)
117. C. Liu, Z. J. Zhang, *Chem. Mater.* **13**, 2092–2096 (2001)
118. M. Willert, R. Rothe, K. Landfester, M. Antonietti, *Chem. Mater.* **13**, 4681–4685 (2001)
119. M. Ghosh, G. Lawes, A. Gayen, G. N. Subbanna, W. M. Reiff, M. A. Subramanian, A. P. Ramirez, J. P. Zhang, R. Seshadri, *Chem. Mater.* **16**, 118–124 (2004)
120. N. Wu, L. Fu, M. Su, M. Aslam, K. C. Wong, V. P. Dravid, *Nanoletters* **4**, 383–386 (2004)
121. S. Utamapaya, K. J. Klabunde, J. R. Schlup, *Chem. Mater.* **3**, 175–181 (1991)
122. P. Jeevanandam, K. J. Klabunde, *Langmuir* **19**, 5491–5495 (2003)
123. M. Li, H. Schnablegger, S. Mann, *Nature* **402**, 393–395 (1999)
124. M. Li, S. Mann, *Langmuir* **16**, 7088–7094 (2000)
125. T. Y. Luo, T. X. Liang, C. S. Li, *Materials Science and Engineering A* **366**, 206–209 (2004)
126. F. Candau, Y. S. Leong, G. Pouyet, S. Candau, *J. Coll. Polym. Sci.* **101**, 167–183 (1984)
127. P. Calandra, A. Longo, V. Turco Liveri, *Coll. Polym. Sci.* **279**, 1112–1117 (2001)
128. C. Giordano, A. Longo, V. Turco Liveri, A.M. Venezia, *Coll. Polym. Sci.* **281**, 229–238 (2003)
129. C. Calvaruso, A. Ruggirello, V. Turco Liveri, *J. Nanoparticle Research* **4**, 239–246 (2002)

130. A. Ruggirello, V. Turco Liveri, *J. Coll. Int. Sci*. **258**, 123–129 (2003)
131. A. Ruggirello, V. Turco Liveri, *Chem. Phys*. **288**, 187–195 (2003)
132. E. Caponetti, D. Chillura-Martino, F. Ferrante, A. Ruggirello, V Turco Liveri, *Langmuir* **19**, 4913–4922 (2003)
133. A. Ruggirello, V. Turco Liveri, *Coll. Polym. Sci*. **281**, 1062–1068 (2003)
134. L. Ceraulo, E Dormond, A. Mele, V. Turco Liveri, *Coll. and Surfaces A* **218**, 255–264 (2003)
135. S. A. Sapp, C. M. Elliot, *Chem. Mater*. **15**, 1237–1241 (2003)
136. J. Chen, J. Zhang, D. Liu, B. Han, G. Yang, *Colloids and Surfaces A, Biointerfaces* **33**, 33–37 (2004)
137. V. Pillai, P. Kumar, M. J. Hou, P. Ayyub, D. O. Shah, *Advances in Colloids and Interface Science*, **55**, 241–269 (1995)
138. L. Jeunieau, F. Debuigne, J. B. Nagy, *Reactions and Synthesis in Surfactant Systems*, (Ed J. Texter, Marcel Dekker Inc, NY, 2001) pp. 609–631
139. T. F. Towey, A. Khan-Lodhi, B. H. Robinson, *J. Chem. Soc. Faraday Trans*. **86**, 3757–3762 (1990)
140. R. P. Bagwe, K. C. Khilar, *Langmuir* **13**, 6432–6438 (1997)
141. C. Petit, P. Lixon, M. Pileni, *J. Phys. Chem*. **97**, 12974–12979 (1993)
142. P. Calandra, M. Goffredi, V. Turco Liveri, *Coll. and Surf. A* **160**, 9–13 (1999)
143. S. Eriksson, U. Nylen, S. Rojas, M. Boutonnet *Applied Catalysis A: General* **265**, 207–219 (2004)
144. Y. Nakaoka, Y. Nosaka, *Langmuir* **13**, 708–711 (1997)
145. A. R. Kortan, R. Hull, R. L. Opila, M. G. Bawendi, M. L. Steigerwald, P. J. Carrol, L. E. Brus, , *J. Am. Chem. Soc*. **112**, 1327–1332 (1990)
146. CJ O'Connor, V Kolesnichenko, E Carpenter, C Sangiorgio, W Zhou, A Kumbhar, J Sims, F Agnoli, *Synthetic Metals* **122**, 547–557 (2001)
147. H. Ohde, F. Hunt, C. M. Wal, *Chem. Mater*. **13**, 4130–4135 (2001)
148. M. Bonini, U. Bardi, D. Berti, C. Neto, P. Baglioni, *J. Phys. Chem. B* **106**, 6178–6183 (2002)
149. O. P. Yadav, A. Palmqvist, N. Cruise, K. Holberg, *Colloid and Surfaces A* **221**, 131–134 (2003)
150. X. Zhang, K. W. Chan, *Chem. Mater*. **15**, 451–459 (2003)
151. M. L. Wu, D. H. Chen, T. C. Huang, *Chem. Mater*. **13**, 599–606 (2001)
152. M. L. Wu, D. H. Chen, T. C. Huang, *Langmuir* **17**, 3877–3883 (2001)
153. T. Tago, Y. Shibata, T. Hatsuta, K. Miyajina, M. Kishida, S. Tashiro, K. Wakabayashi, *J. of Materials Science* **37**, 977–982 (2002)
154. K. K. Yu, C. M. Y. Yeung, D. Thompsett, S. C. Tsang, *J. Phys. Chem. B* **107**, 4515–4526 (2003)
155. J. Fang, K. L. Stokes, J. A. Wiemann, W. L. Zhou, J. Dai, F. Chen, C. J. O'Connor, *Materials Science and Engineering B* **83**, 254–257 (2001)
156. X. Mo, C. Wang, L. Hao, Y. Zhu, . Chen, Y. Hu, *Materials Research Bulletin* **36**, 1925–1930 (2001)
157. S. Chang, L. Liu, S.A. Asher, *J. Am. Chem. Soc*. **116**, 6739–6744 (1994)
158. H. Ohde, M. Ohede, F. Bailey, H. Kim, C.M. Wai, *Nanoletters* **2**, 721–724 (2002)
159. R. Zhang, L. Gao, Q. Zhang, *Chemosphere* **54**, 405–411 (2004)
160. P. S. Khiew, N. M. Hang, S. Radin, M. Ahmad, *Materials Letters* **58**, 762–767 (2004)
161. P. Tartaj, J. Tartaj, *Chem. Mater*. **14**, 536–541 (2002)

162. C. R. Vestal, Z. J. Zhang, *Nanoletters* **3**, 1739–1743 (2003)
163. Y. Deng, L. Wang, W. Wang, S. Fu, A. Elaissari, *J. Magnetism and Magnetic Materials* **257**, 69–78 (2003)
164. S. Santra, R. Tapec, N. Theodoropoulou, J. Dobson, A. Hebart, W. Tan, *Langmuir* **17**, 2900–2906 (2001)
165. D. H. Chen, S. H. Wu, *Chem. Mater*. **12**, 1354–1360 (2000)
166. D. Makovec, A. Kosak, M. Drofenik, *Nanotechnology* **15**, 5160–5166 (2004)
167. A. B. Hungria, A. Martinez-Arias, M. Fernandez-Garcia, A. Igesias-Juez, A. Guerrero-Ruiz, J. J. Calvino, J. C. Conesa, J. Soria, *Chem. Mater*. **15**, 4309–4316 (2003)
168. D. Holzinger, G. Kickebick, *Chem. Mater*. **15**, 4944–4948 (2003)
169. A. J. Zarur, J. Y. Ying, *Nature* **403**, 65–67 (2000)
170. H. Liu, Y. Ni, F. Wang, G. Ying, J. Hong, Q. Ma, Z. Xu, *Colloids and Surfaces A* **235**, 79–82 (2004)
171. H. Xia, Q. Wang, *J. Nanoparticle Research* **3**, 401–411 (2001)
172. S. M. Nuno-Donlucas, J. C. Sanchez-Diaz, M. Rabelero, J. Cortes-Ortega, C. C. Luhrs-Olmos, V. V. Fernandez-Escamilla, E. Mendizabal, J. E. Puig, *J. Coll. Int. Sci*. **270**, 94–98 (2004)
173. F. Debuigne, L. Jeunieau, M. Wiame, J.B. Nagy, *Langmuir* **16**, 7605–7611 (2000)
174. S. P. Moulik, G. C. De, A. K. Pande, B. B. Bhowmik, A. R. Das, *Langmuir* **15**, 8361–8367 (1999)
175. Y. Song, Y. Yang, C. J. Medforth, E. Pereira, A. K. Singh, H. Xu, Y. Yiang, C. J. Brinker, F. Van Swol, J. A. Shelnutt, *J. Am. Chem. Soc*. **126**, 635–645 (2004)
176. F.C. Meldrum, B.G. Heywood, S. Mann, *J. Coll. Int. Sci*. **161**, 66–71 (1993)
177. C. Faure, A. Darrè, W. Neri, *J. Phys. Chem. B* **107**, 4738–4746 (2003)
178. H. S. Zhou, T. Wada, H. Sasabe, H. Komiyama, *Synthetic Metals* **81**, 129–132 (1996)
179. O. V. Vassiltsova, A. L. Chivilin, VN Parmon, *J. Photochemistry and Photobiology A: Chemistry* **125**, 127–134 (1999)
180. H. Jang, L.E. Pell, B. A. Korgel, D. S. English, *J. of Photochemistry and Photobiology, A: Chemistry* **158**, 111–117 (2003)
181. X. Zheng, Y. Xie, L. Zhu, X. Jiang, A. Yan, *Ultrasonics Sonochemistry* **9**, 311–316 (2002)
182. B. A. Korgel, H. G. Monbouquette, *J. Phys. Chem*. **100**, 346–351 (1996)
183. D. W. Kim, S.G. Oh, S. C. Yi, S. Y. Bae, S. K. Moon, *Chem. Mater*. **12**, 996–1002 (2000)
184. K. Kui, Q. Cai, X. Chen, Q. Feng, H. Li, *Microporous and Mesoporous Materials* **78**, 61–64 (2004)
185. M. Taguchi, G. Li, Z. Gu, O. Sato, Y. Einager, *Chem. Mater*. **15**, 4756–4760 (2003)
186. S. Lesiur, C. G. Madelmont, C. Menager, V. Canbil, D. Dadhi, P. Pierrot, K. Edwards, *J. Am. Chem. Soc. (Communications)* **125**, 5266–5267 (2003)
187. I. I. Yaacob, A. C. Nunes, A. Bose, *J. Coll. Inter. Sci*. **171**, 73–84 (1995)
188. M. De Cuyper, P. Muller, H. Lucken, M. Hodenius, *J. Phys. Condens. Matter* **15**, S1425–S1436 (2003)
189. F. Gauffre, D. Roux, *Langmuir* **15**, 3738–3747 (1999)
190. N. M. Correa, H. Zhang, Z. A. Schelly, *J. Am. Chem. Soc*. **122**, 6432–6434 (2000)
191. S. Bhandarkar, A. Bose, *J. Coll. Int. Sci*. **139**, 541–550 (1990)

192. A. Ahmad, S. Senapati, M. I. Khan, R. Kumar, R. Ramani, V. Srinivas, M. Sastry, *Nanotechnology* **14**, 824–828 (2003)
193. R. N. Reese, R. D. Winge, *The Journal of Biological Chemistry* **163**, 12832–12835 (1988)
194. M. Labrenz, G. K. Druschel, T. Thomsen-Erbert, B. Gilbert, S. A. Welch, K. M. Kemner, G. A. Logan, R. E. Summons, G. De Stasio, P. L. Bond, B. Lai, S. D. Kelly, J. F. Banfield, *Science* **290**, 1744–1747 (2000)
195. A. Ahmad, P. Mukherjee, D. Mandal, S. Senapati, M. Islam Khan, R. Kumar, M. Sastry, *JACS Communications* **124**, 12108–12109 (2002)
196. P. Mukherjee, A. Ahmad, D. Mandal, S. Senapati, S. R. Sainkar, M. I. Khan, R. Ramani, R. Parischa, P.V. Ajayakumar, M. Alam, M. Sastry, R. Kumar, *Angew. Chem., Int. Ed.* **40**, 3585–3588 (2001)
197. P. Mukherjee, A. Ahmad, D. Mandal, S. Senapati, S. R. Sainkar, M. I. Khan, R. Parishcha, P. V. Ajaykumar, M. Alam, R. Kumar, M. Sastry, *Nano Lett. (Communication)*; **1(10)**; 515–519 (2001)

Index